PNNL-25395

# Viability Study for an Unattended $UF_6$ Cylinder Verification Station: Phase I Final Report

## May 2016

LE Smith
KA Miller
J Garner
S Branney
B McDonald
J Webster
M Zalavadia
L Todd
J Kulisek
HA Nordquist
N Deshmukh
S Stewart




## DISCLAIMER



PACIFIC NORTHWEST NATIONAL LABORATORY
*operated by*
BATTELLE
*for the*
UNITED STATES DEPARTMENT OF ENERGY
*under Contract DE-AC05-76RL01830*

**Printed in the United States of America**

**Available to DOE and DOE contractors from the**
**Office of Scientific and Technical Information,**
**P.O. Box 62, Oak Ridge, TN 37831-0062;**
**ph: (865) 576-8401**
**fax: (865) 576-5728**
**email: reports@adonis.osti.gov**

**Available to the public from the National Technical Information Service**
**5301 Shawnee Rd., Alexandria, VA 22312**
**ph: (800) 553-NTIS (6847)**
**email: orders@ntis.gov <http://www.ntis.gov/about/form.aspx>**
**Online ordering: http://www.ntis.gov**

This document was printed on recycled paper.
(8/2010)

PNNL-25395

# Viability Study for an Unattended $UF_6$ Cylinder Verification Station: Phase I Final Report

LE Smith
KA Miller[1]
J Garner[2]
S Branney[3]
B McDonald
J Webster
M Zalavadia
L Todd
J Kulisek
HA Nordquist[1]
N Deshmukh
S Stewart[2]

May 2016

Prepared for
the U.S. Department of Energy
under Contract DE-AC05-76RL01830

Pacific Northwest National Laboratory
Richland, Washington 99352

---

[1] Los Alamos National Laboratory, Los Alamos, New Mexico
[2] Oak Ridge National Laboratory, Oak Ridge, Tennessee
[3] Savannah River National Laboratory, Aiken, South Carolina

# Abstract

In recent years, the International Atomic Energy Agency (IAEA) has pursued innovative techniques and an integrated suite of safeguards measures to address the verification challenges posed by the front end of the nuclear fuel cycle. Among the unattended instruments currently being explored by the IAEA is an Unattended Cylinder Verification Station (UCVS), which could provide automated, independent verification of the declared relative enrichment, $^{235}U$ mass, total uranium mass, and identification for all declared uranium hexafluoride ($UF_6$) cylinders in a facility (e.g., uranium enrichment plants and fuel fabrication plants). Under the auspices of the United States and European Commission Support Programs to the IAEA, a project was undertaken to assess the technical and practical viability of the UCVS concept. The U.S. Support Program team consisted of Pacific Northwest National Laboratory (lead), Los Alamos National Laboratory, Oak Ridge National Laboratory, and Savanah River National Laboratory. At the core of the viability study is a long-term field trial of a prototype UCVS system at a Westinghouse fuel fabrication facility. A key outcome of the study is a quantitative performance evaluation of two nondestructive assay (NDA) methods being considered for inclusion in a UCVS: Hybrid Enrichment Verification Array (HEVA), and Passive Neutron Enrichment Meter (PNEM). This report provides context for the UCVS concept and the field trial, potential UCVS implementation concepts at an enrichment facility, an overview of UCVS prototype design, and field trial objectives and activities. Field trial results and interpretation are presented with a focus on the performance of PNEM and HEVA for the assay of over 200 "typical" Type 30B cylinders, and the viability of an "NDA Fingerprint" concept as a high-fidelity means to periodically verify that the contents of a given cylinder are consistent with previous scans. A modeling study, combined with field-measured instrument uncertainties, provides an assessment of the partial-defect sensitivity of HEVA and PNEM for both one-time assay and (repeated) NDA Fingerprint verification scenarios. The findings presented in this report represent a significant step forward in the community's understanding of the strengths and limitations of the PNEM and HEVA NDA methods, and the viability of the UCVS concept in front-end fuel cycle facilities. This experience will inform Phase II of the UCVS viability study, should the IAEA pursue it.

# Executive Summary

The International Atomic Energy Agency's (IAEA's) current enrichment-plant safeguards approaches include attended weighing and nondestructive assay (NDA) of a subset of the plant's cylinder flow and inventory, collection of bulk uranium hexafluoride ($UF_6$) samples for destructive analysis, and environmental sampling for subsequent laboratory analysis. New safeguards measures that are more effective and cost-efficient than contemporary measures are needed, particularly for modern high-capacity plants. Detection of prominent misuse scenarios could be improved at enrichment plants if the IAEA could monitor 100% of material flows and periodically calculate independent uranium and $^{235}U$ mass balances for the facility. However, human and financial resources preclude continuous inspector presence at the facility to measure all of the material flow, using today's attended methods. Further, the portable measurement methods currently used by inspectors have relatively low accuracy for the assay of relative $^{235}U$ enrichment, especially for natural and depleted $UF_6$, and no capability to assay the absolute mass of $^{235}U$, because of the highly localized nature of the instrument geometry and low-energy gamma-ray signature used by today's portable NDA methods. Currently, the IAEA relies primarily on data from operator weighing systems for total uranium mass, with limited independent confirmation using IAEA's portable load cells, which tend to have relatively low precision.

Unattended instruments capable of continuously monitoring material flows, and of performing the routine and repetitive measurements previously performed by inspectors, without additional burden to operators, are central to the new safeguards approaches being considered by the IAEA. One of the instrumentation concepts being considered by the IAEA is an Unattended Cylinder Verification Station (UCVS). UCVS units would be located at key intersections of cylinder movement between material balance areas, or at the operator's accountancy scales (to take advantage of the facility's cylinder weighing operations). The station would include technologies for cylinder identification, NDA of the cylinder contents, video surveillance, and data transmission to an on-site computer or inspectorate headquarters. UCVS units would be owned and operated by the IAEA, but the data streams could be shared with the operator (e.g., for process control) or other regulatory body in conformance with IAEA requirements for shared-use instruments. A notional UCVS is illustrated in Figure ES.1.

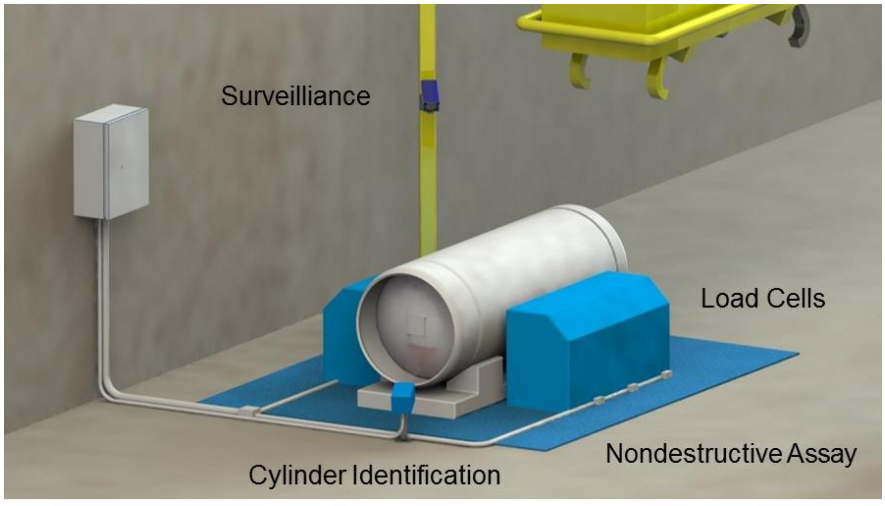


**Figure ES. 1.** Conceptual design of an integrated UCVS that includes unattended NDA instrumentation (blue panels), camera surveillance, and cylinder identification technology.

The NDA components of the UCVS would support several measurement objectives, including: unattended, independent assay of cylinder enrichment ($E_{235}$) and $^{235}$U mass ($M_{235}$) for product, feed, and tails cylinders; independent assay of total uranium mass ($M_U$) as a confidence-building measure on the authenticity of data from operator weighing systems; and the unattended application, verification, and re-verification of an "NDA Fingerprint" to maintain the verification pedigree of the cylinder contents. The NDA Fingerprint concept is not equivalent to a traditional seal, but has the potential to periodically confirm, in an unattended fashion, that the contents of the cylinder are consistent with previous scans and therefore, that diversion has not occurred. Candidate NDA Fingerprint signatures would be similar to or derived from the signatures that are used for the direct assay of $E_{235}$ and $M_{235}$ (e.g., gamma-ray peak ratios or neutron emissions).

An example of how a UCVS might be implemented in an enrichment facility is shown in Figure ES.2, for unblended Type 30B product cylinders. UCVS tracking would begin as the empty cylinder is transferred from the storage material balance area (MBA) to the process MBA (steps 1 and 2). This initial scan would verify that the cylinder is indeed empty by industry standards (i.e., some heel material often remains in an empty cylinder). After the product cylinder is filled and homogenized in the process MBA, a UCVS scan is performed during the transfer back to the storage MBA (steps 3 and 4). In this scan of the full unblended product cylinder, the UCVS would measure, independently, $E_{235}$, $M_{235}$, and $M_U$, and store these data in a way that supports automated comparison to operator declarations of those parameters. The NDA Fingerprint for each filled cylinder would also be collected and archived during this scan. Product cylinders would remain in the storage MBA until the operator is ready to ship the cylinder off-site. As the cylinder is removed from the storage MBA for shipment, the UCVS would re-verify the declared parameters and confirm the consistency of the NDA Fingerprint with previous scans. These UCVS data could be reviewed and approved by a remotely located inspector (e.g., at IAEA headquarters). This automated confirmation process could enable an expedited cylinder release process for facility operators (steps 5 and 6), when compared to today's approaches that involve routine interim inspections and on-site inspector measurements. UCVS-based verification sequences for other cylinder types—for example blended product, tails, and feed—are discussed in more detail in the body of the report.

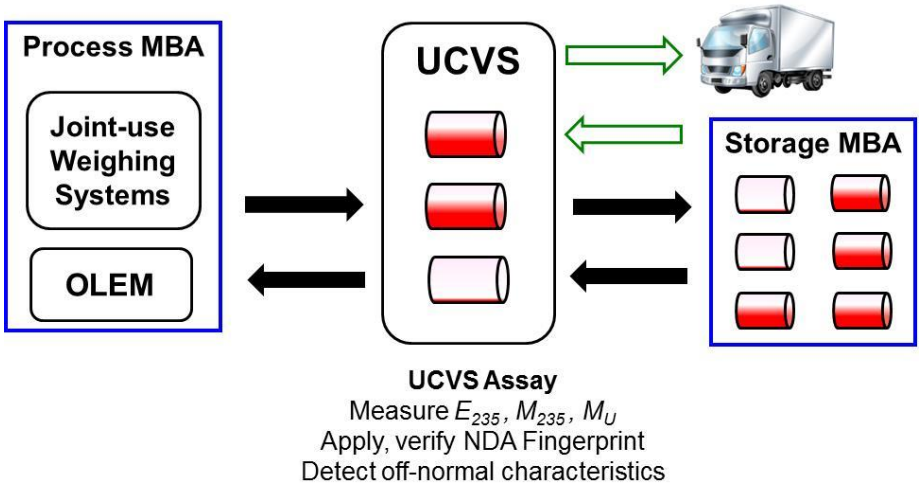


**Figure ES. 2**. Conceptual overview of how an unblended product cylinder could be verified and released from an enrichment facility using a UCVS.

If the potential of the UCVS concept can be realized, such an instrument could significantly enhance the efficiency of IAEA's safeguards approaches at large-capacity enrichment plants, while simultaneously improving effectiveness for deterring and detecting diversion of material from declared flow. A UCVS could also provide benefits to the operators, by easing and expediting the release process for product cylinders, and cylinder tracking for process control.

Though the potential of a UCVS system is understood, its field performance and operational viability in a commercial enrichment facility has yet to be fully tested. Under the auspices of the United States and European Commission Support Programs to the IAEA, a project was undertaken to assess the technical and practical viability of the UCVS concept. Phase I of that project, JNT A 1979, is described in the body of this report. Highlights are provided here, including an overview of candidate NDA methods and the UCVS prototype design, field trial objectives, cylinder populations, analysis results from two candidate NDA methods for the routine assay of "typical" cylinders, and preliminary viability findings for the NDA Fingerprint concept.

***Candidate NDA Methods***

At the inception of JNT A 1979, the IAEA identified two candidate NDA methods for UCVS, both of which were developed under support from the U.S. Department of Energy's (DOE's) Next Generation Safeguards Initiative: the Hybrid Enrichment Verification Array (HEVA) being developed by Pacific Northwest National Laboratory (PNNL), and the Passive Neutron Enrichment Meter (PNEM) being developed by Los Alamos National Laboratory (LANL).

HEVA uses an array of NaI(Tl) spectrometers with specially designed collimators to simultaneously measure the direct 186-keV signature from $^{235}$U, and via high-energy gamma rays induced by neutrons in $^{56}$Fe and the NaI(Tl) itself, the total neutron emission rate from the cylinder. The 186-keV signature provides direct measure of $E_{235}$. Under assumptions of known $^{234}$U/$^{235}$U behavior in the plant, the total neutron signal can be calibrated to total $M_{235}$ in the cylinder. In the Phase I field trial, three HEVA modules were positioned along one side of the cylinder (two-sided implementation was not viable for budget reasons), each module consisting of a 7.5-cm × 7.5-cm cylindrical NaI(Tl) spectrometer coupled to a Canberra Osprey digital photomultiplier tube base, and surrounded by a cylindrical collimator that includes iron and polyethylene layers to enhance neutron-to-gamma conversion. Nonproprietary data acquisition and analysis software was developed by PNNL.

PNEM employs polyethylene-moderated $^{3}$He neutron detectors to measure the singles and doubles neutron count rates from the cylinder. The singles counts come primarily from the $^{234}$U and under an assumption of known $^{234}$U/$^{235}$U behavior, allow determination of $^{235}$U mass, a method used by the Uranium Cylinder Assay System (UCAS) deployed by the operator at a Japanese enrichment plant. PNEM extends beyond singles neutron counting to use the coincidence (i.e., doubles) neutron signature that arises from induced fission in $^{235}$U, thereby allowing quantification of $E_{235}$. The PNEM hardware consists of two polyethylene-moderated detector pods, each containing 12 $^{3}$He tubes at a pressure of 10 atm. Data acquisition and analysis are based on pulse processing electronics from Precision Data Technology (PDT), a Canberra JSR-12 shift register, and standard IAEA software for unattended monitoring systems: Multi-Instrument Collect (MIC), Radiation Review, and the IAEA Neutron Coincidence Counting software (INCC). The PNEM detector pods are commercially available through PDT, and all software is redistributable and available for download online.

### *UCVS Field Prototype Design*

The UCVS team, in consultation with the IAEA, Euratom, and Westinghouse, developed a field prototype design consistent with field-trial objectives, the IAEA's preliminary user requirements, and the characteristics of the field-trial deployment location. A depiction of the UCVS field prototype is given in Figure ES.3. The HEVA and PNEM modules were aligned alongside and below the cylinder support, respectively; load cells were mounted under the cylinder support. Two surveillance cameras were integrated, one with a large field of view to survey the entire field trial location and the other with a field of view focused on the cylinder nameplate (to support confirmation of operator-declared data and troubleshooting). An environmental-sensor package provided temperature, humidity, and dew-point data. A push-button allowed the facility operator to indicate when the cylinder occupancy began, and the associated timer display informed the operator when the 7-minute minimum occupancy period had elapsed. A data acquisition cabinet, filled with components representative of (but not always identical to) IAEA's Unattended Monitoring Systems was located inside a utility building near the assay platform.

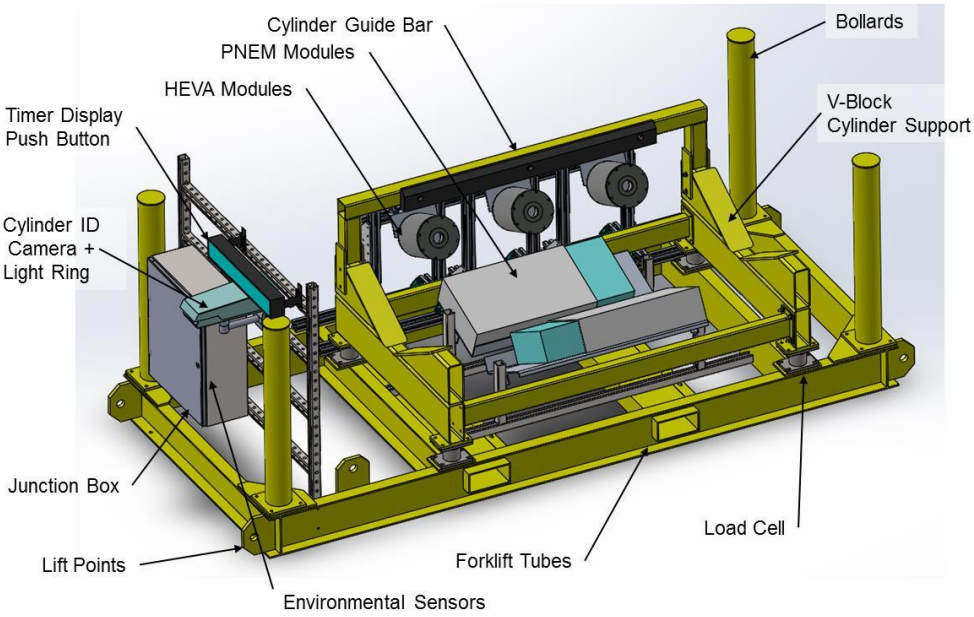


**Figure ES. 3**. Depiction of the UCVS field prototype hardware.

The UCVS software architecture was composed of individual data acquisition modules for each sensor type. Raw data files and state-of-health information were saved to the local data acquisition computer by the modules. A server hosted at PNNL retrieved the raw data daily. No real-time analysis of the raw data was performed in the Phase I study; all interpretation and analysis beyond state-of-health monitoring of the instruments was performed in post-processing. No digital signing of the data was performed but a virtual private network (VPN) tunnel was used for transmission and IAEA's Get RAINSTORM software was used for data retrieval, consistent with IAEA's current remote monitoring processes.

***Overview of Field Trial***

The original objectives of the UCVS Phase I field trial are listed here:

- Perform functional testing, in a realistic operational environment and over an extended time period, of a UCVS prototype that integrates NDA instrumentation, surveillance camera(s), and a data acquisition system representative of IAEA deployments.
- Assay many (ideally, several hundred) typical Type 30B cylinders with enrichment ranging from ~0.2 to 5.0, to support a comparative study of the PNEM and HEVA methods for the determination of $E_{235}$, $M_{235}$, and $M_U$.
- Assay a subset of the larger typical cylinder population on multiple occasions and under different handling conditions, to support study of the NDA Fingerprint concept.
- Perform high-fidelity measurements of a few select typical cylinders to support simulation benchmarking.
- Assay a small population of atypical cylinders that, due to their specific characteristics, are likely to challenge NDA methods.
- Improve understanding of how radiation backgrounds (e.g., from cylinders stored or moving nearby) are likely to affect the performance of the NDA methods and calibration protocols.
- Solicit feedback and recommendations from a facility operator about the potential process-control impacts and international safeguards roles of UCVS.

The UCVS field prototype was deployed at the Westinghouse Fuel Fabrication Facility (WFFF) in South Carolina, U.S.A. in April 2015. The prototype location, relative to the incoming and outgoing truck bays, and the operator's accountancy scale, is shown in Figure ES.4. The UCVS prototype location at WFFF is not wholly representative of envisioned IAEA deployments. First, IAEA deployments are expected to be indoors at an enrichment or fuel fabrication facility. Second, the intensities and variation of the ambient background from nearby cylinder storage and cylinder movements at WFFF are likely much higher than will be realized in permanent installations.

The typical cylinder scanning sequence began weekday mornings after the arrival of a new cylinder shipment (4 to 6 cylinders depending on the trailer used for the daily receipt). Each cylinder was lifted by crane from the transportation overpacks onto the UCVS prototype. After the occupancy period was complete, the cylinder was loaded by crane onto the accountancy scale. A fork truck removed the cylinder from the accountancy scale before processing the next cylinder on the UCVS prototype. The intended full-cylinder handling procedure was not always observed due to time or staffing constraints at WFFF, with the most significant impacts being that cylinders were sometimes left on the accountancy scale, or near the UCVS prototype, during the UCVS occupancy. For a number of occupancies, these nearby background source terms significantly perturbed the PNEM and HEVA signals. Analysis of the raw NDA signatures and camera images was used to identify and remove significantly perturbed occupancies from the cylinder populations used for the viability analysis presented in this report.

During the 8-month field trial, over 300 cylinder occupancies were recorded for Type 30B cylinders containing enrichments from natural to approximately 5 wt%. (The total number of cylinders received by Westinghouse during the trial was significantly higher, but not all incoming cylinders were placed on the

UCVS prototype due to operational time and staffing constraints.) The total number of typical occupancies (i.e., cylinder with typical characteristics and free of significant perturbations from nearby cylinders) during the field trial was 229. The population containing all of these cylinders is labeled "Typical All". It consists predominantly of cylinders produced in URENCO enrichment facilities but also contains cylinders from a conversion plant (natural enrichment) and centrifuge facilities in China and Russia. Subpopulations of the typical cylinders were also defined to support quantitative investigation of facility-specific effects on the fidelity of cylinder assay, particularly as it pertains to the $^{234}U$ /$^{235}U$ behavior and $^{234}U$-derived signatures collected by PNEM and HEVA. These subpopulations are summarized here:

- URENCO All: all URENCO cylinders, including those from Eunice (66), Capenhurst (50), Gronau (16) and Almelo (34), for a total of 166 cylinders.
- URENCO A: from URENCO's gas centrifuge enrichment plant (GCEP) facility in Eunice, New Mexico, 66 cylinders.
- URENCO B: from URENCO's GCEP facility in Capenhurst, UK, 50 cylinders.
- AREVA All: cylinders transferred through the AREVA fuel fabrication facility in the state of Washington, United States, from multiple enrichers around the world for a total of 34 cylinders.

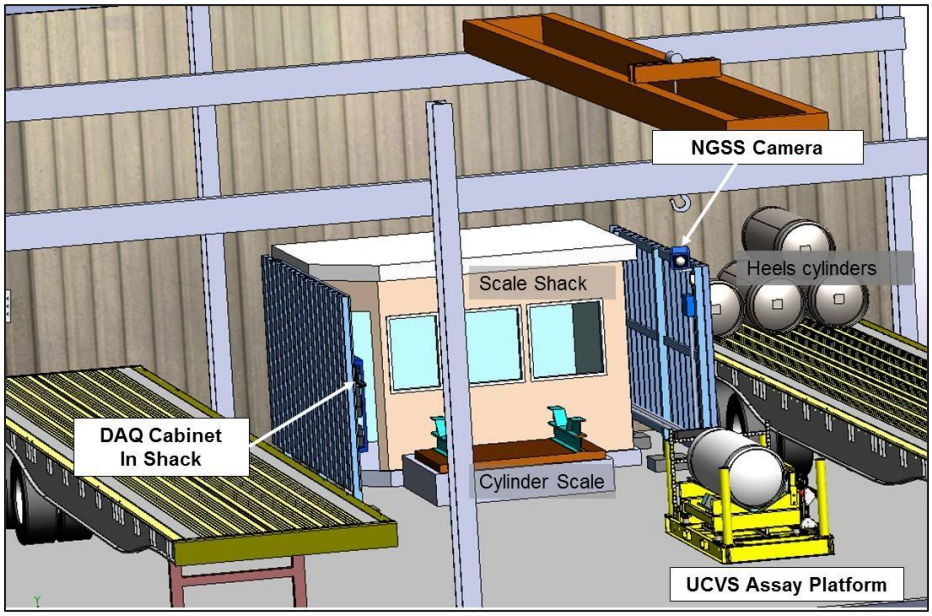


**Figure ES. 4**. Overview of UCVS prototype location at the WFFF facility. The trailer on the left typically contains incoming (full) cylinders in transportation overpacks. The trailer on the right is periodically filled with empty (but with heels) cylinders.

### *Performance Prediction for One-Time Assay of Typical Cylinders*

The radiation signatures, signature collection methods, and data analysis methods employed by HEVA and PNEM are different than the traditional enrichment-meter method (186-keV region of interest) of handheld devices used by the IAEA and Euratom. PNEM achieves direct $^{235}U$ enrichment measurement

using coincidence (i.e., doubles) neutrons induced by self-interrogation ($PNEM_D$). HEVA achieves direct $^{235}U$ enrichment measurement using large-area collection of the traditional 186-keV gamma-ray signature ($HEVA_T$). Both PNEM and HEVA indirectly determine, or *infer*, the $^{235}U$ mass measurement, over the full-cylinder volume using the total neutron emission rate, $PNEM_S$ and $HEVA_{NT}$, respectively.

In addition to these single-signature assay methods, hybrid assay methods were also assessed. Previous work has indicated that the integration of signatures with a low degree of statistical correlation in their uncertainties can provide more precise and revealing verification results than either signature independently. This hybridization, in the analysis presented in this report, is a simple averaging (i.e., equal weighting) of two signatures, and assumes that the total uranium mass is known from the UCVS load cells. In the case of HEVA, $HEVA_T$ and $HEVA_{NT}$ are hybridized to produce $HEVA_{Hybrid}$, a full-volume method for verification of relative cylinder enrichment. For PNEM, $PNEM_S$ and $PNEM_D$ are merged to form $PNEM_{Hybrid}$, also a full-volume assay of relative cylinder enrichment.

In the performance comparisons presented in this report, the primary performance metric is the precision, expressed in relative standard deviation, of the measured enrichment and $^{235}U$ mass as compared to the declared values. Field-measured uncertainties for one-time assay of typical cylinders can be compared to the IAEA's International Target Values (ITVs) for uncertainty in the assay of $UF_6$ in cylinders using handheld spectrometers. The ITVs are based on gamma-ray spectrometers using the traditional enrichment meter analysis technique, a 5-minute count time, a well-calibrated instrument with negligible systematic bias, and the use of wall-thickness corrections using ultrasonic tools. Note that field performance for handheld measurements performed by IAEA and Euratom is often better than the ITVs.

The first performance comparison to be considered in this study is for the assay of relative cylinder enrichment, $E_c$. Table ES.1 and Figure ES.5 show the relative standard deviation of the measured cylinder enrichment, $\sigma_E$, compared to operator declarations. The range of enrichments was 1.5 wt% to 4.95 wt%. Results for HEVA and PNEM for the five populations of typical Type 30B cylinders are given, for both the hybrid-signature and single-signature analysis methods.

The precision of $HEVA_{hybrid}$ and $PNEM_{hybrid}$ is consistently better than $HEVA_T$ (traditional 186-keV signature only) and $PNEM_D$ (doubles only), respectively, confirming prior studies showing the value of signature hybridization. $HEVA_{hybrid}$ performance meets or exceeds ITVs for all populations. $PNEM_{hybrid}$ performance exceeds the ITVs for facility-specific populations, but not for the large mixed-facility population. Not reported here is the performance of HEVA and PNEM for the three natural-enrichment cylinders in the Typical All population. PNEM's accuracy for those cylinders was consistent with results for higher-enrichment cylinders, but HEVA's accuracy for two of the three natural cylinders was very poor (>30% from declared) due to a combination of very weak 186-keV signal and extremely high wall-deposit source terms.

It is important to note that although the hybridization of the direct $^{235}U$ and $^{234}U$-derived signatures provides an attractive option for precision and full-volume reasons, doing so requires knowledge of the total uranium mass in the cylinder, in order to translate the assayed value for $M_{235}$ into a relative enrichment. Under the UCVS concept described earlier, this uranium mass value would be derived from the total cylinder mass provided by the UCVS load cells, and the declared tare weight for the cylinder. In this report, however, the operator's declared uranium mass value was used for this translation because the UCVS load cells were not functional for portions of the field trial. The impact of a load-cell-based total mass value on the hybrid $E_{235}$ performance needs further investigation.

**Table ES. 1**. Relative standard deviation ($\sigma_E$ , in %) of measured enrichment values, as compared to operator declarations. HEVA and PNEM results are shown for five populations (cylinder counts in parenthesis) and two analysis approaches: hybrid and single-signature. IAEA's International Target Values (ITV) for product-cylinder assay using high-resolution and medium-resolution handheld spectrometers are given in blue. Results are reported for cylinder enrichments greater than 1.5 wt%.

| | Typical All (229) | URENCO All (166) | URENCO A (66) | URENCO B (50) | AREVA All (34) |
|---|---|---|---|---|---|
| **ITV** | | **5.4 (HPGe)** | **5.8 (NaI)** | | |
| $HEVA_{hybrid}$ $E_{235}$ | 5.4 | 4.3 | 3.5 | 3.5 | 4.3 |
| $PNEM_{hybrid}$ $E_{235}$ | 10.6 | 4.9 | 1.9 | 3.4 | 5.0 |
| $HEVA_T$ $E_{235}$ (186-keV) | 5.5 | 5.3 | 5.9 | 4.4 | 5.8 |
| $PNEM_D$ $E_{235}$ (Doubles) | 14.8 | 5.7 | 2.4 | 4.9 | 7.6 |
| ITV = International Target Value | | | | | |

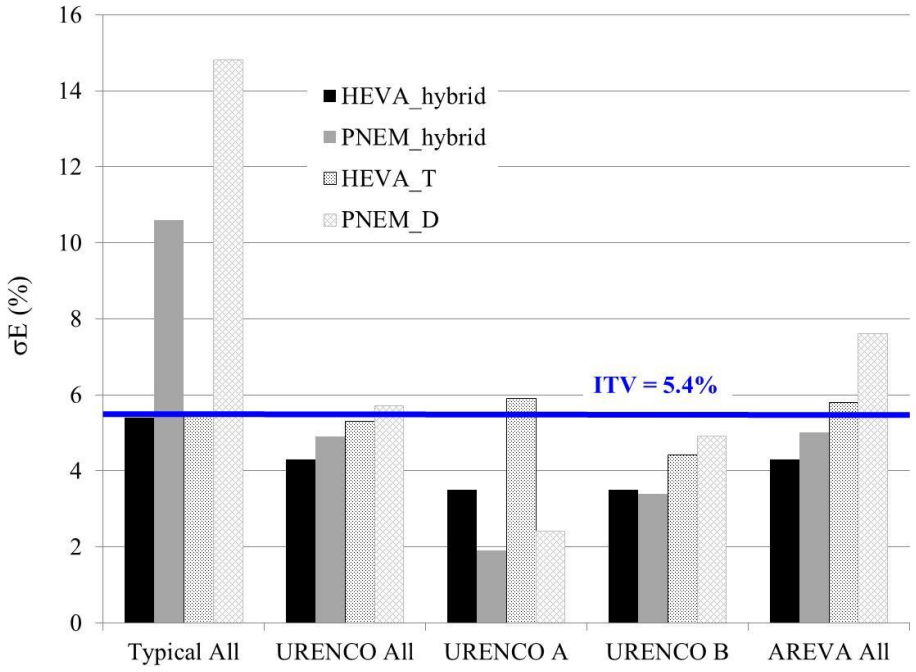


**Figure ES. 5**. Relative standard deviation ($\sigma_E$ , in %) from the operator's declared values for cylinder enrichment, for HEVA and PNEM for the cylinder populations analyzed in the field trial. The International Target Value (ITV) for high-resolution spectrometers is shown as a blue line for comparison.

A summary of the PNEM and HEVA results for the assay of $M_{235}$ is given in Table ES.2 and Figure ES.6. ITVs for $M_{235}$ are not available because the handheld devices used today measure only a small portion (<0.1%) of the $UF_6$ volume in the cylinder and are therefore not capable of assaying the absolute mass of $^{235}U$ in the cylinder. Performance for $HEVA_{NT}$ (singles neutron counting via neutron-gamma conversion) and $PNEM_S$ (singles neutron counting) is very similar over all populations. Both methods appear capable of achieving IAEA's stated UCVS target uncertainties for $^{235}U$ mass assay (i.e., $\sigma_M$ = 3.0%), assuming a facility-specific calibration, as in URENCO A and B. Degraded precision is expected for cylinder populations spanning multiple facilities, as evidenced in the Typical All, URENCO All and AREVA All.

**Table ES. 2.** Relative standard deviation ($\sigma_M$ , in %) from the operator's declared values for $^{235}$U mass. HEVA and PNEM results are shown for all four populations of Type 30B cylinders. IAEA's target values, as given in the UCVS user requirements, are given in blue.

| | Typical All (229) | URENCO All (166) | URENCO A (66) | URENCO B (50) | AREVA All (34) |
|---|---|---|---|---|---|
| **UCVS Target Values** | | | **3.0** | | |
| $HEVA_{NT}$ $M_{235}$ (Singles) | 7.6 | 5.7 | 3.0 | 2.6 | 5.4 |
| $PNEM_S$ $M_{235}$ (Singles) | 7.4 | 4.8 | 2.1 | 2.9 | 3.4 |

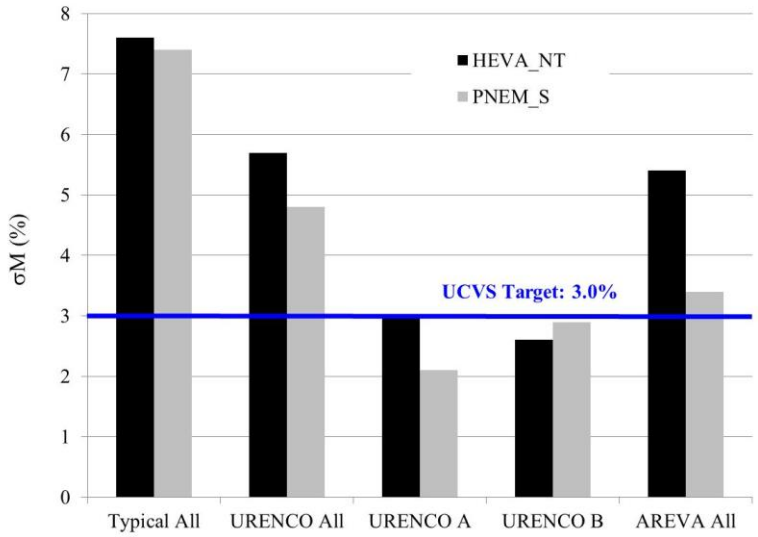


**Figure ES. 6**. Relative standard deviation ($\sigma_M$ , in %) from the operator's declared values for $^{235}$U mass, for HEVA and PNEM for the cylinder populations analyzed in the field trial. The IAEA target value for $^{235}$U mass assay is shown as a blue line for comparison.

Note that the results from Tables ES.1 and ES.2 are based on the as-measured full occupancy period for each cylinder. The occupancy period in the field trial was nominally 7 minutes but some occupancies were considerably longer (e.g., 60 minutes or more) for operational reasons. A fixed occupancy period was not enforced across all subpopulations because the automated event detection feature in the PNEM data analysis software is not configured for this type of analysis and the necessary modifications were not viable in Phase I. However, providing some indication of how the performance of PNEM and HEVA might be affected by a fixed occupancy time consistent with preliminary UCVS User Requirements (i.e., 5 minutes) was deemed important. Therefore, a comparative analysis on a special sub-population called URENCO 97 (97 cylinders from Eunice and Capenhurst), was performed using manual event definition for PNEM. The key finding from this analysis was that there was no statistically significant difference in performance for PNEM, providing empirical support for the assertion that the total uncertainties for PNEM signatures, in the as-deployed hardware configurations, are dominated by systematic, not statistical uncertainties, assuming an assay period of 5 minutes or greater. For HEVA, modest degradation (approximately 10% increase in relative standard deviations for $HEVA_{hybrid}$, $HEVA_T$, and $HEVA_{NT}$) occurred when occupancy period decreased to 5 minutes. This indicates that statistical uncertainties are not insignificant for those signatures.

***Viability of Signatures for NDA Fingerprint***

This field trial presented the first opportunity to explore the NDA Fingerprint concept using PNEM and HEVA signatures on actual cylinders. The key performance metric for the NDA Fingerprint is the total uncertainty, $\sigma_{FP}$ , over a series of repeated measurements. The uncertainty over repeated, relative measurements will have two primary components, $\sigma_{stat}$ and $\sigma_{sys\_ran}$. (The uncertainty associated with calibration of the measured signature to assay enrichment, $\sigma_{sys\_cal}$ , is not relevant for the NDA Fingerprint scenario.)

Five candidate signatures were investigated in this study: $PNEM_S$, $PNEM_D$, $HEVA_{186}$ (gross count rate in the 186-keV region of interest [ROI]), $HEVA_{1001}$ (gross count rate in 1001-keV ROI), and $HEVA_{NT}$. Several series of NDA Fingerprint occupancies were designed to address specific technical questions, for example: How sensitive are the signatures to minor and significant geometry changes between the sensors and the cylinder? How stable are the signatures for repeated occupancies with cylinder handling representative of realistic facility operations? For all of these tests, the duration of NDA Fingerprint occupancies in the UCVS field trial was nominally 7 minutes.

To explore the geometry-sensitivity questions, a carefully controlled "Geometry" cylinder scan sequence was defined that included multiple "Exact Replacements" (ER-1 to ER-5 in the figure below), and intentional changes to the cylinder-sensor geometry (shifts, flips, and rotations; S1, S2, F, and R respectively). Example results for $HEVA_{1001}$ are shown in Figure ES.7, aggregated over scan sequences performed on five cylinders with enrichments ranging from 1.5 wt% to 4.95 wt%. The green shaded box spans the Exact Replacements that were used to "calibrate" a notional alarm threshold (three-sigma). This alarm threshold can then be applied to the intentional geometry changes in the red box. Figure ES.7 shows that at least one of the three HEVA modules would have alarmed for each of the intentional geometry changes (shifts, flip, and roll), indicating that this signature has the potential to detect deliberate geometry changes beyond those expected in routine cylinder handling.

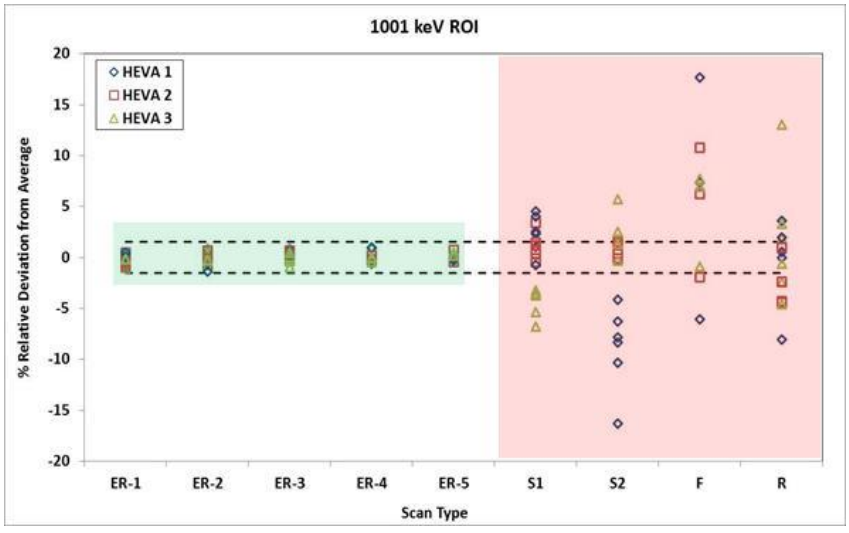


**Figure ES. 7**. Geometry-sensitivity results for candidate NDA Fingerprint signatures, aggregated over five cylinders for $HEVA_{1001}$. The green box indicates occupancies where the cylinder was consistently positioned on the platform. The red box indicates deliberate geometry changes beyond those expected in routine cylinder handling.

To assess the stability of NDA Fingerprint signatures for a more realistic scenario in which no particular care is taken with the placement of the cylinder on the platform, another series of scans on cylinders of various enrichments was performed. Example results from the $PNEM_S$ signature, for a total of 18 occupancies on four different cylinders, are shown in Figure ES.8. These results indicate that this full-volume neutron signature is highly repeatable, with a standard deviation of less than 0.2%, even for cylinders with very different enrichment levels. The stability and full-volume nature of this neutron signature offers the potential for high sensitivity to material substitution or removal scenarios, as discussed below.

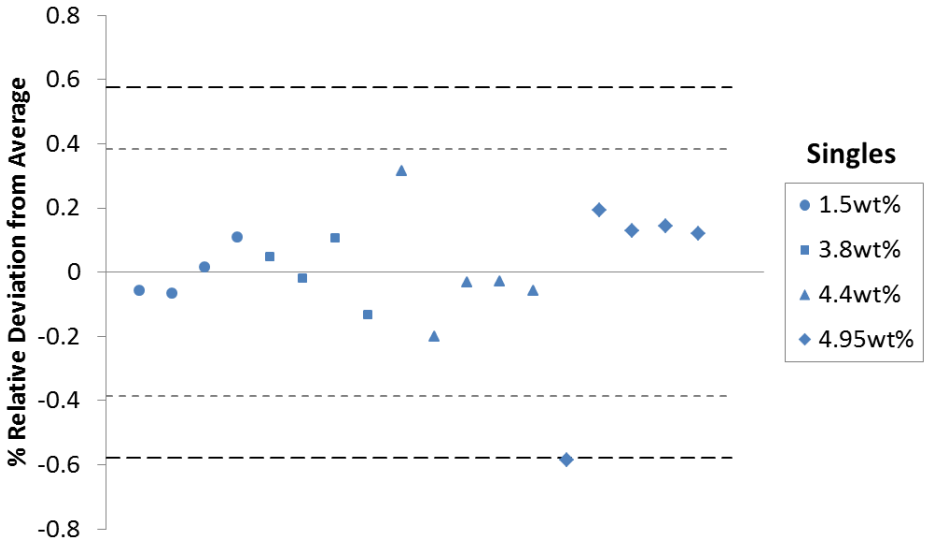


**Figure ES. 8**. Stability of the $PNEM_S$ signature for 18 occupancies aggregated over four cylinders. Two- and three-sigma thresholds are shown.

***Performance Prediction for Assay of Atypical Cylinders***

The cylinder populations analyzed in the tables and figures above include only typical cylinders processed at WFFF and therefore do not contain some of the atypical cylinder types expected to be more challenging to NDA methods, such as product produced from reprocessed feed or tails, partially-filled cylinders, or cylinders other than Type 30B. The performance of HEVA and PNEM for seven atypical cylinders is summarized in Table ES.3. These cylinders were identified as atypical for one of two reasons: 1) designated "WR" as material derived from weapons $r_{ecycl}$e in the former Soviet Union, making it likely that uranium from highly enriched uranium (HEU) downblending (not reactor returns) was used as feed material for the blending process; and 2) originating from a gaseous diffusion rather than centrifuge enrichment facility. Analysis and reporting methods were applied in a manner that seeks to take advantage of the hybrid nature of the HEVA and PNEM methods to identify potentially off-normal cylinder characteristics. If one of the two signatures (e.g., $PNEM_S$ and $PNEM_D$) is sufficiently inconsistent with the other, a flag is thrown regarding the isotopic ratio, as an indicator that the $^{234}U/^{235}U$ ratio behavior (or other characteristics such as material distribution) is not consistent with the assumed calibration and that neutron-based results are likely to be inaccurate. HEVA also reports whether $^{232}U$ is detected at elevated levels as an indicator of atypical material. For the limited atypical population analyzed in this field trial, nearly all of the HEVA and PNEM signatures yielded accurate results based on typical calibration curves. The one exception was the $PNEM_D$ signature for one of the diffusion-plant

cylinders. In that case, PNEM flagged the cylinder for off-normal $^{234}U/^{235}U$ behavior. None of the other cylinders were flagged by HEVA or PNEM. HEVA detected elevated $^{232}U$ levels in all of the cylinders designated as weapons-recycle.

**Table ES. 3**. Results for assay of atypical cylinders, expressed in relative difference ($\Delta E_{235}$, %) from declared relative enrichment. Flags generated by HEVA and PNEM based on indications of a $^{234}U/^{235}U$ ratio outside the calibrated range or the presence of $^{232}U$ (HEVA only) are also shown.

| Cylinder Description | $E_{235}$ (wt%) | HEVA | | | PNEM | |
|---|---|---|---|---|---|---|
| | | $\Delta E_{235}$ (%) | $^{232}U$ observed? | Inconsistent Iso Ratio? | $\Delta E_{235}$ (%) | Inconsistent Iso Ratio? |
| Weapons recycle | 3.23 | 4.8 | X | | 0.47 | |
| Weapons recycle | 3.20 | 6.2 | X | | -2.23 | |
| Weapons recycle | 3.20 | 2.2 | X | | -2.27 | |
| Weapons recycle | 3.20 | 2.8 | X | | -5.50 | |
| Weapons recycle | 3.20 | 3.7 | X | | -3.21 | |
| Diffusion plant | 4.95 | -1.2 | | | 15.36 | X |
| Diffusion plant | 4.95 | -1.1 | | | 0.16 | |

***Modeling-Based Evaluation of Partial-Defect Sensitivity***

Using Monte Carlo N-particle (MCNP) modeling of the neutron-based signatures collected by HEVA and PNEM, partial-defect diversion scenarios were investigated. The two scenarios evaluated here assume that a variable mass of the declared low-enriched $UF_6$ is substituted with either depleted $UF_6$ ($DUF_6$) or with highly enriched $UF_6$ ($HEUF_6$). Figure ES.9 illustrates how the distance, L, is varied to determine the substituted mass of material.

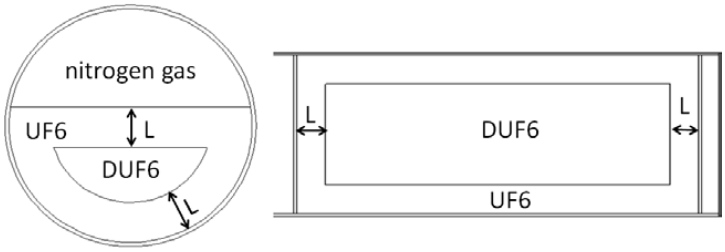


**Figure ES. 9**. Schematic of diversion scenario in which declared $UF_6$ in the center of the cylinder is substituted, in this case with depleted $UF_6$.

In the analysis of detection sensitivity, the magnitudes (i.e., count rates) of the $PNEM_S$ and $HEVA_{NT}$ signatures were based on simulated values, benchmarked to a 4.0 wt% cylinder in the WFFF field trial. The field-measured uncertainties for the assay of $^{235}U$ mass in typical cylinders using facility-specific calibrations (i.e., average of URENCO A and B results), and repeated assay using neutron-based NDA Fingerprint signatures were assumed: $PNEM_S$: $\sigma_{typical}$ = 2.5%, $\sigma_{FP}$ = 0.08%; $HEVA_{NT}$: $\sigma_{typical}$ = 2.8%, $\sigma_{FP}$ = 0.72%. These uncertainties were used to define alarm thresholds corresponding to a false alarm rate of 1%. A 5-minute cylinder occupancy duration was assumed. Example results from the partial-defect study are summarized in Figure ES.10 for the $DUF_6$ substitution scenario.

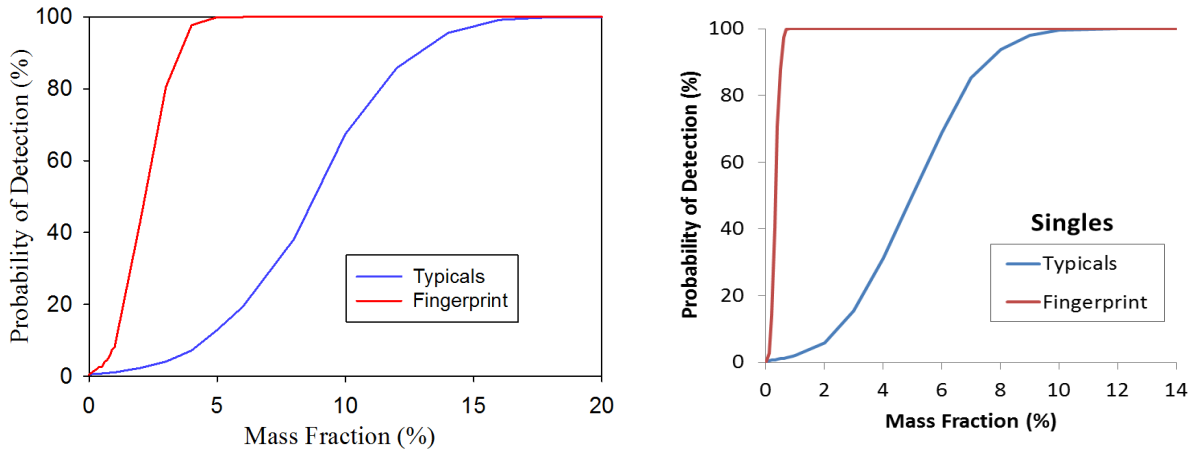


**Figure ES. 10**. Probability of detection versus $DUF_6$ material substitution fraction for $HEVA_{NT}$ (left) and $PNEM_S$ (right). Field-measured uncertainties for one-time assay (Typicals) and repeated assay (Fingerprint) of a Type 30B cylinder at 4 wt% were assumed.

These results indicate that, for one-time, typical cylinder assay, $PNEM_S$ and $HEVA_{NT}$ signatures are capable of detecting $DUF_6$ material substitution fractions of ~8% and ~13%, respectively, when assuming a probability of detection greater than 90% and false alarm rate less than 1%. Not shown graphically are the results for $HEUF_6$ substitution where detection sensitivity is approximately 30 times better, owing to the much higher neutron emission rate from $HEUF_6$. For repeated cylinder assays using the NDA Fingerprint concept, sensitivities for both depleted and highly enriched material are substantially better, particularly for $PNEM_S$, due to the lower uncertainties associated with repeated measurements.

### *Conclusions*

The key findings from the UCVS Phase I study are summarized below.

*Assay of $E_{235}$ Using Hybrid Signatures.* HEVA performance, hybridizing the 186-keV and singles neutron signatures, was better than the ITVs for all populations, including the mixed-facility populations. In comparison to PNEM, HEVA precision was more consistent across the various populations. PNEM performance, based on a hybridization of the singles and doubles signatures, surpassed the ITVs for all but the largest population, which included multiple enrichers. The precision of PNEM-produced $E_{235}$ values varied considerably from population to population. *Both* methods have the potential to provide assay precision comparable to or better than target values for handheld devices, without the need for tedious and laborious wall-thickness corrections. The fact that the hybrid $E_{235}$ approach provides a full-volume assay of cylinder enrichment is notable because today's handheld methods assay less than 1% of the cylinder volume.

*Assay of $M_{235}$ Using Indirect Signatures.* PNEM and HEVA precision for $^{235}U$ mass assay was comparable over all populations, consistent with the fact that both are collecting essentially the same signature (i.e., singles neutrons) and systematic (not statistical) uncertainties dominate. Both methods offer the potential for full-volume assay and therefore, the quantification of $^{235}U$ mass. Under assumptions of a facility-specific calibration for $^{234}U/^{235}U$ behavior, PNEM and HEVA are capable of meeting IAEA's preliminary targets for uncertainty on $^{235}U$ mass quantification (i.e., 3.0%). This would represent a new

capability to safeguards inspectorates and support a significant improvement in the ability to detect material substitution and removal scenarios.

*Viability of NDA Fingerprint for Full-volume Constancy of $UF_6$.* The most promising signatures for verifying the constancy of the $UF_6$ material itself are the two neutron-based signatures: $PNEM_S$ and $HEVA_{NT}$. Both appear capable of highly repeatable ($\sigma_{FP} < 1.0\%$ for product cylinders), full-volume interrogation of the $UF_6$ in the occupancy times considered in this study. PNEM's higher collection efficiency and therefore higher statistical precision, offers the promise of better repeatability. The distribution of HEVA's discrete modules along the length of the cylinder provides more sensitivity to geometry changes than does the current PNEM design.

*Viability of NDA Fingerprint for Cylinder Distinctiveness.* Gamma-ray signatures that can provide insight to the age of the $UF_6$ and the characteristics of the wall deposits at different locations are the most promising signatures for verifying the distinctiveness of a particular cylinder. Of the candidate signatures considered in this study, $HEVA_{186}$ and $HEVA_{1001}$ appear to hold the most potential for this role because they can provide highly repeatable ($\sigma_{FP} < 1.0\%$) confirmation of photon emissions (e.g., the bremsstrahlung and gamma rays from $^{234m}Pa$) from the $UF_6$ itself and wall deposits at multiple locations along the cylinder. Unfortunately, data to quantitatively evaluate this potential were quite limited in the Phase I field trial for two reasons: 1) cylinders assayed at a fuel fabrication plant contain relatively "old" $UF_6$ (i.e., key daughters like $^{234m}Pa$ are already in equilibrium), and 2) efforts to collect data on multiple occupancies of specific-product cylinders separated in time by days and weeks were unsuccessful, in part because the facility operator typically processed incoming cylinders soon after the initial scan.

*Assay of Atypical Cylinders.* The limited set of atypical cylinders from this field trial does not support significant new understanding about the robustness of PNEM and HEVA to off-normal conditions, but the analysis presented here does confirm the need to flag cylinders with a $^{234}U/^{235}U$ ratio outside of the calibration range and ideally, to still report credible values for cylinder enrichment. Prior work has indicated that HEVA offers more robustness for atypical $^{234}U$ conditions because its direct enrichment signature is the 186-keV signature emitted by $^{235}U$. Because the two neutron signatures used in the PNEM method are correlated through the self-interrogation process, off-normal $^{234}U$ concentrations are more problematic. In addition, HEVA is able to detect the presence of $^{232}U$, thereby providing additional evidence about the nature and origin of the $UF_6$ in that cylinder.

*Defect Sensitivity.* Based on measured uncertainties and MCNP modeling of material substitution scenarios, it was demonstrated that the full-volume PNEM and HEVA neutron signatures can provide an unprecedented level of defect sensitivity for IAEA's cylinder verification. For one-time assay of a cylinder, PNEM and HEVA defect sensitivities are:~8% and ~13%, respectively, for depleted uranium (DU) and ~0.5% for HEU substitution scenarios. For repeated cylinder scans using the NDA Fingerprint concept, bias-defect sensitivity, at DU substitution levels less than ~0.5% appears to be achievable using PNEM owing to its more-precise collection of the singles neutron signature and a higher spatial sensitivity to substitution volumes located in the middle of the cylinder.

*Prototype Functionality and Robustness.* The UCVS prototype operated in continuous unattended fashion for over eight months in an outdoor environment. There were no failures of the hardware or data acquisition software modules for PNEM and HEVA. There were, however, failures in the load cells and remote monitoring hardware (i.e., cellular modem and VPN components), and in the supervisory service

running the HEVA data acquisition module. The latter led to the only NDA-related data loss in the trial (i.e., HEVA data for 14 cylinders were corrupted). A preliminary analysis of long-term stability of HEVA and PNEM signatures over approximately 8 months of operation did not reveal any significant instrument drift issues.

*Analysis Software.* The analysis software used for PNEM is available as compiled code for non-expert users, mature (currently in use by the IAEA), and straightforward to implement. No significant challenges were encountered during the Phase I analysis. The HEVA analysis software is written in Python for expert users and still developmental in terms of maturity. The HEVA software is nonproprietary and produces/uses standard input/output file formats (e.g., N42.42) consistent with IAEA's remotely monitored instruments.

*Complementarity of PNEM and HEVA Signatures.* The findings from this field trial confirm a hypothesis that the U.S. Support Program (USSP) team has considered for some time, namely that merging of the best features of PNEM and HEVA offers the potential for performance superior to either acting independently. See below for more discussion.

### *Merging PNEM and HEVA: The Best of Both Methods*

The PNEM and HEVA results presented in this report indicate that both are highly capable NDA methods—either of which could substantially improve on today's handheld methods in terms of assay precision, full-volume interrogation, and defect sensitivity. That said, the UCVS team believes that a new NDA method, one that incorporates the most promising signatures and features from PNEM and HEVA, should be considered. This merged NDA method, here labeled Neutron-Gamma Enrichment Verification (NGEV), would be based on $PNEM_S$ and $HEVA_T$. Supporting logic for NGEV is given here.

- For the full-volume determination of $^{235}U$ mass, $PNEM_S$ can be expected to provide a higher degree of statistical precision and long-term stability than $HEVA_{NT}$. This is particularly true at enrichments below 1.5 wt%, a category of cylinders not included in the Phase I study.
- For determination of relative cylinder enrichment, $HEVA_T$ provides a direct, unambiguous measure of $^{235}U$ concentration that is not dependent on the $U^{234}/U^{235}$ behavior. $HEVA_T$ interrogates only a limited material volume, but assuming the use of $PNEM_S$ in a merged NDA method, full-volume assay is still achieved for the hybrid calculation of $E_{235}$. Inclusion of gamma-ray spectrometry also allows detection of $^{232}U$ as a clear indicator of non-natural feed material.
- For the NDA Fingerprint, $PNEM_S$ is the most precise and stable candidate signature for the verification of $UF_6$ constancy, but in the current hardware configuration it provides limited information about the spatial distribution of the material. The gamma-ray signatures exemplified in $HEVA_{186}$ and $HEVA_{1001}$ are attractive in terms of cylinder distinctiveness, because they provide information about material age, wall-deposit magnitude and spatial variation.
- The $HEVA_T$ spectrometer can be improved and streamlined in NGEV. The use of NaI(Tl) for all HEVA systems to date has been driven by the fact that iodine provides a significant fraction of the $HEVA_{NT}$ signature. If $^3He$ tubes are used to collect the total neutron signature in NGEV, the preferred gamma spectrometer for $HEVA_T$ would be $LaBr_3$. It is expected that the higher resolution of $LaBr_3$ coupled to advanced algorithms to better discriminate against continua produced by wall deposits will

enable more precise determination of enrichment, particularly for natural and depleted enrichments. A more compact collimator design is also possible, since there is no need for the iron/poly layers to serve as neutron-gamma converters.

- The PNEM hardware design can be modified to be more cost-effective and capable for the singles neutron signature. If the doubles signature is not used in an integrated NDA method, the amount of $^{3}$He gas can be significantly reduced through fewer or lower-pressure tubes without significant impact on the statistical uncertainties. Reducing the amount of $^{3}$He used would also lower the cost of the detectors. An array design that provides more uniform efficiency over the length of the cylinder and more spatial sensitivity for NDA Fingerprint measurements should also be considered.

Figure ES.11 shows a notional illustration of NGEV, as it might be implemented in the UCVS prototype. It includes two $^{3}$He pods with multiple tubes (4 atm, 100-cm long) but fewer than in the current PNEM pod design. The two NGEV neutron pods are flanked by four $LaBr_3$ spectrometers, each in a "side-looking" configuration. The streamlined configuration of these integrated neutron-gamma modules should allow deployment flexibility and extensible modularity to Type 48 cylinders (e.g., four panels instead of two). Preliminary statistical analysis that quantitatively supports the complementarity of $PNEM_S$ and $HEVA_T$ is provided in this report.

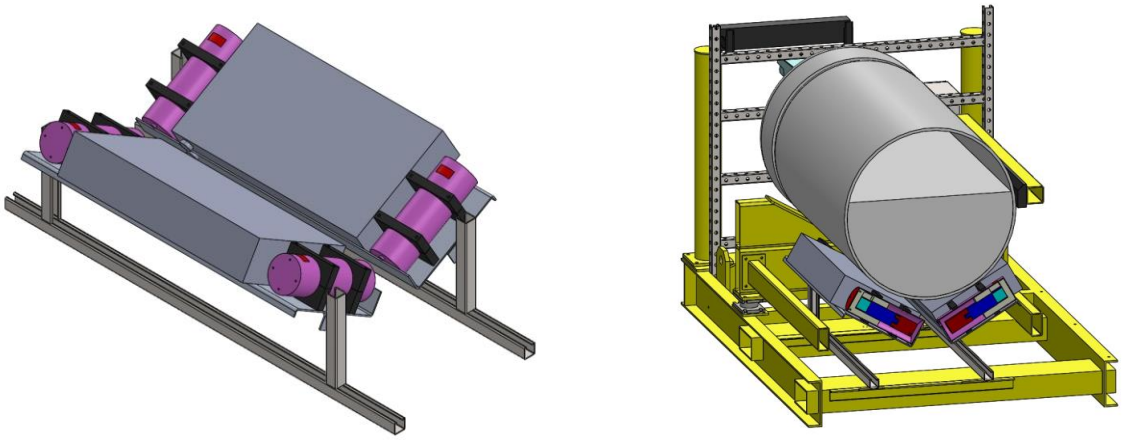

**Figure ES. 11**. Notional illustration of an NDA method that merges the strengths of PNEM and HEVA to create a new method called Neutron-Gamma Enrichment Verification (NGEV). Left: $^{3}$He modules flanked by "side-looking" collimated $LaBr_3$ spectrometers, with NGEV panels in a clamshell configuration. Right: Depiction of the UCVS prototype platform with NGEV modules.

***Preliminary UCVS Cost Estimates***

Preliminary cost estimates were tallied for a UCVS unit under the following assumptions.

- Costs were calculated for a second UCVS prototype, with a design identical to the first unit developed in Phase I, standalone assay platform design for outdoor use. As a second unit, original design costs are not included. The cost of other mechanical designs for the assay platform (e.g., one integrated with a particular accountancy scale or for purely indoor use) may be somewhat different.
- The standard data acquisition cabinet and internal components used by IAEA and the area surveillance camera are not included. This choice is based on the logic that the cabinet cost in a GCEP would likely be shared across multiple instruments, and a surveillance camera dedicated to UCVS may not be required. The cylinder nameplate camera is included in the cost estimate.
- All software and analysis modules are complete and functional—no further development costs are needed.
- Labor costs for fabrication and integration assume nominal DOE laboratory rates. Estimated IAEA costs for the procurement of $^{3}$He are assumed.

Table ES.4 summarizes estimated costs for several UCVS variants: assay platform without NDA, HEVA only, PNEM only, and notional NGEV. Based on these numbers, the UCVS cost is dominated by the assay platform. For the NDA options, the as-deployed PNEM has the highest estimated cost, HEVA the lowest. Because the aggregated UCVS cost is dominated by the platform, the total cost for UCVS variants based on the most- and least-expensive NDA options differ by approximately 30%.

**Table ES. 4**. Cost estimates for the UCVS assay platform and three NDA options.

| | **$K** |
|---|---|
| Assay platform mechanical and electrical components | 12 |
| Load cells and data acquisition module | 15 |
| Cylinder nameplate camera | 5 |
| Operator Interface components | 2 |
| Fabrication and integration (labor) | 173 |
| **Assay Platform Total** | **207** |
| PNEM pods (2) and data acquisition (JSR-12) | **109** |
| HEVA modules (3) and data acquisition (Ospreys) | **29** |
| NGEV neutron pods (2) and gamma modules (4) | **60** |

***Caveats and Recommendations for Continuing Work***

The following caveats on the Phase I findings need to be considered, and can inform potential future work on the UCVS concept.

- *Limitations on material enrichments.* The majority of cylinders in the trial were in a few enrichment bands (e.g., 2.6, 4.0, 4.4, and 4.95 wt%). The facility-specific cylinder populations were relatively small and often had few or no cylinders at enrichments below 1.5%. The effect of these relatively small populations on calibrations and predicted performance is expected to be small but not negligible.
- *Limitations on cylinder type.* Only Type 30Bs were included in the typical populations; performance for Type 48 cylinders with natural and depleted material needs study.
- *Calibration and reporting methods.* All cylinders in a population were used for calibration and reporting of the precision. Blind populations were not used. Future analyses should implement calibration and blind-cylinder approaches similar to those likely to be used by the IAEA in field deployments.
- *Inconsistent cylinder position on assay platform.* The assay platform design did not include indicators or controls to ensure consistent placement of the cylinder. As the NDA Fingerprint studies indicated, even relatively small lateral shifts can produce non-negligible count-rate changes in the NDA instrumentation. Inconsistent lateral position negatively affected the NDA Fingerprint viability study, and likely the reported uncertainties for one-time cylinder assay. Future prototypes should include lateral position controls.
- *Lack of $^{234}U/^{235}U$ calibration data.* No data were available to provide a defensible functional form for "total neutron" calibration. PNEM analysis assumed a quadratic relationship between total neutrons and $^{235}U$ mass; HEVA analysis assumed an exponential relationship. A study of $^{234}U/^{235}U$ behavior across a range of parameters in commercial enrichment facilities is needed, and is under way, funded by DOE.
- *Unknown effect of $UF_6$ distribution and effective density.* Results from the modeling study regarding the impact of $UF_6$ distribution on neutron signatures, and preliminary comparisons of calibration curves for sub-populations analyzed in Phase I, indicate that more study is needed on how facility-specific production processes and cylinder-handling practices affect calibration functions, and measurement precision.
- *Limited NDA Fingerprint data.* While this field trial provided the first data in support of an NDA Fingerprint viability study, the data were significantly short of the original plans, and a number of questions remain, particularly with regards to the viability of gamma-based signatures to reveal and subsequently verify the distinctiveness of each cylinder. Larger datasets and further study are needed.
- *Off-line analysis:* The results presented in this report were based on off-line analysis performed at PNNL and LANL. More software development and field measurements are needed to demonstrate fully unattended operation (e.g., automated occupancy detection), analysis, and reporting. The new iRAP software developed by Euratom and IAEA for unattended monitoring was not ready for deployment in Phase I but could be considered in a follow-on phase.

# Acknowledgments

Funding for this work has been provided by the U.S. National Nuclear Security Administration's (NNSA) Office of Nonproliferation and Arms Control International Nuclear Safeguards (NA-241) program, and the U.S. Support Program (USSP) to the IAEA. The authors are appreciative to Kevin Veal, Karyn Durbin, and Anthony Belian of the NNSA, and Joseph Carbonaro of the USSP for their support and guidance of this project.

The authors would also like to thank James Ely of the IAEA for his oversight of the UCVS development. We are appreciative of Euratom's Peter Schwalbach for his early advocacy and ongoing support from the European Commission perspective, and to Jim Morrissey of Euratom for sharing the inspector's perspective on the potential and challenges associated with the UCVS concept.

The UCVS team is indebted to Westinghouse and the staff at the Westinghouse Fuel Fabrication Facility for supporting this measurement campaign, from the early planning stages through the final reporting. The opportunity to deploy an integrated prototype and test candidate cylinder assay methods in an operational environment has been invaluable to the project and team members. In particular, we would like to thank Frank Clark, Morgan Goff, and Rodney Likes for their day-to-day support of the project, and Wayne Sepitko for management support.

The authors express their appreciation to Chris Orton of Pacific Northwest National Laboratory (PNNL) for his facilitation and coordination of UCVS Phase I activities during his assignment at NA-241, and after his return to PNNL. We are also appreciative to Rick Poland of Savannah River National Laboratory for his coordination efforts with Westinghouse in the planning and preparatory stages of the field trial.

We would also like to recognize the technical contributions of PNNL's Emily Mace (nondestructive assay methods), Erin Fuller (mechanical design), Paul Bruillard (statistical analysis methods) and Bryan Gerber (remote monitoring and data storage); Oak Ridge National Laboratory's Jose March-Leuba (HEVA data viewer software); and Los Alamos National Laboratory's Paul Polk (PNEM environmental enclosures) and Matt Newell and Deeanne Ortiz (PNEM electrical drawings and cables).

# Acronyms and Abbreviations

| | |
|---|---|
| API | application program interface |
| CoK | continuity of knowledge |
| COTS | commercial-off-the-shelf |
| DAQ | data acquisition |
| DOE | U.S. Department of Energy |
| DU | depleted uranium |
| DUF | depleted uranium hexafluoride |
| Euratom | European Atomic Energy Community |
| Euratom safeguards | Directorate Nuclear Safeguards of the Directorate General for Energy of the European Commission |
| GCEP | gas centrifuge enrichment plant |
| HEU | highly enriched uranium |
| $HEUF_6$ | highly enriched uranium hexafluoride |
| HEVA | Hybrid Enrichment Verification Array |
| HPGe | high-purity germanium |
| IAEA | International Atomic Energy Agency |
| ID | identification |
| INCC | IAEA Neutron Coincidence Counting |
| IP | Internet Protocol |
| IR | infrared |
| ITV | International Target Value |
| LANL | Los Alamos National Laboratory |
| LDAQ | Loadcell Data Acquisition |
| LEU | low enriched uranium |
| MBA | material balance area |
| MCNP | Monte Carlo N-Particle |
| MDAQ | Modbus TCP Data Acquisition |
| MIC | Multi-Instrument Collect |
| MUF | material unaccounted for |
| NDA | nondestructive assay |
| NGEV | Neutron-Gamma Enrichment Verification |
| NGSI | Next Generation Safeguards Initiative |
| NGSS | Next Generation Surveillance System |
| NNSA | National Nuclear Security Administration |
| OLEM | online enrichment monitor |

| | |
|---|---|
| ORNL | Oak Ridge National Laboratory |
| PD | probability of detection |
| PDT | Precision Data Technology |
| PNEM | Passive Neutron Enrichment Meter |
| PNNL | Pacific Northwest National Laboratory |
| POE | power over Ethernet |
| ROI | region of interest |
| RSD | relative standard deviation |
| SOH | state of health |
| SRNL | Savannah River National Laboratory |
| SWC | square wave convolute |
| TCP | Transmission Control Protocol |
| UCAS | Uranium Cylinder Assay System |
| UCVS | Unattended Cylinder Verification Station |
| $UF_6$ | uranium hexafluoride |
| USSP | U.S. Support Program |
| VPN | virtual private network |
| WFFF | Westinghouse Fuel Fabrication Facility |
| WR | weapons recycle |

# Contents

# Figures

# Tables

# 1.0 Introduction

In recent years, the International Atomic Energy Agency (IAEA) has pursued innovative techniques and an integrated suite of safeguards measures to address the verification challenges posed by advanced centrifuge technologies and the growth in separative work unit capacity at modern centrifuge enrichment plants (Cooley 2007; Lebrun et al. 2009). These measures would include permanently installed, unattended instruments capable of performing the routine and repetitive measurements previously performed by inspectors. Among the unattended instruments currently being explored by the IAEA is an Unattended Cylinder Verification Station (UCVS) that could provide independent verification of the declared relative enrichment, $^{235}$U mass, and total uranium mass of 100% of the declared cylinders in the plant, as well as the application and verification of a "nondestructive assay fingerprint" (NDA Fingerprint) to preserve verification knowledge on the contents of each cylinder throughout its life in the facility (Smith et al. 2013).

UCVS units would be located at key intersections of cylinder movement between material balance areas (MBAs), or at the operator's accountancy scales to take advantage of the facility's cylinder weighing operations. The station would include technologies for cylinder identification, NDA of the cylinder contents, video surveillance, and data transmission to an on-site computer or to inspectorate headquarters. UCVS units would be owned and operated by the IAEA, but the data streams could be shared with the operator (e.g., for process control) in conformance with IAEA requirements for shared-use instruments (IAEA 2013a). A notional UCVS is illustrated in Figure 1.

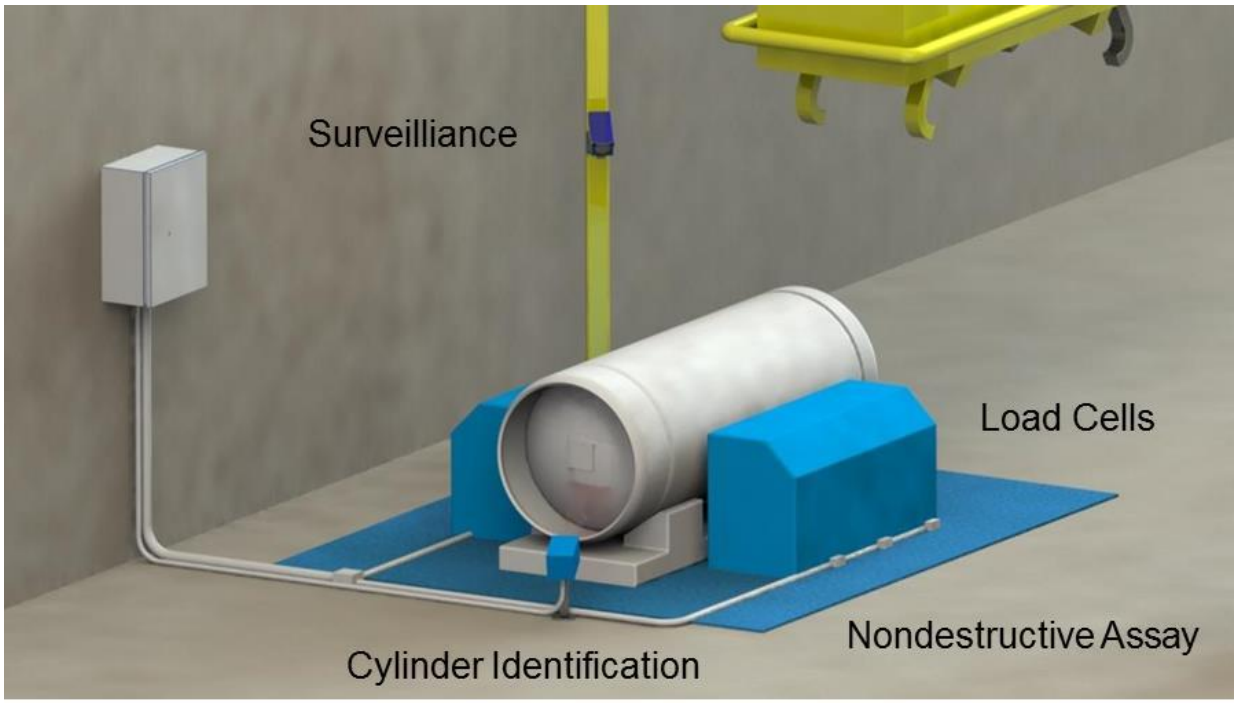


**Figure 1**. Conceptual design of an integrated UCVS that includes unattended NDA instrumentation (blue panels), camera surveillance, and cylinder identification technology.

According to the IAEA, the NDA components of the UCVS will support several measurement objectives, including unattended, independent assay of cylinder enrichment ($E_{235}$) and $^{235}$U mass ($M_{235}$) for product, feed, and tails cylinders; independent assay of total uranium mass ($M_U$) as a confidence-building measure on the authenticity of data from operator weighing systems; and the unattended application, verification, and re-verification of an NDA Fingerprint to maintain the verification pedigree of the cylinder contents and to verify that no partial removal of material has occurred during the cylinder's life at the facility, or during transfer between facilities (IAEA 2013a).

If the potential of the UCVS concept can be realized, such an instrument could significantly enhance the IAEA's efficiency and effectiveness at enrichment plants, and the UCVS might also be considered for use at fuel fabrication plants and uranium conversion facilities. A UCVS could also provide benefits to the operators, by easing and expediting the release process for product cylinders, and cylinder tracking for process control.

Under the auspices of the United States and European Commission Support Programs to the IAEA, a project was undertaken to assess the technical and practical viability of the UCVS concept. Phase I of the UCVS project began in May 2014 and as described in the timeline below, the Phase I field trial and supporting analysis was completed in April 2016 (Figure 2).

This report is the final deliverable for Phase I. It begins with context for the UCVS concept and the field trial, potential UCVS implementation concepts at an enrichment facility, an overview of UCVS prototype design, and field trial objectives and activities. Field trial results and interpretation are then presented, with a focus on the performance of the Passive Neutron Enrichment Meter (PNEM) and the Hybrid Enrichment Verification Array (HEVA) for the assay of over 200 typical Type 30B cylinders, and the viability of an NDA Fingerprint concept as a high-fidelity means to periodically verify that the contents of a given cylinder are consistent with previous scans. A modeling study, coupled to field-measured uncertainties, provides quantitative data about the partial-defect sensitivity of HEVA and PNEM for both the one-time assay and (repeated) NDA Fingerprint verification scenarios. Recommendations for continuing work on the UCVS concept and implementation options are also provided, and are intended to inform Phase II of the UCVS viability study, should the IAEA pursue it.

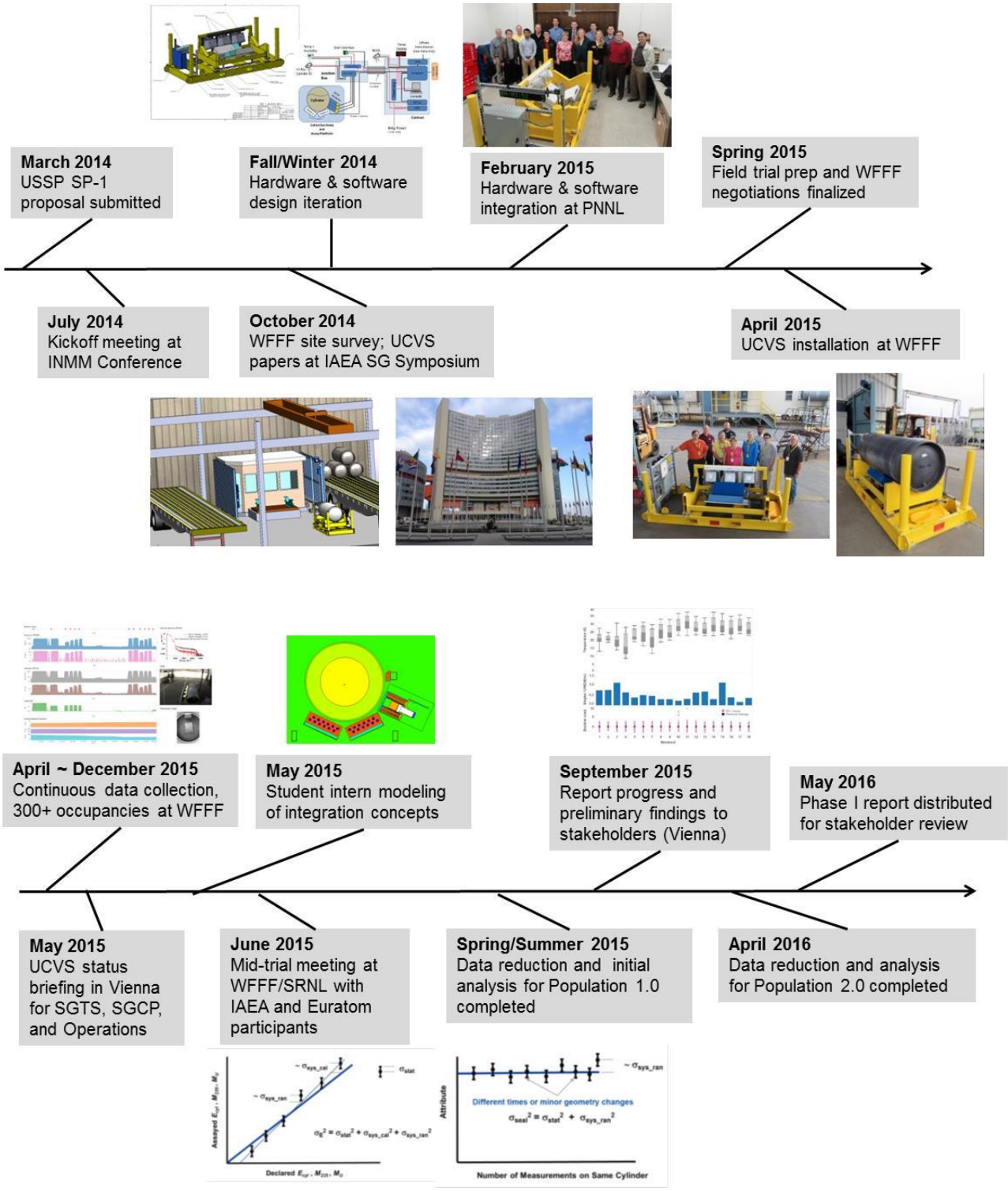


**Figure 2**. UCVS Phase I timeline from proposal to distributions of the Phase I report (this document).

# 2.0 JNT A 1979: Motivation and Objectives

At the inception of UCVS Phase I (JNT A 1979), several objectives were defined by the IAEA:

- Engineering of a UCVS prototype with sufficient hardware and software flexibility to support the initial field evaluation of an instrument operating in unattended mode
- Field testing of the prototype in representative operational conditions, estimate of anticipated life cycle cost, and documentation of implementation considerations
- Quantitative comparison of two candidate NDA methods for the independent measurement of cylinder enrichment and $^{235}U$ mass, and for the collection and verification of an NDA Fingerprint for each cylinder.

The IAEA indicated that the Phase I study would be used in several ways, as described in the UCVS Phase I SP-1 (Support Program task) description. The text below is largely excerpted from the SP-1 description (IAEA 2013b).

***Objective technical and operational review of candidate unattended cylinder NDA methods***

At project inception, it was not clear which candidate NDA method, HEVA or PNEM, was best suited for the UCVS. Technical questions (e.g., total measurement uncertainty and data analysis methodology), implementation questions (e.g., measurement times, physical size, and long-term stability), and life cycle cost questions (e.g., reliability and maintainability) remain. A comprehensive, objective review of HEVA and PNEM based on extended concurrent field testing and in the context of UCVS user requirements was needed to support an IAEA decision about which NDA method (or perhaps combination of methods) should be pursued in a Phase II field prototype and for a possible future production version.

***Evaluation of an integrated field prototype to inform IAEA on UCVS implementation viability***

Though the potential of a UCVS system is understood, its field performance and practical viability to operate in a commercial enrichment facility has yet to be tested. The achievable measurement uncertainties and partial defect sensitivities for various cylinder types, and resistance to spoofing scenarios are among the questions related to the NDA systems. These questions are best addressed with a combination of cylinder measurements and Monte Carlo modeling. The ability of surveillance to help deter and detect tampering (e.g., with the load cells during a UCVS measurement) needs field study. The degree to which emerging IAEA software packages can be used in a UCVS is also of interest.

***Inform the development of new safeguards measures for high-capacity enrichment plants***

The IAEA's intention to simultaneously improve the effectiveness and efficiency of safeguards approaches at enrichment plants, particularly at modern high-capacity centrifuge plants, has been well documented in recent years. The UCVS has the potential to be a key enabling technology in that toolbox, and this project will provide the findings, quantitative data, and recommendations needed by the IAEA to either continue or cease pursuit of the UCVS and related technology development activities. In addition to addressing questions about the viability of the UCVS instrument itself, it is important that the IAEA consider the value of integrating the data streams from the UCVS into a near-real-time analysis of total uranium and $^{235}U$ material balances in the facility. Such calculations could draw, for example, on data from UCVS, On-Line Enrichment Monitors (OLEM) and shared operator weighing systems.

# 3.0 UCVS Collaboration

UCVS Phase I was a joint task accepted by both the US Support Program (USSP) and the European Commission Support Programme (ECSP) to the IAEA. Together, the two support programs provided the diverse array of experience, expertise, and skill sets needed to successfully complete the project, including:

- Familiarity with the IAEA's vision for UCVS roles and measurement objectives
- NDA methods development and system engineering for uranium hexafluoride ($UF_6$) cylinder assay
- Calibration and analysis of NDA methods for safeguards verification scenarios
- Metrics for evaluation of NDA methods against various measurement objectives
- Source terms and modeling of signatures from $UF_6$ cylinders
- Pulse-processing methods and electronics, including those in common use by the IAEA
- Design and implementation of IAEA's unattended monitoring systems
- Principles and application of IAEA's remote monitoring and data security methods
- Application of data acquisition, analysis and review software used by IAEA and Euratom
- Concepts and technologies for cylinder identification
- Principles and technologies for IAEA surveillance systems
- Technologies and methods for operator weighing systems, and potential sharing approaches
- Planning and execution of long-term field deployments
- Relationships and experience working with the operators of facilities handling $UF_6$ cylinders.

UCVS team members are listed below. Members of the team are shown in Figure 3 during the laboratory integration and testing meeting in February 2015 at Pacific Northwest National Laboratory (PNNL).

**USSP**

- USSP Task Officer: Joseph Carbonaro
- U.S. Department of Energy (DOE): Kevin Veal, Karyn Durbin, Anthony Belian and Chris Orton (now at PNNL)
- Technical Lead: Eric Smith (PNNL)
- Deputy Technical Lead: Karen Miller (Los Alamos National Laboratory [LANL])
- PNNL: Ben McDonald, Lindsay Todd, Jennifer Webster, Mital Zalavadia, John Kulisek, Nikhil Deshmukh, Erin Fuller, Bryan Gerber, and Emily Mace
- LANL: Heather Nordquist

- Savannah River National Laboratory (SRNL): Sean Branney, Rick Poland, Nick DeRoller, and Lindsay Sexton
- Oak Ridge National Laboratory (ORNL): Jim Garner, Scott Stewart, and Jose March-Leuba

The ECSP participants included:

- ECSP Coordinator: Joao Goncalves
- Euratom Safeguards: Peter Schwalbach and Jim Morrissey.

From Westinghouse, host for the field trial, the following staff participated: Frank Clark, Rodney Likes, Morgan Goff, and Wayne Sepitko.


**Figure 3**. UCVS team members during integration and testing activities at PNNL in February 2015.

# 4.0 UCVS in Context of Enrichment Plant Safeguards

The IAEA's model safeguards approach for gas centrifuge enrichment plants (Cooley 2007) describes the challenges associated with safeguarding large centrifuge enrichment plants and defines the high-level verification objectives for enrichment plant safeguards approaches, i.e., the timely detection and deterrence of:

- Diversion of natural, depleted or low-enriched $UF_6$ from the declared flow in the plant
- Misuse of the facility to produce undeclared product (at the normal product enrichment levels) from undeclared feed (i.e., excess production)
- Misuse of the facility to produce $UF_6$ at enrichments higher than the declared maximum, in particular highly enriched uranium.

At present, the IAEA's safeguards approaches at enrichment plants are based on a combination of routine and random inspections, during which time a number of verification activities are performed, including environmental sampling for subsequent laboratory analysis, collection of $UF_6$ samples from in-process material and selected cylinders for subsequent destructive analysis in a laboratory, and weighing and NDA of a subset of the plant's cylinder flow and inventory. The weight measurements of cylinders are performed using either operator-owned scales or the IAEA's portable hanging load cells, while the NDA measurements use handheld gamma-ray spectrometers combined with ultrasonic wall-thickness gauges.

Detection of prominent diversion scenarios could be improved at enrichment plants if the IAEA could monitor 100% of material flows and periodically calculate independent uranium and $^{235}U$ mass balances for the facility. However, human and financial resources preclude continuous inspector presence at the facility to measure all of the material flow using today's attended methods. Further, the portable measurement methods currently used by inspectors have relatively low accuracy for the assay of relative $^{235}U$ enrichment because of the highly localized nature of the instrument geometry and low-energy gamma-ray signature used by today's portable NDA methods. Currently, the IAEA relies primarily on data from operator weighing systems for total uranium mass, with limited independent confirmation using IAEA's portable load cells, which tend to have relatively low precision.

The poor accuracy and limited application of today's cylinder verification instruments necessitates additional safeguards measures, including the destructive analysis of $UF_6$ samples drawn from some of the cylinder population. These are among the reasons that the IAEA is exploring how unattended instruments capable of continuously and more accurately verifying material flows (both in-process gas and cylinders) on a quasi-continuous basis could help improve the deterrence and timely detection of protracted diversion scenarios.

These unattended instruments are potential tools in a flexible toolbox of safeguards measures that is aimed at addressing the verification challenges posed by advanced centrifuge technologies and the growth in separative work unit capacity at modern centrifuge enrichment plants (Cooley 2007; Lebrun et al. 2009). Permanently installed, unattended instruments could perform the routine and repetitive measurements previously performed by inspectors, thereby allowing the inspectors to use their time on tasks and investigations that depend more heavily on human intuition and decision making. When combined with other safeguards measures, unattended instruments at centrifuge enrichment plants have

the potential to significantly improve the IAEA's effectiveness to detect and deter the primary diversion scenarios of concern, while simultaneously improving the efficiency of facility-level safeguards approaches (Smith et al. 2013).

The IAEA and its Member States continue to investigate new safeguards measures for gas centrifuge enrichment plants (GCEPs) that could lead to both effectiveness and efficiency improvements. Candidate measures include:

- OLEM to provide continuous measurement of enrichment for 100% of the declared gas flowing through unit header pipes (Younkin et al. 2012; Ely et al. 2014)
- UCVS to provide unattended verification of the declared uranium mass and enrichment in all declared cylinders, and the application and verification of an NDA Fingerprint to preserve verification knowledge on the contents throughout its life in the facility (Smith 2014)
- Joint-use weighing systems on the feed and withdrawal stations to count cylinders introduced to the process and to support a periodic confirmation of mass balance in the plant (Lebrun et al. 2009; Garner et al. 2014)
- Automated facility-wide cylinder monitoring systems based on standardized, machine-readable, authenticable cylinder identification and voluntary enhanced reporting of declared data by operators (Durbin et al. 2014).

A description of how these candidate measures might be used to support unattended verification of in-process gas enrichment and 100% of cylinder flow is provided in this section. In this discussion, it is assumed that unattended identification (ID) readers connect the cylinder ID, both alphanumerically and temporally, to the data streams from the shared load cells, OLEM, and UCVS.

Joint-use weighing stations, with cylinder ID provisions, on each feed and withdrawal station allow the counting of all cylinders introduced to the cascades to ensure that only declared cylinders are used, and provide persistent monitoring of the in-process $UF_6$ material balance that allows the IAEA to calculate an independent, near-continuous material unaccounted for (MUF) on total uranium ("Continuous $MUF_U(t)$" in Figure 4). This material balance is based on the measured feed, product, and tails mass flow rates ($F$, $P$, $T$, respectively) in each enrichment unit, assuming that holdup, sampling, and scrap amounts are negligible. Mass flow rates, $M(t)$, from joint-use weighing systems also allow the IAEA to determine the time periods during which specific cylinders are connected to the process.

The OLEMs on the product and tails header pipes continuously measure the time-dependent relative uranium enrichment, $E(t)$, in weight percent $^{235}U$, of the gas flowing through unit header pipes. OLEM's continuous presence offers significant deterrent value to diversion scenarios involving higher-than declared material, and they also support the determination of a facility-level mass balance on $^{235}U$ ("Continuous $MUF_{U\text{-}235}(t)$" in Figure 4). OLEM data can also be used to calculate the average enrichment of the $UF_6$ in product and tails cylinders, $E_{235}$, and $M_{235}$ in the cylinder, by weighting the $E(t)$ data for each cylinder time window by the $M(t)$ for that same time window. By coupling the joint-use weighing systems and OLEMs in this way, a high-accuracy, independent measurement of $E_{235}$ and $M_{235}$ for all unblended product and tails cylinders is produced. Equivalent data for blended product cylinders come from the UCVS assay of $E_{235}$ and $M_{235}$ (no OLEM data for such cylinders are available). These data streams support a discrete, cylinder-based monitoring of the facility $^{235}U$ mass balance ("Discrete $MUF_{U\text{-}235}(t)$".

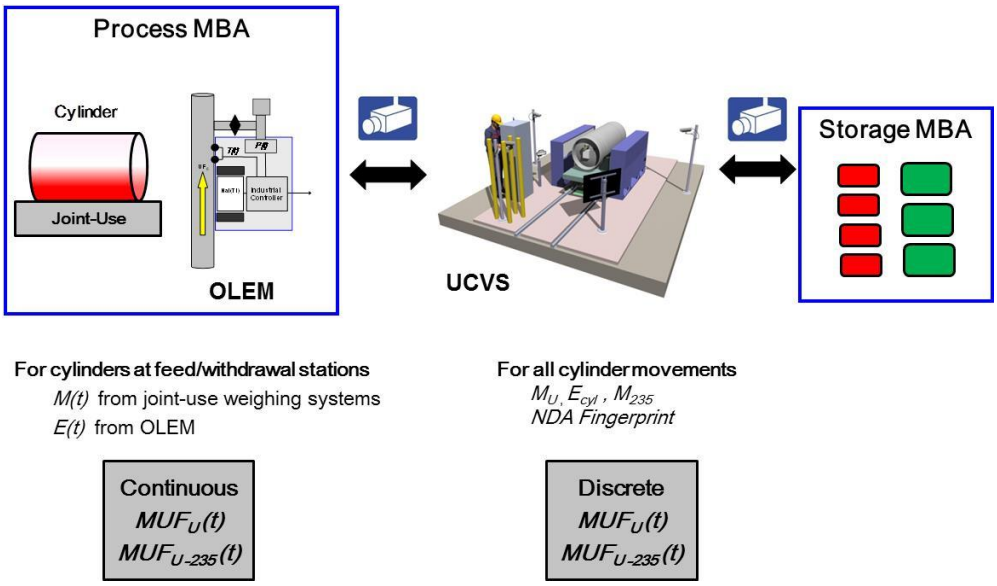


**Figure 4**. Schematic overview of candidate unattended instrumentation in action including joint-use weighing systems on feed/withdrawal stations, OLEM, and UCVS. Cameras and unattended ID readers provide monitoring of cylinder movements and authenticable cylinder identification.

The net uranium mass, $M_U$, in each cylinder can be derived from the sharing of the joint-use weighing instruments at feed and withdrawal stations, but can also be independently measured using the load cells integrated in the UCVS units (assuming tare mass is known). The mass data from the IAEA-owned and operated load cells in UCVS units, which scan all cylinders introduced to and removed from the process MBA, support a discrete form of facility mass balance on total U ("Discrete $MUF_U(t)$" in Figure 4). UCVS units co-located with the operator accountancy scale or at chokepoints for cylinder movements in the facility, scan all cylinders upon entry into the facility, upon exit, and all movements between IAEA-defined MBAs.

The UCVS units could play other important roles, for example in terms of cylinder identification and tracking, and for the verification of the $UF_6$ in blended cylinders for which there would be no associated OLEM-based measurement of $E_{235}$. If OLEM units are not deployed at the facility, UCVS would be the primary means of independent cylinder verification.

There are several potential ways in which facility operators might benefit from UCVS implementation, including an eased and expedited release process for product cylinders. For example, the NDA Fingerprint of a product cylinder ready for off-site shipment could be measured by a UCVS and verified remotely, against previous fingerprint measurements on the same cylinder, by an inspector at IAEA headquarters in Vienna. UCVS scans at entry and exit may be of additional value to operators. Scans of inbound feed cylinders could be used to determine shipper-receiver difference, or aid criticality safety calculations. Outbound scans could ease and expedite the product-cylinder release process for operators, compared to today's methods for holding product cylinders for on-site IAEA verification.

As currently envisaged by the IAEA, UCVS units would be located at key intersections of cylinder movement between MBAs, or at the operator's accountancy scales (in order to take advantage of the facility's cylinder weighing operations). The remotely monitored station would include technologies for

cylinder identification, NDA of the cylinder contents, and video surveillance. UCVS units would be owned and operated by the IAEA, but the data streams could be shared with the operator (e.g., for cylinder tracking and process control) in conformance with IAEA requirements for shared-use instruments. According to the IAEA, the facility-level roles of a UCVS would include (IAEA 2013a):

- Unattended, independent assay of cylinder enrichment ($E_{235}$) and $^{235}$U mass ($M_{235}$) for product, feed, and tails cylinders
- Independent assay of total uranium mass ($M_U$) as a confidence-building measure on the authenticity of data from operator weighing systems
- For product and tails cylinders, the unattended application, verification, and re-verification of an NDA Fingerprint to maintain the verification pedigree of the cylinder contents and to verify that no partial removal of material has occurred during the cylinder's life at the facility
- For feed cylinders, the unattended verification of an NDA Fingerprint to ensure that feed material to the plant is consistent with normal operations using natural feedstock, or consistent with the operator's declaration for non-natural feed
- Detection and reporting of anomalous material, for example non-natural feed that has not been declared by the operator
- Unattended verification of the unique cylinder identifier (e.g., an alphanumeric code stamped on the cylinder nameplate).

## 4.1 NDA Fingerprint

Once the initial verification knowledge on a cylinder (e.g., $E_{235}$, $M_{235}$, and $M_U$) is established, it would be ideal that continuity of knowledge (CoK) on that cylinder and its contents would be maintained from that point forward in that facility and onward to other facilities. Maintaining CoK on cylinders is a particular challenge in gaseous centrifuge enrichment plants since the traditional tool for CoK on nuclear material containers and metal or electronic seals would require very frequent inspector presence to either emplace or remove seals. No practical mechanism for unattended placement *and* removal of such seals exists. (There is a precedent for operators to either emplace or remove seals, but not both.) The NDA Fingerprint concept is intended to compensate for the lack of traditional, continuous CoK on the verified cylinders.

From the technical perspective, the NDA Fingerprint is a collection of radiation signatures (e.g., gamma-ray spectra at multiple locations on a cylinder, and total neutron emissions) that reflect the geometric distribution, isotopic ratios, and isotopic masses of the cylinder contents. There are a number of observable signatures that could be used in the creation of the NDA Fingerprint attributes, and generally speaking, they are the same signatures that are used for the direct assay of $E_{235}$ and $M_{235}$. Viable signatures might include gamma-ray spectra recorded at specific locations on the cylinder wall, gamma-ray peaks (e.g., 1001 keV to 186 keV), or the neutron emissions (total and coincidence) from the cylinder. The constancy (or at least predictability, if decay half-lives are a factor) of these signatures would allow a quantitative check that the key verification parameters for the cylinder are consistent with previous scans, for example, total uranium mass, $M_{235}$, various isotopic ratios (e.g., $M_{234} / M_{235}$ and $M_{232} / M_{235}$), and the spatial distribution of $^{235}$U within the cylinder.

The task of setting and verifying the NDA Fingerprint would be performed by the UCVS. The UCVS scans all cylinders upon entry into the facility, upon exit, and all inter-MBA movements in between. As discussed in the sections below, the UCVS NDA Fingerprint has the potential to play two specific verification roles in an integrated GCEP safeguards approach:

1. A "pseudo-seal" on the contents of all cylinders that periodically confirms, in an unattended fashion, that the contents are consistent with the initial UCVS scan
2. For feed cylinders, precise confirmation that the contents have attributes of typical feed material entering the facility.

In the discussion that follows, the viability of the NDA Fingerprint, for the two roles described, is assumed.

## 4.2 UCVS Implementation Concepts

Building from previous work by the authors and the IAEA, potential concepts of operation for UCVS units deployed in enrichment facilities have been developed. In this discussion, three classes of material and associated cylinders are defined: 1) unblended product and tails cylinders, 2) blended product cylinders, and 3) feed cylinders. Cylinder flow paths and how UCVS-measured data could be used to support unattended verification of each different cylinder type are described, where the primary cylinder verification objectives are to independently confirm $E_{235}$, $M_{235}$, and $M_U$; detect any off-normal characteristics of the cylinder; and preserve the verification knowledge of each full cylinder throughout that cylinder's life at the facility.

### 4.2.1 Unblended Product and Tails Cylinders

As shown in Figure 5, UCVS tracking of a product (Type 30B) or tails cylinder (Type 48) would begin as the empty cylinder is transferred from the storage MBA to the process MBA. This initial scan would verify that the cylinder is indeed empty by industry standards (i.e., some heel material often remains in an empty cylinder). As the product and tails cylinders are being filled in the process MBA, OLEM data would be used to calculate the average enrichment of the $UF_6$ in cylinders, $E_{235}$, by weighting the $E(t)$ data for each cylinder time window by the $M(t)$ for that same time window. By coupling the load cells and OLEMs in this way, high-accuracy, independent measurements of $E_{235}$ and $M_{235}$ are produced. (Here, it is assumed that enrichment level is constant so that only the full-cylinder mass value is needed to calculate $E_{235}$.)

After the cylinder is filled in the process MBA (and homogenized in the case of product cylinders), a UCVS scan is performed during the transfer back to the storage MBA. In this scan of the full unblended product or tails cylinder, the UCVS would measure, in a completely independent fashion, $E_{235}$ and $M_{235}$, (using NDA) and $M_U$ (using the UCVS load cells and a known tare weight) of the cylinder. The NDA Fingerprint for each filled cylinder would also be collected and archived during this scan.

Using the net uranium mass value, $M_U$, measured by the load cells integrated into the UCVS and the OLEM value for $E_{235}$, a high-accuracy determination of $^{235}U$ mass for each unblended product or tails cylinder can be determined because $M_{235} = E_{235} \cdot M_U$.

The UCVS-measured value for $E_{235}$ could be used to confirm the (presumably) higher-accuracy value of $E_{235}$ produced by the OLEM for that cylinder. Importantly, the UCVS measurement of $E_{235}$ would be directly and concurrently connected to the independently verified identification of that cylinder, a connection that is unlikely to be possible for the OLEM cylinder enrichment value.

If OLEMs are not deployed in the facility, or OLEM data are not available for a particular unblended product or tails cylinder (e.g., due to equipment failure), the UCVS would provide the only independent assay of $E_{235}$ as the cylinder exits the process MBA.

The complementarity of the OLEM and UCVS would be similar for the verification of $E_{235}$ in tails cylinders. For tails cylinders, the UCVS scan just prior to entering the storage MBA would likely be the last unattended scan; the tails cylinder would then be transported to the long-term storage area. Should the tails cylinder ever be removed from the long-term storage area, however, a scan by the UCVS and verification of the NDA Fingerprint could ensure that the material inside is consistent with previous scans.

In contrast, product cylinders would remain in the storage MBA only until the operator is ready to ship the cylinder off-site. As the cylinder is removed from the storage MBA for shipment, the UCVS would confirm the constancy of the NDA Fingerprint since previous scans, with review and approval by a remotely located inspector (e.g., at IAEA Headquarters). This automated confirmation process could enable an expedited cylinder release process for facility operators, when compared to today's approaches that involve routine interim inspections and on-site inspector measurements.

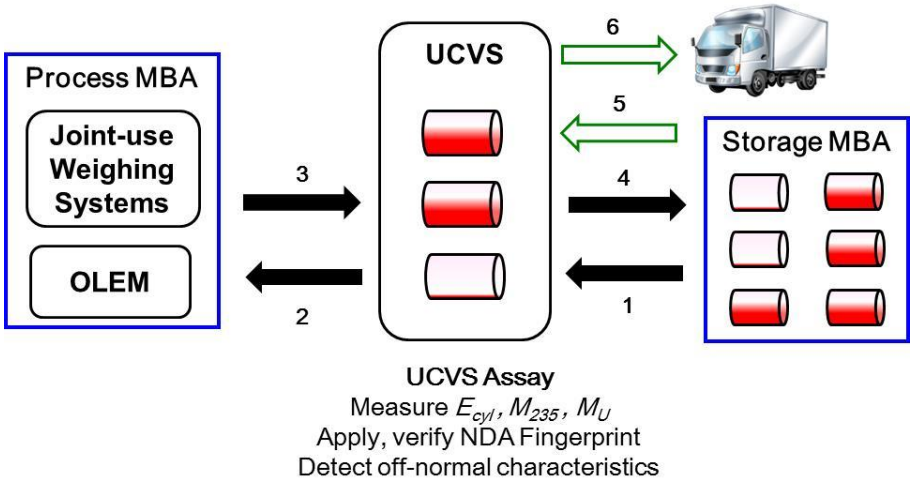


**Figure 5**. Conceptual overview of how an unblended product cylinder could be verified and released from the facility using a combination of OLEM, UCVS, and joint-use weighing stations. The six cylinder movements notionally describe the life cycle of the cylinder from its status as an empty in the storage MBA through off-site shipment. When the operator is ready to ship the cylinder off-site (green arrows at top), the UCVS's NDA Fingerprint capability would be used to verify the constancy of the cylinder contents since production.

### 4.2.2 Blended Product Cylinders

In modern enrichment plants, operators often blend some fraction of product cylinders to achieve a specific enrichment matching a customer's needs. Because an OLEM assay value cannot be maintained on the cylinders involved in the blending process, it is the UCVS assay at the exit of the process MBA that is the first and only opportunity to independently verify $E_{235}$, $M_{235}$, and $M_U$ for blended product cylinders.

The initial flow path for a blended cylinder is the same for an unblended cylinder, but diverges after filling at a withdrawal station is complete. From the withdrawal station, the intermediate unblended product cylinder is moved to the blending station. In some enrichment facilities, the blending station is within the process MBA but in others, a separate blending MBA is defined, as depicted in Figure 6. In such facilities, UCVS scans could be performed on the intermediate unblended product cylinders as they move between the process and blending MBAs, and on the blended product cylinders as they exit the blending MBA. When the operator is ready to ship the blended cylinder off-site, the cylinder's NDA Fingerprint would be verified in a fashion identical to that used for unblended cylinders.

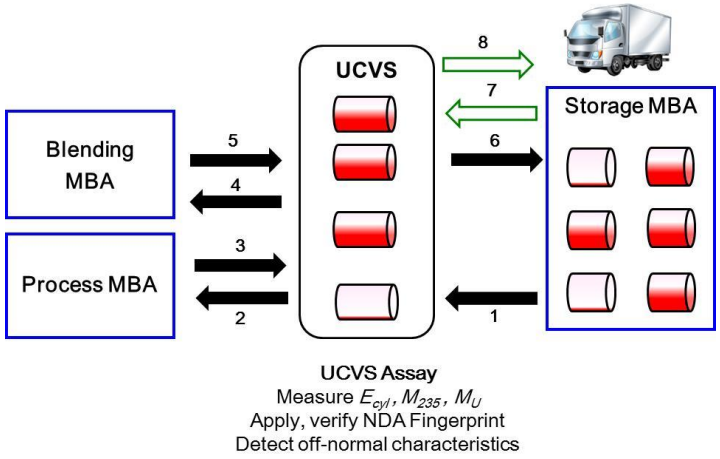


**Figure 6**. Conceptual overview of how a blended product cylinder could be verified and released from an enrichment facility using primarily data from the UCVS. The eight cylinder movements notionally describe the life cycle of the cylinder from its status as empty in the storage MBA through off-site shipment.

### 4.2.3 Feed Cylinders

Verification of feed cylinders presents a particular challenge for unattended measurements systems for several reasons. First, the feed is the largest $^{235}U$ flow rate in the facility, which means that uncertainties in the assay of feed will have a major impact on overall uncertainty in the material balance. There are also some significant hurdles to accurate assay of gas-phase feed material using the OLEM. For example, a pressure-transient wall-deposit calibration approach cannot be used all plants, and likely cannot be used on the feed header pipe since feed-station gas dynamics in the feed header pipe are considerably different than for product and tails header pipes. Further, it is expected that the wall deposits on the feed header pipe may be higher than on product and tails header pipes, since air incursions are more likely to be pulled downstream from the feed cylinder stations, and catalyze wall-deposit formation near the OLEM (Smith et al. 2011).

While all of these factors complicate the use of assay methods to determine $^{235}U$ mass in feed cylinders, there are some potential advantages in the nature of the feed material and cylinders themselves. For example, in contrast to the product and tails material, the isotopic content is known to high precision (assuming natural, not recycled, uranium feed material) and the contents of the cylinder are expected to be highly homogenized. It should be sufficient, therefore, to simply ensure that each new feed cylinder has the attributes of "typical" natural-uranium feed material entering the facility. In practice, this means that an attribute monitor like the NDA Fingerprint could provide all of the necessary quantitative data for verification of the feed material entering the facility. Minor isotopic content, for example $^{234}U$ or $^{232}U$, could also be verified using the NDA Fingerprint and compared to operator declarations based on mass spectrometry. As shown in Figure 7, the NDA Fingerprint for each feed cylinder entered into the storage MBA could be verified to ensure that it is consistent with the operator's declaration and the feed material typically used by the plant. The full feed cylinder would be scanned again prior to placement on a feed station in the process MBA; following the withdrawal process, the empty feed cylinder would be scanned by the UCVS on the way back to the storage MBA.

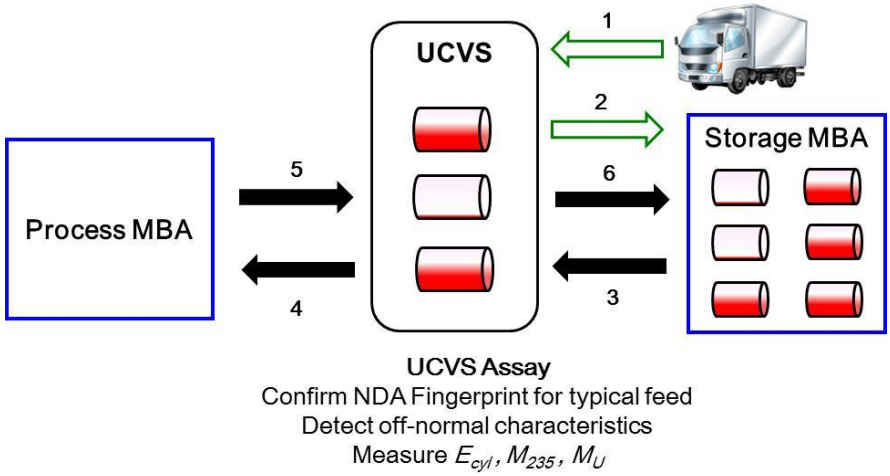


**Figure 7.** Conceptual overview of how a feed cylinder could be verified using the UCVS, beginning with the receipt of the cylinder from off-site. The six cylinder movements describe, notionally, the life cycle of the cylinder from its acceptance onsite as a full feed cylinder through its entry into the storage MBA as an empty.

# 5.0 Candidate NDA Methods

## 5.1 Hybrid Enrichment Verification Array

PNNL has developed a hybrid cylinder assay technique that uses an array of NaI(Tl) spectrometers to simultaneously measure the 1) direct 186-keV signature from $^{235}$U, and 2) singles neutrons via the high-energy gamma rays induced by neutrons in the iodine in the spectrometer crystal and in the $^{56}$Fe of the spectrometer collimators (Figure 8). The traditional 186-keV signature provides a direct measure of $E_{235}$. Under assumptions of known $^{234}$U/$^{235}$U behavior in the plant, the nontraditional total neutron signal can be calibrated to total $M_{235}$ in the cylinder (Smith et al. 2010a; Smith et al. 2010b; McDonald et al. 2011; Smith 2015).

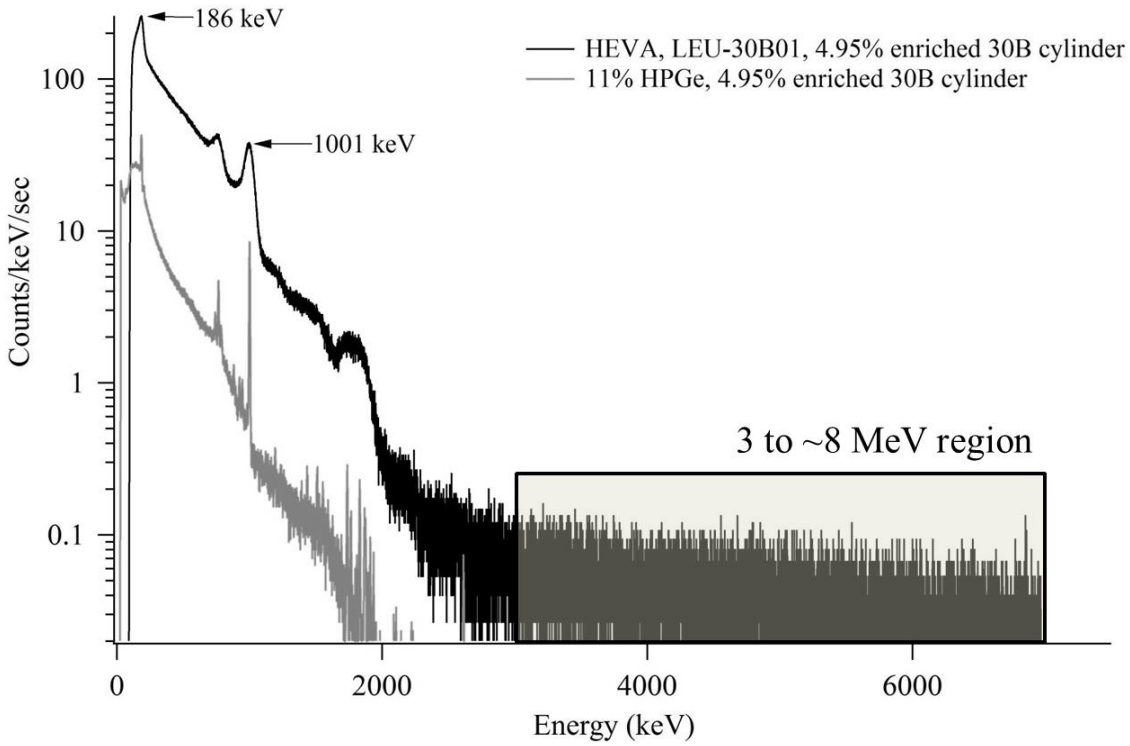


**Figure 8**. Illustration of the traditional (186-keV) and nontraditional (3-8 MeV region corresponding to neutron-induced gamma rays) gamma-ray signatures used by the HEVA method. For comparison, the spectrum from a high-purity germanium (HPGe) spectrometer similar to that used by Euratom and IAEA during inspections, is shown. Note that the high-energy signature is not viable with that smaller, germanium instrument.

Though the HEVA method collects the same 186-keV signature collected by the handheld spectrometers currently used by Euratom and IAEA, there are distinct differences in how wall-thickness variations are addressed, and their impact. In the case of the attended handheld devices, the collection area is very small (~100 cm$^2$), and typically located on the cylinder endcap. Measurements with a separate ultrasonic wall thickness gauge are used to correct the gamma-spectroscopy result, relative to the nominal wall thickness for each cylinder type. In unattended HEVA assay, the collection area is much larger (e.g., multiple spectrometers, each having a field of view somewhat larger than the handhelds), and distributed along the length of cylinder side wall (on both sides, in the nominal unattended system design).

The original hypothesis in early HEVA development was that a large-area, distributed measurement would "average out" any significant wall-thickness effects on the traditional 186-keV signature. Indications that the wall-thickness tolerances on the side wall of a cylinder (rolled steel) tend to be tighter than on the curved, circular end caps, may provide additional advantage for unattended HEVA over typical attended handheld measurements. In several previous field campaigns, some of which also collected ultrasonic wall-thickness data, the original hypothesis has been supported: a calibration based on the aggregate 186-keV signal, summed over multiple NaI(Tl) spectrometers, can produce assay precision comparable to high-resolution handheld devices (Smith et al. 2010b; Jordan et al. 2012; Smith et al. 2014). A separate calibration is needed for Type 30B and Type 48 cylinders, due to the different nominal wall thicknesses and cylinder-detector geometries for those cylinder types.

### 5.1.1 Evolution of the HEVA Modules

Among the findings from studies prior to UCVS Phase I was that the HEVA hardware and software required revision and further development in order to be considered suitable for field trials of an unattended UCVS prototype. For example, the collimator/neutron converter design had an unnecessarily high ratio of mass to sensitivity for the indirect neutron signature. Further, greater flexibility was needed in the collimator mechanical design to better manage the detector field of view so that count rates in each spectrometer can be maintained well below the region where pulse pileup and dead time begin to degrade the quality of the recorded spectra. The pulse-processing electronics used in prior HEVA prototypes were chosen because they were readily available to the developers at no cost—not because they were optimal for this application. Commercially available digital photomultiplier tube bases, used routinely in similar medium-resolution gamma-spectroscopy applications throughout the NDA community, should be used (Smith et al. 2014).

These findings motivated a redesign of the HEVA hardware and software, in preparation for UCVS field trials. PNNL performed modeling and measurements to support a revision of the HEVA module design and data acquisition methods. This work is described in detail by Zalavadia et al (2016); highlights are presented here.

The new HEVA prototype design consists of an array of three ø7.5 cm × 7.5 cm NaI(TI) spectrometers surrounded by specialized collimators consisting of concentric layers of steel and polyethylene. The front side of the collimator assembly is covered with a lead face plate (~1.35-cm thick) with a 2.54-cm wide opening (aperture) to allow a direct path to the detector for the 186-keV gamma-rays from $^{235}$U. The innermost layer around the detectors is a 0.64-cm thick lead layer designed to help manage the count rate and reduce contributions from down-scattered gamma rays. The photomultiplier tubes (PMTs) on each of the three NaI(Tl) detectors are coupled to a Canberra Osprey digital tube base that includes several functions: PMT power, preamplifier, shaping amplifier, analog-to-digital conversion and a multi-channel analyzer. The Osprey was selected for its high degree of flexibility in parameters, robust power and communications options, compact form factor, and familiarity within the IAEA. Figure 9 provides a cross-sectional depiction of the HEVA detector-collimator assembly.

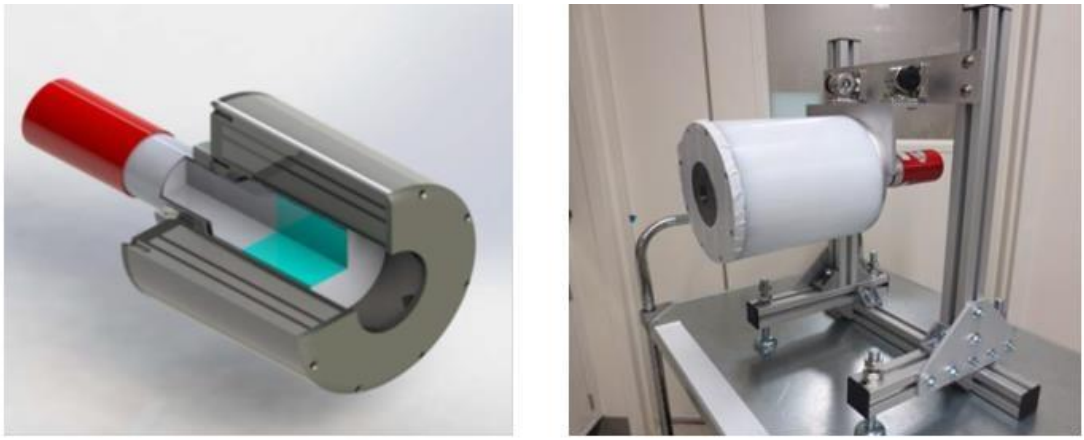

**Figure 9.** Left: Cross-sectional rendering of the HEVA detector-collimator assembly. The Osprey digital tube base is depicted in red on the left, the NaI(Tl) crystal is the light blue object. Surrounding the crystal are layers of lead, polyethylene, and steel to manage the total count rate and enhance neutron-to-gamma conversion. Right: Photograph of the mechanical support for a HEVA module that allows flexibility in terms of orientation angle relative to the cylinder face.

The revised HEVA module design depicted above was informed by a modeling study that allowed prediction of count rates associated with the various cylinder source terms, including the declared $UF_6$ volumes, heels materials, and wall deposits. For the cylinder assay scenario, the HEVA input count rate can vary significantly between cylinders, not just because of varying enrichment levels but also due to the amount of non-$UF_6$ compounds and $^{238}U$ progeny on the bottom and walls of the cylinder. This material is often labeled "heels" and/or "wall deposits" (hereafter, wall deposits for simplicity) and generally speaking, its volume and mass grow with the number of fillings that a given cylinder has experienced. Worst-case assumptions (in terms of expected count rates) about the geometry, elemental composition, and isotopic inventory were adopted in the modeling study, as described by Zalavadia et al. (2016).

The collimator and neutron-gamma converter materials of the new HEVA module design (Figure 9) allow an adaptable detector recess, which can tailor the field of view to manage the gamma-ray flux incident on the detector. With the detector recessed, it is estimated that maximum count rates encountered in the field, even for cylinders with wall deposits, will be less than 30 kcps. The field-trial results presented later in this report have substantiated that modeling-based assertion.

A study of the Osprey parameter space, in the context of the count rates expected for HEVA in the UCVS scenario, was completed. Parameters of interest included: trapezoidal filter parameters, baseline restoration, fast-discriminator threshold, Pile-up Rejection Guard inspection interval (PUR Guard), live-time correction (LTC) and pulse height analysis (PHA) acquisition time. Results indicated that the parameter settings defined through the course of the study strike an appropriate balance between count rate throughput and energy resolution. In addition, these settings should ensure that systematic uncertainties introduced by Osprey pulse-processing parameters will be insignificant in the overall HEVA uncertainty budget, so long as input count rates are maintained less than approximately 50 kcps. As discussed above, the HEVA modules were configured to ensure that count rates stayed well below that level for even the most intense cylinders expected to be encountered. Examples spectra from prior HEVA deployments and the revised modules used in the WFFF field trial are in Figure 10.

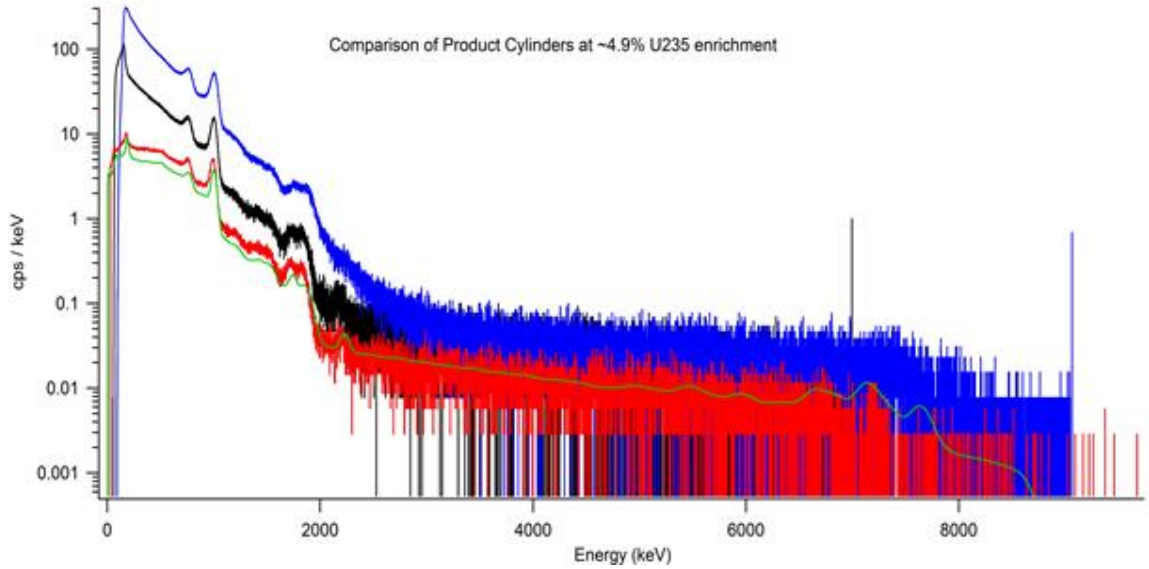


**Figure 10**. Example spectra for 4.9 wt% Type 30B cylinders. Previous field campaigns used a prior HEVA module design measured cylinders with high wall deposits (blue) and lower wall deposits (black). Monte Carlo N-Particle (MCNP) simulations of the new module design for a cylinder had no wall deposits (green) and measured response for the new module design for a cylinder with unknown (but apparently relatively low) wall deposits (red). Sharp spikes are single-channel anomalies from the multi-channel analyzers used in prior field trials.

Laboratory measurement of the intrinsic neutron efficiency for the HEVA nontraditional method produced a value of approximately 0.5%, assuming a gamma-ray region of interest from 3.0 to 8.0 MeV. It was shown that the contribution of the steel layers is relatively small compared to the prompt gamma rays produced in the detector crystal (Zalavadia et al. 2016).

The potential impact of activation of the NaI(Tl) detector medium was investigated, where the dominant contributor was shown to be the production of $^{128}$I (25-minute half-life) via the activation of $^{127}$I. A combination of laboratory, analytical and Monte Carlo N-Particle (MCNP) analysis showed that the $^{128}$I bremsstrahlung spectrum will contribute approximately 10 cps in the 50-2000 keV energy region, at the end of a 5-minute cylinder assay. For a 2-hour assay, the count rate may be nearly eight times higher. It is expected, given nominal total HEVA count rates of 5 to 30 kcps during cylinder assay, that the impact of iodine activation on total HEVA count rate will not be significant.

Appendix A provides more discussion and supporting information regarding the characterization and calibration of the HEVA modules.

### 5.1.2 Overview of HEVA Analysis Algorithms

As discussed above, the HEVA assay approach relies on analysis of two distinct portions of the gamma-ray spectra collected from its array of NaI(Tl) spectrometers: the 186-keV region, required to implement $HEVA_T$, a variant of the "traditional" enrichment meter method; and $HEVA_{NT}$, the high-energy (3-MeV to 8-MeV region) continuum region required to measure the "nontraditional" signature of high-energy

gamma rays emitted following neutron capture in materials proximate to the $UF_6$ cylinder, including the NaI(Tl) spectrometers themselves. The analysis goal in both spectral regions is, first, to construct a calibration curve, mapping spectrometric response versus declared values for each cylinder (enrichment and $^{235}U$ mass), and second, to use the calibrations for assay of subsequent cylinders presented for verification of these declared values. Additional discussion about HEVA analysis algorithms follows.

#### 5.1.2.1 HEVA$_T$ Using the Square Wave Convolute Method

Peak-area extraction in the 186-keV energy region is non-trivial for medium-resolution spectrometers like NaI(Tl) for several reasons. Down-scatter from intense higher-energy lines (most notably, the 766-keV and 1001-keV lines from $^{234m}Pa$, a daughter of $^{238}U$) introduces an often-intense continuum under the 186-keV peak. As predicted by the Klein-Nishina differential scattering cross-section, high-angle scatter is favored so that "backscatter" of the $^{234m}Pa$ lines from the HEVA collimator and pulse-processing electronics creates a very broad, "peak" under the 186-keV peak of interest (Figure 11). In addition, there is bremsstrahlung radiation from the 2269-keV endpoint energy beta particle emitted by $^{234m}Pa$ that produces a broad continuum from near zero to the endpoint energy. This bremsstrahlung source term accounts for approximately half of the total photon emissions from $^{238}U$ and its progeny (for enrichments encountered in commercial enrichment facilities), and over 30% of the counts recorded by a 7.5 cm ×7.5 cm NaI(Tl) detector in the 186-keV energy region (Figure 11).

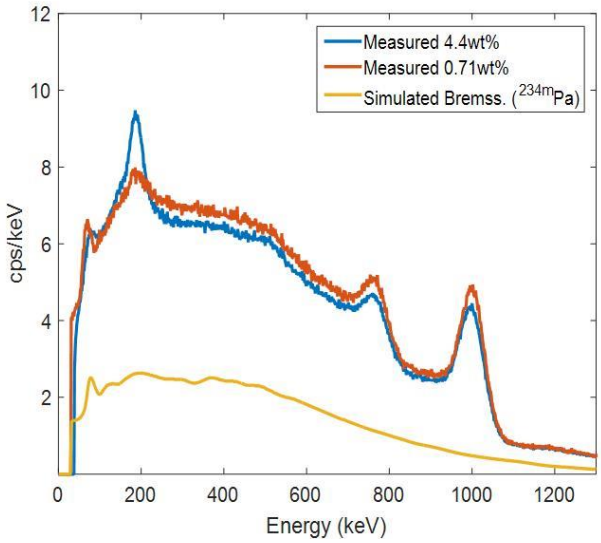


**Figure 11**. Illustration of continuum components presented under the 186-keV peak. Contributions include down-scatter from the 766- and 1001-keV emissions from $^{234m}Pa$, and a bremsstrahlung continuum from $^{234m}Pa$. Measured spectra for cylinders with comparable wall-deposit intensities but very different enrichments are shown (blue and red), along with a simulated bremsstrahlung continuum for natural enrichment (yellow).

$^{234m}Pa$ is present in the bulk $UF_6$ and also in the wall deposits. Particularly for the relatively young $UF_6$ encountered in measurements at enrichment facilities, the wall-deposit contributions may be dominant but for older material such as might be encountered at a fuel fabrication plant like the Westinghouse Fuel Fabrication Facility (WFFF), the $^{234m}Pa$ contribution from the bulk material is significant. Unfortunately, composition of wall deposits and heel material is not well understood. They are commonly thought to be

made of non-uranium, progeny compounds, $UF_4$, or some mix of remaining $UF_6$ (McDonald et al. 2011; Zalavadia et al. 2016). Operationally, heels cylinders are sometimes given time to decay for several weeks before they meet the dose limits for transport, indicating that there are not many uranium atoms left to keep producing radioactive progeny, and that the majority of the wall deposits are made of non-uranium compounds. More investigation is needed on this topic.

Prior studies have shown that the effect of wall deposits on gamma-ray spectra collected from cylinders is highly variable. It depends on the age of the $UF_6$ itself, time since last cleaning, and the enrichment level of *previous* cylinder fillings since it was last cleaned. It is well-known that cylinder-to-cylinder variation is significant and a dominant source of uncertainty for NDA methods using the 186-keV region. This challenge is illustrated in Figure 12 for three natural-enrichment cylinders measured using HEVA during the WFFF field trial.

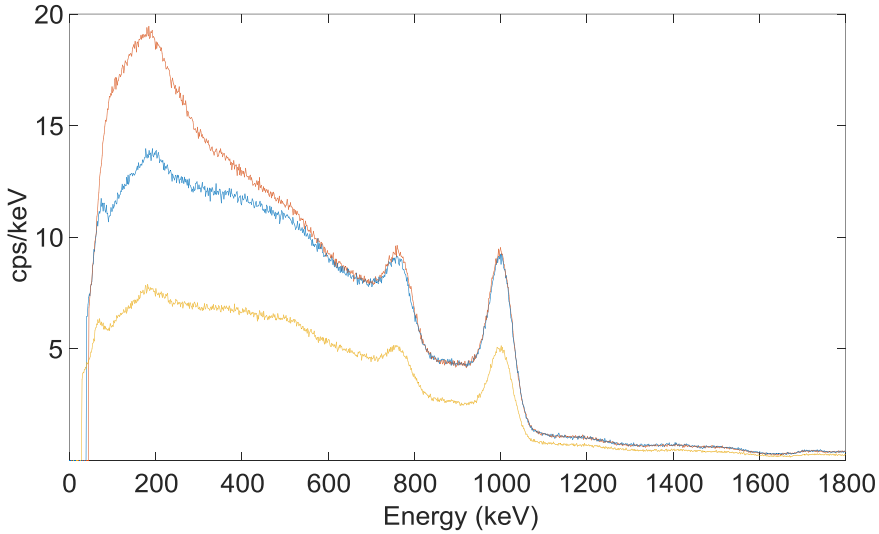


**Figure 12**. Illustration of the high variability in continuum under the 186-keV peak due to varying levels of wall deposit. All three spectra are from cylinders with enrichment of 0.71 wt%.

While cylinder-to-cylinder variation has been assessed previously, less is known about the degree to which the wall-deposit effects vary *within* a cylinder. The WFFF field trial provides additional insight into this question, since the three HEVA modules provide measurements at the ends and middle of the cylinder wall. More discussion on this topic is provided in Sections 9 and 10.

From the analysis algorithm standpoint, the continuum due to down-scatter and bremsstrahlung is difficult to remove using the canonical estimation based upon a linear extrapolation of the continuum above and below the peak region not only because it is highly nonlinear, but also because the shoulders from peaks due to other $^{235}U$ emissions (e.g., 143.8 keV, 163.4 keV, and 205.3 keV) make it difficult to cleanly determine the edges of the 186-keV peak.

For HEVA analysis of cylinders, relatively lightweight algorithms that offer the potential for automated, unattended spectrum analysis were sought. One spectroscopic analysis algorithm adopted for the current work involves application of a discrete form of a so-called zero-area digital filter applied to the pulse-height spectra collected with the NaI(Tl) spectrometers. The convolution of the original spectrum with the

digital filter is referred to as the square wave convolute (SWC) spectrum. Figure 13 illustrates the application of the SWC method to two measured HEVA spectra collected from Type 30B cylinders. Additional detail about the SWC implementation can be found in Appendix B.

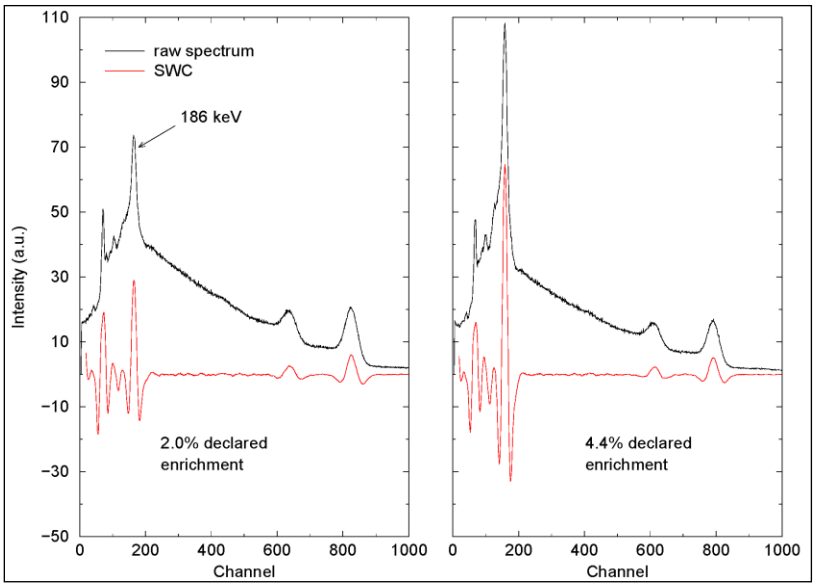


**Figure 13**. Illustration of the square-wave convolute method on two $UF_6$ spectra recorded from Type 30B cylinders with an NaI(Tl) spectrometer.

Previous experience in applying the square-wave filter has indicated that it eliminates linearly varying background quite effectively but exhibits sensitivity to nonlinearities in the continuum shape above the 186-keV region (Smith et al. 2010a; Smith et al. 2010b; McDonald et al. 2011; Jordan et al. 2012). When the intensity of this continuum varies substantially over a cylinder population (e.g., as in Figure 12) or even within a cylinder, the convolute peak amplitude in the 186-keV region reflects not only the intrinsic variation in the 186-keV peak area, but also the impact of the residual continuum shape that is not eliminated completely by the filter. Under these conditions, the impact of continuum shape and intensity distort the simple relationships between enrichment and SWC peak amplitude in the 186-keV, resulting in degraded enrichment assay precision, especially at low enrichments where the $^{235}U$ signal is relatively weak. UCVS Phase I provided an opportunity to more fully test the method's strengths and limitations, on larger and more diverse cylinder populations.

Once the location and magnitude of the 186-keV peak has been determined in this fashion, a linear relationship between this signal and the enrichment of the cylinder is determined using a least-squares linear fit function and the provided declared values, for each population of interest.

#### 5.1.2.2 $HEVA_{NT}$ Analysis Method

The nontraditional total neutron signature, as taken from the summation of counts in the 3-8 MeV range, is calculated for each individual HEVA module, and also summed across the three modules. In contrast to the spectrum analysis in the 186-keV region, the count summation in the nontraditional case is relatively straightforward. Definition of the 3-8 MeV energy window in terms of raw spectrum channels requires an energy calibration, which is currently determined by analysis of the positions of the 186-keV, 766-keV,

and 1001-keV peaks in each NaI(Tl) spectrometer for each 300-second HEVA measurement. An investigation of energy calibration approaches indicated that a linear function is most appropriate for determination of the lower bound of the $HEVA_{NT}$ region of interest (3.0 MeV), when using a three-point calibration based on the 186-keV, 765-keV, and 1001-keV lines expected to be available in each cylinder occupancy spectrum. This three-point linear calibration was used for the $HEVA_{NT}$ analysis presented in this report (Zalavadia et al. 2016).

A least-squares method was used to fit the count rate data to declared $^{235}U$ mass information. As discussed elsewhere, a nonlinear relationship was appropriate based on knowledge of the $^{234}U/^{235}U$ behavior in enrichment facilities. An exponential model was imposed:

$$\ln(\text{cnts}) = a * M_{235} + b$$

where cnts is the total count rate in the NT region, $M_{235}$ is the declared $^{235}U$ mass, and a and b are the fit parameters determined by the least squares method. This method was chosen to reflect the monotonically increasing nature of counts as a function of enrichment and to guarantee a stable inversion that would allow prediction of unique enrichment for any measured count rate.

#### 5.1.2.3 $HEVA_{Hybrid}$ Method for Cylinder Enrichment

Previous statistical analysis by PNNL, using cylinders measured in prior field trials, demonstrated that the uncertainties for the nontraditional (neutron) and traditional (186-keV) signatures show a low degree of correlation, indicating that combining the two signatures will produce more precise verification results than either signature acting independently (Smith et al. 2010a). In this study, this hybrid analysis is performed with a simple averaging (i.e., even weighting) of the traditional and nontraditional signatures. The performance of HEVA, therefore, is reported in terms of $HEVA_T$ and $HEVA_{Hybrid}$ for the verification of relative cylinder enrichment, while $HEVA_{NT}$ is reported for the measurement of the $^{235}U$ mass. Inconsistencies between the enrichment predicted by the traditional and the nontraditional signatures are also flagged, to illustrate how HEVA can identify an off-normal $^{234}U/^{235}U$ ratio in the cylinder, and how such information might ultimately be used in safeguards verification scenarios.

#### 5.1.2.4 HEVA Methods for Detection of Off-Normal Cylinder Characteristics

The gamma-ray spectra collected by the HEVA system can also be used to verify or reveal other information about the contents of a cylinder. For example, feed, product, or tails based on reactor-recycled uranium can be identified by the presence of a strong signal in the 2614-keV gamma-ray peak from $^{208}Tl$, a daughter product of $^{232}U$, assuming that the uranium is sufficiently "old," relative to the last chemical separation, for that daughter to grow in (~6-month equilibrium time). For the UCVS concept, flagging the potential for $^{232}U$ as a contributor to the 2614-keV signal is important because it is an indicator that the $^{234}U/^{235}U$ ratio for that cylinder, and therefore the (alpha, n) neutron emission rate that is central to the $HEVA_{NT}$ and PNEM methods, will be different than is assumed for natural feed material.

It is important to note that $^{208}Tl$ is also a daughter of $^{232}Th$, an ubiquitous naturally occurring isotope. Therefore, a relatively low level of 2614-keV signal is expected from the surrounding environment and depending on the enrichment and therefore higher-energy emission intensity from the cylinder, the ambient contribution to the 2614 keV may not be negligible. It is possible that wall deposits in older cylinders may include daughters emitting at 2614 keV. This is a question that needs further investigation.

A range of 2614-keV intensities is illustrated in Figure 14 using spectra from the WFFF field trial. There, a weak 2614-keV signal, presumably from ambient emissions, is visible even in a low-enrichment cylinder expected to be derived completely from natural uranium. That weak background signature, however, is completely overwhelmed by the non-traditional signature from cylinders with higher enrichments and therefore, not visible in higher-enrichment cylinders with material of natural origin. The very strong 2614-keV signal from cylinders declared to originate from the U.S.-Russia downblending program for highly enriched uranium is clearly evident. Reactor-recycle uranium was commonly used in that program.

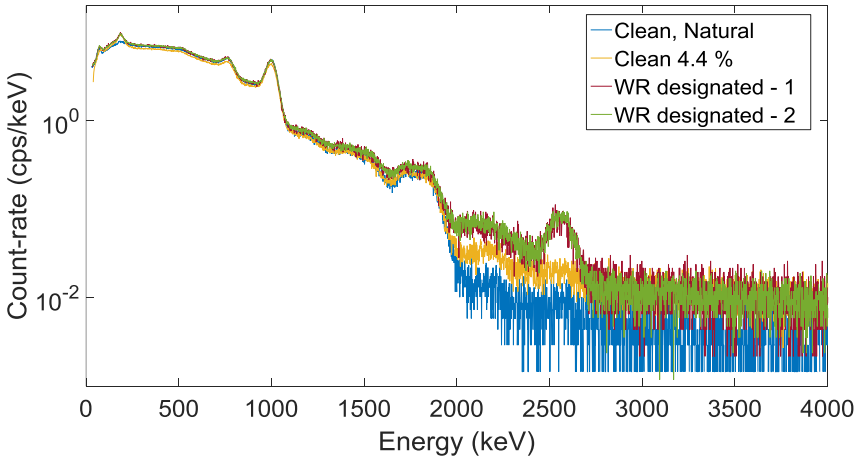


**Figure 14**. Illustration of variation in 2614-keV signal for cylinders of varying characteristics. WR refers to weapons-recycle material that is expected to contain elevated levels of $^{232}U$.

PNNL developed an algorithm to detect an elevated 2614-keV signature and thereby provide a means to flag a cylinder as atypical. The net 2614-keV count rate is calculated by subtracting a fixed continuum from under the 2614-keV peak region of interest (ROI). The intensity of that continuum is determined using a broad ROI that encompasses the $HEVA_{NT}$ signal above 2614 keV. The two ROIs are illustrated in Figure 15. The count rate in the peak ROI, $C_1$, assumes an ROI width of approximately 300 keV. The background count rate, $C_2$, is based on a window spanning 3.0 to 8.0 MeV. The background ROI extents were chosen as a balance between several factors: proximity to the peak region of interest, relatively high statistical certainty, and relatively flat shape.

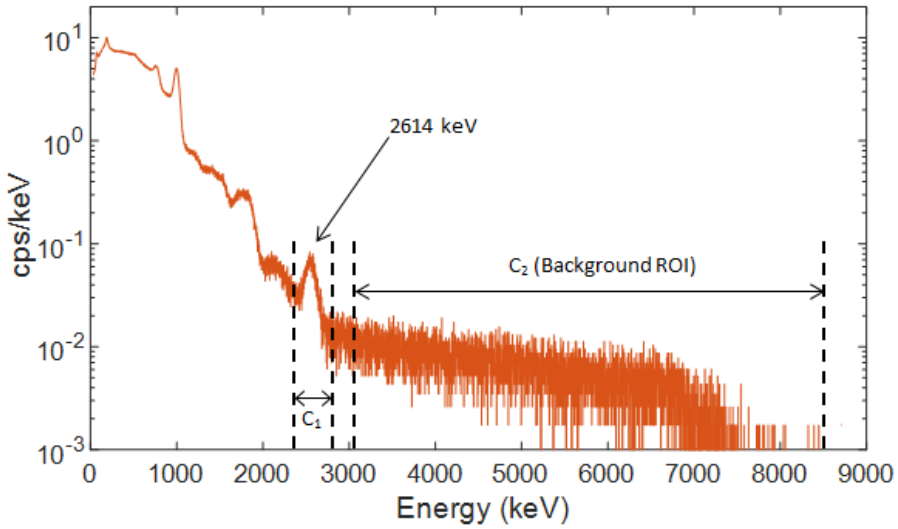


**Figure 15**. The peak and background ROIs used in the calculation of net 2614-keV count rate used to identify $UF_6$ containing elevated levels of $^{232}U$.

To date, the 2614-keV detection algorithm has been applied only to HEVA-2 (center module); results for the outer HEVA modules are expected to be similar. Figure 15 shows the net 2614-keV count rate in HEVA-2 for cylinders measured during the WFFF field trial. All measured cylinders not having significant perturbations, including those not analyzed in this report (e.g., Type 30A at 0.2 wt% and heeled empty cylinders) are shown. Figure 16 illustrates that the algorithm for excess 2614-keV counts is effectively identifying cylinders with high $^{232}U$ content while discriminating against cylinders with relatively strong 2614-keV signals but weak high-energy emissions overall (e.g., depleted enrichment, heels).

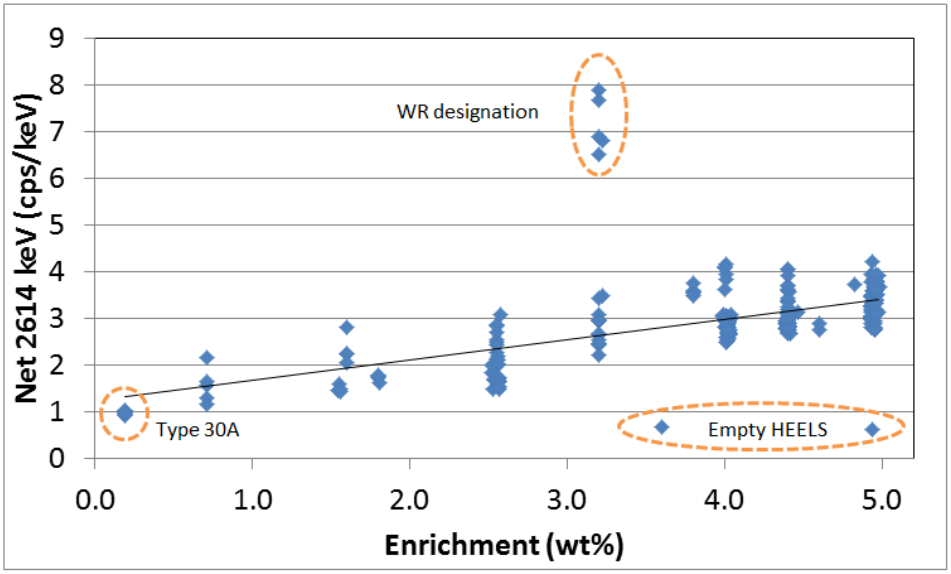


**Figure 16**. Net 2614-keV count rate for cylinders measured during the WFFF field trial. For the identification of off-normal cylinders, a threshold of 4.5 cps was employed.

## 5.2 Passive Neutron Enrichment Meter

Los Alamos National Laboratory's (LANL's) PNEM method uses two $^{3}$He-based neutron detector pods to measure the singles and doubles count rates from the cylinder (Menlove et al. 2010; Miller et al. 2010a; Miller et al. 2012b). The singles counts come primarily from $^{234}$U alpha bombardment of fluorine, giving rise to random (α,n) neutrons. The assumption of known $^{234}$U/$^{235}$U behavior allows determination of $^{235}$U mass (analogous to the indirect neutron signature in the gamma-ray-based HEVA method). This portion of the PNEM methodology is identical to that used by the Unattended Cylinder Assay System (UCAS), another system developed by LANL for operator use at an enrichment plant in Japan (Miller et al. 2010b). PNEM extends beyond singles neutron counting, however, to include the coincidence (i.e., doubles) neutron signature that arises from induced fission in $^{235}$U. The coincident neutron signal also includes the spontaneous fission from the $^{238}$U in the cylinder. The doubles count rate provides a measure of the enrichment level in the cylinder.

The PNEM hardware consists of two polyethylene-moderated detector pods, each containing 12 $^{3}$He tubes and weighing 17.6 kg. The majority of the IAEA's neutron detector systems in routine use employ $^{3}$He proportional counters based on their high efficiency, low sensitivity to gamma interference, reliability, and stability. The PNEM detector pods are shown in Figure 17. The compact preamplifier was designed and built by Precision Data Technology (PDT). The PNEM detector pods are also commercially available through PDT. For the UCVS field trial, the detector pods were contained inside environmental enclosures with a desiccant pack, and a JSR-12 shift register was used for data acquisition. The JSR-12 is the standard IAEA shift register for unattended monitoring systems. A wiring diagram for PNEM is provided in Appendix C.

**Figure 17**. Photograph of the PNEM detector pods, each containing 12 10-atm $^{3}$He tubes and weighing 17.6 kg.

Three prior field trials of the PNEM were at the Rokkasho enrichment plant in Japan, the WFFF in the United States (the same facility as the UCVS deployment), and the URENCO enrichment plant in the Netherlands. The first prototype PNEM detector pods used in the Rokkasho and initial WFFF trials were subsequently replaced with a second prototype. The first and second prototype designs are essentially identical mechanically, the main differences being an increase in $^{3}$He gas pressure from 4 to 10 atm and a simplified amplifier design.

The 2011 field trial in Japan was used as proof-of-concept for a variety of potential PNEM signatures for determining $^{235}U$ mass and enrichment (i.e., singles, doubles, doubles-to-singles ratio, and cadmium ratio) and to study the distribution of $UF_6$ within the cylinders. It included measurements on 36 cylinders including Type 30B and 48Y with depleted, natural, and low-enriched $UF_6$. In the 2012 field trial at WFFF, the PNEM development team continued to study PNEM signatures as well as $UF_6$ distribution inside the cylinders. In this test, the team measured 30 cylinders consisting of Type 30B cylinders only; however, the team gained experience measuring cylinders from both gaseous diffusion and centrifuge enrichment plants as well as highly enriched uranium (HEU) downblend material. In 2013, PNEM was tested at the URENCO plant in the Netherlands as part of a joint field trial including the HEVA system and traditional handheld gamma-ray spectrometers. The field trial included measurements of 45 cylinders including Type 30B and 48Y with depleted, natural, and low-enriched $UF_6$ as well as reprocessed $UF_6$ from reactor returns.

In the 2013 field trial, the LANL team also employed a hybrid metric that combines the $M_{235}$ value obtained from the singles count rate with the operator-declared uranium mass to get an alternative measure of $E_{235}$. That value is averaged with the $E_{235}$ estimate obtained from the doubles to obtain a hybrid enrichment signature. This methodology mirrors the hybrid methodology employed by PNNL for the HEVA system. Inconsistencies between the enrichment predicted by the singles and the doubles signatures are also flagged to illustrate how PNEM can be used to identify a $^{234}U/^{235}U$ ratio outside the calibrated range and how such information might ultimately be used in safeguards verification scenarios. For cylinders with $^{234}U/^{235}U$ ratios far outside the calibrated range, as is typically the case with $UF_6$ from reactor returns, the PNEM can flag the inconsistency but does not provide an accurate measure of enrichment based on the doubles count rate alone. This is because the $^{234}U$-induced $(\alpha,n)$ neutrons serve as the self-interrogation source for the $^{235}U$ induced fission neutrons that provide the doubles counts. To be completely insensitive to the $^{234}U$ content for the enrichment measure, the PNEM can be converted into an active interrogation system (Miller 2012a).

# 6.0 UCVS Prototype Design

A schematic of the UCVS prototype assay platform is shown in Figure 18. The prototype design was driven by the Preliminary UCVS User Requirements (IAEA 2013a) provided by the IAEA, specific objectives of the Phase I field trial, the need to constrain scope of Phase I to essential elements, and the WFFF deployment location. Descriptions of the prototype hardware and software are presented in this section.

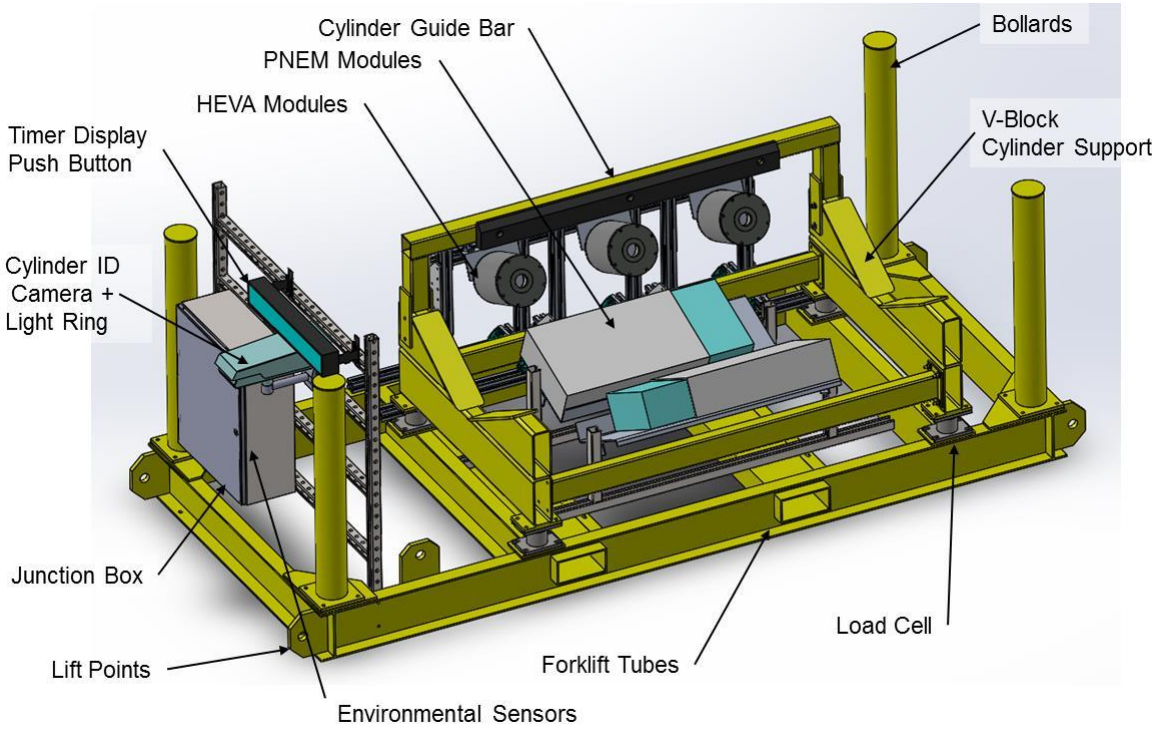


**Figure 18.** Schematic of the UCVS field prototype hardware design.

The prototype design described below does differ from the UCVS User Requirements in several regards:

- Includes environmental sensors (for outdoor field trial) and load cells for gross cylinder mass
- Current version supports only Type 30B cylinders
- No automated cylinder ID technology (nameplate camera images are collected)
- No tamper-indication provisions on instrument, conduit, or enclosures
- No insistence on certified IAEA components (e.g., cabinet, power supplies)
- No real-time automated occupancy detection
- No digital signing of data
- No real-time analysis or state of health (SOH) monitoring
- No formal integration with IAEA data review and analysis software (e.g., iRAP)

## 6.1 Hardware

### 6.1.1 Skid and Mechanical Supports

The mechanical design of the UCVS prototype platform was based on the specific requirements of WFFF deployment location, and a desire to incorporate sufficient adaptability to support (potential) subsequent trials with different characteristics and constraints. Key design characteristics of the UCVS skid and associated mechanical supports follow.

- Provisions for movement via forklift or crane
- Cradles capable of supporting Type 30B cylinders, but the cradle-mounting design is easily adaptable to either/both Type 30B and Type 48 cylinders in the future
- Fixtures for HEVA and PNEM detector modules, load cells, and a junction box
- Junction box to provide environmental protection (National Electrical Manufacturers Association [NEMA4] specifications) for power supply and cabling interconnects
- Fixture for the high-resolution camera used to collect nameplate images
- Conduit and harnesses to protect cabling between sensor modules and junction box
- Shim plates for leveling
- Protective bollards on all four corners
- Physical envelope: $3.048 \times 1.37 \times 1.37$ $m^3$
- Total mass (without cylinder): 1134 kg

### 6.1.2 NDA Modules

Full descriptions of the HEVA and PNEM modules are provided elsewhere; parameters relevant to the platform and data acquisition cabinet are provided here.

- HEVA detector modules (three), including environmental protection
  - Power: power over Ethernet (POE)
  - Communications: Ethernet
- PNEM detector modules (two) including environmental protection
  - Power: 12VDC and 1500VDC (100 μA max)
  - Communications: digital (transistor-transistor logic [TTL])

### 6.1.3 Load Cells

An independent measure of total uranium mass is an important capability in the UCVS concept. Assuming a tare weight for the declared cylinder is known, a measurement of gross cylinder mass using load cells should allow the IAEA to calculate the total $UF_6$ mass and therefore, the total uranium mass. To illustrate this capability, gain experience with the integration and calibration of load cells, and to provide

adaptability for potential future field trials, load cells were incorporated in the UCVS prototype design. Characteristics of the load cells and associated data acquisition are below.

Four Mettler Toledo 0970 Ringmount Weigh Modules were used. Each weigh module included a 5000 kg load cell. The load cells were connected to a junction box installed on the skid. The junction box distributed power and summed the response voltage. The junction box was connected to a IND780 Weighing Indicator, which was mounted on the top of the UCVS Cabinet. The IND780 weighing indicator was connected to the main 120V UCVS cabinet power distribution. The IND780 distributed nominally 10V power to the junction box, digitized the response voltage, and converted it to engineering units. The weighing indicator communicated with the collection computer using the ModbusTCP industrial Ethernet protocol. Figure 19 shows the load cell and weighing indicator.

Parameters are:

- Load Cells: 4 × Mettler Toledo 0970 Ringmount Weigh Modules each with a 5,000 kg load cell
- Standard Mettler Toledo junction box
- IND780 Weighing Indicator with ModbusTCP communications card
- Communications:  ModbusTCP

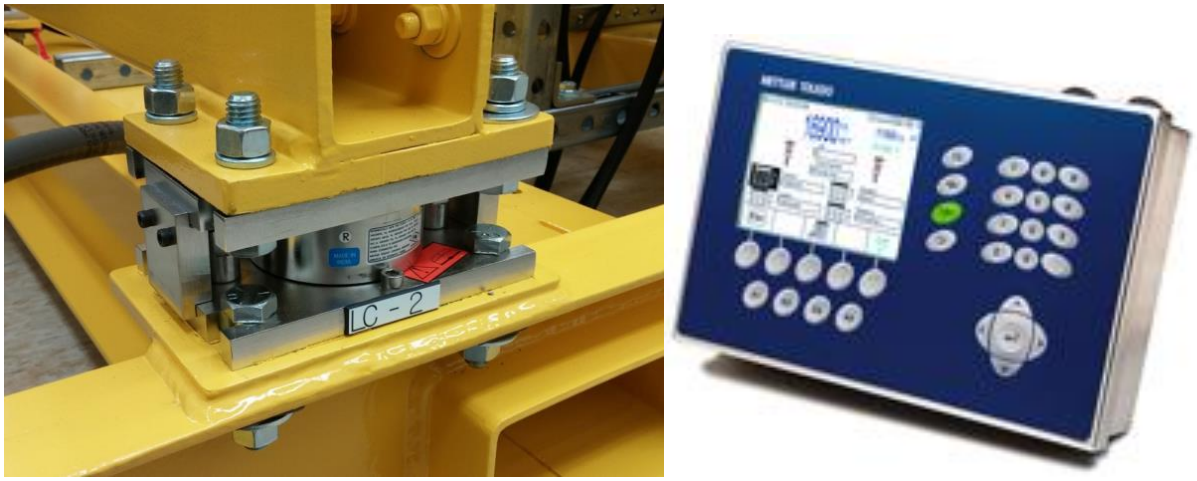


**Figure 19**. The load cells on the platform (left) and IND780 Weighing Indicator (right).

### 6.1.4 Operator Interface

The process to define a user interface for the WFFF field trial sought a balance among the following: the specific operational processes and physical layout at WFFF, a need to avoid scope creep and over-engineering in hardware and software for an initial prototype, a desire for adaptability for potential future field trials, and the IAEA's operational concepts for unattended monitoring systems. In consultation with various stakeholders, primarily WFFF, it was decided that a combination of a push-button and a timer display mounted on the assay platform was appropriate. The parameters are:

- Push button (shown in Figure 20)
  - Interface: Dry Contact switch connected to Phoenix Contact

- Timer display: AutomationDirect ViewMarq NEMA 4 (0 to 60°C, 5 to 95% relative humidity)
  - Power: 24VDC
  - Communications: ModbusTCP
- Digital Logic Controller: Phoenix Contact ModbusTCP bus coupler with eight digital inputs and four digital outputs (Phoenix Contact part number 2703981) with an additional analog output terminal block (Phoenix Contact part number 2700775), shown in Figure 21
  - Power: 24VDC
  - Communications: ModbusTCP

**Figure 20**. Push button (green, upper right) and timer display.

**Figure 21**. Phoenix Contact remote input output module with extra analog output terminal block.

### 6.1.5 Cylinder Identification Camera

Research and development programs in IAEA Member States and Member State Support Program projects have been pursuing cylinder identification technologies for a number of years. Candidate technologies for cylinder identification include barcode readers, image-based optical character recognition, image-based feature matching, active and passive radiofrequency identification, and laser-based surface measurement systems. While the UCVS field prototype developed in this project could

ultimately provide a platform for the testing and evaluation of mature, field-ready cylinder identification technologies, it was deemed outside of UCVS Phase I to integrate and test those technologies.

In this field trial, the primary role of the cylinder-identification camera was to confirm operator declarations for cylinder ID, particularly as needed to resolve data discrepancies or when the occupancy button was not pushed by the operator. The cylinder ID camera was mounted on the cylinder platform near the junction box and had a small field of view to capture images of the valve end of each cylinder, including the nameplate. A series of images at varying light intensities was automatically captured when the operator pressed the push button. These images are stored on the UCVS computer and can be viewed with any standard commercial-off-the-shelf (COTS) image viewing tool. Figure 22 shows the infrared (IR) light panel with the camera behind it.

**Figure 22**. Infrared Light Panel with high-resolution camera behind it.

Parameters for the camera are:

- Camera: COTS high-resolution
  - Model: Axis P1428E Network Camera (Figure 23)
  - Resolution: 8.3 MP
  - Power: POE
  - Communications: Ethernet.

**Figure 23**. Axis P1428E[1].

Parameters for the lighting are:

- Lighting: infrared
  - Model: SmartVision Lights, DLPW-H67-300x300-850 (Figure 24)
  - Power: 24VDC
  - Communications: Intensity controlled with analog output of the Phoenix Contact device.

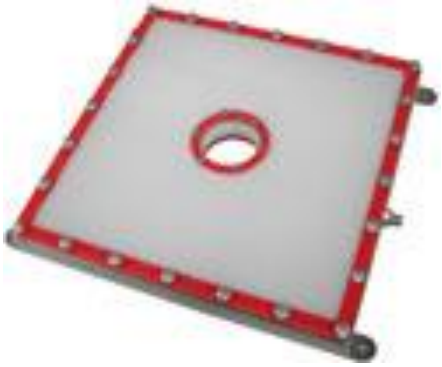

**Figure 24**. SmartVision Lights, DLPW-H67-300x300-850[2].

Parameters for the imaging are:

- Imaging sequence: multiple images with different lighting conditions, triggered by button push (color image with ambient light, monochrome image with the IR filter removed with light intensity of 0, 25, 50, 75, and 100%)
- Software: JPEG images could be viewed with standard COTS viewing tools.

### 6.1.6 Area Surveillance Camera

A second camera was mounted on a wall a few meters behind the platform to provide surveillance of the area in and around the UCVS prototype. In an actual IAEA unattended monitoring system installation,

[1] http://www.axis.com/us/en/products/axis-p1428-e
[2] http://smartvisionlights.com/products/diffuse-ring-light-panels

such a camera would be used to detect and deter tampering, and to document nearby personnel or cylinder movements that might perturb the UCVS scan. In the WFFF field trial, it was used only for the latter. Activities of particular interest include the unloading process from inbound overpacks, the loading status of the empty heels trailer just behind the prototype, and the movement of cylinders to/from the accountancy scale near the prototype. Parameters of the system are:

- Camera
  - IAEA's DCM-C5, hereafter Next-Generation Surveillance System, "NGSS" (Figure 25)
  - Resolution: 1.3 megapixel images
  - Power: 24VDC
  - Communications: Ethernet
- Lighting: none
- Imaging Sequence: 1 image per minute (no coupling to push-button)
- Software: IAEA's MPEG2 graphical user interface (GUI) viewing software.

**Figure 25**. Deployment location for the area surveillance camera (left) and NGSS (DCM-C5) camera shown with front back and top panels open (right).

## 6.2 Environmental Sensor Module

An environmental sensor module was included to record ambient conditions during the trial and to support the analysis of long-term stability with temperature, pressure, and humidity. This module (Figure 26) was mounted on the wall near the platform (near the Scene-Monitoring Camera). Parameters include:

- Model: OMEGA iBTHX-W-5 measuring pressure (mBar), temperature (°C), humidity (%), dewpoint (°C)
- Power: 12 VDC
- Communication: Ethernet
- Location: extending from junction box on north curtain wall

The OMEGA porous polyethylene probe cap for wet environments (iP-PCI-10P) was placed on the environmental sensor head to prevent damage to the sensor from rain. The north curtain wall is somewhat covered by roof overhang, but winds may blow rain sideways into the UCVS components.

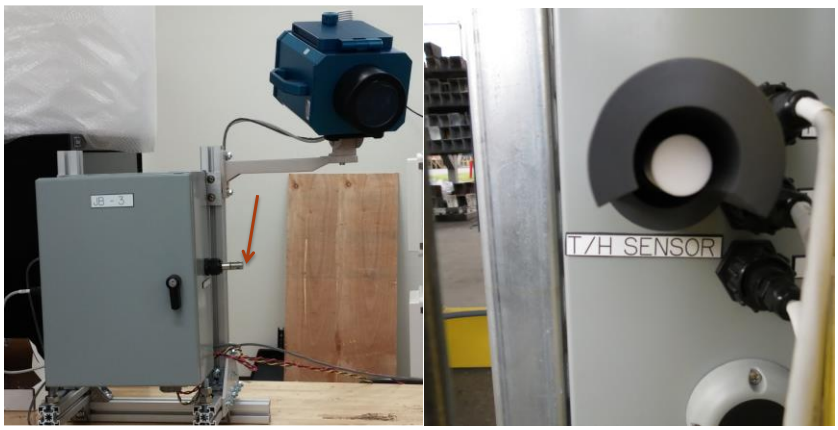


**Figure 26**. Left: Environmental sensor (red arrow) on junction box of the Scene-Monitoring camera. Right: Polyethylene cap and additional "umbrella" over the sensor head for protection from rain and sun.

## 6.3 Data Acquisition Cabinet

The data acquisition cabinet (DAQ) was located in the WFFF's accountancy scale shack (Figure 27). It contained power distribution component, the data collection computer and backup data storage, shift register for PNEM acquisition, uninterruptible power supply (UPS) and provisions for data viewing and download by UCVS team members. Parameters for the cabinet and components are:

- Cabinet
  - Model: BUD ER-16622-RB
  - Nominal dimensions: 1.2 m (high), 0.56 m (wide), 0.79 m (deep)
- UPS
  - Model: APC Smart-UPS SMX2200RMLV2U
  - Output Power Capacity: 1850W/ 2200VA
  - Nominal Output Voltage: 120V
  - Input Voltage: 120V @ 50/60 Hz
- Computer
  - Model: Industrial Computers INC. (ICI) 4UXEONFRXT
  - 4U Dual Intell Xenon 10 – X8 piE
  - 48-cm (19-in.) Rack Mount Frame
  - 4 GB DDR3 Reg/ECC/SR, 500GB SATA3 Hard Drive
  - CD/DVD-RW Drive

  - Raid 1 Mirroring with four 500GB redundant Drives
  - Windows 7 Pro – 64 BIT
- Power Supply- 12/24V
  - Model: Altronix Maximal 133$^{RD}$
  - Rack Mount
  - Input: 115 VAC, 60 Hz, 3.8A
  - Outputs: 12VDC or 24VDC @ 12A total current
    - Power Supply #1: 12VDC @ 6A or 24VDC @ 6A
    - Power Supply #2: 8 outputs: 12VDC @ 6A or 24VDC @ 6A
- Power Supply – 48V
  - Model: Innovative Circuit Technology (ITC)  ICT690-48S
  - Rack Mount
  - Input: 100-265VAC @ 50/60 Hz
  - Output: 55.2 VDC @ 12.5 amp continuous
- POE Switch
  - Model: TP-Link TL-SF1008P
  - 8 10/100/1000Mbps RJ45 port
  - With four POE ports
- JSR-12 Neutron Coincidence Analyzer
  - Model: Canberra JSR-12
- LCD + Keyboard Console
  - Model: APC AP5717
  - 43-cm LCD console
  - 1U Rack Mount
- VPN & Bridge/Modem – See Section 6.4 Communications for descriptions
- Scale Display
  - Model: Mettler Toledo IND 560 Controller with 0970 Load Cells
  - See Section 6.1.3 Load Cells for additional information.

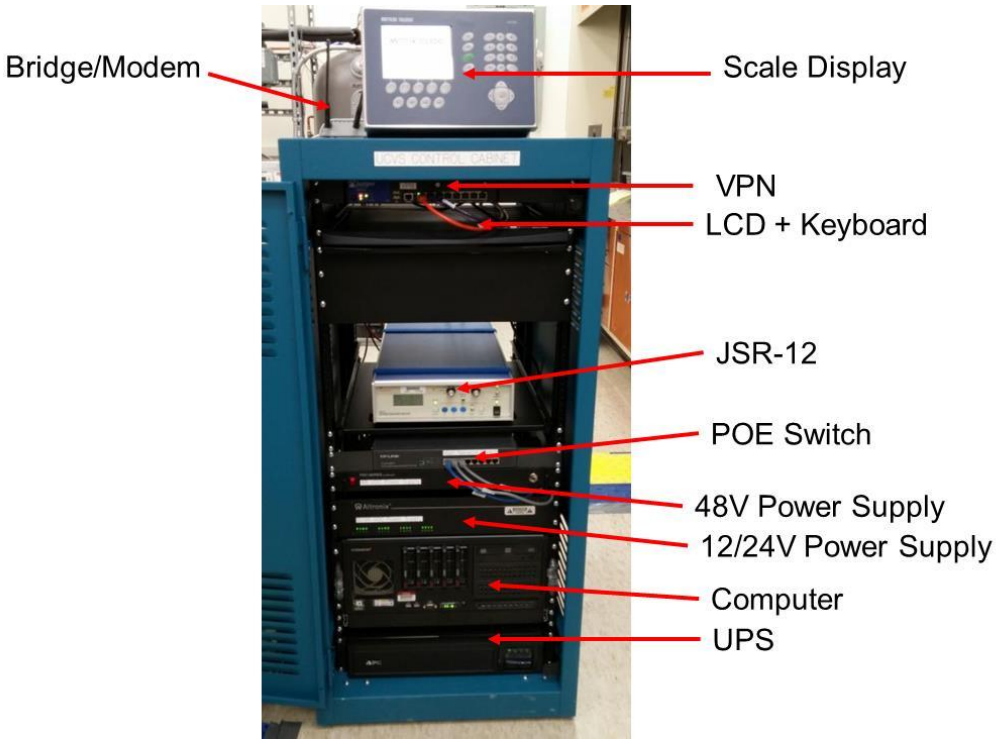


**Figure 27**. Data acquisition cabinet for UCVS field prototype.

## 6.4 Communications

Remote data transmission permitted researchers to retrieve data in a timely manner and diagnose issues with fewer disruptions to the Westinghouse site and staff (Figure 28). Parameters are:

- Security Appliance: Juniper SRX210
  - Power: 12VDC provided by dedicated transformer
  - Location: In cabinet.
- Cellular Link:
  - Juniper CX111 with Juniper CX-MC200LE-VZ cellular modem.
  - Power: 12VDC provided by dedicated transformer
  - Location: On top of cabinet.

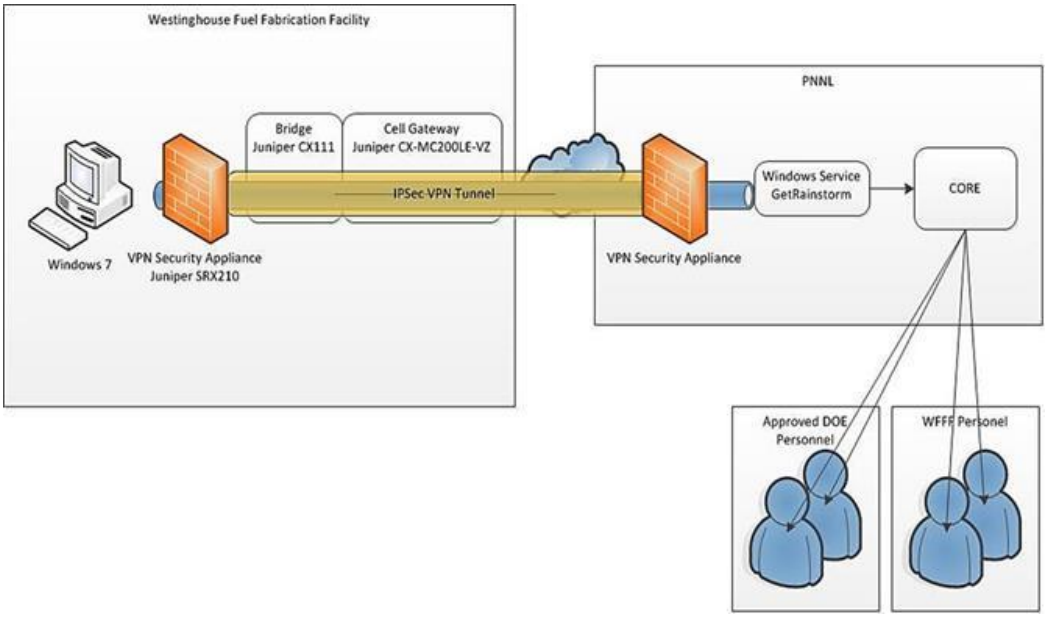


**Figure 28**. Off-site communication was enabled using a Juniper SRX210 with CX111 bridge and CX-MC200LE-VZ cellular modem.

## 6.5 Software

The software for UCVS Phase 1 was developed with simplicity and modularity in mind, and a recognition that the IAEA (and Euratom) have existing high-level remote monitoring and inspector review software. For the UCVS field prototype, a relatively simple supervisory control approach was adopted in which the individual data acquisition modules (DAQs) were run as separate services (Figure 29). No attempt was made at an integrated data acquisition and analysis software solution.

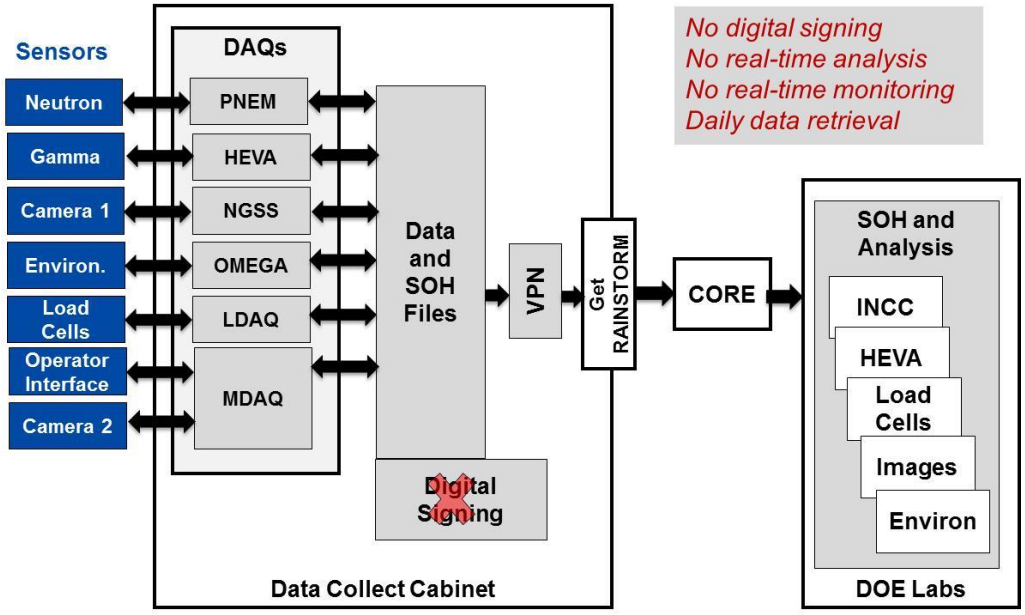


**Figure 29**. Conceptual schematic of the UCVS software architecture.

### 6.5.1 PNEM

The PNEM software is all based on standard IAEA software for unattended monitoring systems. Multi-Instrument Collect (MIC) acquires data continuously from the shift register. It produces three files per day including a binary data file (.JSR) and two plain text log files (.PFM and .CEV). Radiation Review is a graphical program used to display and analyze safeguards data. For the UCVS field trial, it was used for offline analysis of the data files generated by MIC. Radiation Review has a "Determine Measurements" feature that allows it to automatically identify cylinder occupancies and generate .NCC files over those periods. Alternatively, the user can also define a time window for analysis manually using the graphical interface. The .NCC files are then read by the IAEA Neutron Coincidence Counting (INCC) software to calculate the singles and doubles counting rates for each cylinder. A summary of the results can be output from INCC as a .CSV file. For the field trial, count rates and calibration curves were analyzed offline. In practice, for verification measurements, INCC can store multiple calibration functions (for singles and doubles), calculate the estimated $^{235}$U mass and enrichment of each cylinder, and calculate differences from the operator declarations. The PNEM software process flow is shown in Figure 30.

MIC, Radiation Review, and INCC are redistributable and available for download on GitHub (https://github.com/hnordquist).

Requirements/Dependencies are: 32 bit Win 7, Visual C++ Redistributable.

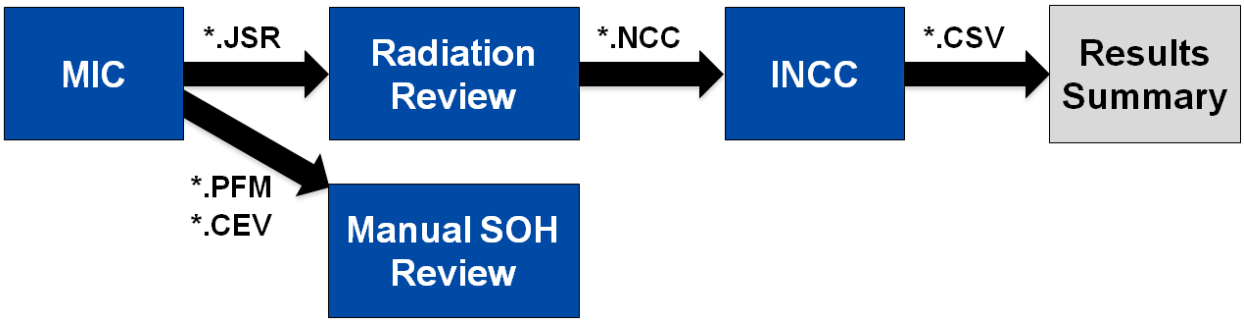


**Figure 30**. Process flow for PNEM software.

### 6.5.2 HEVA

The primary function of PNNL's HEVAOspreyDaq software is to acquire pulse-height spectra and single-channel analyzer (SCA) data from the three Canberra Osprey units attached to the NaI(Tl) gamma-ray spectrometers. Pulse-height spectra are acquired at one-minute intervals, as defined in the HEVA module characterization study (Zalavadia et al. 2016). The SCA data are collected in six energy windows with (approximate) energy bounds set to reflect gross count rates (40 to 10,000 keV) and key ROIs: 186 keV ROI (145 to 220 keV), 765 keV ROI (725 to 880 keV), 1001 keV ROI (950 to 1050 keV), 3-5 MeV, and 5-8 MeV. SCA data are recorded at 1-second intervals. The pulse-height spectra are saved in .N42 format; the SCA data are included in that file. Raw data files generated by the HEVA DAQ are saved to an output folder, which is created at the start of each day, and contains the date as part of its name.

The Ospreys are connected to the DAQ computer using Ethernet, and are assigned fixed Internet Protocol (IP) addresses. To provide the user flexibility in choosing the IP addresses of the Osprey, the acquisition intervals and the many acquisition parameters that the HEVAOspreyDaq software supports, an XML config file is used. Errors are logged to a log file. If an Osprey does not respond during an acquisition cycle, but subsequently starts responding again, the OspayDaq software can log the situation and recover from it. The code is written in C++ using Visual Studio and intended to run on a 32 bit Windows 7 machine. The Osprey drivers and Visual C Redistributable are expected to be available on the system.

Requirements/Dependencies are: 32 bit Win 7, Visual C++ redistributable, Osprey driver version 1.0.4, Firmware Version 1.04.1408.15.00, FPGA Version 0349.

### 6.5.3 Environmental Sensors

The EnvSensor DAQ software acquires environmental data from the Omega iBTHX-W temperature/pressure/humidity/dewpoint sensor. The device supports HTTP Get commands, implemented via a HTTPGet utility provided by the vendor, to acquire data. The DAQ developed by PNNL is essentially a smart wrapper around this utility to support a config file for input, log file for output, and file management for the daily output file.

The software style is quite similar to HEVAOspreyDaq and the user creates a config file, which provides the IP address/port number of the sensor and the acquisition interval. A new file is created at the start of each day and the environmental data are written to it at a user selected period.

Requirements/Dependencies are: 32 bit Win 7, Visual C++ Redistributable, HTTPGet.exe, which is a utility provided by the manufacturer, and must be installed on the system.

### 6.5.4 IAEA NGSS Online

The DCM-C5 camera (NGSS) was configured to take one picture per minute and stored the images as 1 MPG per hour. The IAEA's NGSS-Online software was installed on the data collect computer and pulled the MPGs stored on the DCM-C5's SD card to the collect computer. The IAEA's Mpeg2 GUI software could be run on the data collect computer or on workstations at the DOE national laboratories to split the MPGs into their respective individual image files and review them.

### 6.5.5 Modbus TCP Data Acquisition (IMDAQ)

ORNL developed the MDAQ application in C# to communicate with the Phoenix Contact digital logic controller, and to trigger various actions based on user input. The MDAQ program communicated with the COTS high-resolution camera, the Phoenix Contact device, and the LED display panel. The program also contained logic to recover from a loss of communication with any of the hardware devices. The industrial push button and IR illuminator were connected to the Phoenix Contact device. A diagram of these interactions is included in Figure 31 below.

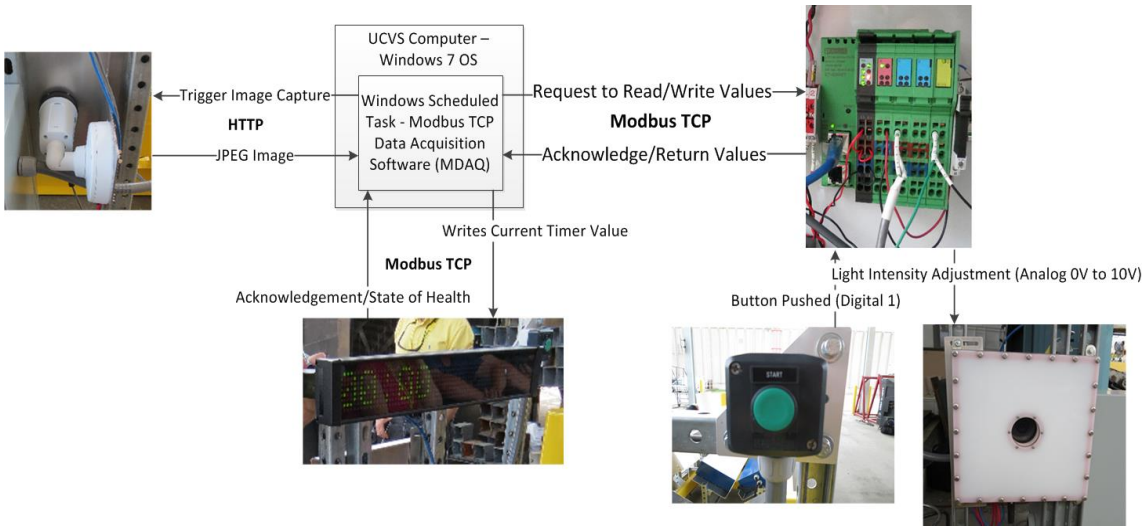


**Figure 31**. MDAQ Software Interaction Diagram.

Typical Modbus communications involve reading and writing to various registers exposed on a device to trigger various actions, or monitor for certain conditions. For Modbus Transmission Control Protocol (TCP), these read and write operations are wrapped in TCP/IP packets to be sent over an Ethernet network. The MDAQ software application used this paradigm by constantly monitoring the registers on the LED display, as well as the registers on the Phoenix Contact device. The industrial push button would indicate that it was being pressed by allowing a digital input line on the Phoenix Contact device to be connected to a 5V source. This change would then be indicated in the Modbus registers of the Phoenix Contact device and sensed by the MDAQ application when it checked those registers. The button press then triggers several actions.

First, the time of that button press is recorded by the MDAQ application to support off-line data analysis. Then the application starts an internal countdown timer, and writes the time remaining in that timer to the LED display several times per second to indicate the time remaining to the operator. The button press also triggers a series of images to be captured with the COTS high-resolution Cylinder ID camera.

The COTS Cylinder ID camera has an outward facing web interface that includes an application program interface (API) which can be used by other applications to change camera settings or capture images if they access the camera with the proper username and password. When the start button is pressed, the MDAQ application sends a series of image capture requests to the Cylinder ID camera API. The MDAQ application then receives a stream of bytes representing the image captured by the camera using the camera's current configuration settings and writes that image to disk. After the first image is captured, the MDAQ application removes the IR cut filter from the Cylinder ID camera by driving one of the digital output lines of the Phoenix Contact controller high, and turns on the IR illuminator. The application then continues taking a series of images at 25, 50, 75 and 100%IR light intensities. The IR light intensity is controlled through the analog output module of the Phoenix Contact device. Once these images are captured, the IR illuminator is turned off, and the IR cut filter is put back in place.

In future deployments for the UCVS, additional modules to monitor for environmental conditions or trigger measurements could be integrated into the Phoenix Contact device and controlled by the MDAQ program.

### 6.5.6 Load Cell Data Acquisition

ORNL developed the Load Cell Data Acquisition (LDAQ) application in C# from the same codebase as the MDAQ application. The LDAQ program communicates with the IND780 Weight Indicator over Modbus TCP. The weight indicator converts the summed response from the load cells into engineering units and updates its Modbus registers with that information periodically. The LDAQ application then reads these registers several times per second, and writes that engineering value to a file at a user-defined interval (which was set to 1 minute for the UCVS field trial). The LDAQ application also contains disaster-recovery logic to recover from communication errors. A diagram of these interactions is included in Figure 32.

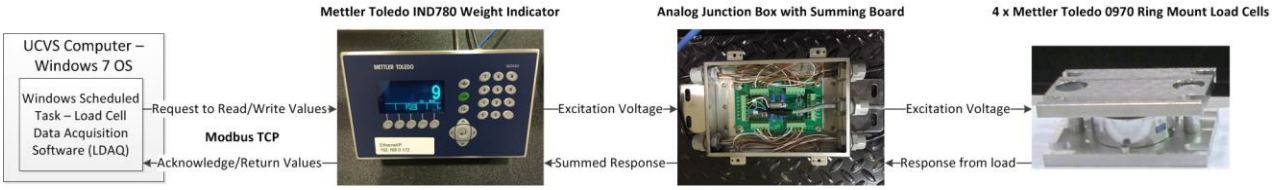


**Figure 32**. LDAQ Software Application Interaction Diagram.

In the future, the LDAQ application could easily be integrated into the MDAQ software application. This was not included as part of the MDAQ software application for ease of troubleshooting during the field trial.

### 6.5.7 Remote Transmission

Typical IAEA unattended and remotely monitored systems have a data collect computer located near the sensors. This local data collect computer interfaces with the various sensors and stores the raw or processed data. The UCVS prototype followed this model. Data were collected on Windows 7 workstation in the cabinet. Secure remote transmission of the data was provided using an IPSec VPN tunnel over a cellular link. A Juniper SRX210 security appliance was used with a Juniper CX111 bridge and CX-MC-200-LE-VZ cellular modem at the WFFF. The other end of the IPSec VPN terminated on a Cisco ASA security appliance.

The IAEA has begun adopting the Real-time And INtegrated STream-Oriented Remote Monitoring (RAINSTORM) protocol to transport data from remote sites to headquarters (Morgan, 2014). The RAINSTORM protocol was configured on the data collect computer at WFFF. The IAEA's GetRainstorm application was installed and configured on a workstation at PNNL. GetRainstorm pulled data through the IPSec VPN from WFFF to the workstation. Scripts were then developed to copy the data to the Common Operating and Response Environment™ (CORE) repository (see below).

### 6.5.8 Data Archiving and Sharing

UCVS Phase I used an existing data archiving and sharing framework called the CORE (http://analytics.pnnl.gov/docs/CORE_Flier_v3.pdf). This framework has been developed for over a decade at PNNL to enable automated data collection and processing from field measurements. It consists of a database and web interface and requires two-factor authentication for non-PNNL users. The data are available from a web interface and in the case of the UCVS field trial, were configured to store zipped files containing all of the data collected from the instrument in a given day. Figure 33 is an example screenshot of the UCVS Core web interface. Each file has a zipped file upload with a number of files that was typically around 1441. The number fluctuated depending on whether the occupancy button was pressed or if some files were missed in previous uploads due to transmission problems. For instance, note that several dates before 4 January 2016 had zero files and that date had 8854 files, indicating that there was some transmission issue.

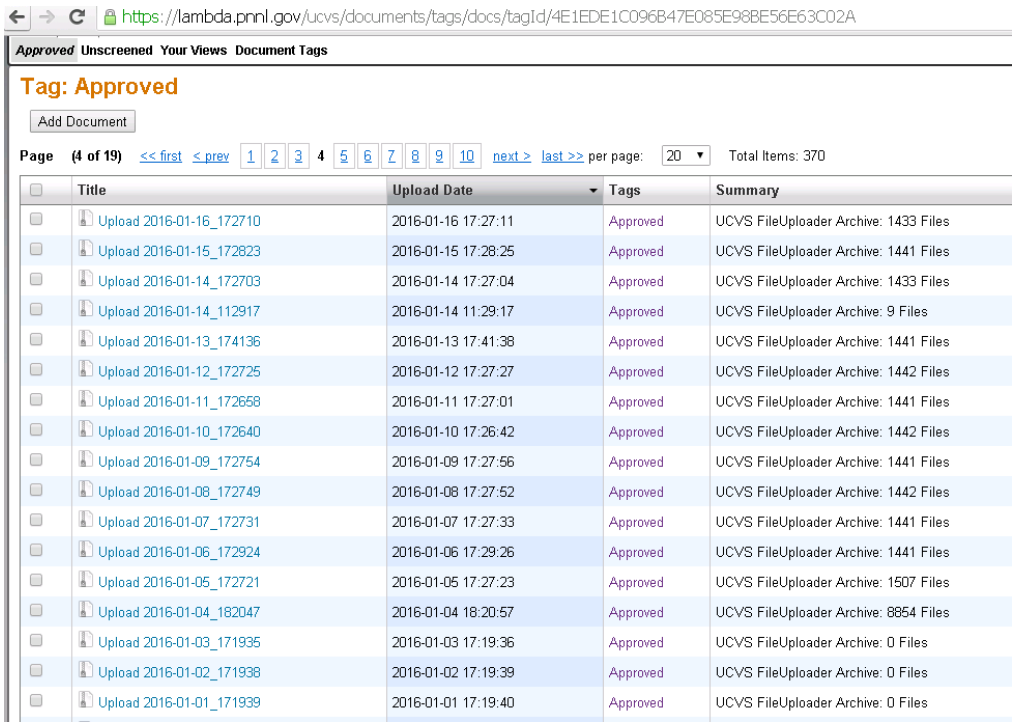


**Figure 33**. Screenshot of the CORE web interface as implemented for UCVS Phase I.

Each zipped folder is approximately 24 MB and 108 MB unzipped for a day with no occupancies. On days with cylinder occupancies with a push-button trigger, the sizes are somewhat larger due to the additional data associated with each occupancy (e.g., nameplate images). Figure 34 shows the breakdown of disk usage by the different UCVA sensor systems. The HEVA NDA system requires by far the largest fraction of the disk storage. Each HEVA file is approximately 70kB; three such files (three modules) are created every minute of acquisition time.

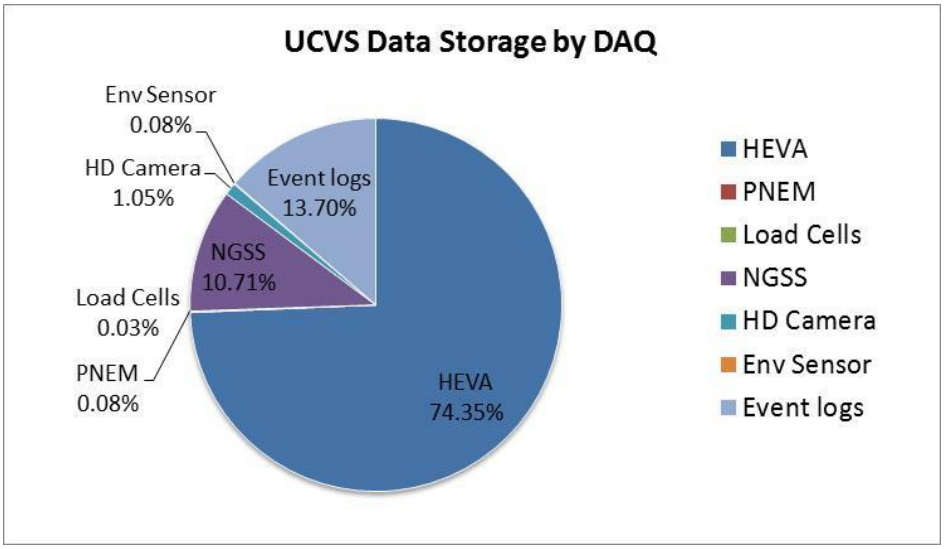


**Figure 34**. Distribution of data storage utilization during the UCVS field trial. Over 11 months of data acquisition, the total uncompressed disk storage was ~73 GB.

# 7.0 Field Trial: Overview

Previous field campaigns with HEVA and PNEM were based on proof-of-principle prototypes operating in an attended mode and relatively small numbers of cylinders. Further study of the NDA signatures and methods, longer field trials, and large, diverse cylinder populations, along with refined versions of HEVA and PNEM hardware and software were needed to enable a more definitive evaluation of NDA capabilities relevant to unattended cylinder verification. Per the original SP-1 guidance, the IAEA was also interested in a preliminary evaluation of operational factors, stability, maintainability, and estimated cost associated with a UCVS prototype that includes NDA, surveillance, data acquisition, and remote monitoring capabilities.

During the latter half of 2015 and early 2016, DOE staff members, the UCVS team and Westinghouse collaborated to define when, how and where a UCVS field prototype could be deployed at WFFF. The facility was attractive for many reasons, not the least of which was Westinghouse's willingness to host previous Next Generation Safeguards Initiative (NGSI) technology trials, and their interest in supporting the global nonproliferation regime more generally. In terms of the facility itself, the relatively high rate of cylinder processing (typically more than 50 per month) offered the opportunity for a large population of cylinders to be studied. Unfortunately, the diversity of the inbound cylinders processed by WFFF is relatively limited: no Type 48 cylinders, and very few cylinders at enrichments of natural and below.

Based on discussions among the IAEA, WFFF, the UCVS project team and other key stakeholders, the following objectives were defined for the Phase I field trial at WFFF:

1. Perform functional testing, in a realistic operational environment and over an extended time period, of a UCVS prototype that integrates NDA instrumentation, a surveillance camera, and a data acquisition system representative of IAEA deployments.
2. Assay of many (ideally, several hundred) "typical" Type 30B cylinders with enrichment ranging from ~0.2 % to 5.0%, to support a comparative study of the PNEM and HEVA methods for the determination of $E_{235}$, $M_{235}$, and $M_U$.
3. Assay a subset of the larger "typical" cylinder population on multiple occasions and under different handling conditions, to support study of the NDA Fingerprint concept.
4. Perform high-fidelity measurements of a few select typical cylinders to support simulation benchmarking.
5. Assay a small population of atypical cylinders that, due to their specific characteristics, are likely to challenge NDA methods.
6. Improve understanding of how radiation backgrounds (e.g., from cylinders stored or moving nearby) are likely to affect the performance of the NDA methods and calibration protocols.
7. Solicit feedback and recommendations from a facility operator about potential process-control impacts and the international safeguards role of UCVS.

The sections that follow describe the prototype deployment location at WFFF, the various types of cylinder scans performed during the field trial to address specific technical questions posed by the IAEA and the project team, a typical cylinder scan sequence, and activities in the vicinity of the prototype location that can lead to perturbed cylinder occupancies for PNEM, HEVA or both.

## 7.1 Prototype Deployment and Scan Procedures

The UCVS field prototype was sited near the WFFF accountancy scale, between the receiving and shipping bays, as shown in Figure 35. This location was chosen based on several factors: anticipated gamma and neutron background levels and their variability, desire to minimize impact on WFFF operations (especially fork-truck operations near the scale), and environmental effects. A brief description of WFFF's cylinder handling practices, and the corresponding UCVS siting considerations is given here.

At least one and sometimes two WFFF staff members perform the cylinder-handling operations on each weekday morning. Full cylinders (4 to 6 depending on the trailer used for the daily receipt) are lifted by crane from transportation overpacks on the trailer in the receiving bay (left) onto the WFFF accountancy scale (between two blue curtain walls, near scale shack in Figure 35). WFFF personnel record the accountancy scale value using an interface inside the scale shack. The cylinder on the accountancy scale is then removed via fork truck and the next cylinder is transferred via crane from the trailer to the scale.

Empty cylinders (either clean or heeled) are loaded, via crane, onto trailers in the shipping bay (right). Up to 30 cylinders are loaded on the trailer, over the course of 1-2 weeks. A trailer filled with heeled empties can present challenging background levels for the UCVS, primarily for the gamma-ray-based HEVA method. Fortunately, the background from the shipping-bay trailer is generally constant during each daily batch of UCVS assays since empties are not typically loaded on the trailer during WFFF's unloading of new, full cylinders.

While the empty-cylinder trailer and emissions from cylinders on the accountancy scale favored siting the UCVS station further away from those background sources, weather effects encouraged a location well inside of the roofline. To avoid direct rainfall on the UCVS prototype, a location approximately 3 m from the end of the blue curtain wall was selected.

All cylinder movements in the vicinity of the UCVS Assay Platform can introduce background variations that could perturb the neutron and gamma-ray signatures collected by PNEM and HEVA, and therefore degrade the measurement results for a given cylinder occupancy. Increasing distance between the UCVS prototype and nearby cylinders, and reducing the duration of the movements during a UCVS assay is desirable. The UCVS team worked with WFFF to define a cylinder-handling sequence that sought to minimize ambient background changes and impact on WFFF operations (see Section 7.1.2 through 7.1.4).

The UCVS prototype location at WFFF is not wholly representative of envisioned IAEA deployments. First, IAEA deployments are expected to be inside an enrichment or fuel fabrication facility. Second, the intensities and variation of the ambient background from nearby cylinder storage and cylinder movements may have been higher during the field trial than will be realized in permanent installations. Therefore, the findings of the field trial may provide a "worst-case" scenario for the study of UCVS NDA accuracy and precision, the NDA Fingerprint concept, and environmental effects on instrument drift and calibration.

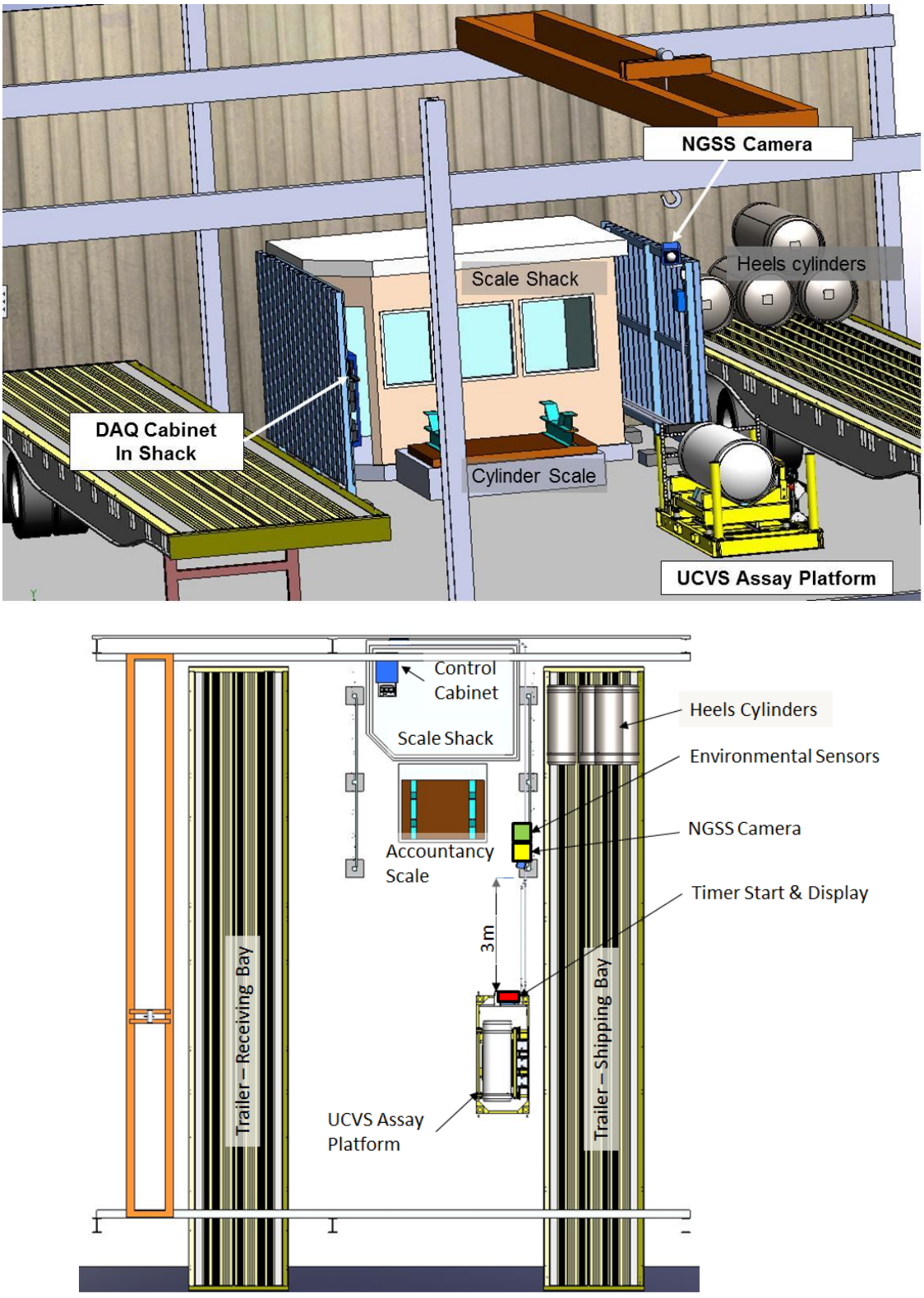


**Figure 35**. Top: Depiction of UCVS field prototype location (cylinder on yellow platform) at WFFF, including the receiving (left) and shipping bays (right), accountancy scale (light blue stand) and scale building. Bottom: plan view showing location of the assay platform and other UCVS prototype components.

The prototype UCVS was installed at the WFFF April 7-10, 2015. Figures 36-38 are photos from the installation. During the installation visit, basic functionality was tested for all components and processes: continuous collection of data by HEVA and PNEM; collection of data at prescribed intervals or triggers for cameras, IR lighting, and environmental sensors; local storage of raw data in the secure instrumentation cabinet, with redundant storage; and automatic transfer of a subset of the raw data (as approved by WFFF's security review) to the CORE system at PNNL. After functional testing and calibration were completed, cylinders scans began. A total of 16 cylinders were assayed during the last two days of the deployment visit.

**Figure 36.** Installation of the HEVA (left) and PNEM (right) NDA modules on the platform.

**Figure 37**. Forklift placement of the platform at the deployment location (left); placement of first cylinder on the UCVS prototype platform using the overhead crane (right).

**Figure 38**. Area surveillance camera mounted on the curtain wall (left); environmental cover intended for placement on UCVS after each measurement sequence is completed (right).

### 7.1.1 Cylinder Scan Variants

To meet the high-level objectives of the UCVS field trial, several different types of cylinder assay were defined, as described below.

***Typical Cylinder Scans***

- Anticipated total number of cylinders: several hundred
- Characteristics: full Type 30B cylinders, natural-origin material (no recycled uranium or re-enriched tails)
- Number of scans per cylinder: 1
- Orientation: cylinder valve toward guard scale shack (typical direction)
- Nominal occupancy duration: 7 minutes

***Atypical Cylinder Scans***

- Anticipated number of cylinders: 10+
- Characteristics: for example, diffusion plant, reactor recycle, tails recycle, partial fill
- Number of scans per cylinder: 1
- Orientation: cylinder valve toward scale shack (typical direction)
- Nominal occupancy duration: 7 minutes

***NDA Fingerprint Scans***

The key question for the NDA Fingerprint concept is the consistency and reproducibility of repeated measurements on the same cylinder. Potential sources of variability to study include major geometry effects such as valve direction, minor geometry effects such as small lateral or rotational changes from

one scan to another, age effects, handling effects on material distribution inside, and ambient background effects including other cylinders or large volumes of moderating materials nearby.

- Anticipated number of cylinders: ~10
- Characteristics: typical and atypical cylinders (see this section, above)
  - Ideal Geometry Sequence: 5+ "placements" of a specific cylinder on the UCVS by the crane, in a short time period (e.g., 1 hour) and at specific position offsets (e.g., 10 cm off center) and rotations defined by UCVS team members on-site during the campaign.
  - Ideal Time+Geometry Sequence: 10+ scans separated in time by days or weeks. For example, 12 scans of each fingerprint cylinder, one every two weeks over a 6-month trial. Orientation would be same as for the typicals described above.
- Nominal occupancy duration: 7 minutes per cylinder placement.

***Benchmarking Scans***

- Anticipated total number of cylinders: ~3
- Characteristics: typical and atypical cylinders
- Number of scans per cylinder: 1
- Orientation: cylinder valve toward scale shed (typical direction)
- Nominal scan time: 30 minutes or more depending on operational constraints

### 7.1.2 Nominal Cylinder Scan Procedure

Figures 39-41 show the nominal cylinder scan procedure. Note that the benchmark and NDA Fingerprint scan procedures may differ significantly.

**Figure 39**. Retrieve a full cylinder from overpack (or other on-site location) and place cylinder on the UCVS platform using the overhead crane. For a typical cylinder scan, the valve/nameplate end of the cylinder should be facing the scale shack.

**Figure 40**. Initiate cylinder assay using the green START button on the UCVS assay platform. The remaining assay time is displayed on the digital display.

**Figure 41**. Left: Once the remaining assay time has expired, remove the cylinder from the UCVS assay platform and transfer it to the accountancy scale using the overhead crane. Right: Remove the cylinder from the accountancy scale using the fork truck before placing the next cylinder on the UCVS assay platform. Removal of the cylinder from the scale before, rather than during, the next UCVS occupancy prevents radiation background variation.

### 7.1.3 Declared Data from WFFF

Transmission of declared cylinder data from WFFF was performed using password-protected spreadsheets sent via email to the UCVS Data Team. Approximately every few weeks, WFFF provided declared data to the UCVS Data Team, for all cylinders assayed since the previous report. The data declarations were generated from a query of WFFF's accountancy system, and include data from WFFF's mass spectrometry analysis. Data fields include:

- Cylinder ID
- Shipper's facility code
- Date of receipt at WFFF
- Date and time of accountancy-scale measurement by WFFF
- Shipper's data
  - Gross mass (kg)
  - Net mass (kg)
  - Tare mass (kg)
  - U elemental percentage
  - $^{235}$U isotope mass (kg)
  - $^{235}$U enrichment (wt%)
- Receiver's (WFFF's) data
  - Gross mass (kg)
  - Net mass (kg)
  - Tare mass (kg)
  - U elemental percentage
  - $^{235}$U isotope mass (kg)
  - $^{235}$U enrichment (wt%)
  - $^{234}$U concentration (wt%)
  - $^{236}$U concentration (wt%)

### 7.1.4 Operational Experience from Field Trial

Generally speaking, the 8-month field trial at WFFF ran smoothly and according to the original planning by the stakeholders. However, a number of problems and issues arose. Descriptions and observations of those challenges are included here and may be useful to future UCVS inquiry, should the IAEA choose to continue in that direction.

#### 7.1.4.1 UCVS Hardware and Software Issues

*HEVA DAQ and Supervisory Control Software.* An issue arose with the supervisory control software in which multiple copies of the HEVA DAQ were found to be running at the same time, creating a "race" condition that led to lost data during three of the field trial days (on September 16, 21, and 30). HEVA data for 14 cylinders were lost during this time period. A solution to this problem, in the form of a Python scheduling script that reduced the frequency of checks performed by the Windows scheduler, was devised and tested, but not deployed. The logic for this decision was that modifying the DAQ software remotely, in the middle of the field trials, was deemed to be relatively risky, compared to the relatively low risk of additional data loss due to the race condition—assuming frequent monitoring of HEVA data retrievals. No further data loss occurred during the course of the trial and the solution is ready for use in the future, as appropriate.

*Load cell drift.* The UCVS platform incorporated four Mettler Toledo weigh modules with load cells specified to be temperature-compensated by the vendor. Immediately after installing the platform at the Westinghouse site, the team discovered a drift in the weight data from the load cells. The zero was slowly oscillating with a range of about 40 kg around zero in a manner that seemed correlated to temperature. ORNL visited the site with a Mettler Toledo technician to troubleshoot the problem. The technician concluded the load cells were working properly, but the drift continued. Load cell 4 was replaced and the drift issue was dramatically reduced. Weigh modules with load cells typically are installed easily and perform within specifications. This installation proved challenging, but it is unclear if the issue was caused by a load cell that had a manufacturing defect or if it was damaged during shipping or assembly. The problem seems to have been nonroutine as the most experienced Mettler Toledo technician in the region tested the load cells and found them to be working properly. For future installations, it would be valuable to install and test the load cells before they are deployed in the field.

*PNEM remote data retrieval.* The remote retrieval of the JSR files produced by PNEM and upload to the CORE site was erratic for much of the field trial. The problem is likely due to conflicts in the timing of read/write commands for the JSR files and remote retrieval process, but the issue was not resolved during the field trial. Instead, a manual retrieval via remote desktop was performed (a simple process due to the small size of PNEM data files).

*CORE and RAINSTORM conflicts.* IAEA's RAINSTORM was intended to download partial files, identify new appended data since the prior retrieval, and create a directory structure at the destination. In the WFFF field trial, the raw data files were compressed before RAINSTORM was called for retrieval. This appears to have caused problems with the data files and is a possible explanation for the PNEM retrieval issues identified above. Also, CORE's efficiency for unzipping and sharing data was laborious—improved methods should be considered for any future trials.

*Remote data transmission issues.* One party needs to be responsible for the remote data transmission system. At one point, communications failed and initial troubleshooting was not done by the same party that initially configured the system, making troubleshooting more challenging.

#### 7.1.4.2 Cylinder Handling and Ambient Conditions

*Consistent Cylinder Positioning.* No provisions for consistent lateral positioning of the cylinders were included in the UCVS prototype design. This oversight leads to additional uncertainty, for both one-time and repeated assays, due to lateral shifts of the detectors relative to the $UF_6$ volume. Future prototypes/instruments should include robust lateral positioning provisions to reduce this uncertainty.

*Inconsistent Cylinder Processing Procedure.* WFFF operators did not always follow the cylinder handling procedure described above. For example, it was not uncommon for the preceding cylinder to be left on the accountancy scale during the UCVS scan of the next cylinder. Depending on the relative enrichments of the two involved cylinders, minor perturbations on the UCVS-measured signatures may have resulted. Analysis by the UCVS team indicated that the effects were likely to be minor, and consequently were ignored.

*Bypassing UCVS.* When time or manpower was in short supply, WFFF bypassed the UCVS. The bypass rate increased over time. By early November, very few of incoming cylinders were placed on the UCVS.

*Button Push.* WFFF operators did not always push the scan start button, which meant that the camera image of the cylinder ID was not triggered. This created challenges in data reduction and troubleshooting. In the future, automated occupancy determination algorithms coupled to surveillance cameras would be advantageous.

*Heels Trailers.* The trailers on which heels cylinders are loaded, located directly behind the UCVS prototype, had a profound effect on the background count rate in the HEVA modules. Additional analysis showed, however, that these effects did not appear to have significant negative effects on the $HEVA_T$ precision or accuracy for the affected cylinders. As expected, the heels cylinders had no effect on the neutron signatures collected by PNEM and $HEVA_{NT}$, since neutron emission from heels is negligible.

#### 7.1.4.3 Other Lessons Learned

*PNEM module design.* As described in Section 7.2, the PNEM singles count rate is sensitive to nearby cylinder movements and major changes in background (the doubles count rate is not very sensitive to background variations). In order to reduce this sensitivity, the PNEM detector pods can be wrapped in a thin layer of cadmium, which will absorb thermal neutrons from the room background. The addition of cadmium would reduce the efficiency of the detectors. With the current PNEM design and a 5-minute measurement time, the singles counting statistics would likely remain well below 1%; however, it may have a more noticeable impact on the doubles counting statistics.

*PNEM operating parameters.* In this field trial, the data collection cycle time for PNEM was set to 30 seconds, which proved to be much longer than necessary. Shortening the cycle time to 5 seconds or less is recommended to provide better-defined transitions for cylinder occupancies, and thus more accurate automated event detection, as well as better outlier rejection in INCC for perturbed occupancies and spallation neutron events.

*Cylinder ID Camera Illuminator.* As mentioned previously, MDAQ controlled the IR illuminator and the cylinder ID camera to take a sequence of images at varying light intensities. The majority of full color

images did not suffer from glare or other specular reflections, and were sufficient to allow a human to confirm the identity of the cylinder. The color images benefited from a diffuse lighting environment that resulted from the orientation of the camera relative to the sun, location of the system under the canopy and the large junction box directly behind the camera blocking other light sources. Due to the dependence on installation environment, supplemental lighting should be included in future field trials until it is proven unnecessary in all cases.

## 7.2 Cylinder Populations: Overview

During the course of the 8-month field trial, over 300 occupancies were recorded for the UCVS prototype. Approximately 60 of those occupancies were specific to the NDA Fingerprint study, several were used for benchmarking simulations, and seven were characterized as atypical (see below). Of the approximately 260 typical occupancies, approximately 15 were perturbed and discarded from the analysis (see below), and another 14 cylinders were not analyzed because of the HEVA data acquisition failure. Note that the total number of cylinders received by Westinghouse during the trial was significantly higher that the populations described here because not all incoming cylinders were placed on the UCVS prototype due to operational time and staffing constraints.

The cylinders measured by the UCVS prototype during the field trial contained material enrichments ranging from natural to approximately 5 wt%. Using the declared data provided by WFFF, image data from the cylinder identification camera and raw data from the UCVS sensors, the UCVS team analyzed every occupancy to determine if surrounding activities created perturbations in the ambient background. If those perturbations were deemed sufficient to skew the HEVA or PNEM analysis, those occupancies were removed from the analysis populations. Associated imagery, raw data traces, and analyst notes were preserved for each perturbed occupancy. Examples of such data are given in Figure 42.

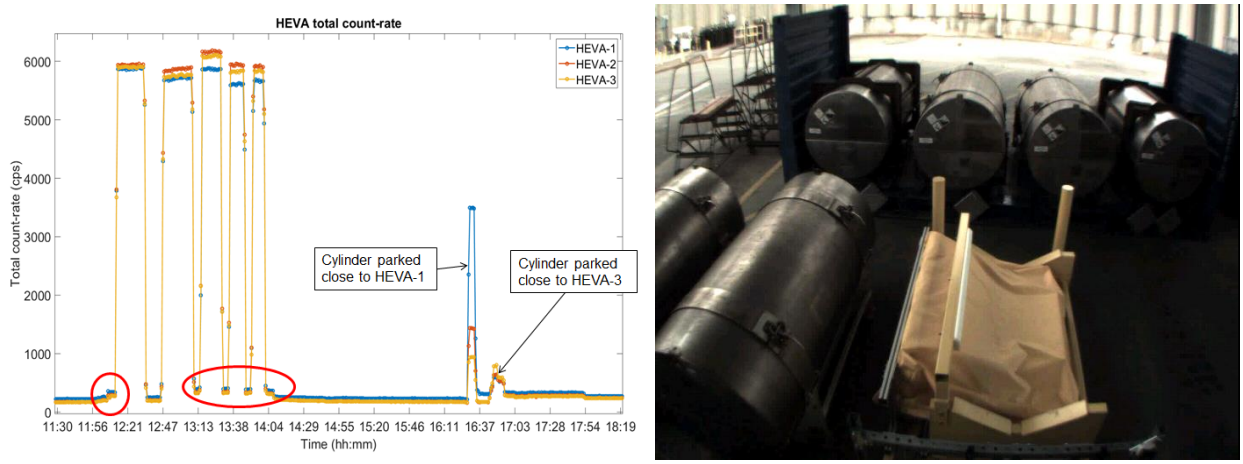


**Figure 42**. Examples of the HEVA raw data (left) and NGSS imagery used to identify perturbed occupancies. Red circles on the left indicate the effects of a cylinder on the accountancy scale during the UCVS assay.

Perturbed occupancies for PNEM were identified using the graphical interface in Radiation Review. An example is given in Figure 43, which shows a screenshot of the Radiation Review data viewer with the total counts (singles) plotted as a function of time on top and reals counts (doubles) plotted below. During a cylinder occupancy, the plateaus showing increased count rates are expected to be flat. The plot of

singles counts in Figure 43 (top pane) shows that there were likely cylinder movements nearby during the occupancy. Note that doubles counts are not highly affected by perturbations and background noise.

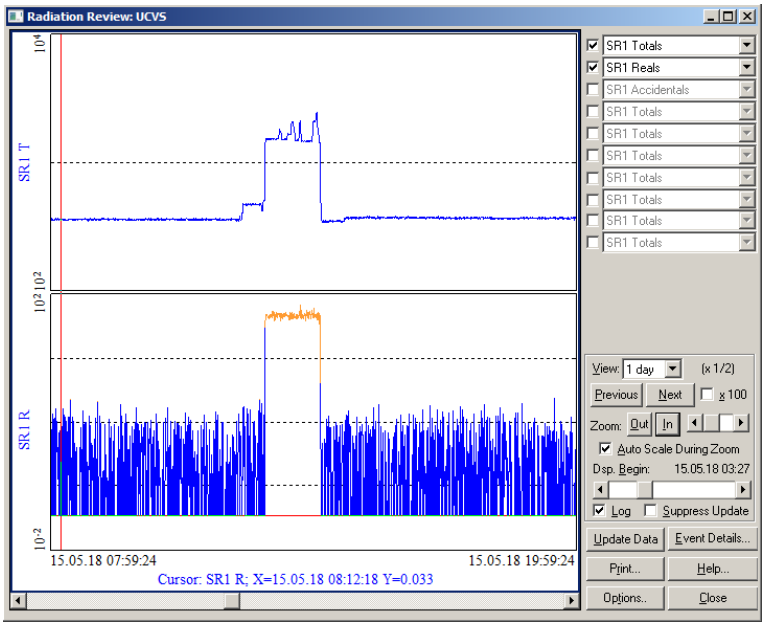


**Figure 43**. Example of a perturbed occupancy for PNEM identified using the Radiation Review graphical interface.

### 7.2.1 Typical Cylinder Populations

The total number of "Typical" occupancies (free of significant perturbations from nearby cylinders, and typical cylinder characteristics) during the field trial was 229. For the Type 30B cylinders assessed in this field trial, typical cylinders are filled to licensed capacity and homogenized, and are derived from natural feed. The population containing all of these cylinders is labeled "Typical All." It consists predominantly of cylinders produced in URENCO enrichment facilities but also includes cylinders from a conversion plant (natural enrichment) and centrifuge facilities in China and Russia. Subpopulations of the typical cylinders were also defined to support quantitative investigation of facility-specific effects on the fidelity of cylinder assay, particularly as it pertains to the $^{234}U/^{235}U$ behavior and $^{234}U$-derived signatures collected by PNEM and HEVA. These subpopulations are summarized here:

- URENCO All. All URENCO cylinders from Eunice (66), Capenhurst (50), Gronau (16) and Almelo (34); a total of 166 cylinders.
- URENCO A. From URENCO's GCEP facility in Eunice, New Mexico; 66 cylinders.
- URENCO B. From URENCO's GCEP facility in Capenhurst, UK; 50 cylinders.
- AREVA All. Cylinders transferred through the AREVA fuel fabrication facility in Washington State, United States; from multiple enrichers around the world; 34 cylinders.
- URENCO 97: A subset of URENCO All, i.e. chronologically the first 97 cylinders. This population was used only to support a specific analysis related to occupancy duration (see Section 8.1).

A description of each cylinder population is given in Table 1.

**Table 1**. Overview of the typical cylinder populations analyzed in this study.

| | Shipping Facilities | Number of Cylinders | Range of Enrichment (wt%) | Most common Enrichments (wt%) | Occupancy Duration |
|---|---|---|---|---|---|
| Typical All | 5+ GCEP facilities, one conversion facility | 229 | 0.71 to 4.95 | 2.5, 4.4, 4.95 | Variable |
| URENCO All | URENCO's USA, Capenhurst, Almelo and Gronau plants | 166 | 1.5 to 4.95 | 4.0, 4.4, 4.95 | Variable |
| URENCO A | URENCO USA | 66 | 2.5 to 4.95 | 4.0, 4.4 | Variable |
| URENCO B | URENCO Capenhurst | 50 | 1.5 to 4.95 | 2.5, 4.95 | Variable |
| AREVA All | Multiple enricher facilities | 34 | 1.5 to 4.4 | 2.6, 3.2 | Variable |
| URENCO 97 | URENCO's Capenhurst and USA plants (subset of URENCO A and B) | 97 | 1.5 to 4.95 | 4.0, 4.4, 4.95 | Variable 5 minutes |

The "typical" cylinder populations represent the set of cylinders that would be used for initial calibration of the HEVA and PNEM instruments in an actual implementation scenario. In effect, the NDA methods are trained on these typical cylinders, which allows calibration between the radiation detection signatures and the operator's declared parameters. Once the calibration relationships are fixed for a specific instrument in a specific facility, all subsequent cylinders would be considered "unknowns." Note that this type of "unknown" analysis was not performed in the Phase I study—all cylinders in a given population were used for calibration and performance reporting.

### 7.2.2 NDA Fingerprint Cylinders

The collection of NDA Fingerprint cylinders was selected to span a range of product enrichments (i.e., above natural). A tabular summary of those cylinders, their characteristics and the specific type of fingerprint scan(s) performed on each is provided in Table 2 below. A Type 30A cylinder used by WFFF as a weight standard is included in the table for completeness. That cylinder was measured multiple times by the UCVS but because of its very different characteristics (depleted enrichment and significantly thicker wall), results from that cylinder are not included in the performance analysis in this report.

**Table 2**. Information on cylinders and scan sequences used for NDA Fingerprint studies.

| Proxy ID | U Mass (kg) | Enrichment (wt %) | $^{235}$U Mass (kg) | Geometry Scan | Time+Geometry Scan | Comment |
|---|---|---|---|---|---|---|
| 235 | | 1.54 | 23.2 | | Yes | |
| 123 | 1511.3 | 1.54 | 23.3 | Yes | | Case-study scans |
| 510 | 1511.4 | 1.80 | 27.2 | Yes | | Case-study scans |
| 355 | 1457.7 | 3.20 | 46.7 | Yes | | WR designation, case-study scans |
| 251 | 1526.8 | 3.80 | 58.1 | | Yes | |
| 476 | 1507.2 | 4.40 | 66.4 | | Yes | |
| 586 | 1512.0 | 4.95 | 74.8 | | Yes | |
| 367 | 1511.9 | 4.95 | 75.2 | Yes | | |
| 551 | 1511.5 | 4.98 | 75.2 | Yes | | |
| 389 | 1517.3 | 0.19 | 2.9 | | Yes | Type 30A |

### 7.2.3 Atypical Cylinders

Atypical cylinders are those that have characteristics outside the typical cylinders used for calibration of the NDA methods, for example: partially filled, derived from non-natural feed (e.g., reactor-recycle uranium or tails recycle), produced by diffusion plants, or nonhomogenized. In the WFFF field trial, no partial fill or nonhomogenized cylinders were available, but cylinders designated as "WR" (derived from weapons in the former Soviet Union) were observed. Table 3 summarizes data for the seven atypical cylinders.

**Table 3**. Cylinder information for the Atypical population.

| Proxy ID | U Mass (kg) | Enrichment (wt %) | $^{235}$U Mass (kg) | Occupancy time (min) | Comment |
|---|---|---|---|---|---|
| 371 | 1499.6 | 3.23 | 48.3 | 15 | U-232 detection, WR designation |
| 886 | 1503.2 | 3.20 | 48.1 | 7 | U-232 detection, WR designation |
| 885 | 1484.3 | 3.20 | 47.5 | 11 | U-232 detection, WR designation |
| 643 | 1502.6 | 3.20 | 48.1 | 10 | U-232 detection, WR designation |
| 519 | 1505.5 | 3.20 | 48.2 | 6 | U-232 detection, WR designation |
| 657 | 1454.0 | 4.95 | 72.0 | 159 | diffusion |
| 002 | 1493.6 | 4.95 | 73.9 | 51 | diffusion |

The analysis of atypical cylinders is helpful in understanding the robustness of the calibration of a particular NDA method, aids the understanding of strengths and limitations of various NDA methods that use different radiation signatures and collection methods, and gives the NDA development teams insights relatively early in the NDA methods development life cycle about the analysis and reporting challenges that could arise in actual implementation of unattended cylinder verification at fuel cycle facilities.

# 8.0 Analysis Approach: Overview

All of the analysis of the WFFF field trial data presented in this report was completed after the campaign; real-time analysis and reporting was deemed outside of Phase I scope. Key assumptions for the analyses and a description of the performance metrics used to compare HEVA and PNEM are described.

## 8.1 Occupancy Duration

International Target Values (ITVs) for $UF_6$ cylinder verification using handheld instruments are based on 5-minute assay times (Zhao 2010), and the UCVS User Requirements (IAEA 2013a) that state: "total cylinder measurement and verification time for a production-version UCVS will be 5 minutes." The User Requirements also recognize, however, that longer assay times may be used in field-prototype devices, for example to accommodate a signature collection efficiency less than envisioned for a production version, or to support analysis of specific technical objectives (e.g., benchmarking of simulations).

To ensure that the HEVA and PNEM data for each occupancy were at least 5 minutes in length (taking into consideration the 1-minute spectral acquisition period of HEVA), the timer for the operator interface was set to 7 minutes. All occupancies in the field trial were at least 7 minutes in duration, and as Figure 44 shows, many were substantially longer due to the flow of WFFF's cylinder-handling operations, or pauses in the work day (e.g., break or lunch period). Per early discussions with the UCVS team, it was understood that longer occupancies could be of value in the team's analysis (e.g., studying interplay between systematic and statistical uncertainties) and therefore, WFFF did not enforce a strict 7-minute occupancy period. A graphical summary of the occupancy durations for the 229 occupancies in the Typical All population is given in Figure 44 below. As noted there, the mean and median duration were 11 minutes and 8 minutes, respectively.

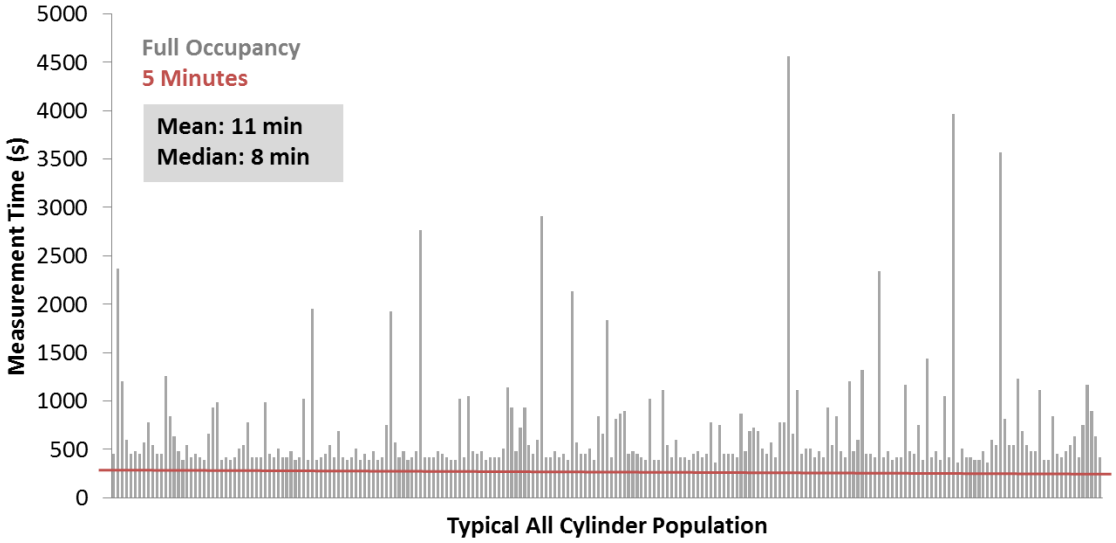


**Figure 44**. Duration of the 229 occupancies in the Typical All cylinder population, and the associated mean and median values. The UCVS prototype timer was set to 7 minutes; UCVS User Requirements from the IAEA indicate a 5-minute occupancy in a future production-version UCVS.

All occupancy durations discussed in this report are based on the real, clock time recorded by the data acquisition software. For the HEVA instrument, however, the live time of an occupancy may be slightly shorter than the real clock time presented, due to dead time in the pulse processing electronics, an effect that was typically less than 2%, and even for cylinders with particularly high count rates (highest recorded in the trial was 17.4 kcps) was only 4%. The PNEM neutron measurements have negligible associated dead time.

The UCVS team recognizes that the occupancy duration can have an impact on the uncertainties reported in the performance comparisons, and that those impacts will vary depending on the signature. For example, statistical uncertainties associated with $PNEM_S$ are very low and performance results are expected to be very similar for the range of occupancy durations shown in Figure 44. For $PNEM_D$ and $HEVA_{NT}$, however, statistical uncertainties can be appreciable, particularly at lower enrichments, and therefore occupancy duration is an important consideration in performance prediction.

Ideally, the PNEM and HEVA data for all occupancies would have been partitioned to a consistent 5-minute real time for all of the analysis presented in this report. However, there is no automated mechanism to do "X-minute" partitioning in the analysis software used in the PNEM analysis (i.e., RadReview+INCC); adapting the software or performing the partitioning manually for the 250-plus occupancies was not possible under the budget and schedule of Phase I.

So that the Phase I analysis could include a preliminary investigation of occupancy-duration effects, LANL performed manual partitioning of data for the first 97 cylinders included in the URENCO All population. PNNL adopted these LANL-specified start/stop times so that the PNEM and HEVA results for the "URENCO 97 5-MIN" population are based on a consistent 5-minute duration for all occupancies.

## 8.2 Calibration Function for $^{234}U/^{235}U$ Ratio

Population-specific calibrations were used to determine the relationships between measured signatures (e.g., net 186-keV count rate, total and coincidence neutrons) and two operator-declared parameters: $^{235}U$ mass ($M_{235}$), $^{235}U$ enrichment ($E_{235}$). The need for a calibration procedure that connects the singles neutrons to the $^{235}U$ mass is described in more detail here, as it is an important consideration in the evaluation of both the PNEM and HEVA methods.

The use of total neutron count rate as a means of determining $M_{235}$ is based on the production of neutrons in $^{19}F(\alpha,n)$ reactions, with the dominant alpha emitter being $^{234}U$ for all enrichments above natural (Walton et al. 1974; Miller et al. 2012a; Smith et al. 2010b). The highly penetrating nature of this signature offers the potential for full-volume interrogation of the cylinder, and therefore, absolute measurement of $^{235}U$ mass. However, because this signature is driven by $^{234}U$, it requires knowledge of the $^{234}U/^{235}U$ ratio as a function of enrichment in order to infer $M_{235}$.

Previous studies have analyzed the natural variation in the $^{234}U/^{235}U$ ratio in the natural uranium typically used as feed in commercial enrichment plants. Work by Richter et al. (1999) analyzed mass spectrometry measurements of various uranium ore samples from around the world and set the extremes of the natural variation. Another source of isotopic variation is that modern enrichment plants, depending on the price of uranium, may recycle tails as feed material, with potential impacts on the $^{234}U/^{235}U$ ratio in the product

cylinders. Commercial enrichers may also use reactor-recycle uranium that typically has much higher $^{234}U/^{235}U$ ratios than natural-origin material.

In this work and in the rest of the discussion in this section, it is assumed that the typical feed in the enrichment facility is of natural origin. Further, it is assumed that a facility-specific calibration for NDA methods using the $^{234}U$-derived signatures would incorporate knowledge about how the $^{234}U/^{235}U$ ratio changes as a function of enrichment in each unit/facility. This calibration could be informed, for example, by the IAEA's archival data of uranium isotopic ratios from destructive analysis on $UF_6$ samples drawn from the process or cylinders.

Though knowledge about the $^{234}U/^{235}U$ ratio may ultimately come from independent sources such as IAEA archives of bulk sample analysis, in this study it is derived from operator declarations. Figure 45 shows a plot of operator-declared $^{234}U$ versus $^{235}U$ values for Typical All and URENCO All cylinders measured in the first half of the field trial. In those figures, the data are fit using a quadratic function and appear to represent the data reasonably well, but the exact nature of this isotopic ratio behavior over the range of enrichments from depleted to 5% is not yet fully understood. Nor have the calculations been performed to determine how that isotopic ratio behavior will translate to neutron flux at the surface of the cylinder or counts in specific sensor types, after considering effects such as neutron self-shielding that may change as a function of enrichment, the energy spectrum of the neutron flux incident on the sensors, and neutron multiplication in the $UF_6$ volume itself. It is a functional relationship between measured singles-neutron signal, and the declared $^{235}U$ mass for a cylinder, that was needed by the UCVS team for calibration of PNEM and HEVA neutron-based signatures.

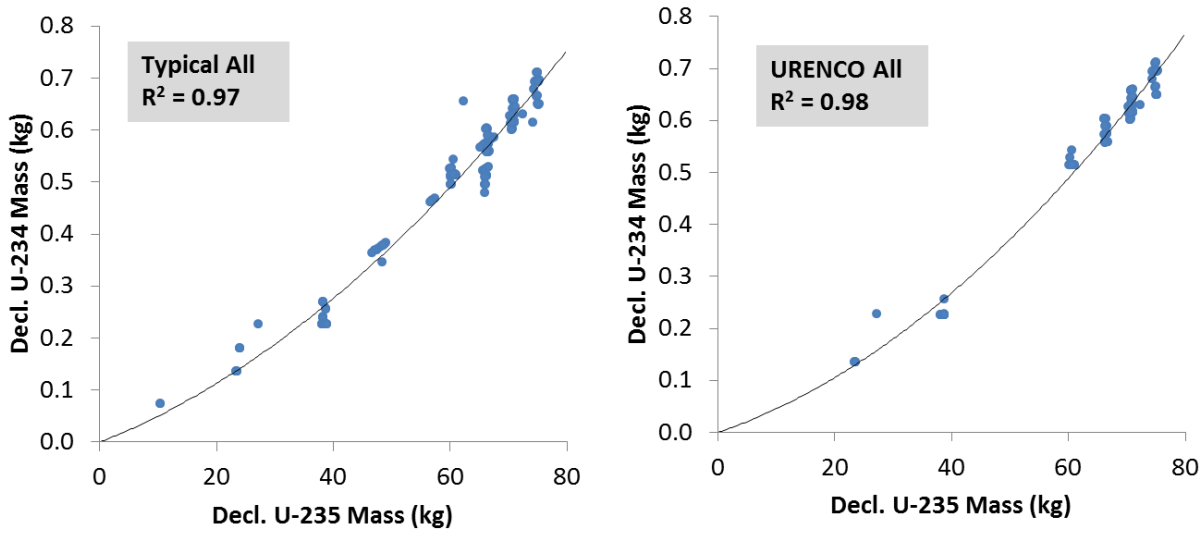


**Figure 45**. Declared $^{234}U$ vs. $^{235}U$ values for a subset of the Typical All (left) and URENCO All (right) cylinder populations, and a quadratic fit to those data.

Building from the data in Figure 45, the UCVS team enforced the following characteristics on the calibration functions for neutron signatures:

- Nonlinear and concave up
- Always positive, even at the lowest $^{235}U$ mass values, due primarily to $^{238}U$ spontaneous fission in the cylinder (approximately half of the total emission at natural enrichment)
- Monotonically increasing.

$HEVA_{NT}$ analysis implemented a matrix-based analytic solution to avoid common optimization issues, and chose an exponential model for the relationship between emitted neutrons and $^{235}U$ mass. Analysis of $PNEM_S$ and $^{235}U$ mass, and the calibration between $PNEM_D$ and relative enrichment, assumed a montonically increasing quadratic model. Analysis presented in this report indicates that the two models produce very similar results, with some modest departures for lower-mass cylinders (of which there are very few in this field trial).

More study of the $^{234}U/^{235}U$ behavior is needed, over a plausible range of the parameters encountered in commercial enrichment, for example: natural ore variations; use of low-assay feed (i.e., depleted $UF_6$ as feed); use of reactor-recycle material as feed; enrichment method (i.e., centrifuge or diffusion); cascade-specific parameters and operational practices (e.g., blending). A project recently initiated by the National Nuclear Security Administration's (NNSA's) NGSI program is targeting this challenge, and could inform a UCVS Phase II, should the IAEA pursue it.

## 8.3 Hybridization of NDA Signatures

As discussed earlier, previous field trials and statistical analysis the UCVS team (Smith et al. 2010b; Smith et al. 2014) have indicated that combining multiple signatures from assayed cylinders is advantageous in terms of reducing overall assay uncertainty for calculating $E_{235}$. In this study, the UCVS team has continued to perform analysis in this way.

It is important to recognize that applying this hybrid analysis method requires knowledge of the total uranium mass in the cylinder, to translate the assayed value for $M_{235}$ (from the singles neutron signature) into a relative enrichment. In past analyses, and in this report, the operator's declared uranium mass value is used for this translation because the UCVS load cells were not fully functional and calibrated in the field trial. Assuming load cells would be incorporated in a fielded UCVS, the total $UF_6$ mass value would be derived from the load cells and the declared tare weight for the cylinder.

If the UCVS units of the future do not include load cells, the total $UF_6$ mass value must be taken from operator declarations. This means that the hybrid assay method will have lost some degree of independence in terms of verification. Whether or not this reduction in the independence of the hybrid method is important is a question to be posed to Euratom and the IAEA.

## 8.4 Performance Metrics

### 8.4.1 Typical Occupancies

Analysis of the relative differences between the measured and the declared values of a parameter (e.g., average cylinder enrichment) is the most common way of reporting predicted performance of cylinder verification instruments and is the performance metric used in this study (as well as previous field trials of PNEM and HEVA). A more statistically rigorous gauge of expected performance would be to consider one or more of the typical cylinders in a population (e.g., URENCO A) as unknowns, and to use the remaining typical cylinders in that population for the calibration. This is often referred to as an "all but *N*" analysis method, where *N* is the number of typical cylinders extracted from the population to serve as unknowns. Such analysis should be considered for future UCVS work.

"Typical" occupancies are those for which the cylinder is a Type 30B and the contents have none of the "atypical" characteristics described earlier (e.g., derived from non-natural feed, diffusion plant origin, or partial fill). The assay of the cylinder is a one-time event (unlike the NDA Fingerprint scenario described in Section 8.4.2 below) and measurement outcome is absolute (e.g., $E_{235}$ in wt% $^{235}$U), similar to the cylinder verification measurements performed currently by IAEA and Euratom inspectors.

The two primary metrics of interest for typical occupancies are the precision and accuracy, relative to the operator declarations, of measured values for $E_{235}$ and $M_{235}$. In keeping with the approach typically employed by Euratom and IAEA in the assessment of field instrumentation for cylinder assay, performance in this report is quantified by evaluating:

- The relative standard deviation, $\sigma$, of the differences between the declared and measured values (e.g., $\sigma_M$ for $^{235}$U mass $\sigma_E$ for cylinder enrichment). When the declared value has a much lower uncertainty, as is assumed in this application, $\sigma$ can be considered as the performance characteristic of the verification method, which then can be compared with an appropriate ITV. Note that $\sigma$ covers both the random and the short-term systematic uncertainty components, as described in definitions given in the ITV document (Zhao 2010).
- The mean of the relative differences between declared and measured values, $\mu$. Because the expectation value for $\mu$ in a well-calibrated instrument is zero, $\mu$ can be used to indicate, for example, calibration issues with an instrument.

In this report, the operator's declared values (from mass-spectrometry analysis) are considered to be the true values and further, to carry negligible uncertainty compared to the uncertainties of the NDA methods.

Quantitative assay of $E_{235}$ and $M_{235}$ relies on a calibration relating the measured signatures to the enrichment level. The total uncertainty of the measured value $\sigma_{tot}$ will have several components, described here and depicted graphically in Figure 46:

- $\sigma_{stat}$ is the random statistical uncertainty of the signatures measured by HEVA, for example in the net count rate under the 186-keV gamma-ray peak, or in the singles neutron count rate.
- $\sigma_{sys\_ran}$ is the random systematic uncertainty of the measured signatures. Random systematic uncertainties might include wall thickness variations, cylinder age, material distribution in the cylinder, ambient background changes (e.g., nearby cylinder movements), instrument drift (e.g.,

gamma-spectrometer gain drift with temperature), small changes in the measurement geometry from one scan to the next (e.g., cylinder position on trolley, or rotation).

- $\sigma_{sys\_cal}$ is the error in the calibration relationship between the absolute value of the measured signature and the true value of the parameter to be determined. Sources of calibration uncertainty might include an incomplete understanding of the $^{234}U/^{235}U$ ratio behavior in the facility or error in the absolute collection efficiency of the detectors.

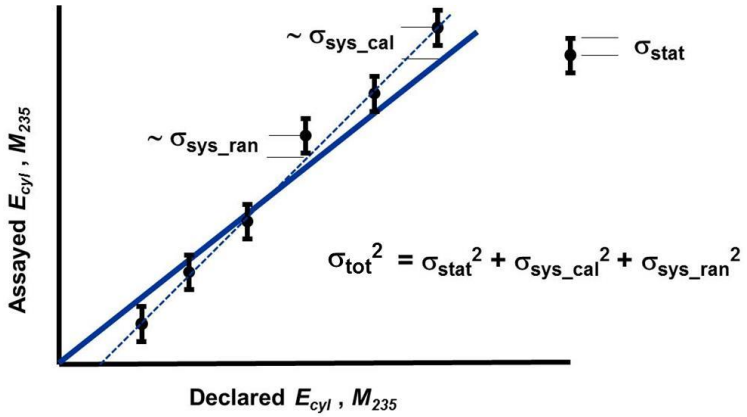


**Figure 46**. Components of uncertainty for the quantitative NDA of $^{235}U$ enrichment using the UCVS, where the assay enrichment of each cylinder is determined from a single measurement of that cylinder.

### 8.4.2 NDA Fingerprint Occupancies

NDA Fingerprint occupancies are those that were specifically designed to investigate the consistency and repeatability of the fingerprint signatures collected by PNEM and HEVA. The key scan variables of interest are the relative geometry between the sensors and the cylinder (e.g., translational shifts or rolls) and the time between scans. The assay of the cylinder is a repeated event where the measurement outcome is a *relative* difference from the prior scan.

The key performance metric for the NDA Fingerprint is the total uncertainty, $\sigma_{FP}$ , over a series of repeated measurements (Figure 47). The total uncertainty will have two primary components, $\sigma_{stat}$ and $\sigma_{sys\_ran}$ (Figure 47). The uncertainty associated with calibration of the measured signature to assay enrichment, $\sigma_{sys\_cal}$ , is not relevant to NDA Fingerprint scans, which ideally, makes it possible to achieve significantly lower uncertainty values than are possible for direct NDA of $E_{235}$ and $M_{235}$. Each NDA Fingerprint signature (e.g., PNEM Singles or HEVA 1001-keV ROI) is likely to exhibit a different relative mix of uncertainty components.

For the NDA Fingerprint scans, contributors to $\sigma_{sys\_ran}$ are similar to those described above for the typical occupancies: small changes in the measurement geometry from one scan to the next (e.g., cylinder position on trolley, rotation), cylinder age (i.e., grow-in of daughters), changes in the material distribution in the cylinder (e.g., due to handling movements or heat/cold in the storage yard), ambient background changes (e.g., nearby cylinder movements), and instrument drift (e.g., gamma-spectrometer gain drift with temperature).

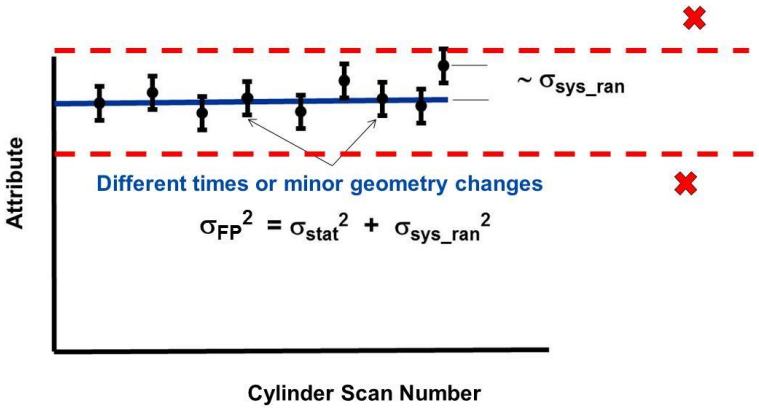


**Figure 47**. Components of uncertainty for the application and re-verification of an NDA Fingerprint, where the fingerprint attribute is measured multiple times (e.g., as the cylinder is moved between MBAs) on the same cylinder. Notional alarm thresholds (e.g., ±3σ) are shown in red, along with red icons representing scan values that would signal a significant change in the characteristics of the cylinder and therefore, a "fingerprint alarm."

### 8.4.3 Flagging Anomalous Cylinder Characteristics

The hybrid analysis method employed with HEVA and PNEM offers the potential to flag inconsistencies between the enrichment predicted by the full-volume (nontraditional signature for HEVA; singles for PNEM) and the direct $^{235}$U (traditional signature for HEVA; doubles for PNEM) signatures, and therefore to detect a $^{234}$U/$^{235}$U ratio in a cylinder that is outside the calibrated range. Using the atypical cylinder population, the viability of this capability is preliminarily explored. In that analysis, a threshold of 3σ is defined as the threshold to raise an anomaly flag, where σ is taken from the results for the typical cylinder populations. That is, if the value of $E_{235}$ based on the direct $^{235}$U signature is more than 3σ different from the $E_{235}$ value based on the full-volume signature (and the declared total uranium mass), a flag is noted for that cylinder. Details of the analysis steps are given here:

1. Calculate $E_{235}$ using $HEVA_T$ ($PNEM_D$).
2. Calculate $M_{235}$ using $HEVA_{NT}$ ($PNEM_S$) and the facility-specific calibration on the $^{234}$U/$^{235}$U ratio.
3. Translate the measured $M_{235}$ into a measured $E_{235}$ using the operator-declared value for total uranium mass.
4. If the two values of $E_{235}$ differ by less than 3σ (from the calibration populations for $HEVA_{NT}$ and $PNEM_S$), both HEVA and PNEM report the hybrid enrichment values for the cylinder.
5. If the two values of $E_{235}$ differ by more than 3σ, flag as anomalous $^{234}$U/$^{235}$U ratio.
    i. For HEVA, report only the measured $E_{235}$ value based on the direct $^{235}$U signature: $HEVA_T$.
    ii. For PNEM, report only a flag indicating that the $^{234}$U concentration is outside of the calibrated range.

In addition to the $^{234}$U flag, HEVA spectra are also used to flag $UF_6$ of non-natural origin using the 2614-keV peak. This peak is indicative of the presence of feed, product or tails based on reactor-recycled uranium and therefore, could be useful to safeguards inspectorates in the cylinder verification process

# 9.0 Results: Cylinder Verification

The results for HEVA and PNEM analysis are presented in this section for the typical cylinder populations, NDA Fingerprint studies, and atypical cylinders.

## 9.1 Typical Cylinder Populations

Results for the assay of $E_{235}$ and $M_{235}$ for the typical cylinder populations are discussed here.

### 9.1.1 HEVA Analysis

The results of the HEVA analysis for $E_{235}$ in the typical cylinder populations are shown in Figures 48 and 49 and Table 4. There, the calibration relationships between $HEVA_T$ (the traditional 186-keV signature, as calculated using the SWC method) and declared $E_{235}$ are indicated, along with the relative standard deviation (RSD) values for that population. These $HEVA_T$ results are an aggregation of the SWC signals from all three HEVA modules. (The calculation of the SWC signal is performed for each detector individually, then summed.) These results show that the $HEVA_T$ calibration relationship is quite consistent across all five populations—the slope and offset vary little from facility to facility. This is the expected result since the 186-keV signature is a direct measurement of $^{235}U$ enrichment and as such, should have no variation with facility-specific factors such as centrifuge type or feed material. For similar reasons, it is expected that the RSD values for the five typical populations would be relatively consistent, and the data support that assertion: Typical All, 5.5%; URENCO All, 5.3%; URENCO USA, 5.9%; URENCO Capenhurst, 4.4%; and AREVA All, 5.8%.

Note that the RSDs reported above are for enrichments greater than natural, which is only relevant to the Typical All population because no other populations include natural-enrichment cylinders. The top pane of Figure 48 shows that the SWC results for two of the three natural cylinders are erroneously high. It is well documented that the accuracy of traditional enrichment-meter approaches degrades for low-enrichment cylinders, particularly those with significant wall deposits, because a relatively weak 186-keV signature is riding on a relatively intense continuum from the $^{234m}Pa$ ($^{238}U$ daughter). This effect is clearly illustrated in Figure 51 where HEVA spectra from two cylinders are compared. The first (top pane) exhibits modest and spatially consistent $^{234m}Pa$ signatures, presumably from a relatively consistent spatial distribution of wall deposits along the length of the cylinder wall viewed by the HEVA modules. For that cylinder, the SWC results are as expected for all detectors (i.e., SWC values ~15 in Figure 48). The spectra from the second cylinder (bottom pane of Figure 46) show a high degree of spatial variability in the wall deposits (as evidenced by the different intensities for each detector), and even variation in the shape of the underlying continuum. The SWC results from HEVA-1 and HEVA-3, for that cylinder, are significantly higher than expected, which results in a significant bias for a cylinder enrichment assay value based on the average of all three modules. Note that HEVA-2 produced an accurate enrichment value for that cylinder.

The key messages from the poor performance of SWC on two of the natural cylinders are that more investigation is needed into: 1) why the shape and intensity of the continuum changes so dramatically between HEVA-1 and HEVA-3, even though the $^{234m}Pa$ lines (1001 and 766 keV) show similar intensities, 2) how the SWC parameters might be adapted to better discriminate highly variable continua.

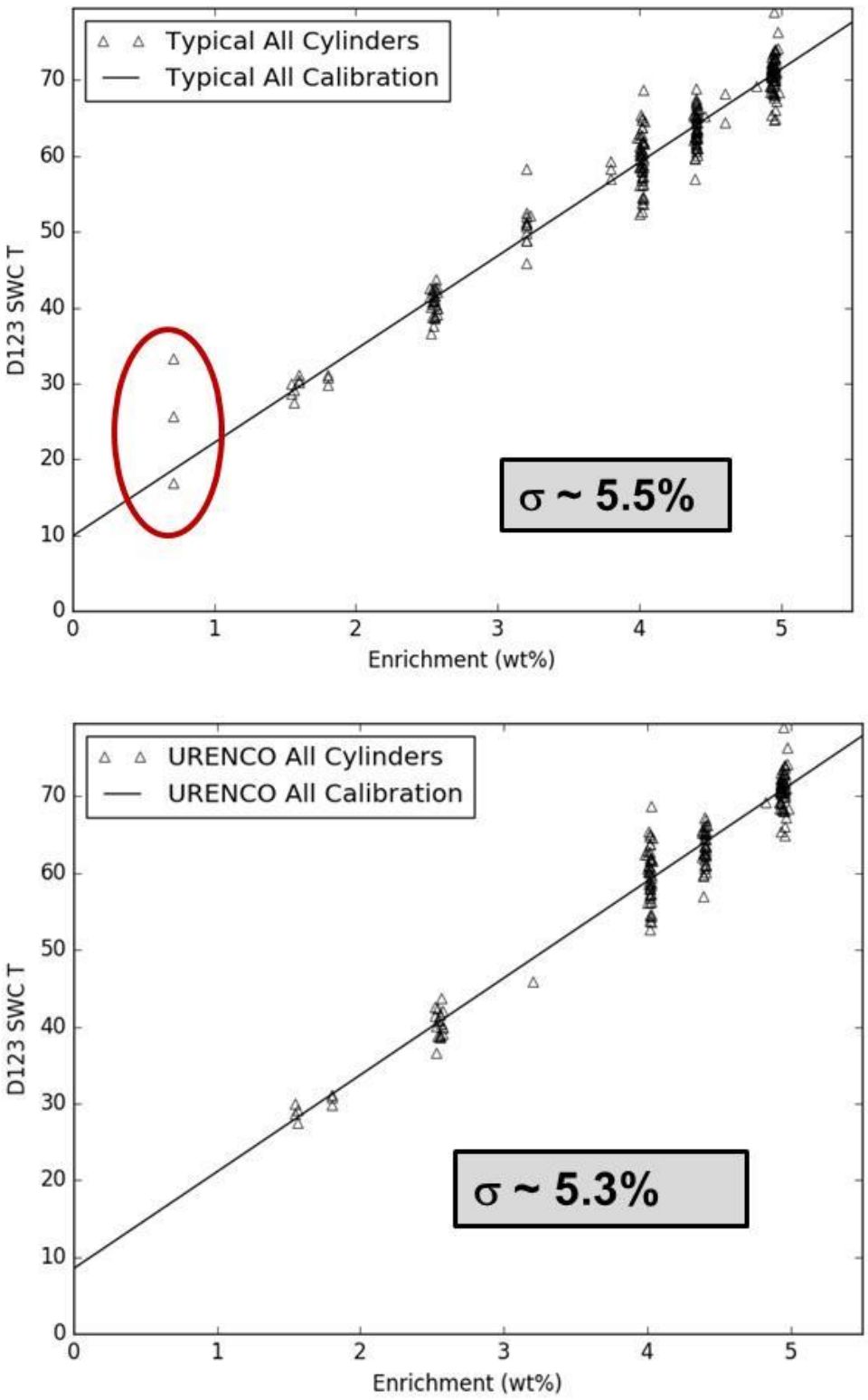


**Figure 48**. Calibration relationships between the HEVA traditional signature (based on a SWC analysis algorithm) and declared $^{235}U$ enrichment for two populations: Typical All (top, 229 cylinders, 226 product) and URENCO All (bottom, 166 cylinders). "D123" is the summed SWC signal from all three HEVA modules.

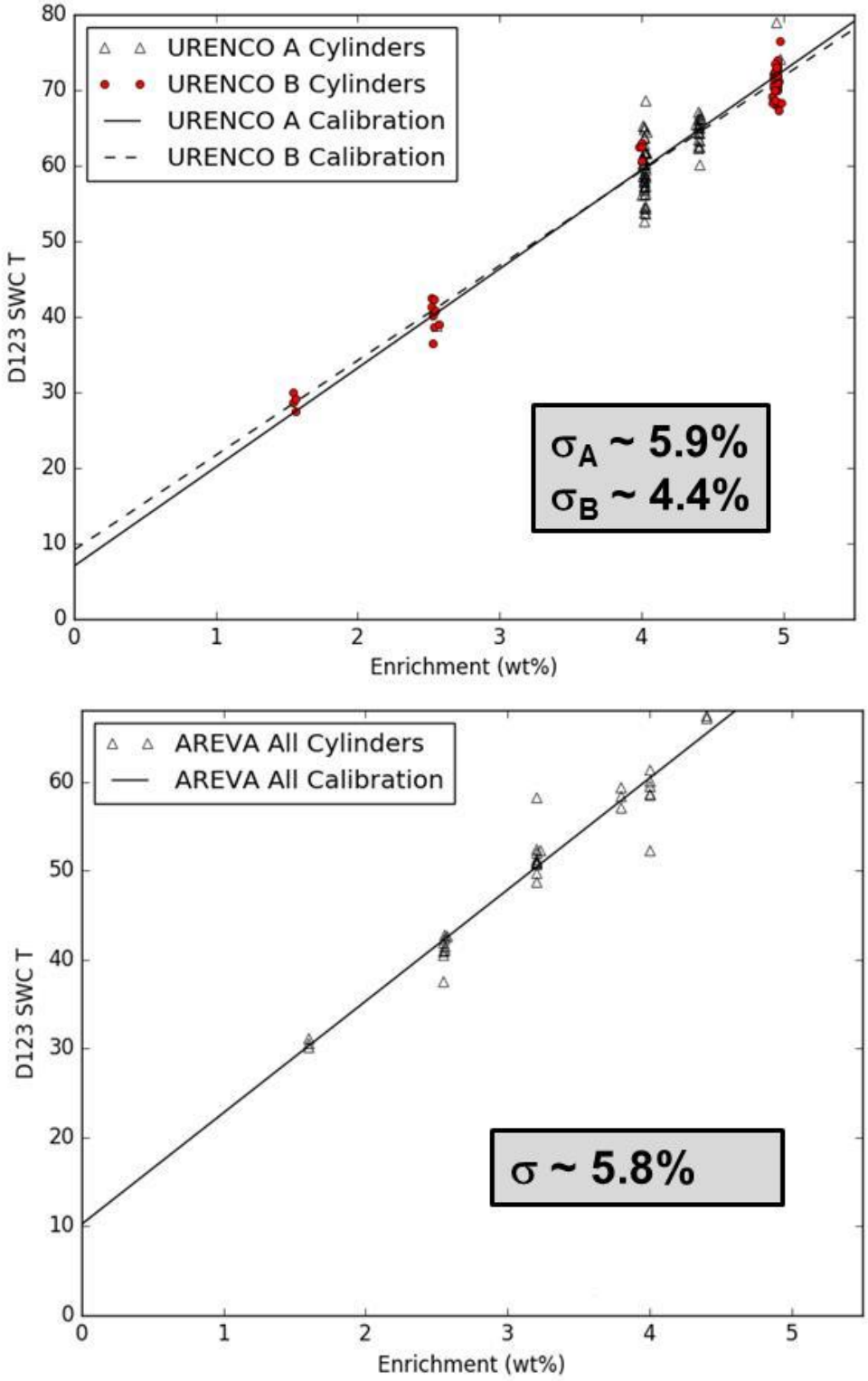


**Figure 49**. Calibration relationships between the HEVA traditional signature (based on a SWC analysis algorithm) and declared $^{235}U$ enrichment for three populations: URENCO A, URENCO B (top, 66 and 50 cylinders, respectively),and AREVA All (34 cylinders). "D123" is the summed SWC signal from all three HEVA modules.

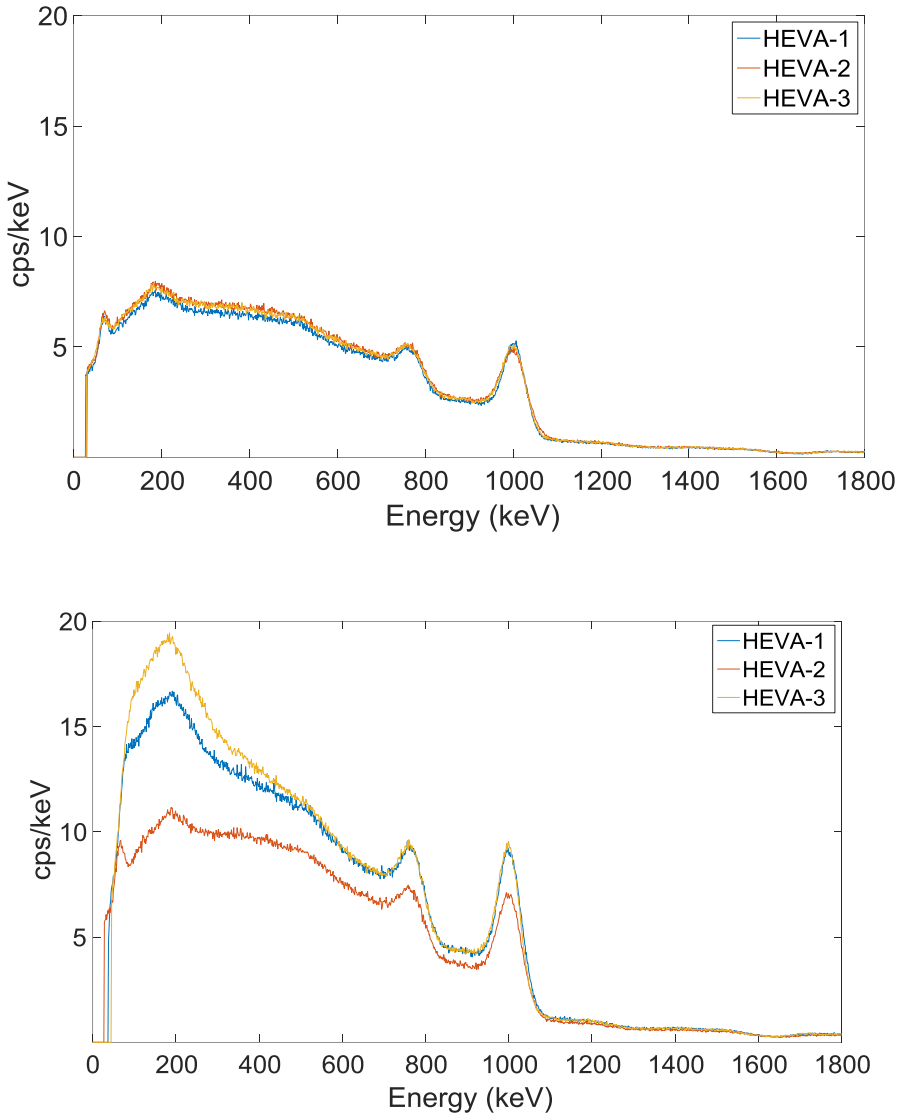


**Figure 50**. HEVA spectra (from all three modules) for two natural enrichment cylinders producing very different SWC results. Top: cylinder with accurate SWC results for all three HEVA modules. Bottom: cylinder with erroneously high SWC result for HEVA-1 and HEVA-3.

The results of the HEVA analysis for $M_{235}$ in the typical cylinder populations are given in Table 4 Figure 50 and Figure 51 where the calibration relationships between $HEVA_{NT}$ (indirect totals neutron signature) and the declared $M_{235}$ values are shown along with RSD values. The $HEVA_{NT}$ results are based on a summation of the 3 to 8 MeV region for all three HEVA modules. These reults show that the $HEVA_{NT}$ calibration relationship varies substantially across the five typical populations. As discussed previously, this is expected since $HEVA_{NT}$ is driven by the $^{234}U$ mass, and the $^{234}U/^{235}U$ behavior is dependent on facility-specific factors such as centrifuge type and feed material. The results are generally consistent with expectation in that cross-facility populations (e.g., Typical All, URENCO All and AREVA All) have somewhat higher RSD values: Typical All, 7.6%; URENCO All, 5.7%; URENCO USA, 3.0%; URENCO Capenhurst, 2.6%; and AREVA All, 5.4%.

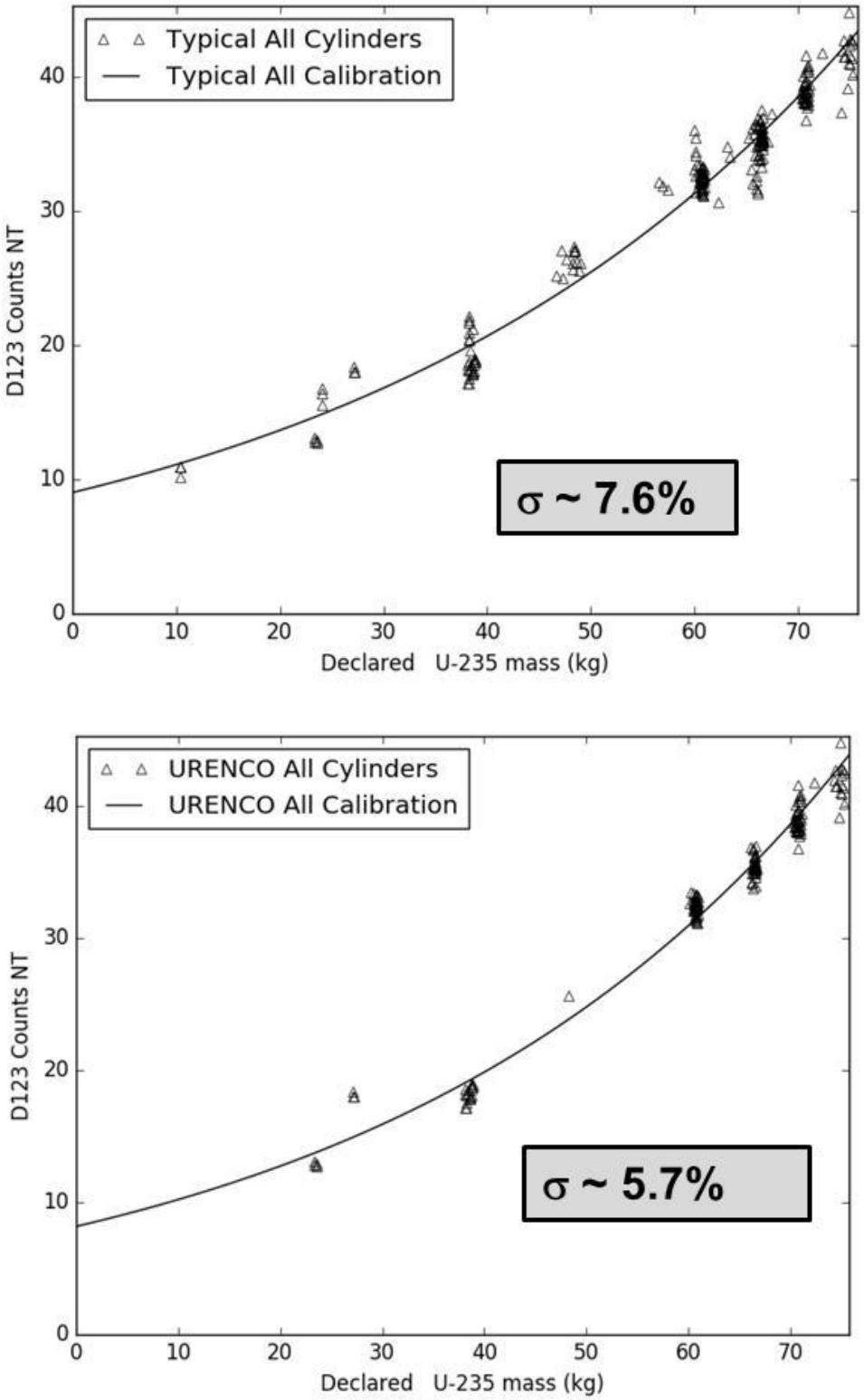


**Figure 51**. Calibration relationship between the HEVA non-traditional signature (count rate in 3-8 MeV region of interest) and declared $^{235}U$ mass for two populations: Typical All (top, 229 cylinders, 226 product) and URENCO All (bottom, 166 cylinders). "D123" is the sum over all three HEVA modules.

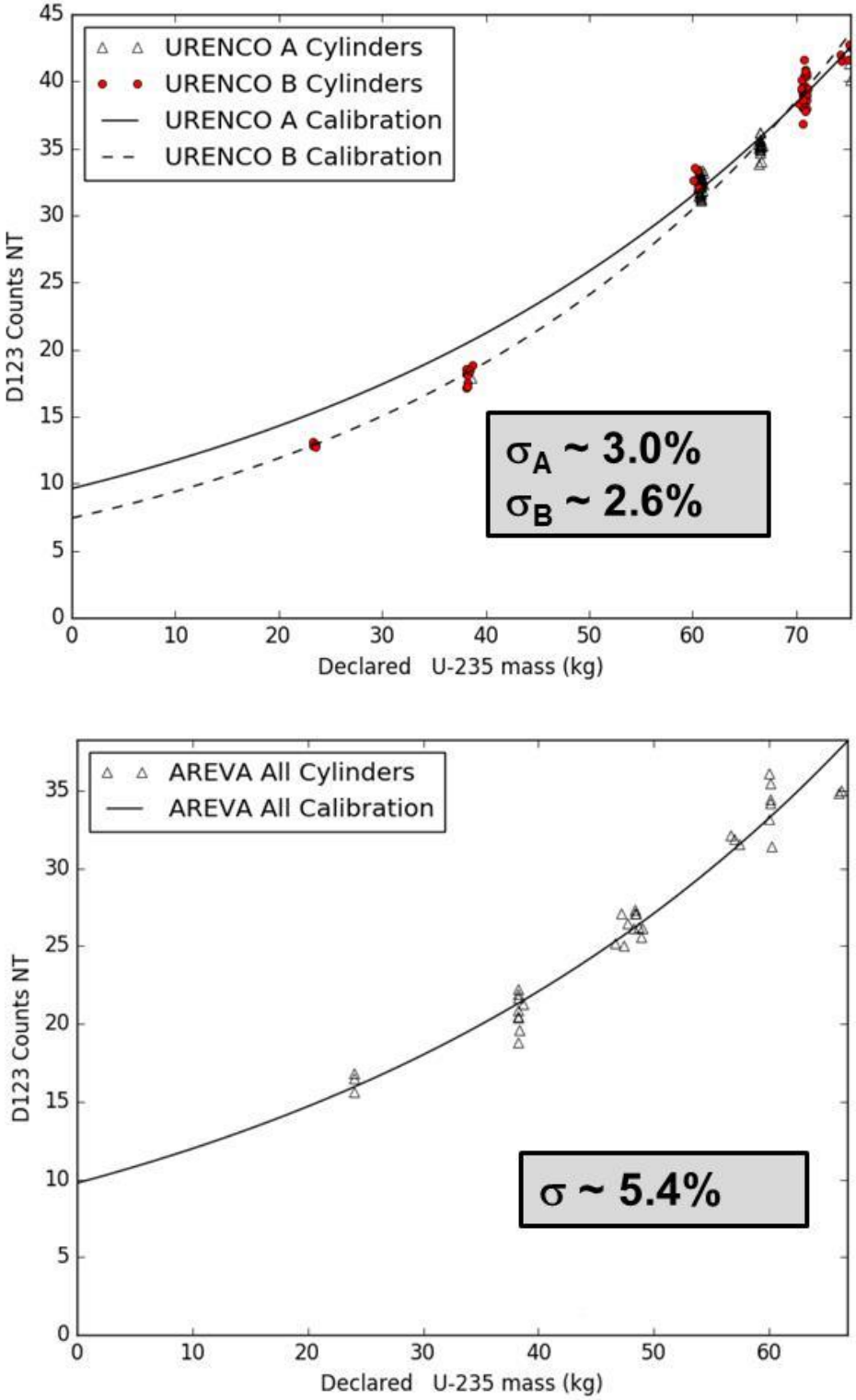


**Figure 52**. Calibration relationship between the HEVA non-traditional signature (count rate in 3-8 MeV region of interest) and declared $^{235}$U mass for three populations: URENCO A, URENCO USA B (top, 66 and 50 cylinders, respectively), and AREVA All (34 cylinders). "D123" is the sum over all three HEVA modules.

As discussed previously, the two independent HEVA signatures can be hybridized: assuming a known total uranium mass in each cylinder (e.g., from UCVS load cells or declared data), the $HEVA_{NT}$ values for $M_{235}$ can be translated to a second value for $E_{235}$. This hybrid enrichment value can be considered a full-volume assay value, owing to the penetrability of the non-traditional neutron signature. Prior work has shown that the hybrid enrichment precision is consistently superior to the $HEVA_T$ precision, and the same is true for the UCVS Phase I populations. RSD values for $HEVA_{Hybrid}$ were: Typical All, 5.4%; URENCO All, 4.3%; URENCO USA, 3.5%; URENCO Capenhurst, 3.5%; and AREVA All, 4.3%.

A graphical comparison of the $HEVA_{hybrid}$ and $HEVA_T$ $E_{235}$ values are shown in Figure 53 for the URENCO All population. It is evident there is the reduction in uncertainties when hybridizing two HEVA signatures that have a low degree of statistical correlation of errors, as asserted by prior work (Smith et al. 2010a). To confirm this prior finding, a statistical analysis of the $HEVA_T$ and $HEVA_{NT}$ signatures for the URENCO All population was performed. The correlation coefficient of the relative errors was calculated to be 0.18 (perfectly correlated data would have a value of 1.0, perfectly uncorrelated 0, and perfectly anti-correlated -1.0).

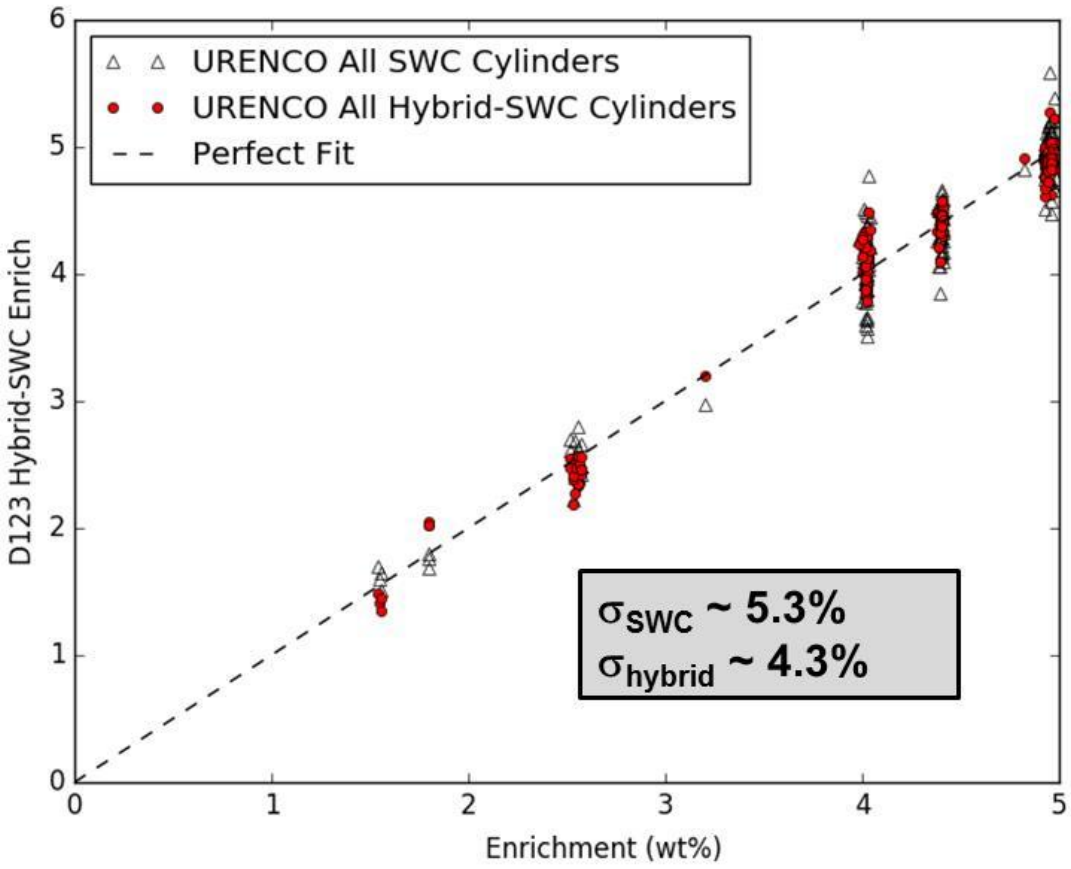


**Figure 53**. Comparison of hybrid and SWC-based values for $^{235}U$ enrichment for the URENCO All population (166 cylinders).

A comparison of the HEVA results for the URENCO 97 population, using the full and 5-minute occupancy durations, are shown in Figure 54. The key finding from this analysis was that there were modest increases (an ~10% increase in RSDs for $HEVA_{hybrid}$, $HEVA_T$, and $HEVA_{NT}$). This analysis provides empirical support for the assertion that the total uncertainties for HEVA signatures, in the as-deployed hardware configurations, are dominated by systematic, not statistical uncertainties, assuming an assay period of 5 minutes or greater. The degradation in the RSD for the $HEVA_{NT}$ assay for the 5-minute occupancy period was consistent with expectations because—particularly for low-enrichment cylinders—the statistical contribution to uncertainty can be significant. The degradation in the $HEVA_T$ RSD was not expected. More investigation is needed into the source of that increase.

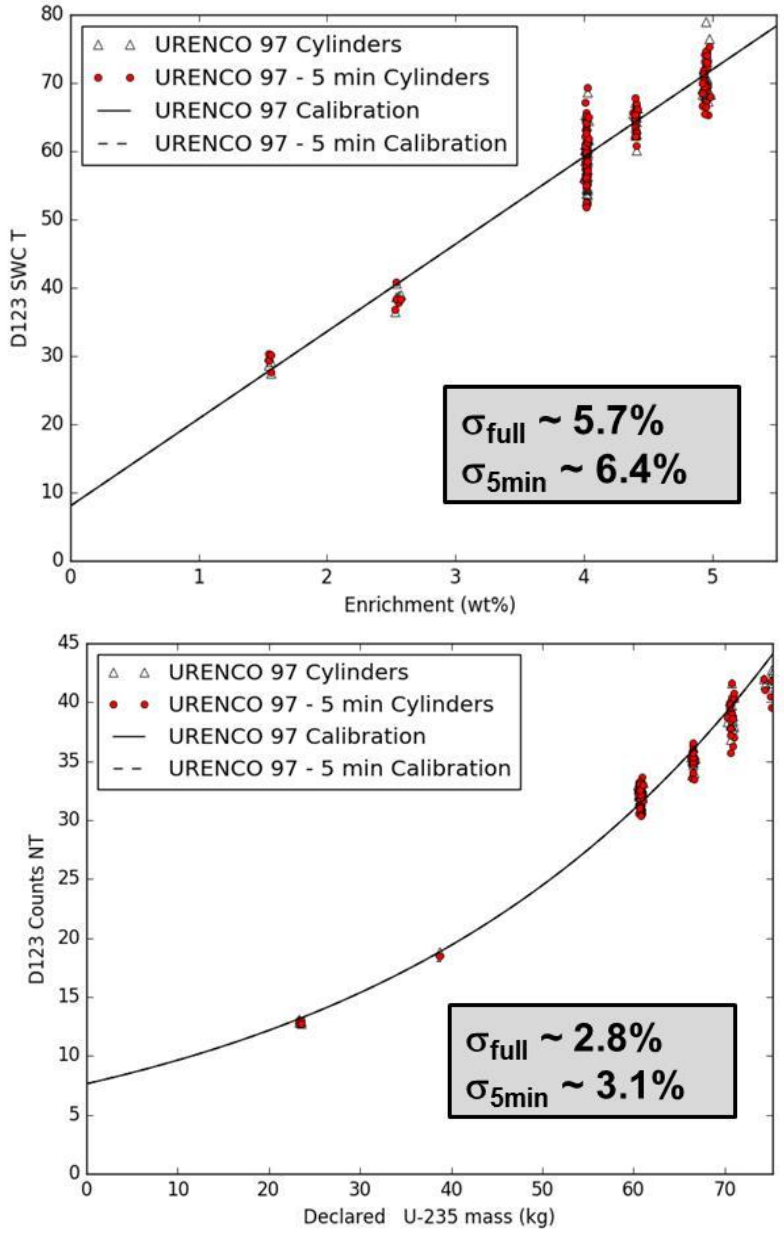


**Figure 54**. Comparison of HEVA results for full (i.e., variable) and 5-minute occupancy durations for the URENCO 97 (97 cylinders) population. Top: SWC-based values for $^{235}U$ enrichment. Bottom: HEVA non-traditional signature for $^{235}U$ mass.

The effect of heels cylinders present on the heels trailers during cylinder occupancies was investigated, as documented in Figure 55 and Figure 56 below. As Figure 55 illustrates, the heels trailers presented significantly elevated gamma-ray backgrounds below approximately 2 MeV. This was particularly evident for the second heels trailer, where the background count rate of 1526 cps was over seven times higher than the nominal value of 200 cps when heels trailers were not present. WFFF indicated that the cylinders on the second trailer were particularly intense in terms of gamma-ray emissions because there was a much shorter time between cylinder withdrawal and loading on the trailer, and therefore a shorter time for decay of daughters in the heels. Figure 56 shows that there appears to be no significant negative impact of the heels trailers on $HEVA_T$ precision: the precision of cylinders measured during the multi-day loading periods for the heels cylinders are comparable to precision for other populations.

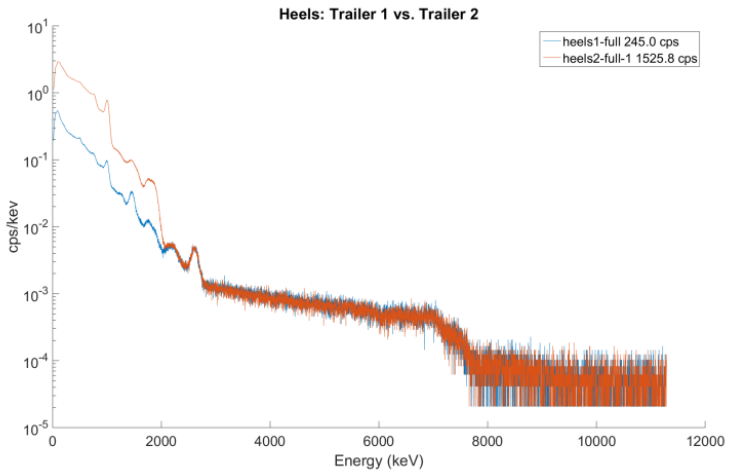


**Figure 55**. Comparison of background count rates in a single HEVA module for filled heels trailer 1 and filled heels trailer 2.

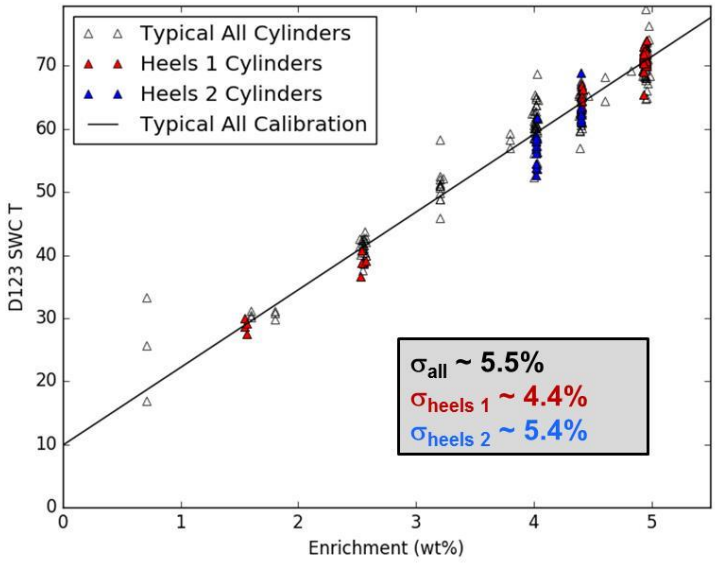


**Figure 56**. Comparison of SWC-based values for $^{235}U$ enrichment for cylinders assayed during the multi-day loading processes for two different trailers loaded with empty cylinders containing heels. The RSD values for the cylinders assayed with heels cylinders nearby are compared to the Typical All value.

As noted above, the HEVA results presented in this report are based on analysis methods without background subtraction. An analysis with background subtraction was also performed, for all of the cylinder populations reported above. In that analysis, the nominal background for each day (and each detector) was defined to be a spectrum averaged over 7 hours between 0000 and 0700, when it was assumed that the area around the UCVS prototype was free of filled cylinders and no cylinder movements would take place. A comparison of RSDs for HEVA with and without background subtraction is given in Table 4. Observations from that data include:

- Background subtraction has a negligible effect on $HEVA_T$ precision, an unsurprising result because the background count rate in the 186-keV region is negligible compared to the very high signal from a cylinder, even for low-enrichment cylinders.
- Background subtraction actually degrades $HEVA_{NT}$ performance. More investigation is needed to definitively explain this trend, but the fact that the nontraditional neutron signal, on a per-detector basis, is relatively weak, means that background uncertainty (statistical and systematic) is a significant contributor to the total uncertainty of a background-subtracted signal.

One potential source of systematic uncertainty in the background-subtracted $HEVA_{NT}$ assay values is an effect called "background suppression." Background suppression refers to a measurement scenario in which a large sample shields the detectors from some portion of the background radiation fields that those detectors view when the sample is not present. Background suppression is a well-known effect in vehicle/container portal monitors. In the case of UCVS and HEVA, the placement of the Type 30B cylinder on the platform shields the HEVA modules from neutrons and gamma rays that are collected from the sensors' field of view when the cylinder is not present. When a background measured with no cylinder present is subtracted from a cylinder occupancy, systematic errors can arise. Additional investigation, including whether the degradation in precision is most significant at lower enrichments, might help to address this technical question.

**Table 4**. Comparison of HEVA RSDs without and with (red values) background subtraction.

| | **Typical All* (229)** | **URENCO All (166)** | **URENCO A (64)** | **URENCO B (35)** | **AREVA All (34)** |
|---|---|---|---|---|---|
| HEVA $E_{235}$ (Hybrid) | 5.4 / 5.6 | 4.3 / 4.5 | 3.5 / 3.6 | 3.5 / 3.6 | 4.3 / 4.3 |
| HEVA $E_{235}$ (SWC) | 5.6 / 5.4 | 5.3 / 5.3 | 5.9 / 5.9 | 4.4 / 4.3 | 5.8 / 5.6 |
| HEVA $M_{235}$ ("Singles") | 7.6 / 10.6 | 5.7 / 6.0 | 3.0 / 3.5 | 2.6 / 2.9 | 5.4 / 5.5 |

### 9.1.2 PNEM Analysis

The results of the PNEM analysis for $M_{235}$ and $E_{235}$ on the five data sets for typical cylinders—Typical All, URENCO All, URENCO A, URENCO B, and AREVA All—are provided in this section along with a comparison between the full occupancy and 5-minute data cut for a subset of 97 URENCO cylinders. Plots of the five data sets are shown in Figure 57 through Figure 61, where the calibration curves were constructed by fitting a monotonically increasing, second-order polynomial with a positive y-intercept through the data points. In each figure, the plot on the left shows the singles count rate as a function of declared $^{235}$U mass and the plot on the right shows the doubles count rate as a function of declared enrichment.

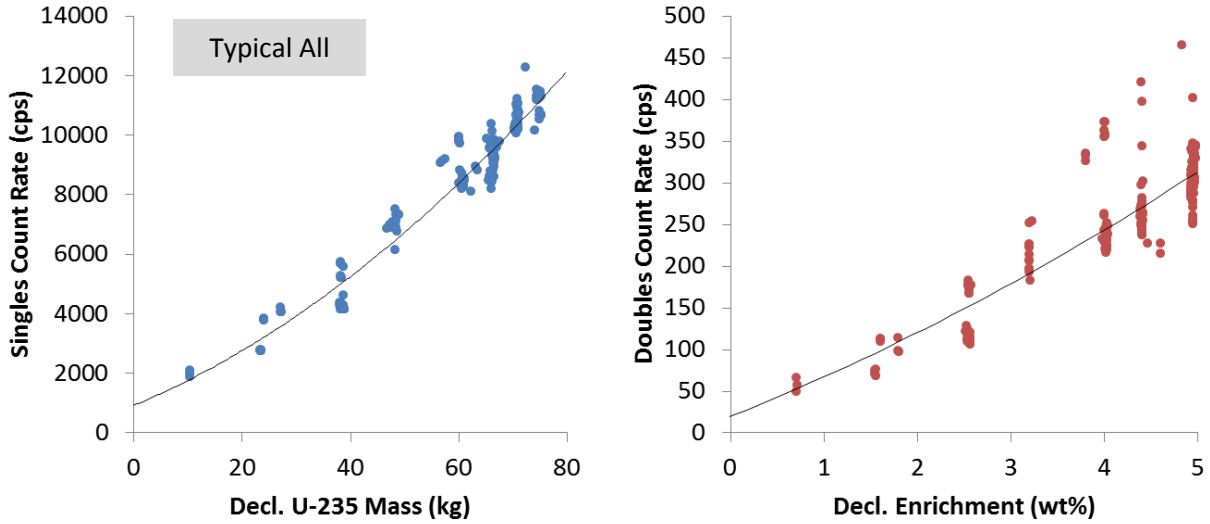


**Figure 57**. PNEM results showing results for $^{235}$U mass based on the singles count rate (left) and enrichment based on the doubles count rate (right) for the Typical All population.

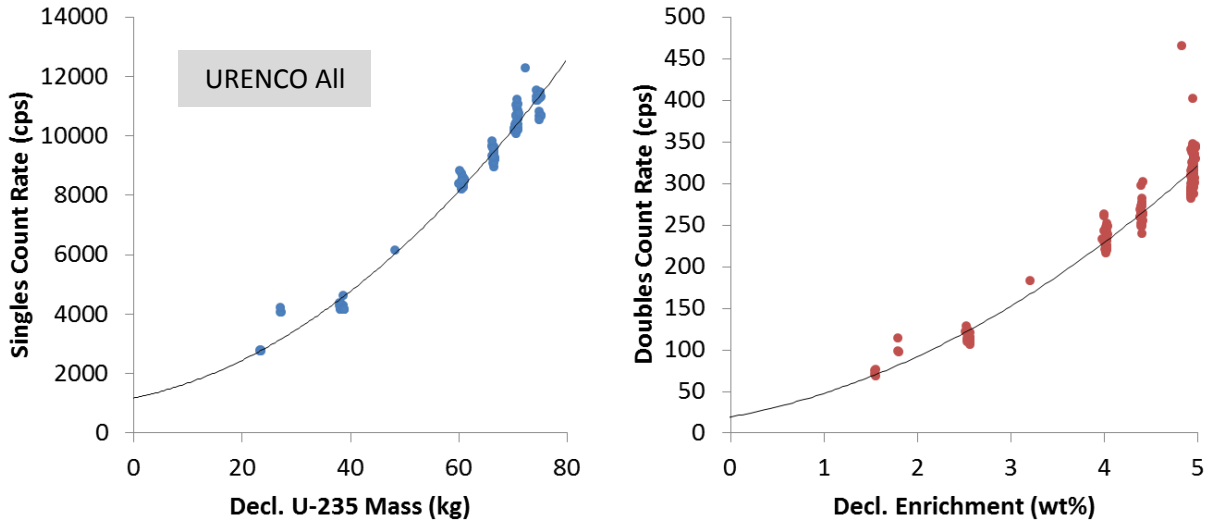


**Figure 58**. PNEM results showing results for $^{235}$U mass based on the singles count rate (left) and enrichment based on the doubles count rate (right) for the URENCO All population.

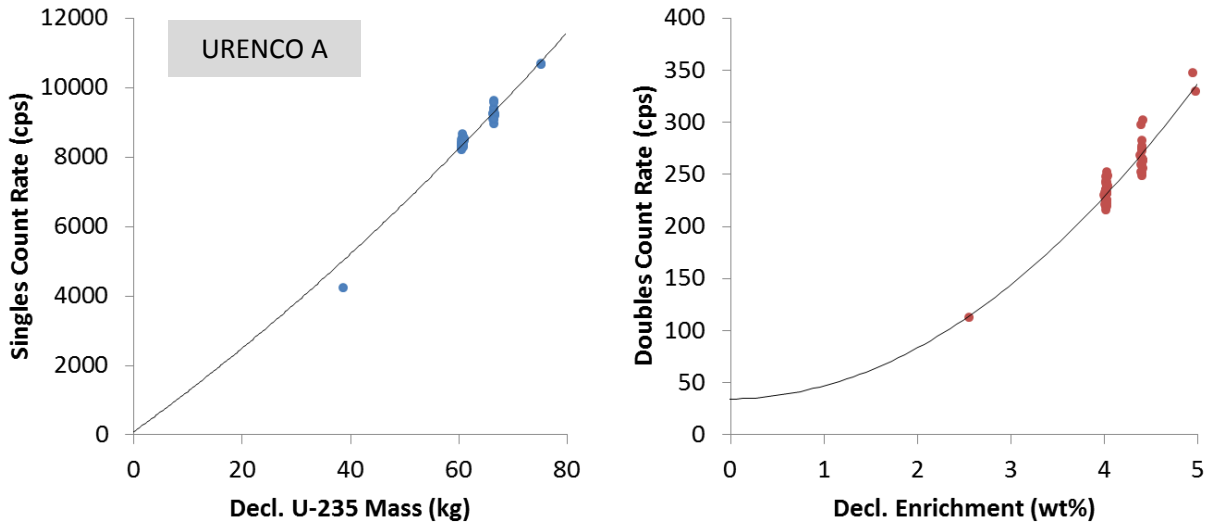


**Figure 59**. PNEM results showing results for $^{235}U$ mass based on the singles count rate (left) and enrichment based on the doubles count rate (right) for the URENCO A population.

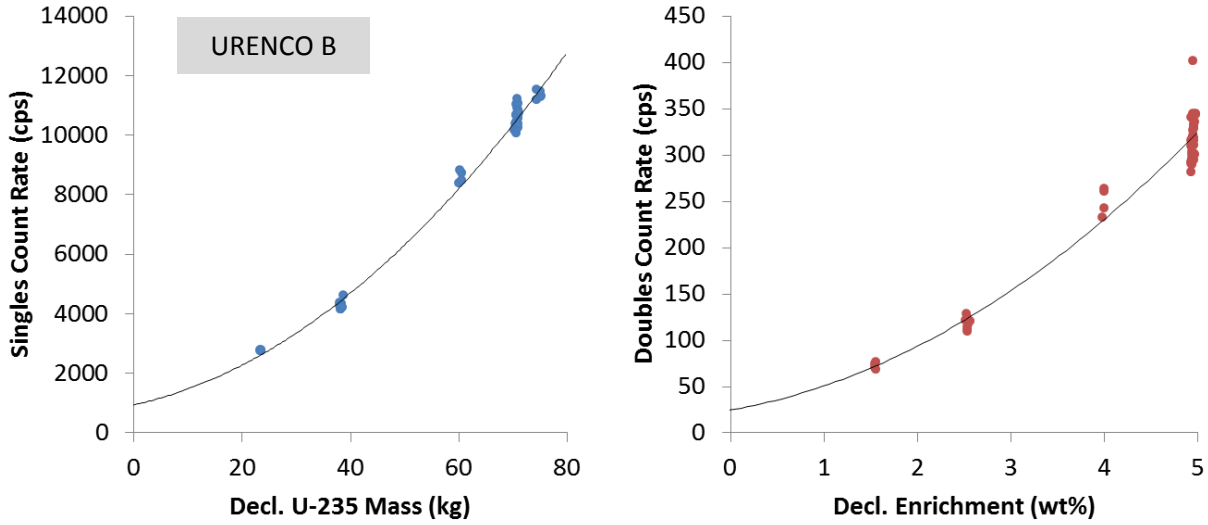


**Figure 60**. PNEM results showing results for $^{235}U$ mass based on the singles count rate (left) and enrichment based on the doubles count rate (right) for the URENCO B population.

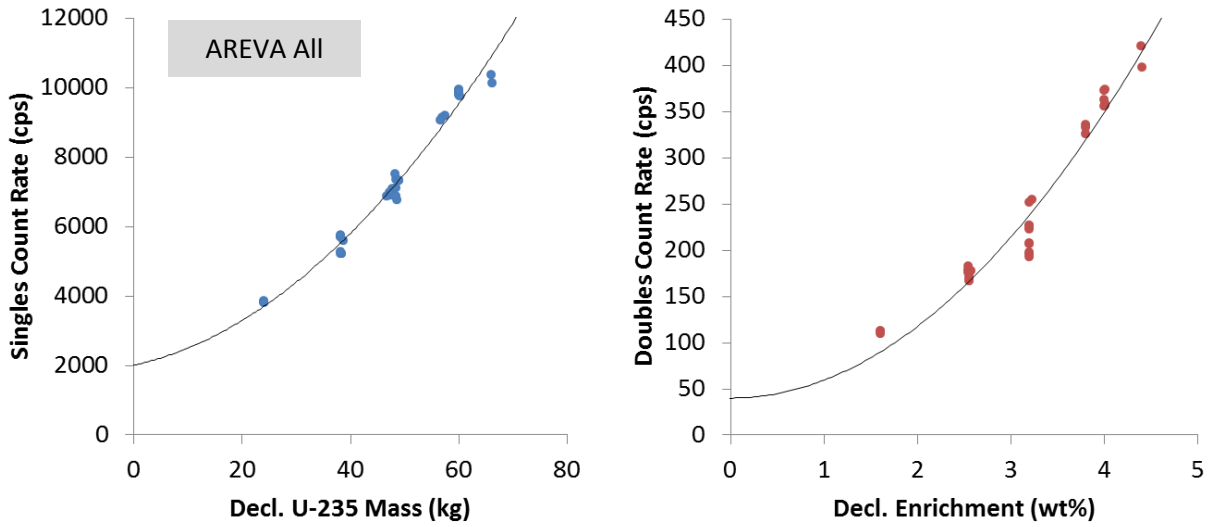


**Figure 61**. PNEM results showing results for $^{235}$U mass based on the singles count rate (left) and enrichment based on the doubles count rate (right) for the AREVA All population.

The results for each sample population are summarized in Table 5. The table provides the RSD between the operator declaration and the value calculated using the PNEM calibration curves for cylinders with enrichment greater than 1%. This includes the value for $^{235}$U mass using the singles count rate and enrichment using both the doubles count rate and hybrid method.

**Table 5**. Relative Standard Deviation from Operator Declared Values for the PNEM System and Typical Cylinder Populations with Enrichment >1%.

| | **Typical All (226)** | **URENCO All (166)** | **URENCO A (66)** | **URENCO B (50)** | **AREVA All (34)** |
|---|---|---|---|---|---|
| PNEM $M_{235}$ (Singles) | 7.4% | 4.8% | 2.1% | 2.9% | 3.4% |
| PNEM $E_{235}$ (Doubles) | 14.8% | 5.7% | 2.4% | 4.9% | 7.6% |
| PNEM $E_{235}$ (Hybrid) | 10.6% | 4.9% | 1.9% | 3.4% | 5.0% |

As discussed in Section 8.1, the UCVS team carved out a subset of 97 cylinders from the URENCO All population on which to compare results of the NDA systems for the full occupancies measured during the field trail against a consistent 5-minute occupancy time. For full occupancies, the "Determine Measurements" feature of Radiation Review was used for automated event selection. Because PNEM used a relatively long 30-second collection cycle for this field trial, the automated event selection picked up the leading and tailing edges on the count rate plateaus as shown highlighted in orange in Figure 62. For 5-minute occupancies, analysis windows were selected manually in the Radiation Review graphical interface, where the leading edges were not included. The "cleaner" occupancy definitions in the 5-minute analysis is expected to reduce systematic uncertainties compared to the full-occupancy analysis, but statistical uncertainties will be higher for the shorter occupancy period. Table 6 shows that in the case of the $^{235}$U mass estimate using the singles count rate, the relative standard deviation actually decreased for the 5-minute occupancy from 2.2% to 2.0%. The reduction in systematic error appears to have been greater than any small increase in the statistical error of a (very precise) singles signature. In the case of

the enrichment estimate using the doubles count rate, the relative standard deviation increased from 3.6% to 3.7%. The statistical uncertainty appears to have been greater than the reduction in systematic errors, for the doubles rate. In any case, there is no significant difference in PNEM results for the full and 5-minute occupancy analyses.

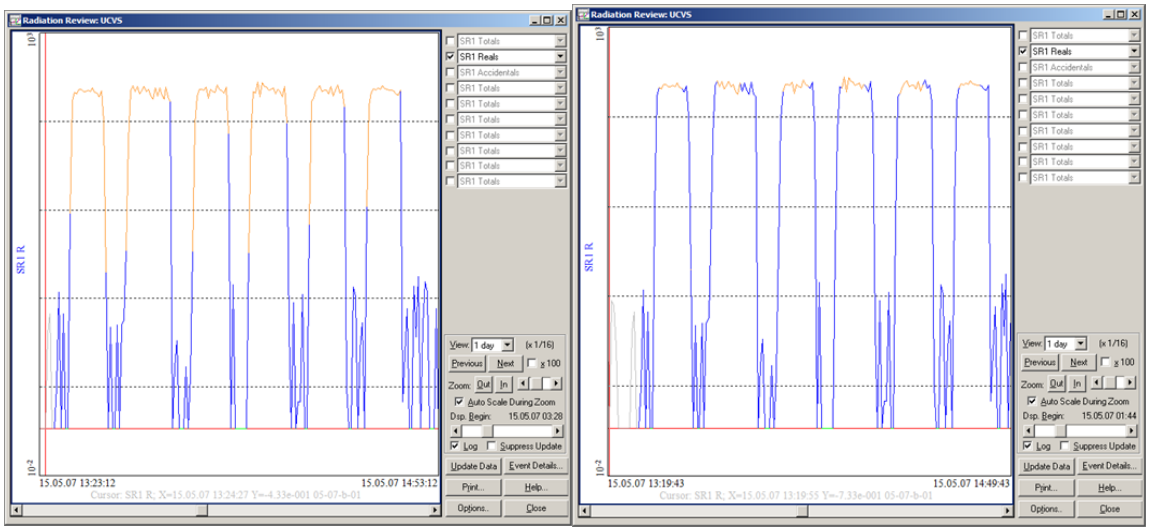


**Figure 62**. PNEM event selection for full occupancies using automated event detection in Radiation Review (left) versus manual selection of analysis window (right).

**Table 6**. Relative Standard Deviation from Operator Declared Values for the PNEM System based on Occupancy Time.

| | PNEM $M_{235}$ (Singles) | PNEM $E_{235}$ (Doubles) |
|---|---|---|
| Full Occupancy | 2.2% | 3.6% |
| 5-Minute Count | 2.0% | 3.7% |

## 9.2 NDA Fingerprint Occupancies

Performance metrics for the NDA Fingerprint viability study were described previously. Analysis and findings for several technical questions associated with the NDA Fingerprint concept are provided below: short-term ("best-case") stability, geometry stability; and time-geometry stability. Several potential NDA Fingerprint signatures were analyzed:

- $PNEM_S$ (total neutron)
- $PNEM_D$ (coincident neutron)
- $HEVA_{186}$ (gross 186-keV)
- $HEVA_{1001}$ (gross 1001-keV ROI; $^{234m}$Pa source terms are wall deposit and $UF_6$)
- $HEVA_{NT}$ (indirect total neutron)

As discussed previously, performance is judged in terms of $\sigma_{FP}$, the total RSD associated with a series of repeated measurements. The total RSD is characterized using two constituents, $\sigma_{stat}$ and $\sigma_{sys\_ran}$.

### 9.2.1 Short-term Stability

A first step in assessing the viability of the NDA Fingerprint concept is understanding the short-term, best-case stability associated with each of the candidate signatures. To address this question, long-dwell cylinder assays of several cylinders were partitioned into 7-minute time segments. Because the cylinder placement is unchanged, no cylinders are moving nearby, and long-term drift is not of concern, $\sigma_{sys\_ran}$ should be negligible and this data series should illustrate the highest achievable repeatability in the signatures and data acquisition equipment. In theory, $\sigma_{FP}$ should be dominated by $\sigma_{stat}$.

Plots of the results for each of the candidate signatures are given in Figure 63 and Figure 64, for a 1.81 wt% cylinder and a total assay time of 35 minutes, partitioned into five, 7-minute segments. Note that the absolute magnitude of the candidate signatures will vary with enrichment (except HEVA 1001-keV), but the stability analysis was performed on the relative difference from the mean, for each time segment. Table 7 provides the total RSD values ($\sigma_{FP}$) for each candidate signature, and estimates on the constituent statistical and systematic contributions, for that specific cylinder.

For both PNEM and HEVA, the expected results were realized: $\sigma_{stat}$ dominated $\sigma_{FP}$ and in some cases, exceeded it, presumably due to the relatively small number of samples (i.e., five) used in this case study. The exception to this is the $HEVA_{186}$ signature, where the statistical and systematic contributions are similar in magnitude. A limited number of samples is the likely explanation, but cannot be confirmed based on this dataset.

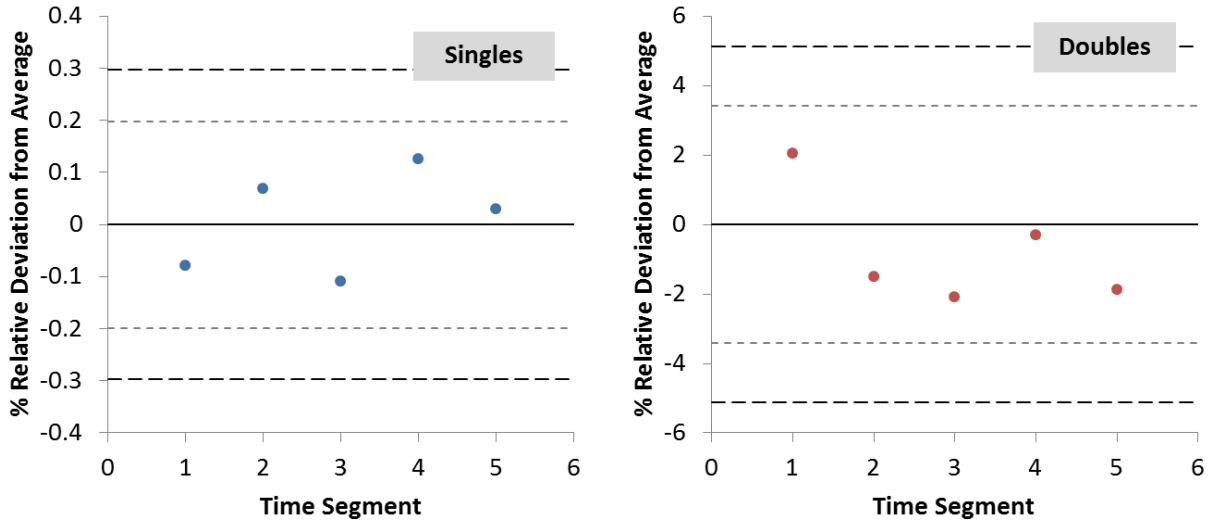


**Figure 63**. Short-term stability results for a 1.81 wt% cylinder for candidate NDA Fingerprint Signatures for PNEM: $PNEM_S$ (left) and $PNEM_D$ (right). Two- and three-sigma thresholds are shown.

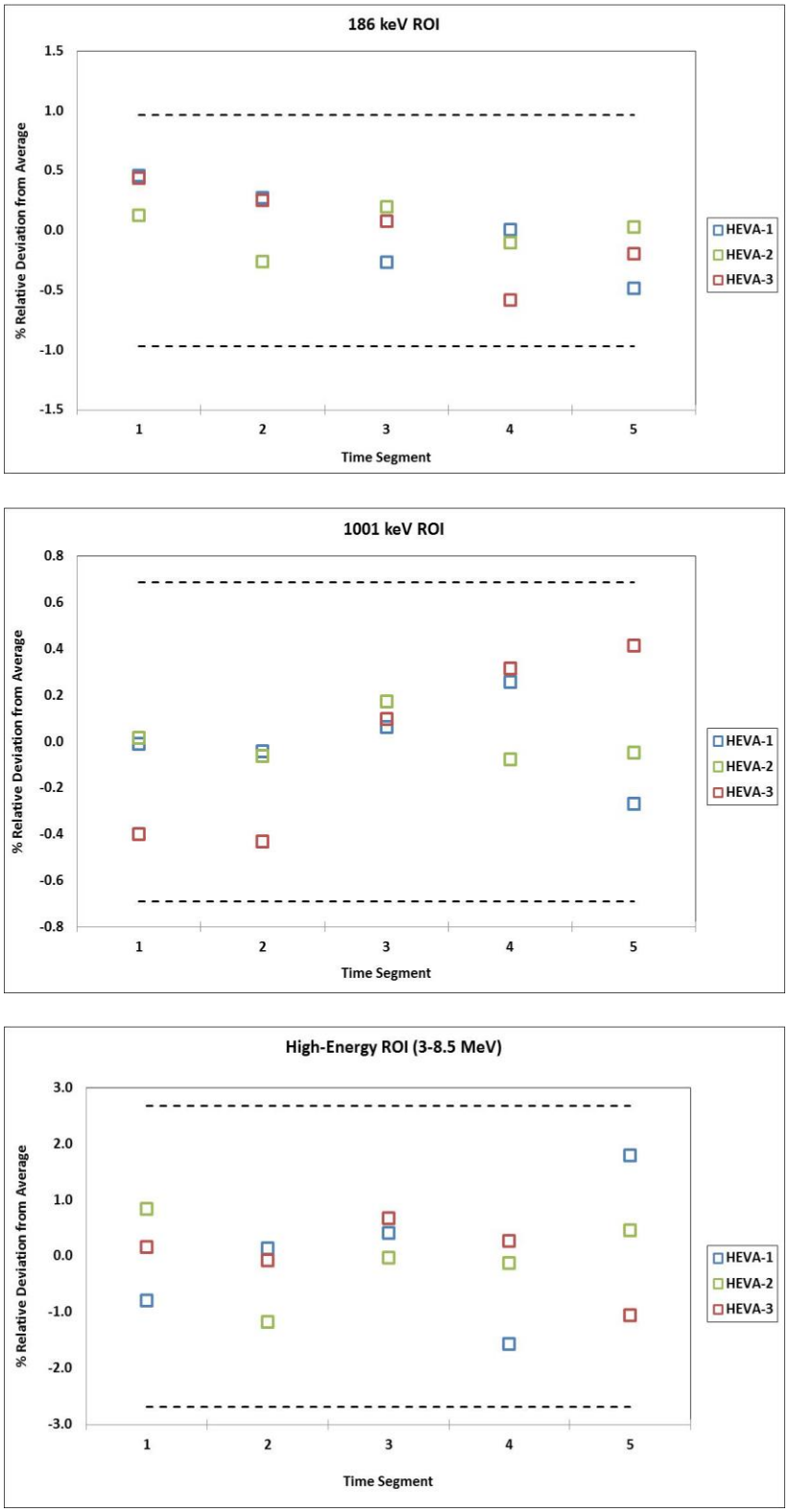


**Figure 64**. Short-term stability results for a 1.81 wt% cylinder for candidate NDA Fingerprint Signatures for HEVA: $HEVA_{186}$ (top), $HEVA_{1001}$ (middle) and $HEVA_{NT}$ (bottom). Three-sigma thresholds are shown.

**Table 7**. Relative standard deviations (in %) for short-term stability of candidate NDA Fingerprint signatures, as measured from a 1.81 wt% cylinder.

| | $\sigma_{FP}$ | $\sigma_{stat}$ | $\sigma_{sys\_ran}$ |
|---|---|---|---|
| $PNEM_S$ | 0.1 | 0.09 | -- |
| $PNEM_D$ | 1.7 | 2.7 | -- |
| $HEVA_{186}$ | 0.32 | 0.22 | 0.23 |
| $HEVA_{1001}$ | 0.23 | 0.21 | 0.08 |
| $HEVA_{NT}$ | 0.39 | 0.65 | -- |

### 9.2.2 Geometry Effects

A cylinder scan sequence was defined to explore the geometry effects on NDA Fingerprint uncertainty, as shown in Figure 65. The sequence begins with multiple (e.g., three or more) "Exact Replacements" in which the operator entirely removed the cylinder from the platform, then made careful efforts (using pen marks on the cylinder) to replace the cylinder in the same location on the platform. The uncertainty associated with these Exact Replacements provides the total RSD, $\sigma_{FP}$, for the repeated replacement of cylinders on the UCVS platform, assuming alignment indicators or controls are integrated in the platform (but were unfortunately, not included in the prototype design). These RSD values were then used to define nominal alarm thresholds for the detection of significant geometry changes, as exemplified in the three-sigma thresholds shown in Figure 66.

The remaining scans in the sequence are deliberate perturbations on the cylinder-sensor geometry. The shifts translate the cylinder 12 cm in one direction or the other. The flip places the valve end of the cylinder in the direction opposite from normal, while striving to maintain (approximately) the same relative position of the $UF_6$ volume and the PNEM/HEVA sensors. The roll consisted of a 45-degree rotation of the cylinder in the azimuthal direction (Figure 65).

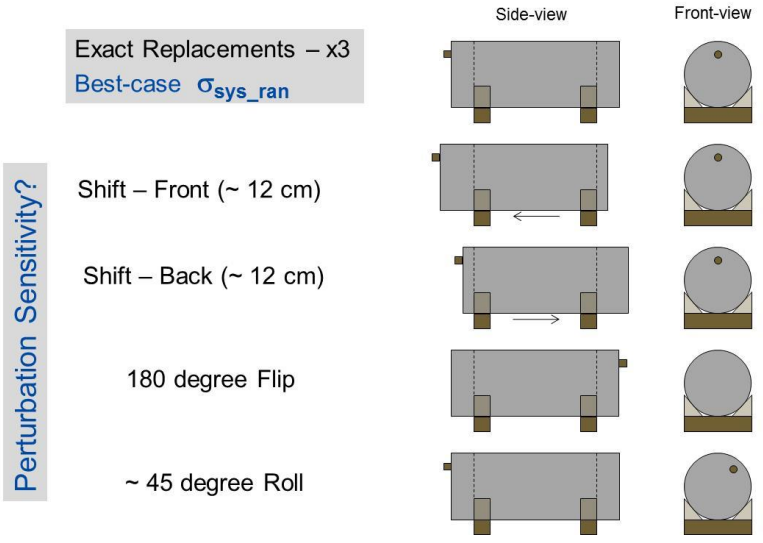


**Figure 65**. Depiction of the cylinder scan sequence used to explore geometry effects on NDA Fingerprint uncertainty.

Plots of the results for each of the candidate fingerprint signatures are given in Figure 66 (PNEM) and Figure 67 (HEVA), for five cylinders with enrichments ranging from approximately 1.5 wt% to 5 wt%. A total of 20 Exact-Replacement occupancies were performed using these five cylinders (a minimum of three, maximum of five occupancies per cylinder). The green box indicates occupancies where the cylinder was consistently positioned on the platform. The red box indicates deliberate geometry changes beyond those expected in routine cylinder handling. For HEVA, results are shown for each of the three modules; $HEVA_{186}$ is not shown but is very similar to $HEVA_{1001}$. Table 8 provides a summary of the RSD values calculated for each candidate signature, based on the exact replacements.

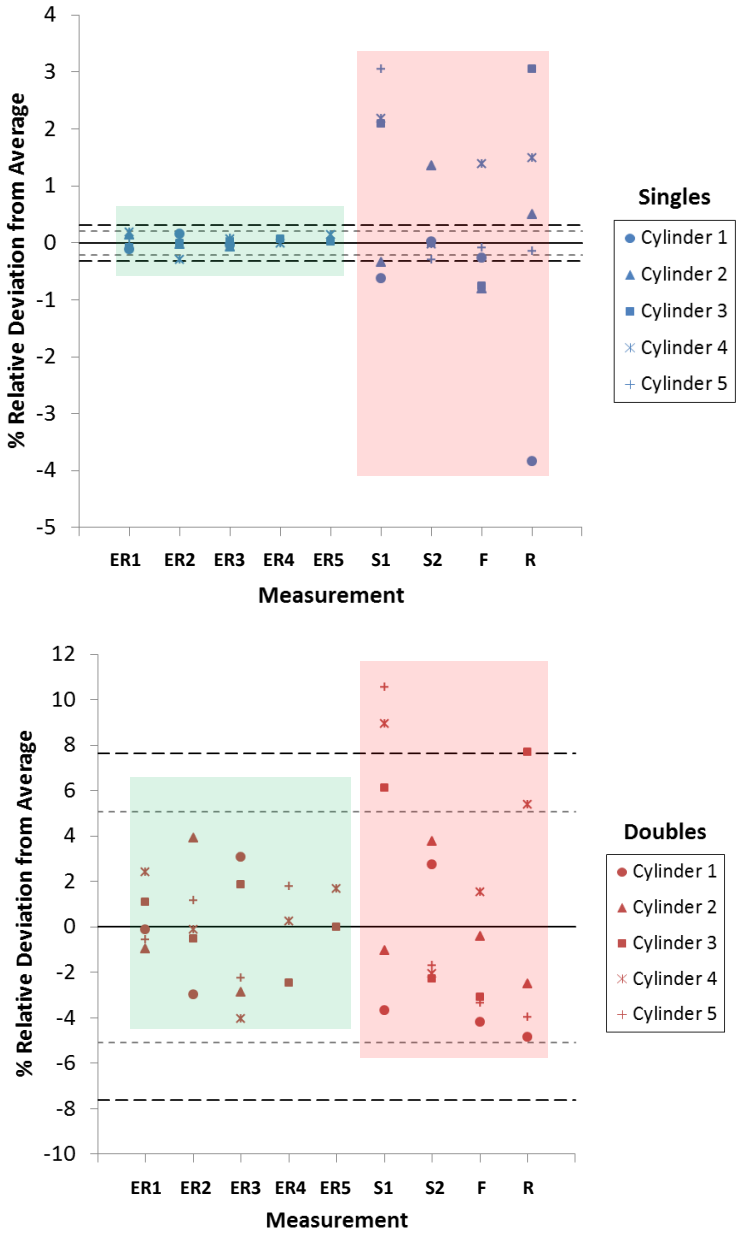


**Figure 66**. Geometry variation results for candidate NDA Fingerprint Signatures from PNEM, based on five Type 30B cylinders (1.5 wt% to 4.95 wt%): $PNEM_S$ (top) and $PNEM_D$ (bottom). Two and three-sigma thresholds are shown.

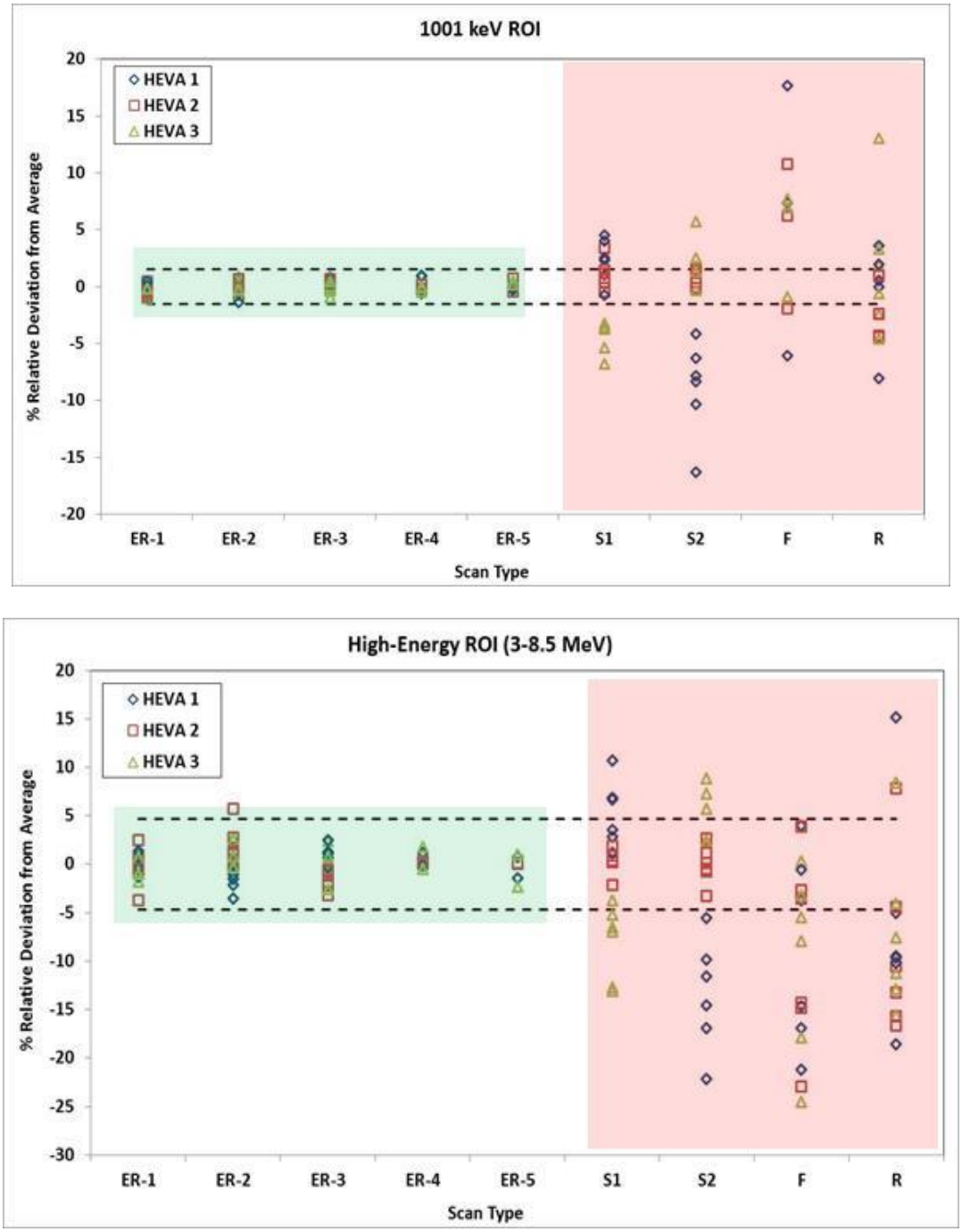


**Figure 67**. Geometry variation results for candidate NDA Fingerprint Signatures from HEVA, based on five Type 30B cylinders (1.5 wt% to 4.95 wt%): $HEVA_{1001}$ (top) and $HEVA_{NT}$ (bottom). Three-sigma thresholds are shown. Some $HEVA_{1001}$ data points with very high relative differences are off scale.

**Table 8**. Relative standard deviations (in %) for candidate NDA Fingerprint signatures, as determined through a series of Exact Replacements on five different cylinders (total of 20 occupancies). Statistical uncertainties assume a 4.0 wt% cylinder and are therefore approximate.

| | $\sigma_{FP}$ | $\sigma_{stat}$ | $\sigma_{sys\_ran}$ |
|---|---|---|---|
| $PNEM_S$ | 0.10 | ~0.07 | 0.10 |
| $PNEM_D$ | 2.5 | ~2.2 | 1.8 |
| $HEVA_{186}$ | 0.55 | ~0.17 | 0.52 |
| $HEVA_{1001}$ | 0.52 | ~0.21 | 0.47 |
| $HEVA_{NT}$ | 0.77 | ~0.65 | 0.42 |

Interpretative comments on the geometry effects study are given here.

- $PNEM_S$ has the highest precision (i.e., lowest $\sigma_{FP}$) of the five candidate signatures for Exact Replacements, and has relatively good sensitivity to deliberate geometry changes (shifts, flips, and rolls). In this initial study, most of the geometry changes would have produced an alarm for most of the cylinders, assuming a three-sigma threshold.
- $PNEM_D$ has the poorest precision of the five candidate signatures and not surprisingly, has poor sensitivity to deliberate geometry changes. The relatively weak doubles signature has high statistical uncertainty that precludes detection of the relatively small systematic effects introduced by the shifts, flips, and rolls.
- $HEVA_{186}$ and $HEVA_{1001}$ have relatively good overall precision, and exhibit relatively high sensitivity to deliberate geometry changes. In several cases, the relative change was greater than 30% (off-scale, not shown in figures above). At least one HEVA module would have alarmed for all deliberate geometry changes. This high geometry sensitivity is due largely to two factors: 1) HEVA employs three distinct modules located along the length of the cylinders, and 2) the gross count rate in the 186- and 1001-keV ROIs are significantly influenced by the thickness and age of the wall deposits, and the characteristics of the $UF_6$ volume, in the collimated field of view for each HEVA module. HEVA-2, generally speaking, shows less variation with the shifts because it is less sensitive to end effects on the cylinders.

$HEVA_{NT}$ has higher variability than $PNEM_S$ due to its relatively low-signal intensity, but may be more sensitive to geometry changes through the use of three distinct neutron detection modules. These preliminary results indicate that $PNEM_S$ and $HEVA_{1001}$ exhibit a number of desirable fingerprint characteristics for the detection of geometry changes. More investigation of their potential is needed, including: analysis of how PNEM singles neutron sensitivity can be tailored to improve geometry-change sensitivity without sacrificing precision, and exploration of $HEVA_{1001}$ (and/or other gamma-ray peak regions) to provide a distinctive, spatial fingerprint of that cylinder via its wall-deposit characteristics. For the latter, the effect of wall-deposit and $UF_6$ age needs investigation—the WFFF field trial provided no data to support an investigation into variations expected from "young" $UF_6$ (i.e., where $^{234m}Pa$ is not yet in equilibrium.)

### 9.2.3 Realistic Scenario: Time + Geometry Effects

A reasonably realistic NDA Fingerprint scenario is one in which some time has passed between repeated cylinder scans (e.g., hours, days or weeks), and the geometry variability is consistent with routine cylinder handling practices and the use of cylinder-positioning provisions on the UCVS to ensure a repeatable geometry. The UCVS team sought to perform this kind of a "Time+Geometry" study at WFFF, but for a number of reasons, the study falls short of the desired conditions.

First, the Time+Geometry occupancies (18 total) are only minutes apart and the $UF_6$ is relatively "old" so that all daughters are in equilibrium. Unfortunately, repeated occupancies with days in between were not realized at WFFF, in large part because cylinders are typically processed soon after arrival (and the initial UCVS scan). Second, because the UCVS platform did not include a positioning indicator for cylinder placement, relatively significant lateral shifts of several cm or more would be expected each time the crane emplaces a cylinder. The exact effects of these shifts are not known, but a comparison of HEVA's detector-to-detector variation for the exact replacements described in the geometry sequences (where lateral position was controlled), and the "inexact replacements" used in the Time+Geometry study is revealing. Detector-to-detector variation was less than 10% for the $HEVA_{1001}$ signature in the exact replacements, but more than 50% for the Time+Geometry occupancies. This variation translates to higher $\sigma_{FP}$ values for the HEVA signatures in Table 9, and likely, negative impacts on the PNEM precision as well. This finding highlights the need for cylinder-positioning controls on a future UCVS, in order to reduce systematic errors for repeated-assay (and one-time assay) scenarios.

A summary of the Time+Geometry results for PNEM and HEVA signatures are given in
Table 9, Figure 68 and Figure 69, for a set of four Type 30B cylinders with enrichments ranging from 1.5 wt% to 4.95 wt%. As in the short-term and geometry stability analyses, the relative difference, from the mean value for the cylinder, was calculated for each occupancy. The cylinder-specific RSDs are reported in Table 9, along with an aggregated RSD taken over the four cylinders and 18 occupancies. For $HEVA_{186}$ and $HEVA_{1001}$, graphical results are shown for each of the three modules but the tabular data are based on an average of the three modules. For $HEVA_{NT}$, the sum over all three modules is plotted and tabulated, to allow a direct comparison to $PNEM_S$.

Also tabulated in Table 9 is the Time+Geometry data for repeated assays (six) of a Type 30A cylinder used by WFFF as a weight standard. The assays are separated in time by weeks—exactly the kind of repeated occupancies the UCVS team intended to study during the WFFF field trial. However, the Type 30A occupancies are poorly matched to the fingerprint study objectives for several reasons. First, the very low enrichment (0.2 wt%) is not representative of the product cylinders of greatest interest, which leads to statistical contributions to overall uncertainty that are much higher (e.g., 4.9% for $HEVA_{NT}$) than they would be for higher enrichments. Second, the thicker wall of the Type 30A (~18 mm) significantly changes the gamma signatures. Third, the occupancy durations range from the typical 7 minutes to more than 2 hours. Also, the Type 30A provides very little insight into temporal effects on the signatures from the actual $UF_6$ material and wall deposits because it has been in the WFFF a long period (years), so that all daughters are in equilibrium and therefore no variation in time is expected. Finally, the occupancies for this atypical cylinder were not analyzed for perturbations caused by cylinder movements nearby. Given the unusually high uncertainty for $PNEM_S$ and $HEVA_{NT}$, it appears likely that nearby cylinder movements did occur during one or more occupancies, some of which were very long in duration. Further evidence is that for this cylinder, the uncertainty of $PNEM_D$ (not sensitive to ambient background changes) is actually

less than the uncertainty for $PNEM_S$. For these reasons, the Type 30A data are set apart from the Type 30B data in Table 9 and were not used in the quantitative analysis described below.

The findings from the Geometry stability study are largely echoed in the results here: $PNEM_S$ shows the highest precision, $PNEM_D$ the lowest; HEVA gamma-ROI signatures are comparable and show modest precision; $HEVA_{NT}$ is inferior to $PNEM_S$ in terms of precision. Uncertainties are somewhat higher than for the exact replacements in the Geometry study, due to the (presumably) larger variation in the cylinder placement on the platform.

**Table 9**. Relative standard deviations ($\sigma_{FP}$ in %) for candidate NDA Fingerprint signatures in the Time+Geometry study. RSDs are shown for each of the four Type 30B cylinders (number of occupancies indicated in parenthesis, e.g. "5X"), an aggregate value over all four Type 30B cylinders. For comparison, the results for a Type 30A cylinder with much higher variability in terms of time and geometry parameters, is also shown.

| | **$PNEM_S$** | **$PNEM_D$** | **$HEVA_{186}$** | **$HEVA_{1001}$** | **$HEVA_{NT}$** |
|---|---|---|---|---|---|
| **$\sigma_{stat}$** (4 wt%) | ~0.05 | ~2.2 | <0.2 | ~0.2 | ~0.6 |
| Type 30B (1.5 wt%, 4X) | 0.08 | 1.2 | 0.62 | 0.79 | 0.34 |
| Type 30B (3.8 wt%, 5X) | 0.10 | 0.67 | 0.59 | 0.56 | 1.36 |
| Type 30B (4.4 wt%, 4X) | 0.19 | 2.7 | 0.82 | 0.88 | 0.41 |
| Type 30B (4.95 wt%, 5X) | 0.33 | 3.5 | 1.3 | 1.1 | 0.83 |
| **Aggregate $\sigma_{FP}$ *** | **0.19** | **2.2** | **0.81** | **0.79** | **0.72** |
| | | | | | |
| Type 30A (0.2 wt%, 6X)** | 2.4 | 2.1 | 1.04 | 0.90 | 5.05 |

*Based on all four Type 30B cylinders, total of 18 occupancies, 7-minute occupancies.
**Long and variable occupancy times (~18, 9, 7, 12, and 127 minutes), ~weekly assays

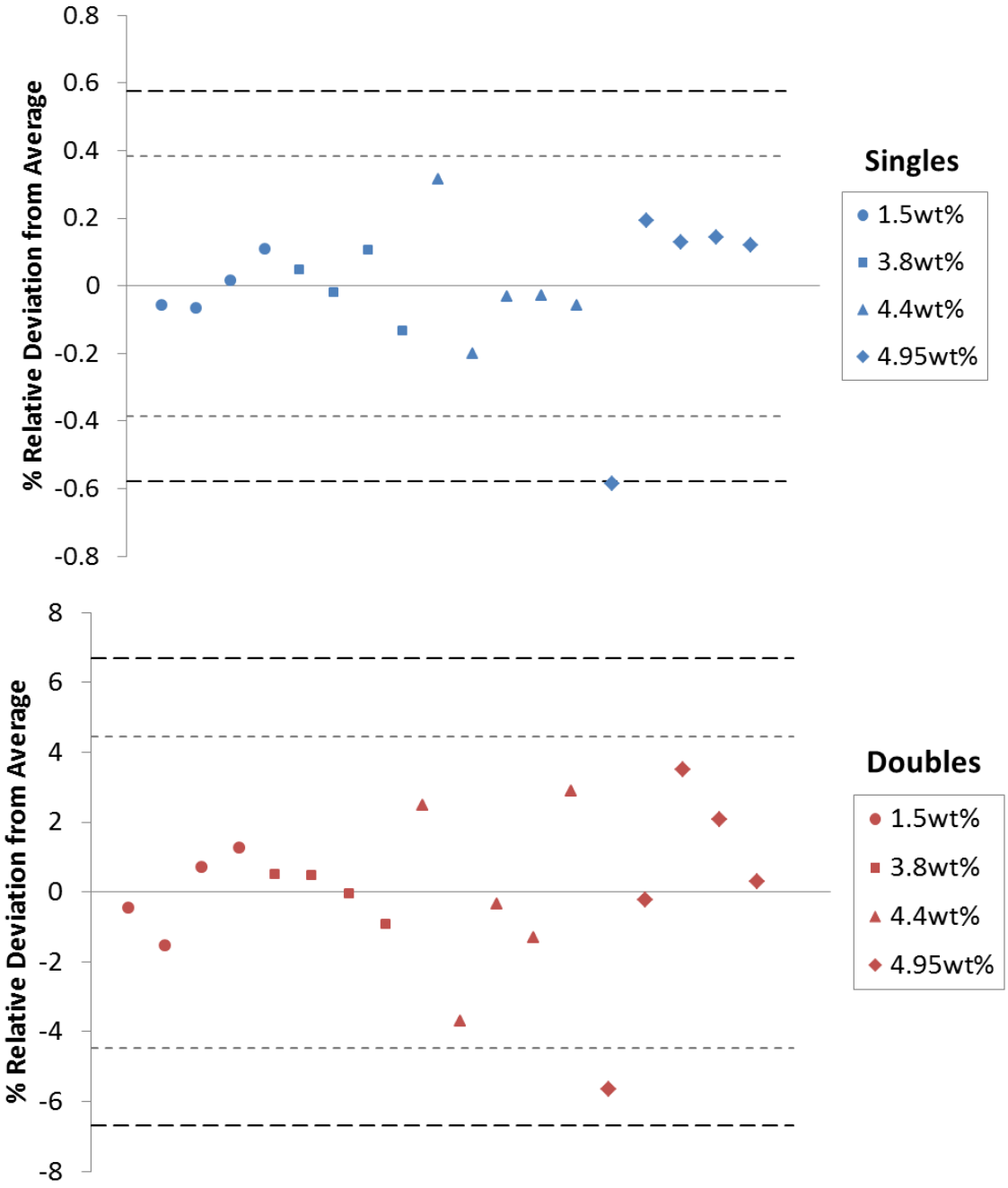


**Figure 68**. Example NDA Fingerprint results for a series of "inexact replacements" over four cylinders and a total of 18 occupancies for $PNEM_S$ (top) and $PNEM_D$ (bottom). Two and three-sigma thresholds are shown.

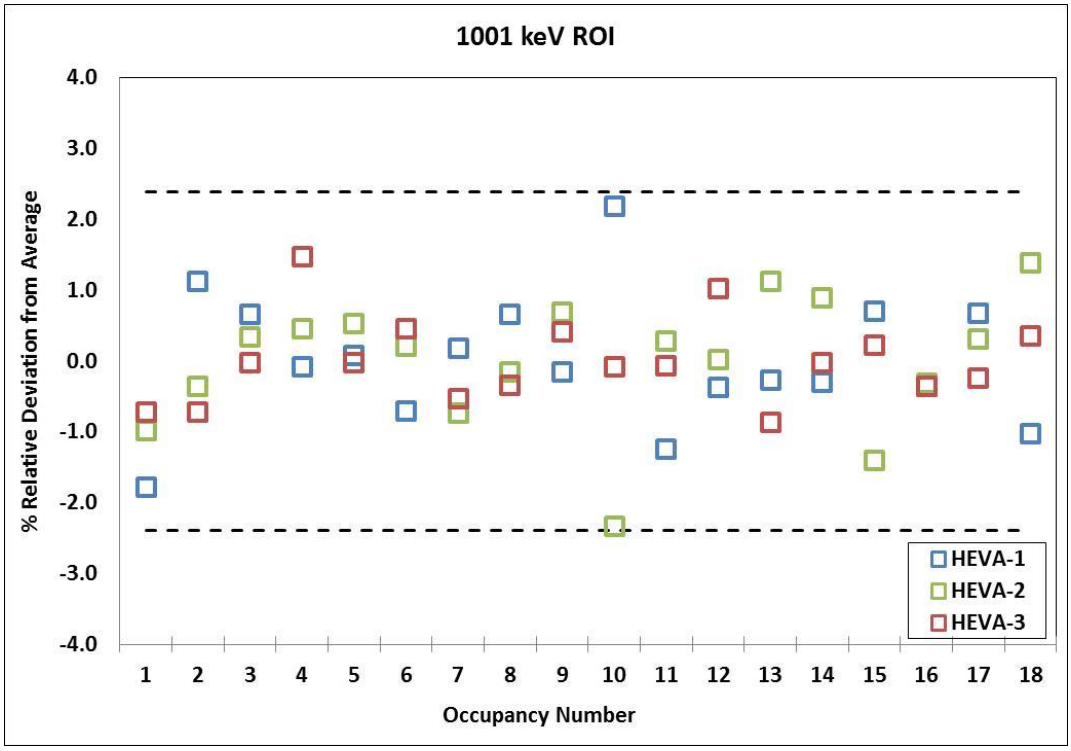


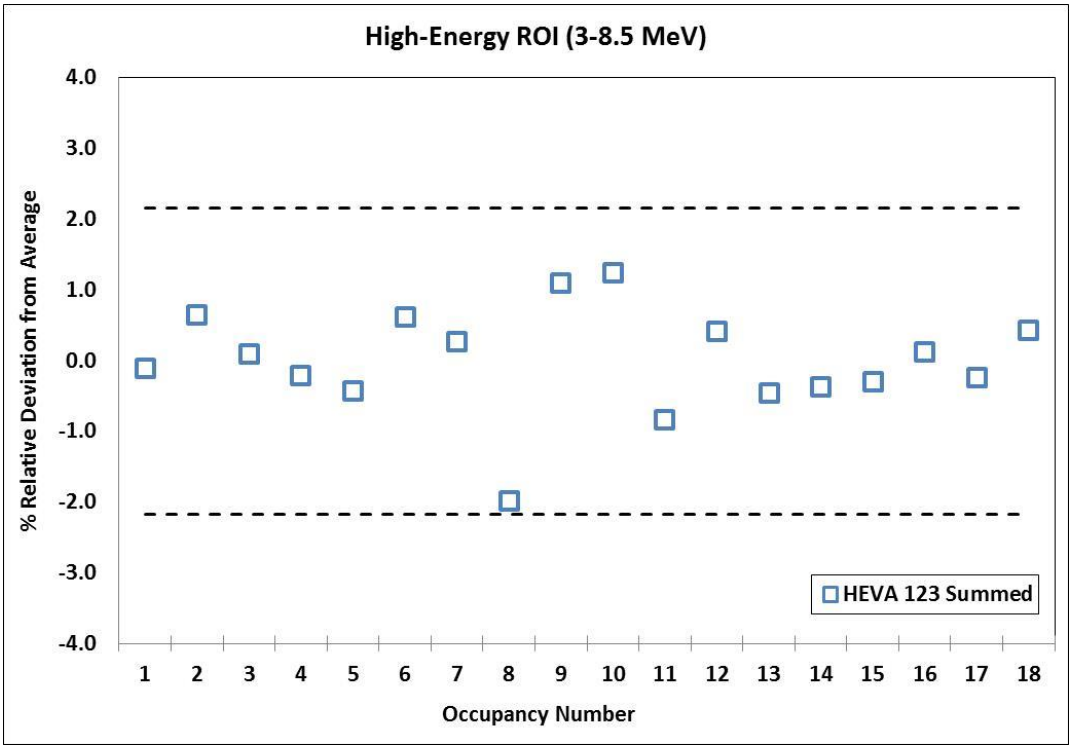


**Figure 69**. Example NDA Fingerprint results for a series of "inexact replacements" over four cylinders and a total of 18 occupancies for $HEVA_{1001}$ (top) and $HEVA_{NT}$ (bottom). Three-sigma thresholds are shown.

### 9.2.4 Preliminary Test Cases for NDA Fingerprint Concept

The "Time+Geometry" results discussed in the previous section were used to support preliminary test cases of the NDA Fingerprint concept. For these test cases, the "Aggregated $\sigma_{FP}$" values for each candidate signature in Table 9 were used to support analysis of repeated assays for a different set of "unknown" cylinders. The fingerprint test cases performed in Phase I are summarized here:

1. For each test-case cylinder, calculate the relative difference, from the initial baseline occupancy, for each candidate fingerprint signatures.
2. Use the Aggregate $\sigma_{FP}$ values to translate that relative difference to a multiple of $\sigma_{FP}$. For example, if $\sigma_{FP}$ $HEVA_{NT}$ is 0.72% and the relative difference for the second cylinder occupancy is 1.54%, then $N\sigma_{FP} = 2.0$.

A summary of the results for the NDA Fingerprint test cases, using three cylinders with enrichments of 1.5 wt%, 1.8 wt%, and 3.2 wt% are shown in Table 10. $HEVA_{186}$ is not reported here because it largely mirrors $HEVA_{1001}$ for these case studies. The case study results use only HEVA-2 signatures; HEVA-1 and HEVA-3 signatures exhibited large variations due to inconsistent lateral positioning of the cylinders in the NDA Fingerprint calibration scans (see previous section). Only data from the center module, HEVA-2, were deemed appropriate for a case study analysis that assumes consistency in lateral positioning of the cylinder on the platform.

**Table 10**. Summary of results for NDA Fingerprint test cases. The absolute value of the relative difference of each signature from the initial baseline occupancy is expressed in terms of $N\sigma_{FP}$.

| **Proxy ID** | **E (wt%)** | **Date** | **$PNEM_S$** $\sigma_{FP}$=0.19% | **$PNEM_D$** $\sigma_{FP}$=2.2% | **$HEVA_{1001}$** $\sigma_{FP}$=0.79% | **$HEVA_{NT}$** $\sigma_{FP}$=0.72% |
|---|---|---|---|---|---|---|
| 123 | 0.2 wt% | 2015-6-15 | – | – | – | – |
| | | 2015-6-23 | 1.5 | 2.5 | 1.6 | 3.3 |
| 510 | 1.8 wt% | 2015-6-23 | – | – | – | – |
| | | 2015-11-04 | 8.6 | 2.4 | 4.8 | 9.2 |
| | | 2015-11-30 | -2.3 | -0.04 | 2.4 | 1.0 |
| 355 | 3.2 wt% | 2015-11-04 | – | – | – | – |
| | | 2015-11-30 | -2.7 | -0.6 | 3.8 | 1.8 |

The $N\sigma_{FP}$ values from these case studies provide a preliminary indication of the threshold levels that might be used for each candidate signature, in order to minimize false alarms. The very limited dataset from the WFFF field trial, and the lack of a lateral-positioning indicator on the prototype preclude any definitive assessment of the NDA Fingerprint concept using these case studies. However, it is clear that the second occupancy for the 1.8 wt% cylinder shows far higher relative differences than other occupancies, for both NDA methods. The imagery for that occupancy showed no indication of nearby cylinders.

## 9.3 Atypical Cylinders

The Atypical cylinder population includes five AREVA cylinders with the WR designation (all of which were flagged for elevated $^{232}$U content by HEVA) and two cylinders from diffusion plants (one of which was Chinese). Because the majority of the Atypical cylinders are known to be from AREVA and the Typical All calibration curve is heavily biased for URENCO cylinders, the AREVA All calibrations for HEVA and PNEM were used to analyze the Atypicals.

Figure 70 shows a plot of the declared $^{234}$U versus $^{235}$U mass for the AREVA All population as well as that for the Atypical cylinders. The Chinese-origin cylinder is not included in the plot because the $^{234}$U content was not declared. The cluster of AREVA WR cylinders does show a higher $^{234}$U content than the typical AREVA cylinders, which is expected for HEU downblend material, but the variance is not on the order of what might be seen for reprocessed material from reactor returns, for example. The gaseous diffusion cylinder at the high end of the plot is consistent with the $^{234}$U/$^{235}$U behavior from the AREVA All population. Two key questions for the Atypical analysis were: 1) whether these cylinders could be analyzed accurately with the PNEM and HEVA calibration curves for AREVA All and 2) if not, whether PNEM and HEVA would flag these elevated $^{234}$U concentrations as off-normal.

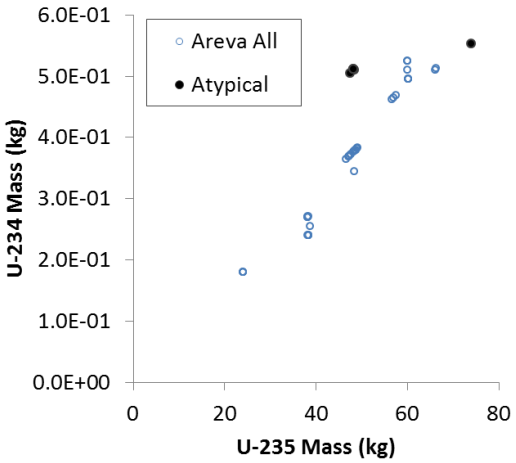


**Figure 70**. $^{234}$U versus $^{235}$U behavior for AREVA All and Atypical cylinder populations, not including the Chinese-origin cylinder.

### 9.3.1 HEVA Analysis

Table 11 provides a summary of the HEVA results relative to the declared values, using the analysis and reporting approach detailed in Section 8.4.3. The 'N*$\sigma_M$' column provides the difference between the two enrichment calculations, $HEVA_T$ and $HEVA_{NT}$ (using the declared total U mass), measured by the number of standard deviations, N, and where $\sigma_M$ is the $HEVA_{NT}$ value of 5.4% for the AREVA All population. If the difference between the two measured enrichment values is more than 3*$\sigma_M$, then a consistency flag is raised indicating that the $^{234}$U concentration is outside the calibrated range of the instrument. In that case, HEVA reports only the $HEVA_T$ result, since that signature is not dependent on $^{234}$U. For this set of cylinders, no $^{234}$U flags were raised and therefore, $HEVA_{hybrid}$ was reported for all of them. The relative differences from the declared enrichment values ($\Delta E_{235}$) for all seven cylinders were consistent with the AREVA All population.

**Table 11**. HEVA results for assay of Atypical cylinders.

| Proxy ID | Decl. $E_{235}$ (wt%) | Meas. $E_{235}$ (wt%) | | | $N\sigma_M$ | $^{234}U/^{235}U$ Iso Flag | $^{232}U$ Detect | $\Delta E_{235}$ (rel%) (**Trad** or Hybrid) |
|---|---|---|---|---|---|---|---|---|
| | | $HEVA_T$ | $HEVA_{NT}$ | $HEVA_{Hybrid}$ | | | | |
| 371 | 3.23 | 3.39 | 3.37 | 3.38 | 0.11 | | X | 4.8 |
| 886 | 3.20 | 3.36 | 3.44 | 3.40 | 0.44 | | X | 6.2 |
| 885 | 3.20 | 3.19 | 3.39 | 3.27 | 1.16 | | X | 2.2 |
| 643 | 3.20 | 3.06 | 3.51 | 3.29 | 2.74 | | X | 2.8 |
| 519 | 3.20 | 3.28 | 3.36 | 3.32 | 0.47 | | X | 3.7 |
| 657 | 4.95 | 5.04 | 4.90 | 4.89 | 0.52 | | | -1.2 |
| 002 | 4.95 | 4.91 | 4.92 | 4.90 | 0.03 | | | -1.1 |

### 9.3.2 PNEM Atypical Analysis

Table 12 provides a summary of the PNEM results for the atypical cylinders. The table lists the cylinder ID, operator-declared $E_{235}$, measured $E_{235}$ for $PNEM_D$ and $PNEM_S$ (using the declared total U mass) , where the average of these two values is equal to $PNEM_{Hybrid.}$ The relative differences between the operator-declared and measured $E_{235}$ values. The second-to-last column provides the difference between the two enrichment calculations, $PNEM_D$ and $PNEM_S$, measured by the number of standard deviations, N. The $\sigma_M$ values used was 3.4% corresponding to the AREVA All typical cylinder results. If the difference between the two measured enrichment values is more than $3\sigma_M$, then a $^{234}U/^{235}U$ consistency flag is raised indicating that something about the cylinder, most likely the assumption of a known $^{234}U/^{235}U$ behavior, is outside the calibrated range of the instrument. This is shown explicitly in the final column in Table 12. In other words, the concept is that if two different methods for measuring the same value generate results that are significantly different, then that is an indicator that the results are questionable. Whether or not $3\sigma_M$ is the best threshold to employ needs further study, but it is used here for demonstration purposes.

**Table 12**. PNEM results for the assay of atypical cylinders

| Proxy ID | Decl. $E_{235}$ (wt%) | Meas. $E_{235}$ (wt%) | | $\Delta E_{235}$ (rel%) | | $N\sigma_M$ | $^{234}U/^{235}U$ Iso Flag? |
|---|---|---|---|---|---|---|---|
| | | $PNEM_D$ | $PNEM_S$ | $PNEM_D$ | $PNEM_S$ | | |
| 371 | 3.23 | 3.21 | 3.25 | -0.47 | 0.67 | 0.37 | |
| 886 | 3.20 | 3.27 | 3.37 | 2.23 | 5.28 | 0.90 | |
| 885 | 3.20 | 3.27 | 3.37 | 2.27 | 5.33 | 0.90 | |
| 643 | 3.20 | 3.38 | 3.43 | 5.50 | 7.18 | 0.44 | |
| 519 | 3.20 | 3.30 | 3.33 | 3.21 | 3.92 | 0.27 | |
| 657 | 4.95 | 4.19 | 4.70 | -15.36 | -4.98 | 3.58 | X |
| 002 | 4.95 | 4.94 | 4.90 | -0.16 | -1.02 | 0.24 | |

In all but one instance, the accuracy of the measured $E_{235}$ values for the atypical cylinders are in line with what would be expected compared with analysis of the AREVA All typical cylinders. The exception is the $E_{235}$ value calculated with the doubles for the cylinder of Chinese origin, which would stand out as an

outlier. The $E_{235}$ calculated via the singles for that cylinder is relatively accurate. There is a discrepancy between the two enrichment estimates of $3.58\sigma_M$, meaning the $^{234}U/^{235}U$ isotopics flag is raised for that cylinder as shown in Table 12. Unfortunately, the $^{234}U$ content of the Chinese origin cylinder is not available, so there is no way to know whether the discrepancy is related to the $^{234}U/^{235}U$ behavior for that cylinder, but it is promising that the one erroneous result has a consistency flag associated with it.

# 10.0 Other Analysis and Findings

A summary of the long-term stability analysis for the NDA methods, and analysis of the load-cell data collected during the field trial, are given here.

## 10.1 Long-term Environmental Stability Analysis

In accordance with UCVS User Requirements (IAEA 2013a) , the thermal stability of the NDA methods is essential to ensure stable and accurate measurements over long periods, and an analysis of thermal stability was requested by the IAEA in Phase I of the project. This section describes the long-term stability analysis for PNEM and HEVA.

As noted previously, the UCVS prototype was installed outdoors at the Westinghouse facility and subject to relatively large swings in environmental conditions over the length of the field trial. Data from the environmental sensors was used to evaluate the stability of the NDA instruments with respect to changes in temperature, humidity, pressure, and dewpoint. Generally speaking, no cylinder movements are made at the facility over the weekends, so 48-hour weekend blocks were used for this analysis. Figure 71 contains box-and-whisker plots of the environmental sensor data for 35 weekends between April and December 2015. Each box shows the spread of the data over 48 hours, assuming 30-second measurement intervals, and the whiskers extend to the maximum and minimum points over each weekend. The temperature range covered in this analysis is 2ºC to 37ºC.

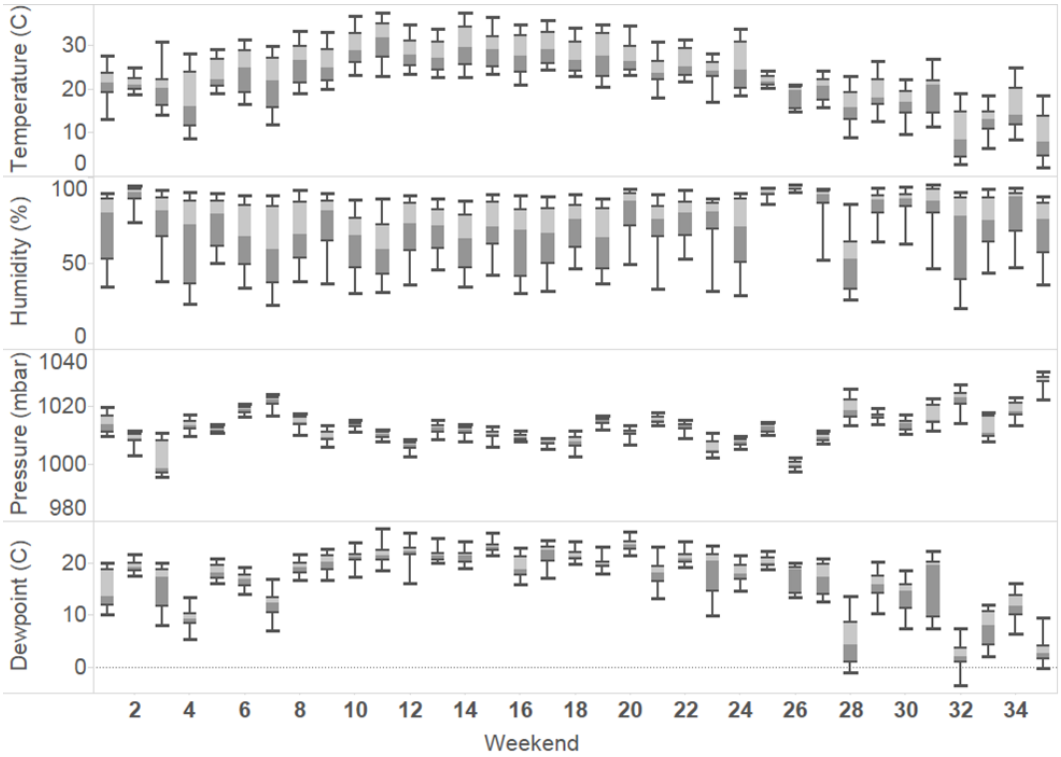


**Figure 71**. Box-and-whisker plots showing the environmental sensor data over 35 weekends from April to December 2015, based on 30-second measurement intervals.

In order to evaluate stability of the NDA systems, it was assumed that the RSD of the background signals is a combination of counting statistics and environmental effects added in quadrature: $\sigma^2_{weekend} = \sigma^2_{stat} + \sigma^2_{env}$. Figure 72 and Figure 73 show the stability analyses for PNEM and HEVA, respectively, over the 35-week range. The temperature variation data during the same period is plotted for comparison. A summary of the RSD values for the long-term stability analysis is given in Table 13.

The long-term variability in PNEM signals is shown in Figure 72: RSD values for $PNEM_S$, based on 30-second measurement intervals in each 48-hour period, distribution of $PNEM_D$ samples (also 30-second intervals), and the weekend average. As expected, the doubles background is stable at ~0 counts per second (RSD for doubles is undefined/infinite because of division by ~0). Notably, an anomalously high value occurs at week 27. Review of the NGSS feed from that weekend showed that there was activity on site including cylinder movements near the UCVS. The data for that weekend are not included in the analysis for Table 13. The average RSD value for $PNEM_S$ was 1.2%.

Based on the mean singles background count rate, the statistical contribution to that total is 1.0%. This translates to an estimated long-term stability of approximately 0.7% on the background count rate. In terms of actual count rate, this is less than 5 cps, a negligible rate compared to the singles rate for a full cylinder in the range of 2000 to 12000 cps. Furthermore, PNEM singles and doubles show no indication of significant drift or trending with temperature.

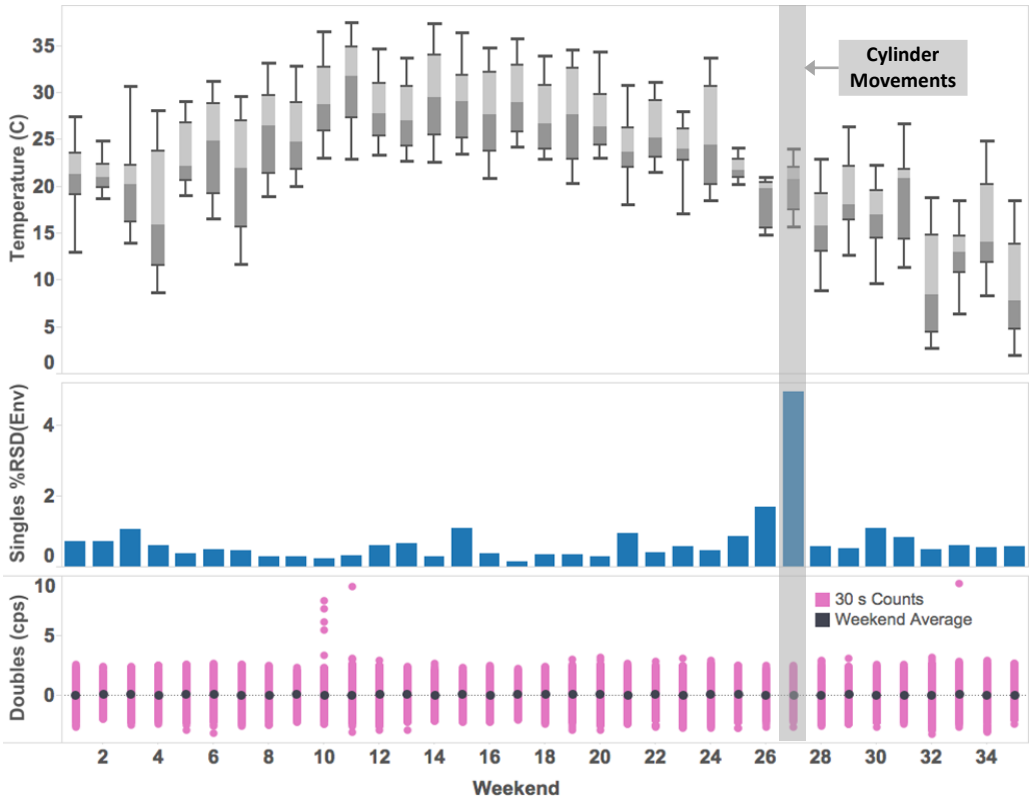


**Figure 72**. Long-term environmental stability analysis of the PNEM data.

A similar analysis was performed for HEVA using the gross count rates in three gamma-ray ROIs: 1460 keV from naturally occurring $^{40}$K, 2614 keV from naturally occurring $^{208}$Tl (daughter of $^{232}$Th), and the 3 to 8 MeV ROI corresponding to indirect neutron detection with HEVA. A time interval of 4 hours was used to achieve a high enough statistical precision to reveal any long-term drift. Figure 73 illustrates that the RSDs for all three ROIs are quite stable over the 35-week period, with the lowest uncertainty for the high-energy (i.e., singles neutron) ROI. Note that seven weekends are excluded from the HEVA RSD analysis: three in July because heels cylinders were on the nearby trailer during that time, and four in September and October due to HEVA data acquisition failures during that time. As with PNEM, week 27 is also excluded due to nearby cylinder movements. The Table 13 data show that the long-term stability is between 0.4% and 0.6% for the three background ROIs. In terms of absolute count rates, this level of drift is negligible compared to the high rates (few kcps or more) expected in each module for full cylinders. These preliminary findings give no indication of significant drift or trending with temperature, for the HEVA instrumentation.

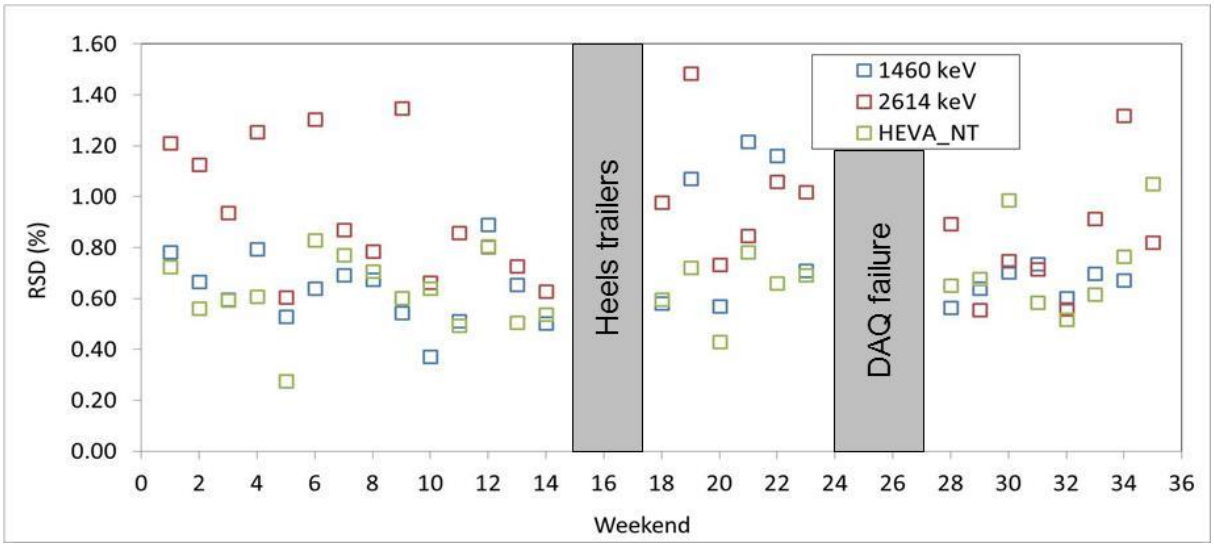


**Figure 73**. Long-term environmental stability analysis of the HEVA data**.**

**Table 13**. Summary of Long-Term Environmental Stability Results for PNEM and HEVA.

| | $\sigma_{weekend}$ | $\sigma_{env}$ | $\sigma_{stat}$ |
|---|---|---|---|
| PNEM$_S$ | 1.2% | 0.7% | 1.0% |
| HEVA 1460 keV ROI | 0.7% | 0.6% | 0.4% |
| HEVA 2614 keV ROI | 0.9% | 0.4% | 0.8% |
| HEVA 3 to 8 MeV ROI | 0.7% | 0.5% | 0.5% |

## 10.2 Load-Cell Analysis

Though not a part of the original SP-1 scope, four Mettler Toledo 0970 weigh modules were installed as part of the UCVS platform, based on guidance from NNSA and the IAEA. These load cells were connected to a junction box which was in turn connected to a weighing indicator. When the UCVS platform was installed at the WFFF site, the shipping blocks were removed, the UCVS platform was leveled with shims, and the shims were welded in place.

The weighing system was calibrated using a two-point calibration: the zero was set with the platform empty, and the WFFF weight standard (filled, Type 30A cylinder) was used to set the full span weight. These same weighing components were set up at ORNL's platform scale testing center in a similar manner and in a series of preliminary tests, performed within specifications.

Soon after the weighing components were calibrated, the UCVS team observed that the zero was drifting significantly more than expected: up to ~40 kg and in a manner that seemed correlated with daily temperature fluctuations. A team from ORNL and SRNL returned in June 2015 to troubleshoot the issue. The team disconnected all but a single load cell, recalibrated, and observed how each load cell drifted for approximately 30 minutes. This testing revealed that a single load cell was drifting significantly more than the others.

For the subsequent month, the suspect load cell was left disconnected, leaving only three in operation. In late July 2015, a team from ORNL and SRNL returned to WFFF with the master technician from the local Mettler Toledo distributor. The Mettler Toledo technician isolated each load cell and tested them against expected resistance measurements. The technician found all of the load cells to exhibit the proper resistance. He reconfigured the weighing indicator to use less precision, recalibrated and considered the problem resolved. The ORNL team released the Mettler Toledo technician. The test weight cylinder was left on the scale for approximately 2 hours. Drift of approximately 2 kg was observed during that time but after the test cylinder was removed, the "zero" or empty scale weight had drifted upwards approximately 4 kg. The team decided to replace the suspect load cell; the system was then re-zeroed, and recalibrated.

From that point forward, the load cell data were much improved, based on a preliminary analysis. When vacant, the scale reports a weight much closer to zero but anomalous short-term excursions have been observed. More investigation is needed, but one possible explanation is the effects of direct sunlight heating the load cells unevenly.

Because the installation and analysis of load cells were not part of the original SP-1 scope, a complete analysis of the data is not included in this report. That analysis will be released separately by ORNL.

# 11.0 NDA Modeling and Simulation Study

Per the original SP-1 guidance, a modeling and simulation study was undertaken to complement the UCVS field trial. The main objectives of this study were to address questions that cannot be addressed easily through field trials. Examples include investigating the interrogation depth of the signatures collected by HEVA and PNEM and the sensitivity of those methods to partial-defect scenarios of interest to the IAEA.

The UCVS team adopted a consistent set of modeling assumptions, radiation transport methods, and analysis methods. Table 14 provides a list of neutron emission rates for each uranium isotope and reaction used to calculate source terms (Reilly et al. 1991; Miller et al. 2014a). Monte Carlo N-Particle (MCNP) V6 (Goorely et al. 2012) was used in the development of their HEVA and PNEM models, respectively. The team collaborated to develop the "full-scene" MCNP model of the as-built prototype (i.e., cylinder, platform, and surroundings) that was then used in the study described here.

**Table 14**. Source Yields for Uranium Isotopes in $UF_6$.

| Isotope | F(α,n) (n/s/g) | Spontaneous Fission (n/s/g) |
|---|---|---|
| $^{234}U$ | 4.74E+02 | 5.02E-03 |
| $^{235}U$ | 8.00E-02 | 2.99E-04 |
| $^{236}U$ | 2.90E+00 | 5.49E-03 |
| $^{238}U$ | 2.80E-02 | 1.36E-02 |

This section begins with a description of benchmarking performed using a cylinder measured during the field testing, then continues with a discussion of spatial mapping of neutron signal efficiencies to assess the interrogation depth of the PNEM and HEVA methods. This section concludes with an analysis of the probability of detection for two partial defect scenarios.

## 11.1 Benchmarking MCNP Models

To provide confidence in accuracy of the PNEM and HEVA models used in the spatial mapping and partial defect analysis, MCNP modeling of the as-built UCVS prototype was benchmarked against a specific cylinder measured in the field trial. The cylinder was selected because it had an enrichment in the middle of the typical product-cylinder range (i.e., 4 wt% enrichment and 60.8 kg $^{235}U$), and because it appeared to be relatively "clean" in that the level of wall deposits was lower than other cylinders at that enrichment. The isotopic composition of the benchmark cylinder, as declared by the operator and modeled in MCNP, is provided in Table 15.

**Table 15**. $UF_6$ Isotopic Composition of the Benchmark Cylinder.

| Isotope | Composition (wt%) |
|---|---|
| $^{234}U$ | 2.30E-02 |
| $^{235}U$ | 2.72 |
| $^{236}U$ | 6.76E-04 |
| $^{238}U$ | 64.9 |
| $^{19}F$ | 32.4 |

One of the most significant sources of modeling uncertainty for large $UF_6$ cylinders such as the Type 30B is the distribution of $UF_6$ within the cylinder. The $UF_6$ profile inside the cylinder is generally believed to be a function of how the cylinder was filled, whether it has been sampled or homogenized, and environmental factors such as storage and handling conditions. This study adopted a $UF_6$ cylinder modeling convention developed by Berndt et al. (2010) wherein an x-factor is defined that describes the percentage of $UF_6$ covering the inner cylinder wall with a layer of constant thickness and assuming a uniform density as shown in Figure 80. These filling profiles represent extreme bounding cases. The true range of filling profiles is likely a smaller subset of that shown in Figure 80 with more nuanced geometry and density gradients. A variety of experimental studies of the filling profiles of $UF_6$ cylinders (both published and unpublished) have resulted in conflicting conclusions as to the most likely filling profile, so this remains an open question for simulation (and assay) of $UF_6$ cylinders. For this study, detector responses for the two extreme cases of x=0 and x=100 are reported and compared for HEVA and PNEM. For neutron-based signatures, the difference in estimated detector response between the x=0 and x=100 cases increases with increasing enrichment level due to neutron multiplication effects.

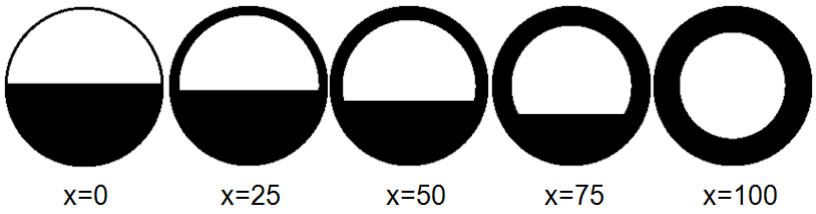


**Figure 74**. Theoretical filling profiles inside $UF_6$ cylinders used for modeling and simulation.

For the HEVA system, representation of the deposit on the bottom and walls of the cylinder may also be a significant source of modeling uncertainty. This material is often labeled “heels” and/or “wall deposits”. Generally speaking, its volume and mass grow with the number of fillings that a given cylinder has experienced. The radiation from the heel is predominantly from the progeny of $^{238}U$, particularly $^{234m}Pa$. The heel may contribute significantly to the overall gamma-ray spectrum below 2 MeV but does not contribute to $HEVA_{NT}$, which is evident by the results shown in Figure 75. In the top pane of Figure 75, the simulated spectrum, with and without a heel component, is compared with the measured spectrum for the benchmark cylinder. Since the heel had no effect on the simulated spectrum above 2 MeV, only the simulated data for a clean cylinder (no heel or wall deposits) are shown in the high-energy spectra in the bottom pane of Figure 75.

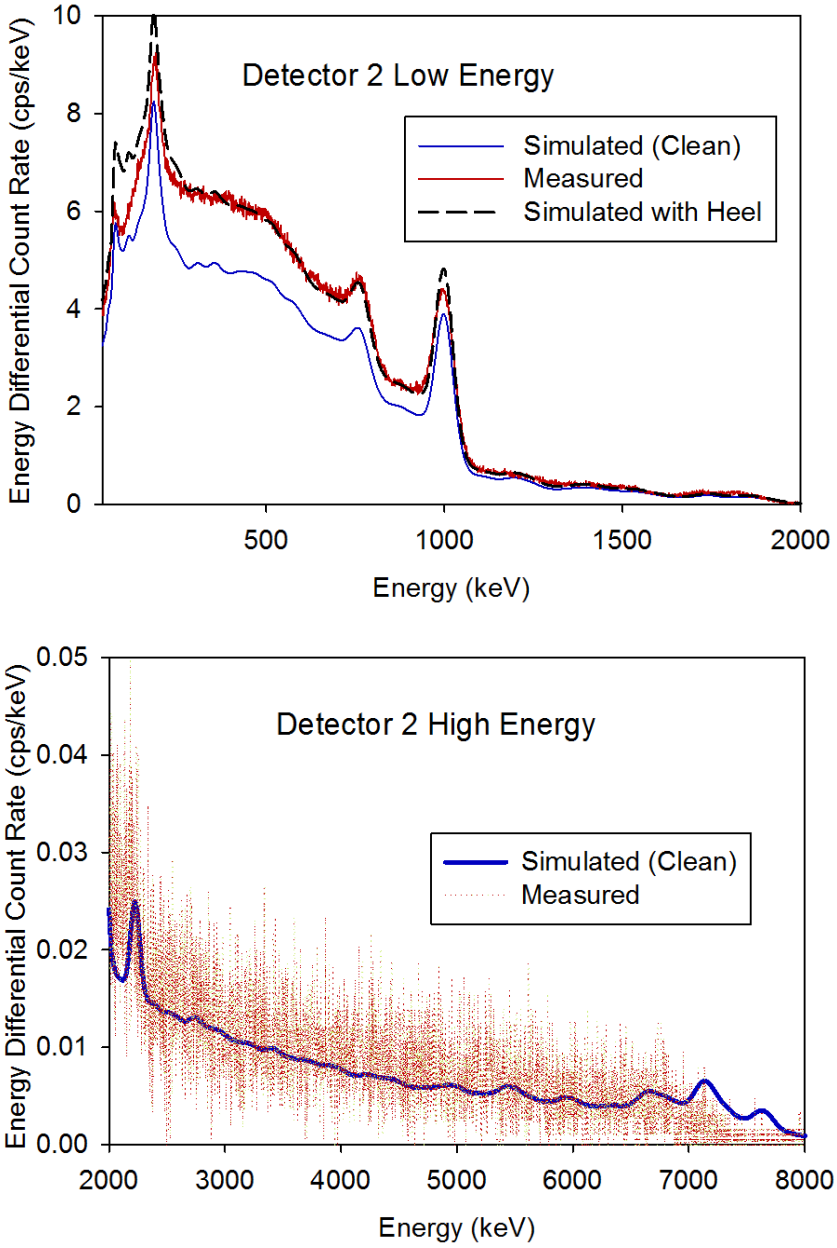


**Figure 75.** Comparison of measured and simulated gamma-ray spectra from the middle HEVA detector for lower energies (top) and higher energies (bottom) for assay of the benchmark cylinder.

Table 16 and Table 17 provide the benchmark results for PNEM and HEVA (with no added heel) for the 4 wt% benchmark cylinder. For both systems, the estimated signals from simulation fall between the two bounding cases of x=0 and x=100, which helps provide confidence that MCNP simulations can provide an estimate of count rates for each system. It is, however, disconcerting to note that HEVA favors the x=0 case whereas PNEM favors the x=100 case. No additional spatial measurements were made on the benchmark cylinder to provide evidence to support either case, so this discrepancy remains unresolved.

**Table 16**. PNEM MCNP Benchmark Results.

| Case | Singles Count Rate (cps) | Singles Diff. (%) | Doubles Count Rate (cps) | Doubles Diff. (%) |
|---|---|---|---|---|
| Measured | 8365.8 ± 4.3 | – | 221.8 ± 4.7 | – |
| PNEM, x=0 | 10280.4 | 22.9% | 509.3 | 129.4% |
| PNEM, x=100 | 7899.9 | -5.6% | 214.9 | -3.2% |

**Table 17**. HEVA MCNP Benchmark Results.

| Case | $HEVA_T$ | Diff. (%) | $HEVA_{NT}$ | Diff. (%) |
|---|---|---|---|---|
| Measured | 1941 ± 2 | – | 85.9 ± 0.4 | – |
| HEVA, x=0 | 1712 | -11.8% | 84.3 | -1.9% |
| HEVA, x=100 | 1739 | -10.4% | 75.4 | -12.2% |

## 11.2 Spatial Mapping of Neutron Signal Efficiencies

One of the key advantages that PNEM and HEVA provide over the traditional enrichment-meter methods used today by the IAEA and Euratom is a significantly larger interrogation depth. This section describes an assessment of interrogation depth for the total-neutron-based signatures (i.e., $PNEM_S$ and $HEVA_{NT}$) using the 4 wt% benchmark cylinder and the x=0 source distribution. The SCX tally in MCNP provides an indicator of detection efficiency as a function of the neutron emission cell. In this case, the SCX tally includes the spontaneous fission and F(α,n) neutron source particles and their progeny from a particular cell. In other words, it includes the induced fission daughter neutrons regardless of whether the induced fission event occurred in the original source emission cell or not.

The $UF_6$ volume inside the cylinder was discretized into 7656 approximately equal-volume voxels as shown in Figure 76 for both the PNEM and HEVA simulations. Each of the voxels is colored according to its contribution to the detector response. Voxels having the maximum contribution, closest to the detectors, are red; whereas, at the other extreme, voxels colored in dark blue contribute the least amount to the response. The same spatial mappings of the total neutron signal efficiencies for PNEM and HEVA are shown in histogram form in Figure 77 and Figure 78.

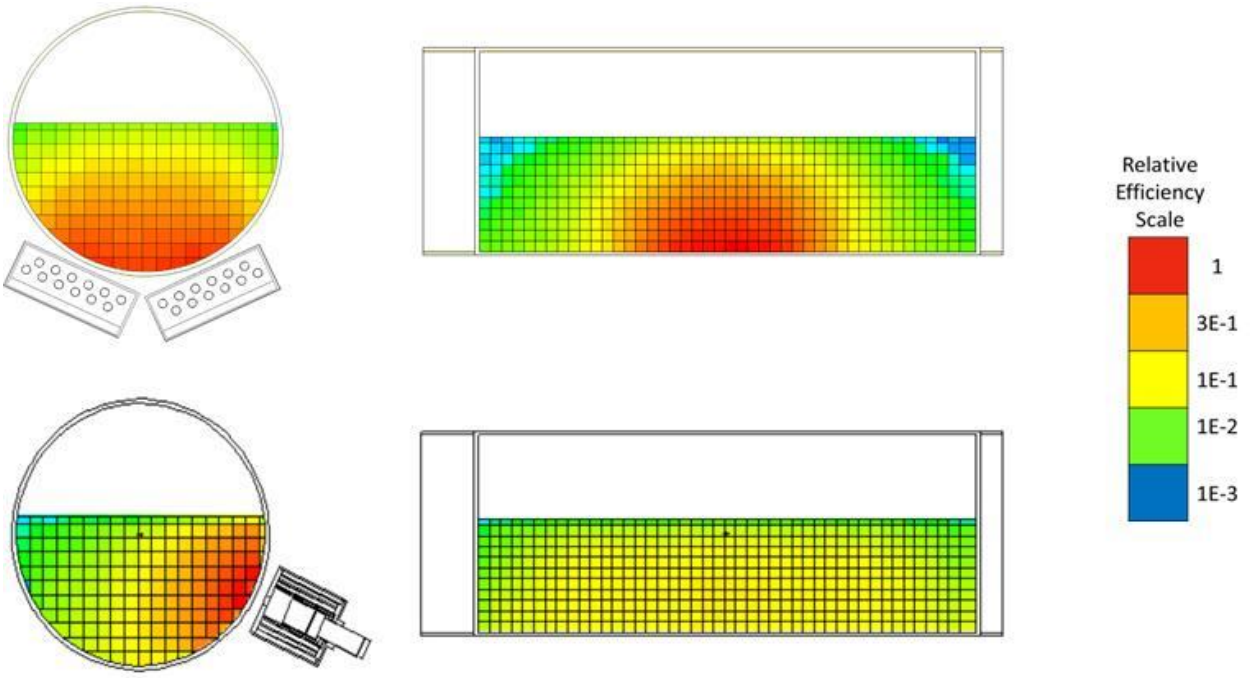


**Figure 76.** Images depicting the $UF_6$ discretization and the relative contribution to the overall detector response for the as-built PNEM (top) and HEVA (bottom) configurations in the UCVS prototype.

Ideally, the response for each NDA method would be uniform over the entire volume of the $UF_6$ in order to minimize sensitivity to parameters such as material distribution. This ideal is not practically achievable, so it is important to understand the strengths and limitations of each method. These observations trend with intuition based on the as-deployed hardware designs for PNEM and HEVA. For PNEM, the cross-sectional sensitivity is quite uniform near the axial center of the cylinder, but because the neutron pods are centered axial on the cylinder, the collection efficiency is quite low for neutrons emitted near the upper, end portions of the cylinder. The opposite is true for HEVA: The one-sided, as-deployed version has poor sensitivity to cylinder regions on the opposite side of the cylinder, but the three modules along the axial length translate to quite uniform axial efficiency. A comparison of the PNEM and HEVA spatial efficiency histograms indicates that, in aggregate, their relative efficiency are quite similar, depending on where material is substituted or removed, their sensitivity to partial defects could be quite different.

The designs of the HEVA and PNEM NDA modules in the as-built UCVS were chosen based on existing prototype instrumentation, overall size constraints to minimize impact to the operator, and consistency with previous field trials; however, a more optimal configuration of detectors designed to flatten the response profile could be envisioned and designed using calculations similar to those presented here.

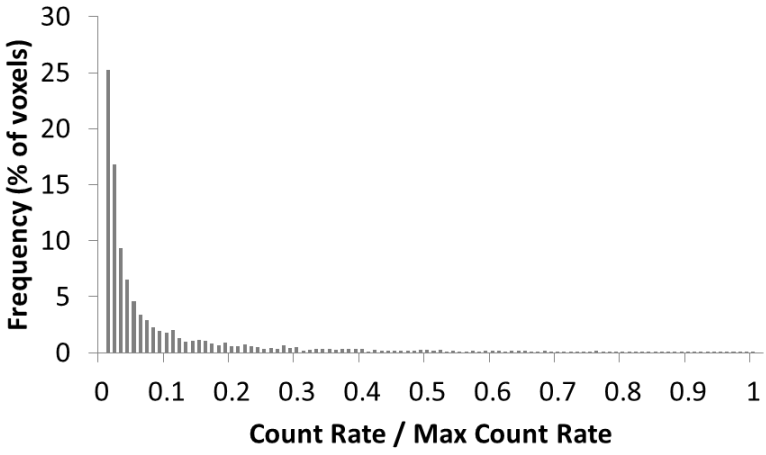


**Figure 77**. Histogram depicting total neutron signal efficiency map for $PNEM_S$.

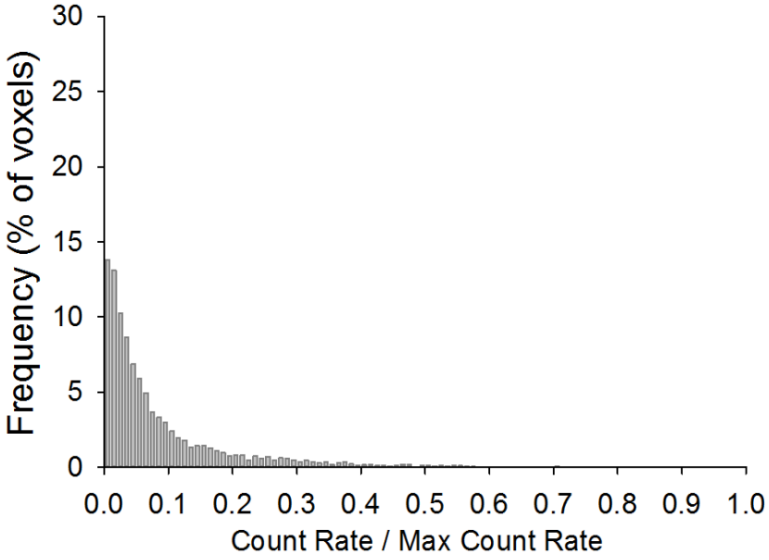


**Figure 78.** Histogram depicting total neutron signal efficiency map for $HEVA_{NT}$.

## 11.3 Partial Defect Sensitivity

The UCVS User Requirements set performance targets for partial-defect detection and here, a combination of MCNP modeling and field-measured uncertainties are used to predict PNEM and HEVA partial-defect sensitivity. The geometry assumed for the partial defect scenarios is shown in
Figure 79 (Kulisek et al. 2014). In this example scenario, $DUF_6$ has replaced a portion of the $LEUF_6$ in the interior of the cylinder such that there is a uniform thickness $L$ of $LEUF_6$ surrounding the diverted material. This geometry was chosen because it represents the most difficult scenario to detect and, thus, provides a conservative estimate of detection probability.

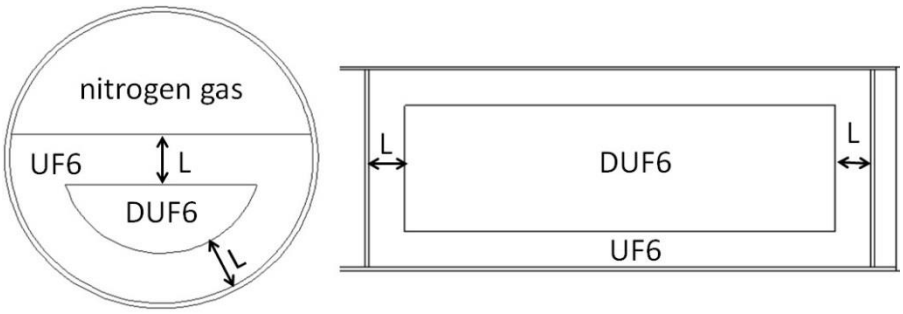


**Figure 79**. Schematic of partial defect scenario in which $LEUF_6$ in the center of the cylinder is replaced with $DUF_6$. The dimension *L* is varied to create partial defects of varying relative mass fractions.

Performance predictions for partial defect detection were calculated in terms of the probability of detection, at a given false alarm rate, for various levels of diverted material. A false alarm rate of 1% was enforced by defining alarm thresholds above and below the mean net counts expected for a cylinder filled with material enriched to the declared value, assuming a normal distribution: $\mu \pm 2.58\sigma$, where $\mu$ is the expected, mean count rate for a cylinder with no material diversion and $\sigma$ is the corresponding relative standard deviation.

The probability of detection (PD) for each mass fraction level of diverted material is determined using the probability density function (again, assuming a normal distribution) of the count rate for the corresponding cylinder with diverted material. For scenario A in which $LEUF_6$ is replaced with $DUF_6$, the fraction of the probability density function of the diverted cylinder that falls below the lower alarm threshold, which is set based on the distribution of the cylinder with no diversion, is the detection probability. For scenario B in which $LEUF_6$ is replaced with $HEUF_6$, the detection probability is defined as the fraction of the probability density function of the cylinder with diverted material that falls above the upper alarm threshold. This method for determining the PD for a fixed alarm rate and fixed amount of $UF_6$ diversion is depicted in Figure 80.

For this study, the $\sigma$ values for typical cylinder assay and fingerprint measurements are derived from the UCVS field trial measurements. The typical cylinder assay values $\sigma_{typ}$ come from the average of results for the two facility-specific calibration populations, URENCO A and URENCO B. The fingerprint values $\sigma_{FP}$ come from the fingerprint measurements that encompass both time and geometry effects. The values are given in Table 18.

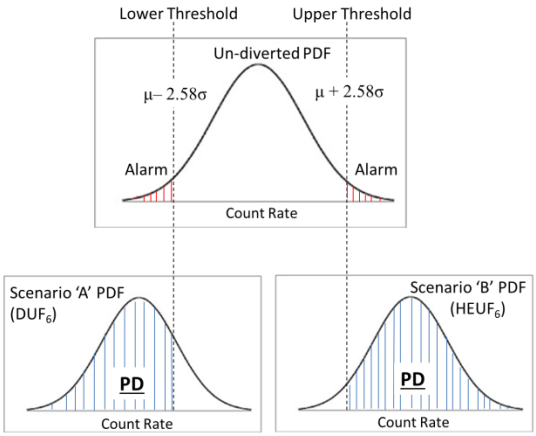


**Figure 80**. Method of determining PD for diversion of a fixed amount of $UF_6$ and false alarm rate for scenarios A and B.

**Table 18**. PNEM and HEVA Uncertainty Values Used for Probability-of-Detection Calculations.

| Signature | $\sigma_{typ}$ (rel%) | $\sigma_{FP}$ (rel%) |
|---|---|---|
| $PNEM_S$ | 2.5% | 0.19% |
| $PNEM_D$ | 3.7% | 2.2% |
| $HEVA_{NT}$ | 2.8% | 0.72% |

The probability-of-detection curves for PNEM and HEVA for scenario A ($DUF_6$ in $LEUF_6$) are shown in Figure 81 and Figure 82 for a 1% false alarm rate. The plots show results for both one-time typical cylinder assay as well as repeated NDA Fingerprint measurements.

These results indicate that PNEM can detect mass defects of greater than 8% with greater than 90% confidence in the one-time cylinder assay scenario. HEVA sensitivity is somewhat lower, at approximately 15% for the same confidence level. The reasons for superior PNEM sensitivity include a marginally lower field-measured uncertainty for singles neutrons (2.5% versus 2.8% for HEVA) and higher spatial sensitivity over the cylinder region in which the material substitution occurred. A comparison of Figures 79 and 76 shows that PNEM's sensitivity to a centralized substitution volume is more uniform than HEVA's as-deployed one-sided configuration.

For the repeated-assay, fingerprint scenario, the sensitivity of the two methods is much higher than for one-time assay. For PNEM, detection of mass defects as low as 1% are possible at 90% confidence and a 1% false alarm rate. $HEVA_{NT}$ sensitivity is inferior to $PNEM_S$ for the same reasons stated above: $PNEM_S$ has higher field-measured precision and higher spatial sensitivity to a substitution volume in the center of the cylinder.

For scenario B ($HEUF_6$ in $LEUF_6$), the $HEUF_6$ neutron emission rate is large enough that a very small diversion would be easily detected. In this case, all of the PNEM and HEVA neutron-based signatures are

expected to have a 100% detection probability with less than 1% mass fraction of diverted material (~15 kg $UF_6$).

Very important to note here is that these preliminary findings indicate that these advanced NDA methods have the potential to provide the IAEA with not only partial-defect sensitivity for one-time assay scenarios but also *bias-defect* sensitivity for repeated assay scenarios. The potential implications on a new-generation of safeguards approaches deserves more discussion.

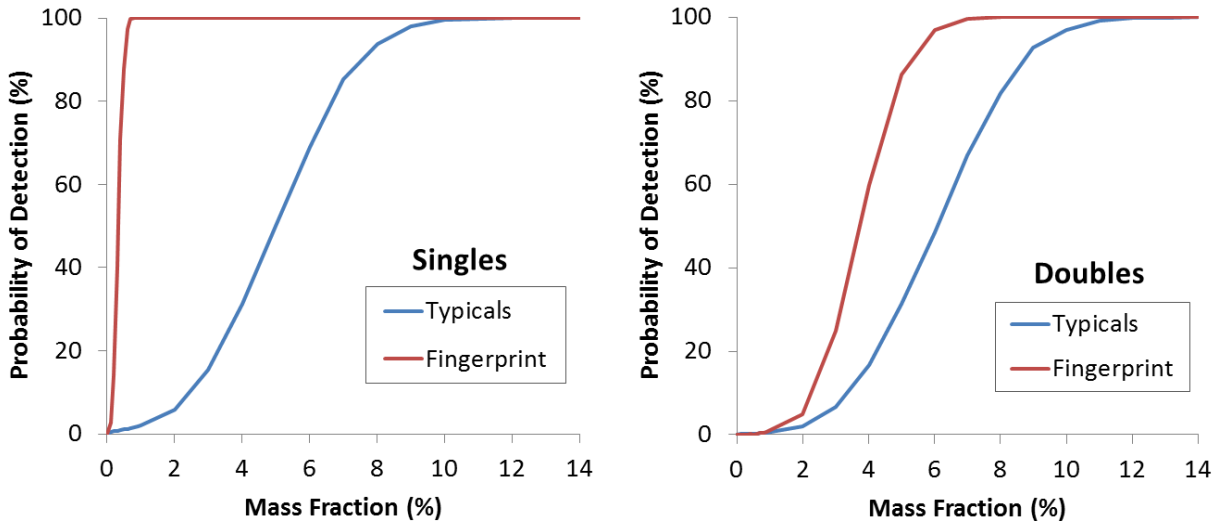


**Figure 81**. Probability-of-detection curves for $PNEM_S$ (left) and $PNEM_D$ (right) for scenario A ($DUF_6$).

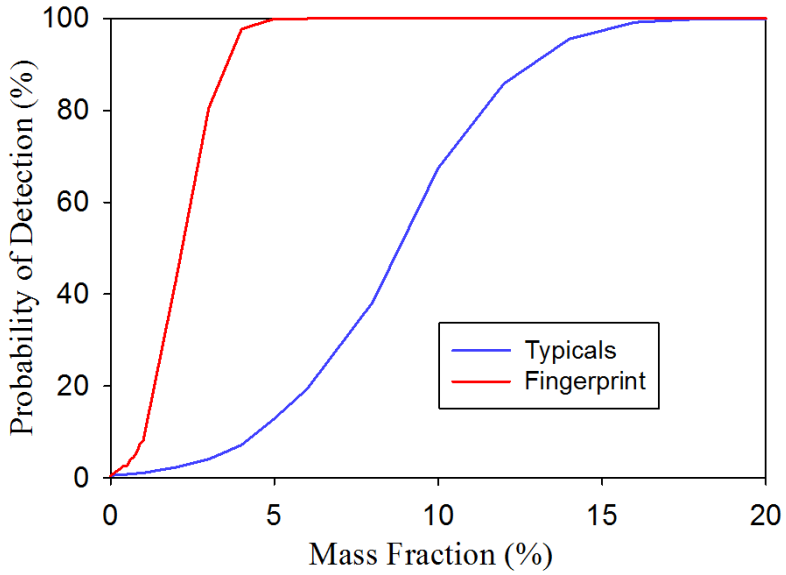


**Figure 82**. Probability-of-detection curves for $HEVA_{NT}$ for scenario A ($DUF_6$).

# 12.0 Merging HEVA and PNEM: Best of Both Methods

The PNEM and HEVA results presented in this report indicate that both are highly capable NDA methods, either of which could substantially improve on today's handheld methods in terms of assay precision, full-volume interrogation and defect sensitivity. That said, the UCVS team believes that a new NDA method, one that incorporates the most promising signatures and features from PNEM and HEVA, should be considered. This merged NDA method, here labeled Neutron-Gamma Enrichment Verification (NGEV), would be based on $PNEM_S$ and $HEVA_T$. Supporting logic for NGEV is given here.

For the full-volume determination of $^{235}U$ mass $PNEM_S$ and $HEVA_{NT}$ collect essentially the same singles-neutron signature. Figure 83 illustrates the high degree of correlation for these two signatures, as determined through an analysis of the correlation coefficients on the relative differences from declared values. The correlation is especially strong for enrichments above natural where the statistical uncertainty in $HEVA_{NT}$ is lower, and the systematic biases that appear to result from different singles calibration functions (i.e., exponential for HEVA, quadratic for PNEM) are not as evident. While $PNEM_S$ and $HEVA_{NT}$ collect the same signature, $PNEM_S$ can be expected to provide a higher degree of statistical precision and possibly long-term stability than $HEVA_{NT}$. This is particularly true at enrichments below 1.5 wt%, a category of cylinders not studied extensively in the Phase I study. Therefore, a variant of $PNEM_S$ is the recommended method for collecting the singles neutron signature and the determination of $^{235}U$ mass.

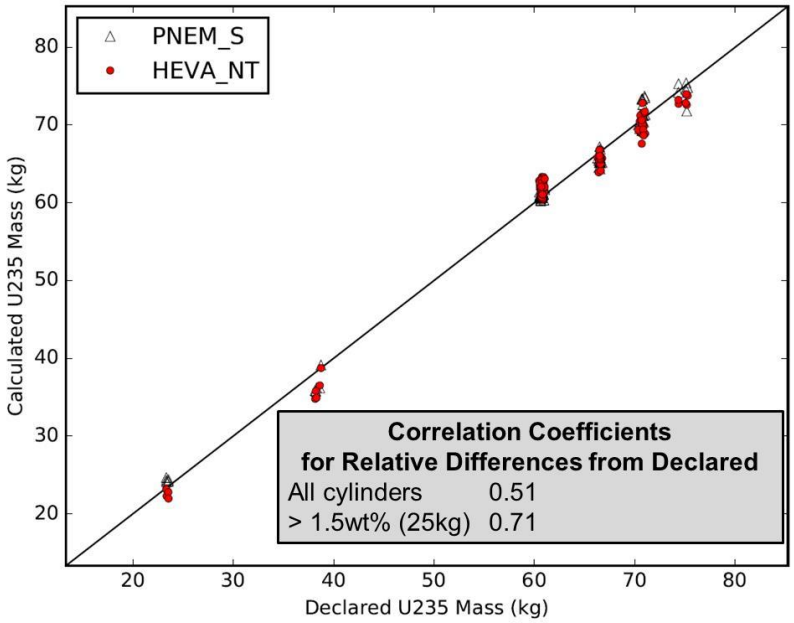


**Figure 83**. $PNEM_S$ and $HEVA_{NT}$ assay versus declared values for $^{235}U$ mass. Correlation coefficients, for the relative differences from declared for each method, are shown. These results are based on the URENCO 97 population (full occupancy period).

For determination of relative cylinder enrichment, $HEVA_T$ provides a direct, unambiguous measure of $^{235}U$ concentration that is not dependent on the $^{234}U/^{235}U$ behavior. Though $HEVA_T$ interrogates only a limited material volume, the use of a totals neutron signature in a merged NDA method (i.e., $PNEM_S$) ensures that full-volume assay is still achieved for the hybrid calculation of $E_{235}$. Inclusion of gamma-ray spectrometry also allows detection of $^{232}U$ as a clear indicator of off-normal material. For these reasons, $HEVA_T$ is the recommended method for the direct determination of cylinder enrichment, and hybridization with $PNEM_S$ to provide full-volume enrichment assay. The statistical rationale for hybridizing these two signatures was preliminarily examined using data from the Phase I field trial. In that analysis, the correlation coefficient for the relative errors of $PNEM_S$ and $HEVA_T$ was calculated. A low value is desirable and as illustrated in Figure 84, was realized. The correlation coefficients, especially for enrichments above 1.5 wt%, quantitatively confirm their independence and practicably speaking, their potential for hybridization.

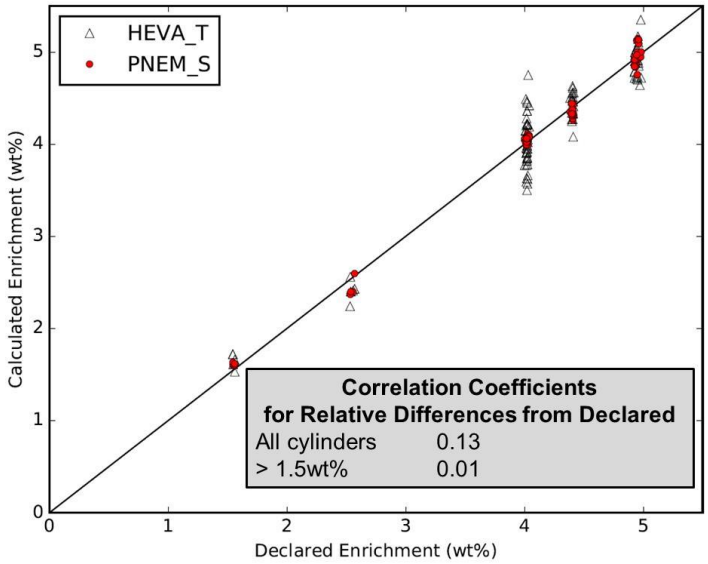


**Figure 84**. $PNEM_S$ and $HEVA_T$ assay versus declared values for cylinder enrichment, and the correlation coefficients for relative errors. These results are based on the URENCO 97 population.

For the NDA Fingerprint, $PNEM_S$ is the most precise and stable candidate signature for the verification of $UF_6$ constancy, but in the current hardware configuration it provides limited information about the spatial distribution of the material. The gamma-ray signatures exemplified in $HEVA_{186}$ and $HEVA_{1001}$ (other ROIs not studied here may prove more useful) are attractive in terms of cylinder distinctiveness, since they provide information about material age, wall-deposit magnitude and spatial variation.

The $HEVA_T$ spectrometer can be improved and streamlined in NGEV. The use of NaI(Tl) for all HEVA systems to date has been driven by the fact that iodine provides a significant fraction of the $HEVA_{NT}$ signature. If $^3He$ tubes are used to collect the total neutron signature in NGEV, the preferred gamma spectrometer for $HEVA_T$ would be $LaBr_3$. It is expected that the higher resolution of $LaBr_3$ and advanced algorithms to better discriminate against continua produced by wall deposits will enable more precise determination of enrichment, particularly for natural and depleted enrichments. A more compact collimator design is also possible, because there is no need for the iron/polyethylene layers to serve neutron-gamma converters.

The PNEM hardware design can be modified to be more cost-effective and capable for the singles neutron signature. If the doubles signature is not used in an integrated NDA method, the number of $^{3}$He tubes can be reduced without significant impact on the statistical uncertainties. Lower-pressure tubes, and thus, lower $^{3}$He costs may also be preferable. An array design that provides a flatter efficiency profile and more spatial information should also be considered (building from experience with the UCAS installed at Rokkasho Enrichment Plant in Japan).

Figure 85 presents a notional illustration of NGEV, implemented in the UCVS prototype. It includes $^{3}$He tubes (4 atm, 100-cm long) but fewer and at lower pressure than in the current design. The two neutron pods are flanked by four $LaBr_3$ spectrometers, each in a "side-looking" configuration. The streamlined configuration of these integrated neutron-gamma modules should allow deployment flexibility and extensible modularity to Type 48 cylinders (e.g., four panels instead of two).

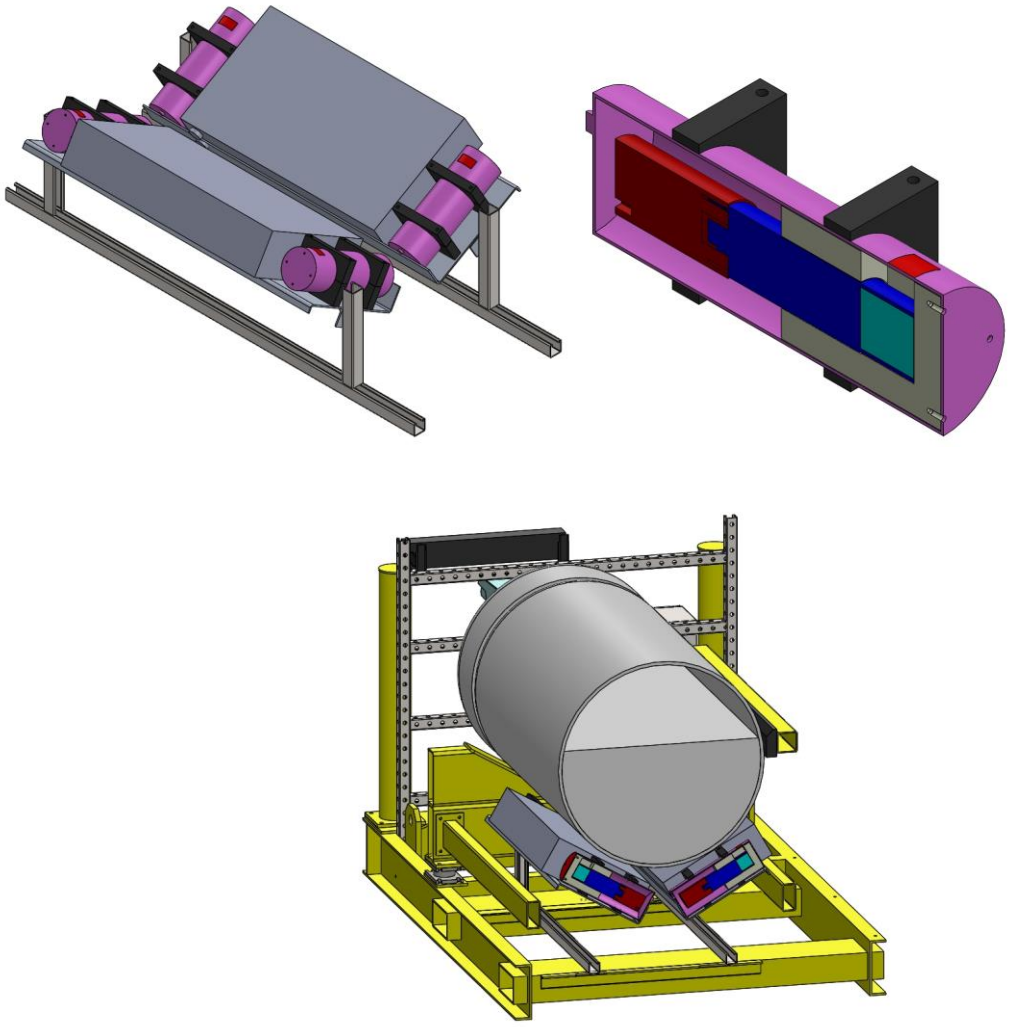

**Figure 85**. Notional illustration of an NDA method that merges the strengths of PNEM and HEVA to create a new method called Neutron-Gamma Enrichment Verification (NGEV). Top left: $^{3}$He modules flanked by "side-looking" collimated LaBr spectrometers, with NGEV panels in a clamshell configuration. Top right: Cross-section of the LaBr module showing collimator (grey) and LaBr crystal (light blue). Bottom: Depiction of a UCVS prototype with NGEV modules.

A preview of the potential for NGEV is given in Figure 86 where $HEVA_T$ and $PNEM_S$ signatures, collected separately during the WFFF field trial, are hybridized to produce full-volume enrichment assay for the URENCO 97 population. The precision of NGEV is improved when compared to $HEVA_{hybrid}$ for the sample population: NGEV produced an RSD of 3.2%, the $HEVA_{hybrid}$ value was 3.9%.

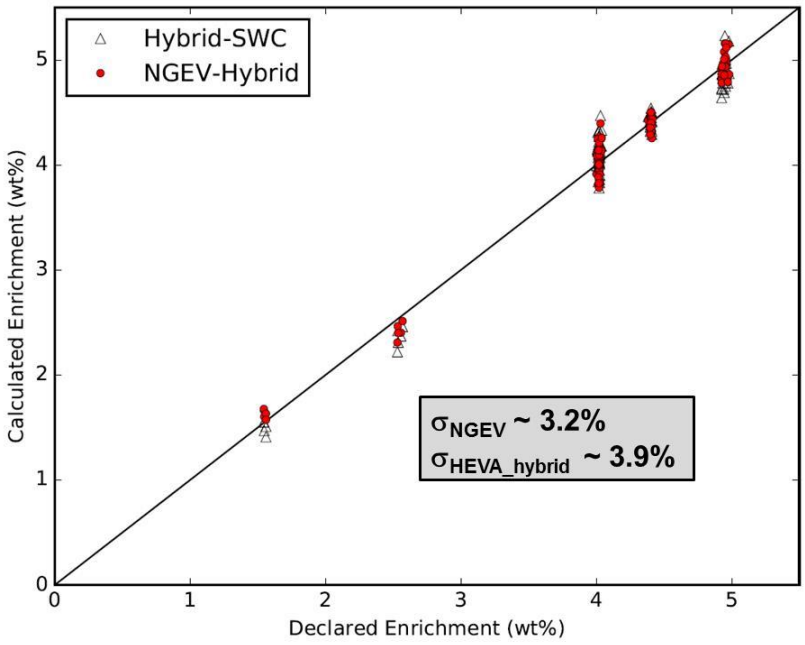


**Figure 86**. Comparison of NGEV and $HEVA_{hybrid}$ results for the URENCO 97 population.

# 13.0 Preliminary UCVS Cost Estimates

Preliminary cost estimates were tallied for a UCVS unit under the following assumptions.

- Costs were calculated for a second UCVS prototype, with a design identical to the first unit developed in Phase I: standalone assay platform designed for outdoor use. As a second unit, original design costs are not included. The cost of other mechanical designs for the assay platform (e.g., one integrated with a particular accountancy scale or for purely indoor use) may be somewhat different.
- The "standard" data acquisition cabinet and internal components used by IAEA and the area surveillance camera are not included. This is based on the logic that the cabinet cost in a GCEP would likely be shared across multiple instruments, and a surveillance camera dedicated to UCVS may not be required. The cylinder nameplate camera is included in the cost estimate.
- All software and analysis modules are complete and functional—no further development costs are needed.
- Labor costs for fabrication and integration assume nominal DOE laboratory rates. Estimated IAEA costs for the procurement of $^{3}$He are assumed.

Table 19 summarizes estimated costs for several UCVS variants: assay platform without NDA; HEVA only, PNEM only, notional NGEV. Based on these numbers, the UCVS cost is dominated by the assay platform. For the NDA options, the as-deployed PNEM has the highest estimated cost, HEVA the lowest. Because the aggregated UCVS cost is dominated by the platform, the total cost for UCVS variants based on the most- and least-expensive NDA options differ by approximately 30%.

**Table 19**. Cost estimates for the UCVS assay platform and three NDA variants (PNEM-only, HEVA-only, NGEV-only).

| **Assay Platform** | | | | | |
|---|---|---|---|---|---|
| **Description** | **Vendor** | **Quantity** | **Unit Price ($)** | **Total** | **Notes** |
| Environmental Sensor Package | Omega | 1 | 450 | 450 | |
| Junction Boxes | Hammond Manufacturing | 2 | 400 | 800 | |
| Steel Materials | Multiple | | | 3,500 | |
| Elecrical Materials | Multiple | | | 2,500 | |
| Fixtures and Fasteners | Multiple | | | 5,000 | |
| Skid Fabrication | | | | 32,000 | US DOE Labor rates |
| Operator interface components | Multiple | | | 2,000 | |
| Load Cells | Mettler Toledo | 4 | 2,625 | 10,500 | |
| Weight Display Module | Mettler Toledo | 1 | 4,084 | 4,084 | |
| Cylinder ID Camera | AXIS | 1 | 1,069 | 1,069 | |
| Cylinder ID Light Bar | Smart Vision Lights | 1 | 2,740 | 2,740 | |
| Bridge/Gateway | Juniper | 1 | 900 | 900 | |
| Labor to integrate platform components | | | | 141,656 | US DOE Labor rates |
| | | | **TOTAL** | **207,199** | |
| **HEVA NDA** | | | | | |
| NaI(Tl) module (7.5x7.5cm) | Canberra | 3 | 1,500 | 4,500 | |
| Osprey PMT base | Canberra | 3 | 5,500 | 16,500 | |
| Collimator and fixtures | Multiple | 3 | 1,300 | 3,900 | |
| HEVA Weather Shield Box | ZERO | 3 | 1,250 | 3,750 | |
| | | | **TOTAL** | **28,650** | |
| **PNEM NDA** | | | | | |
| Detector body | Precision Data Technology | 2 | 11,850 | 23,700 | |
| Empty He-3 tubes | GE Reuter-Stokes | 24 | 1,500 | 36,000 | |
| He-3 gas, 52.8 L | GE Reuter-Stokes | 1 | 36,960 | 36,960 | Based on estimated IAEA cost: $700/L |
| Neutron Coincidence Analyzer | Canberra | 1 | 10,200 | 10,200 | |
| Environmental enclosures | Continental Machining Co. | 1 | 3,050 | 3,050 | |
| | | | **TOTAL** | **109,910** | |
| **NGEV NDA** | | | | | |
| Neutron module detector body | Precision Data Technology | 2 | 11,850 | 23,700 | |
| Empty He-3 tubes | GE Reuter-Stokes | 8 | 1,500 | 12,000 | Assumes He-3 sensitivity ~30% of Phase I PNEM design |
| He-3 gas, ~18L | GE Reuter-Stokes | 1 | 12,000 | 12,000 | Based on estimated IAEA cost: $700/L |
| Neutron Coincidence Analyzer | Canberra | 1 | 10,200 | 10,200 | |
| Neutron pod environmental enclosures | Continental Machining Co. | 1 | 3,050 | 3,050 | |
| LaBr(Tl) module (3.8x3.8cm) | Canberra | 4 | 7,500 | 30,000 | |
| Osprey PMT base | Canberra | 4 | 5,500 | 22,000 | |
| Collimator and fixtures | Multiple | 4 | 1,300 | 5,200 | |
| Environmental Enclosures | ZERO | 4 | 700 | 2,800 | |
| | | | **TOTAL** | **60,000** | |

# 14.0 Conclusions

## 14.1 Key Findings

The key findings from the UCVS Phase I study are summarized below.

*Assay of $E_{235}$ Using Hybrid Signatures.* HEVA performance, hybridizing the 186-keV and singles neutron signatures, was better than the ITVs for all populations, including the mixed-facility populations. In comparison to PNEM, HEVA precision was more consistent across the various populations. PNEM performance, based on a hybridization of the singles and doubles signatures, surpassed the ITVs for all but the largest population, which included multiple enrichers. The precision of PNEM-produced $E_{235}$ values varied considerably from population to population. *Both* methods have the potential to provide assay precision comparable to or better than target values for handheld devices, without the need for tedious and laborious wall-thickness corrections. The fact that the hybrid $E_{235}$ approach provides a full-volume assay of cylinder enrichment is notable because today's handheld methods assay less than 1% of the cylinder volume.

*Assay of $E_{235}$ using Direct Signatures.* HEVA's performance using the $^{235}U$ signature (i.e., 186-keV peak region) was comparable or better than the ITVs, and quite consistent across all populations, as expected since it has no $^{234}U$ dependence. PNEM's performance, based only on the direct $^{235}U$ signature (i.e., doubles neutrons) surpassed the ITVs for the subpopulations where a facility-specific calibration that accurately characterizes the $^{234}U/^{235}U$ ratio was assumed. For the large cylinder population spanning multiple facilities, the uncertainty was significantly degraded. PNEM's direct signature collects over a much larger material volume than does HEVA's.

*Assay of $M_{235}$ using Indirect Signatures.* PNEM and HEVA precision for $^{235}U$ mass assay was comparable over all populations, consistent with the fact that both are collecting essentially the same signature (i.e., singles neutrons) and systematic (not statistical) uncertainties dominate. Both methods offer the potential for full-volume assay and therefore, the quantification of $^{235}U$ mass. Under assumptions of a facility-specific calibration for $^{234}U/^{235}U$ behavior, PNEM and HEVA are capable of meeting IAEA's preliminary targets for uncertainty on $^{235}U$ mass quantification (i.e., 3.0%). This would represent a new capability to safeguards inspectorates and support a significant improvement in the ability to detect material substitution and removal scenarios.

*Viability of NDA Fingerprint for Full-volume Constancy of $UF_6$:* The most promising signatures for verifying the constancy of the $UF_6$ material itself are the two neutron-based signatures: $PNEM_S$ and $HEVA_{NT}$. Both appear capable of highly repeatable ($\sigma_{FP} < 1.0\%$ for product cylinders), full-volume interrogation of the $UF_6$ in the occupancy times considered in this study. PNEM's higher collection efficiency and therefore higher statistical precision, offers the promise of better repeatability. The distribution of HEVA's discrete modules along the length of the cylinder provides more sensitivity to geometry changes than does the current PNEM design.

*Viability of NDA Fingerprint for Cylinder Distinctiveness:* Gamma-ray signatures that can provide insight to the age of the $UF_6$ and the characteristics of the wall deposits at different locations are the most promising signatures for verifying the distinctiveness of a particular cylinder. Of the candidate signatures

considered in this study, $HEVA_{186}$ and $HEVA_{1001}$ appear to hold the most potential for this role because they can provide highly repeatable ($\sigma_{FP} < 1.0\%$) confirmation of photon emissions (e.g., the bremsstrahlung and gamma rays from $^{234m}Pa$) from the $UF_6$ itself and wall deposits at multiple locations along the cylinder. Unfortunately, data to quantitatively evaluate this potential were quite limited in the Phase I field trial for two reasons: 1) cylinders assayed at a fuel fabrication plant contain relatively "old" $UF_6$ (i.e., key daughters like $^{234m}Pa$ are already in equilibrium), and 2) efforts to collect data on multiple occupancies of specific product cylinders separated in time by days and weeks were unsuccessful, in part because the facility operator typically processed incoming cylinders soon after the initial scan.

*Assay of Atypical Cylinders.* The limited set of atypical cylinders from this field trial does not support significant new understanding about the robustness of PNEM and HEVA to off-normal conditions, but the analysis presented here does confirm the need to flag cylinders with a $^{234}U/^{235}U$ ratio outside of the calibration range and ideally, to still report credible values for cylinder enrichment. Prior work has indicated that HEVA offers more robustness for atypical $^{234}U$ conditions because its direct enrichment signature is the 186-keV signature emitted by $^{235}U$. Because the two neutron signatures used in the PNEM method are correlated through the self-interrogation process, off-normal $^{234}U$ concentrations are more problematic. In addition, HEVA is able to detect the presence of $^{232}U$, thereby providing additional evidence about the nature and origin of the $UF_6$ in that cylinder.

*Defect Sensitivity.* Based on measured uncertainties and MCNP modeling of material substitution scenarios, it was demonstrated that the full-volume PNEM and HEVA neutron signatures can provide an unprecedented level of defect sensitivity for IAEA's cylinder verification. For one-time assay of a cylinder, PNEM and HEVA defect sensitivities are ~8% and 13% respectively for DU, and ~0.5% for HEU substitution scenarios. For repeated cylinder scans using the NDA Fingerprint concept, bias-defect sensitivity, at material substitution levels less than ~0.5% appear to be achievable using PNEM, owing to its more precise collection of the singles neutron signature, and a higher spatial sensitivity to substitution volumes located in the middle of the cylinder.

*Prototype Functionality and Robustness.* The UCVS prototype operated in continuous unattended fashion for over eight months in an outdoor environment. There were no failures of the hardware or data acquisition software modules for PNEM and HEVA. There were, however, failures in the load cells and remote monitoring hardware (i.e., cellular modem and VPN components), and in the supervisory service running the HEVA data acquisition module. The latter led to the only NDA-related data loss in the trial (i.e., HEVA data for 14 cylinders were corrupted). A preliminary analysis of long-term stability of HEVA and PNEM signatures over approximately 8 months of operation did not reveal any significant instrument drift issues.

*Analysis Software.* The analysis software used for PNEM is available as compiled code for non-expert users, mature (currently in use by the IAEA), and straightforward to implement. No significant challenges were encountered during the Phase I analysis. The HEVA analysis software is written in Python for expert users and still developmental in terms of maturity. The HEVA software is nonproprietary and produces/uses standard input/output file formats (e.g., N42.42) consistent with IAEA's remotely monitored instruments.

*Complementarity of PNEM and HEVA Signatures.* The findings from this field trial confirm a hypothesis that the UCVS team has considered for some time: merging of the best features of PNEM and HEVA offers the potential for performance superior to either acting independently (see below).

*UCVS Cost Estimates.* The preliminary estimate for the cost of a second UCVS prototype assay platform (identical to the first, excluding data acquisition cabinet and area surveillance camera) is $209K, the majority of which is labor for fabrication and integration. The incremental cost of the NDA modules for PNEM, HEVA and NGEV are $109K, $29K and $60K respectively.

## 14.2 Caveats

The findings above represent a significant step forward in the community's understanding of the strengths and limitations of the PNEM and HEVA NDA methods, and the viability of the UCVS concept in front-end fuel cycle facilities. There are caveats on the Phase I findings that need to be considered, and that can inform potential future work on the UCVS concept.

- *Limitations on material enrichments.* The majority of cylinders in the trial were in a few enrichment bands (e.g., 2.6, 4.0, 4.4 and 4.95 wt%). The facility-specific cylinder populations were relatively small and often had few or no cylinders at enrichments below 1.5%. The effect of these relatively small populations on calibrations and predicted performance is expected to be small but not negligible.
- *Limitations on cylinder Type.* Only Type 30B cylinders were included in the Typical populations, performance for Type 48 cylinders with natural and depleted material needs study.
- *Calibration and Reporting Methods:* All cylinders in a population were used for calibration and reporting of the precision. Future analyses should implement calibration and blind-cylinder approaches similar to those likely to be used by the IAEA in field deployments.
- *Inconsistent cylinder position on assay platform.* The assay platform design did not include indicators or controls to ensure consistent placement of the cylinder. As the NDA Fingerprint studies indicated, even relatively small lateral shifts can produce non-negligible count-rate changes in the NDA instrumentation. Inconsistent lateral position negatively affected the NDA Fingerprint viability study, and likely the reported uncertainties for one-time cylinder assay. Future prototypes should include lateral position controls.
- *Lack of $^{234}U/^{235}U$ Calibration Data.* No data were available to provide a defensible functional form for total neutron calibration. PNEM analysis assumed a quadratic relationship between total neutrons and $^{235}U$ mass; HEVA analysis assumed an exponential relationship. A study of $^{234}U/^{235}U$ behavior across a range of parameters in commercial enrichment facilities is needed, and is currently under way under DOE funding.
- *Unknown effects of $UF_6$ distribution and effective density.* Results from the modeling study regarding the impact of $UF_6$ distribution on neutron signatures, and preliminary comparisons of calibration curves for sub-populations analyzed in Phase I, indicate that more study is needed on how facility-specific production processes and cylinder handling practices affect calibration functions, and measurement precision.
- *Limited NDA Fingerprint Data.* While this field trial provided the first data in support of an NDA Fingerprint viability study, the data were significantly short of the original plans and a number of questions remain, particularly with regards to the viability of gamma-based signatures to reveal and verify the distinctiveness of each cylinder. Larger datasets and further study are needed.

# 15.0 References


Berndt R, E Franke and P Mortreau. 2010. "$^{235}$U Enrichment or $UF_6$ Mass Determination on $UF_6$ Cylinders with Non-Destructive Analysis Methods," *Nuclear Instruments and Methods in Physics Research A*, 612.

Cooley JN. 2007. "Model Safeguards Approach and Innovative Techniques Implemented by the IAEA at Gas Centrifuge Enrichment Plants," *INMM Annual Meeting Proceedings*.

Durbin K., et al. 2014. "NGSI's $UF_6$ Cylinder Monitoring Project Update: Technology Survey and Evaluation," INMM Annual Meeting.

Ely J, T Pochet, J Younkin, J Garner, J March-Leuba, LE Smith, and A Lebrun. 2014. "On-Line Enrichment Monitor (OLEM): Supporting Safeguards at Enrichment Facilities". Proc. IAEA Symposium on International Safeguards.

Garner J, et al., 2014. "A Monte Carlo Analysis of Gas Centrifuge Enrichment Plant Product and Tails Withdrawal Station Load Cell Data", INMM Annual Meeting.

Goorley T, M James, T Booth, J Brown, L Cox, et al. 2012. "Initial MCNP6 Release Overview," *Nuclear Technology*, vol. 180, pp. 298-315.

IAEA – International Atomic Energy Agency. 2013a. *Unattended Cylinder Verification Station (UCVS) User Requirements*. SG-UR-12186. Department of Safeguards, International Atomic Energy Agency, Vienna, Austria.

IAEA – International Atomic Energy Agency. 2013b. "Viability of an Unattended Cylinder Verification Station." SP-1 proposal. IAEA Department of Safeguards, International Atomic Energy Agency, Vienna, Austria.

Janssens F and JP Francois. 1991. "Evaluation of Three Zero-Area Digital Filters for Peak Recognition and Interference Detection in Automated Spectral Data Analysis." *Analytical Chemistry* 63(4):320-31.

Jordan D, C Orton, E Mace, B McDonald, J Kulisek, and L.E. Smith. 2012. *Automated $UF_6$ Cylinder Enrichment Assay: Status of the Hybrid Enrichment Verification Array (HEVA) Project*. PNNL-21263, Pacific Northwest National Laboratory, Richland, Washington.

Kulisek JA, et al., 2014. "Hybrid Enrichment Verification Array: Investigations of the High-Energy Gamma-Ray Signature Origin and Use for Partial Defect Detection," proc. INMM Annual Meeting, Atlanta, Georgia, USA, 20-24 July 2014.

Lebrun AR, et al. 2009. "Improved Verification Methods for Safeguards Verifications at Enrichment Plants," Proceedings of the ANIMMA Conference.

McDonald BS, DV Jordan, CT Orton, EK Mace, RS Wittman, and LE Smith. 2011. "Model and Algorithm Evaluation for the Hybrid $UF_6$ Container Inspection System." Proceedings of the 52nd INMM Annual Meeting, Palm Desert, California, 2011.

Menlove HO, MT Swinhoe, and KA Miller. 2010. "A More Accurate and Penetrating Method to Measure the Enrichment and Mass of $UF_6$ in Storage Cylinders Using Passive Neutron Self-Interrogation." Proceedings of the 51st INMM Annual Meeting, Baltimore, Maryland, 2010.

Miller KA, HO Menlove, MT Swinhoe, and JB Marlow. 2010. "A New Technique for Uranium Cylinder Assay Using Passive Neutron Self-Interrogation." Proc. IAEA Symposium on International Safeguards.

Miller KA. 2010 "The Uranium Cylinder Assay System for Enrichment Plant Safeguards." *Journal of Nuclear Materials Management* (39).

Miller KA, HO Menlove, MT Swinhoe, and JB Marlow. 2011. *The Passive Neutron Enrichment Meter for Uranium Cylinder Assay*. ESARDA Bulletin.

Miller KA, HO Menlove, MT Swinhoe, and JB Marlow. 2012. "Monte Carlo Feasibility Study of an Active Neutron Assay Technique for Full-Volume $UF_6$ Cylinder Assay Using a Correlated Interrogation Source." *Nuclear Instruments and Methods in Physics Research A*, 703.

Miller KA, MT Swinhoe, HO Menlove and JB Marlow. 2012. *Status Report on the Passive Neutron Enrichment Meter (PNEM) for $UF_6$ Cylinder Assay*. LA-UR 12-21058, Los Alamos National Laboratory, Los Alamos, New Mexico.

Miller KA, et al. 2014. "Measured F(α,n) Yield from $^{234}U$ in Uranium Hexafluoride," *Nuclear Science and Engineering*, Volume 176, (1):98-105.

Morgan, K and C Brunhuber. 2014. "Evolution of RAINSTORM," Proc. IAEA Symposium on International Safeguards.

Op de Beeck, BJ. 1975. "Gamma-Ray Spectrometry Data Collection and Reduction by Simple Computing Systems." *Atomic Energy Review*, 13(4):743.

Reilly D, N Ensslin, H Smith, and S Kreiner. 1991. *Passive nondestructive assay of nuclear materials*. NUREG/CR-5550, LA-UR-90-732, U.S. Nuclear Regulatory Commission, Washington, D.C.

Richter S, A Alonso, W De Bolle, R Wellum, and PDP Taylor. 1999. "Isotopic 'fingerprints' for natural uranium ore samples." *International Journal of Mass Spectrometry*, 193(1):9-14.

Smith LE, DV Jordan, AC Misner, EK Mace, and C Orton. 2010a. *Hybrid Enrichment Assay Methods for a $UF_6$ Cylinder Verification Station.* PNNL-19854, Pacific Northwest National Laboratory, Richland, Washington.

Smith LE, EK Mace, and AC Misner. 2010b. "Signatures and Methods for the Automated Nondestructive Assay of $UF_6$ Cylinders at Uranium Enrichment Plants." *IEEE Transactions on Nuclear Science* (57).

Smith LE and AR Lebrun. 2011. "Conceptual Design and Modeling for Online Uranium Enrichment Monitoring." 2011 IEEE Nuclear Science Symposium, Valencia, Spain, October 2011.

Smith LE, AR Lebrun, and R Labella. 2013. "Potential Roles of Unattended Safeguards Instrumentation at Centrifuge Enrichment Plants." *Journal of Nuclear Materials Management*, Vol. 42(1).

Smith LE, KA Miller, J Garner, R Poland, B McDonald, H Nordquist, J March-Leuba. 2014. "An Unattended Verification Station for $UF_6$ Cylinders: Implementation Concepts and Development Status." Proc. IAEA Symposium on International Safeguards.

Smith LE, D.V. Jordan, J. Kulisek, B. McDonald, E.K. Mace, "Viability of $UF_6$ Cylinder Verification using the Hybrid Enrichment Verification Array," Journal of Nuclear Materials Management, Vol. 43(4), July 2015.

Walton RB, TD Reilly, JL Parker, JH Menzel, ED Marshall, and LW Fields. 1974. "Measurements of $UF_6$ Cylinders with Portable Instruments," *Nuclear Technology*, (21). pages

Younkin JR, JR Garner, NC Rowe, and LE Smith. 2012. "A Robust and Flexible Design for Gas Centrifuge Enrichment Plant Unattended Online Enrichment Monitoring," 9th International Conference on Facility Operations-Safeguards Interface.

Zalavadia MA, LE Smith, BS McDonald, JA Kulisek, EK Mace, NS Deshmukh. 2016. *Hybrid Enrichment Verification Array: Module Characterization Studies*. 2016. PNNL-25066, Pacific Northwest National Laboratory, Richland, Washington.

Zhao K. 2010. *International Target Values 2010 for Measurement Uncertainties in Safeguarding Nuclear Materials*. IAEA STR-368, IAEA Department of Safeguards, International Atomic Energy Agency, Vienna, Austria.

# Appendix A

# Overview of HEVA Characterization Study

# Appendix A

# Overview of HEVA Characterization Study

The HEVA module design changed considerably between the U.S.-Euratom field trial at Almelo (May 2013) and the inception of the UCVS Phase I project. In order to fully characterize the new design and prepare for the WFFF field trial, PNNL performed a study to assess the revised HEVA modules. That study is fully documented by Zalavadia et al. (2016); highlights are provided here to complement the HEVA results and findings in the body of the report.

A method for measuring the intrinsic efficiency of this "nontraditional" neutron signature, and the results from a benchmark experiment are presented. Also discussed are potential perturbing effects on the nontraditional signature, including short-lived activation of materials in the HEVA module. Modeling and empirical results are presented to demonstrate that such effects are expected to be negligible for the envisioned cylinder assay scenario.

## A.1 Count Rate Predictions for UCVS Assay Scenario

For the UCVS cylinder assay scenario, the HEVA input count rate can vary significantly among cylinders, not just because of varying enrichment levels but also of the amount of non-$UF_6$ compounds and $^{238}U$ progeny on the bottom and walls of the cylinder. MCNP modeling and analysis by PNNL demonstrated that, via an adaptable design for detector recess, the field of view can be used to manage the count rate incident on the detector. Modeling indicated that the HEVA count rates could extend as high as ~80 kcps for a worst-case heels scenario, but it was predicted that maximum count rates encountered in the field, even for very dirty cylinders, would be less than 30 kcps. The WFFF field trial results were consistent with the modeling-based predictions: the highest single-module count rate recorded during the trial was 17.4 kcps.

## A.2 Osprey Parameter Study

Characterization and refinement of the Osprey parameters was completed over a range of input count rates defined by the worst-case scenario modeled above. Osprey parameters of interest included: trapezoidal filter parameters, baseline restoration, fast-discriminator threshold, Pile-up Rejection Guard inspection interval (PUR Guard), live-time correction (LTC) and pulse height analysis (PHA) acquisition time. Table A.1 lists the recommended settings for each of the parameters.

**Table A.1**. List of recommended settings for the Canberra Osprey with a NaI(Tl) scintillator, for the UCVS cylinder assay scenario

| Parameter | Value/Setting |
|---|---|
| High Voltage | User defined and/or follow manufacturer's recommendation |
| PHA Acquisition times | 60 seconds |
| Gain (Coarse × Fine) | 1×1 |
| Rise-time | 1 µs |
| Flat-top | 0.5 µs |
| BLR Mode | HARD |
| LTC | ON |
| PUR Guard | 2.5x |
| FDisc Mode | Auto |
| FDisc Shaping | Normal |
| Preset | Real-time |
| Dynamic MCA Range | 8192 channels |
| LLD | 0.5 |
| ULD | 100 |

The field trial confirmed that these settings struck an appropriate balance between count rate throughput and energy resolution. In addition, these settings ensured that systematic uncertainties introduced by Osprey pulse-processing parameters were insignificant in the overall HEVA uncertainty budget, so long as input count rates were less than approximately 50 kcps, as they were during the field trial.

## A.3 $HEVA_{NT}$ Intrinsic Neutron Efficiency

HEVA's nontraditional signal can be viewed as an indirect totals neutron detector and as such, it is important to quantify the intrinsic neutron detection efficiency of the HEVA module. Measurements were performed using one of the HEVA detector modules used in the prototype UCVS, for these experiments (Figure A.1). A bare $^{252}Cf$ neutron source, emitting $3.5\times10^4$ neutrons per second, was placed 5.16 cm away from the detector. Note that this is roughly one order of magnitude lower than the expected neutron emission rate from a 5 wt% Type 30B $UF_6$ cylinder.

Figure A.2 compares the MCNP-simulated and measured spectra in the high-energy indirect neutron detection region. As illustrated there, excellent agreement was observed between the simulated and measured spectra within this high-energy region. An agreement of within 2%, with respect to $HEVA_{NT}$ gross counts, was observed between the simulated and measured results. Similar agreement was observed between simulations and measurements from cylinder assays made in the WFFF field trial.

The intrinsic neutron efficiency is defined as the number of neutron-induced counts in $HEVA_{NT}$ divided by the number of neutrons incident over the entire front face of the HEVA module. The intrinsic efficiency of the HEVA module was calculated to be 0.37% from the MCNP simulation. This value can be compared to a typical moderated, multi-tube $^3He$ pod efficiency of greater than 5%.

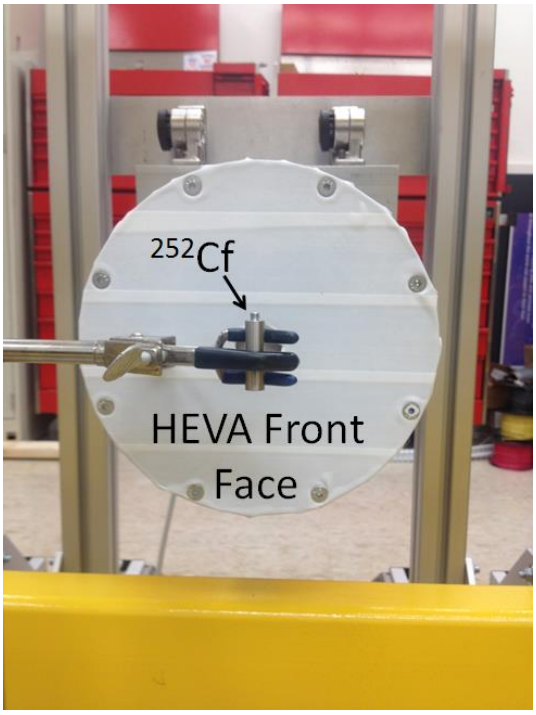


**Figure A.1**. Experimental configuration for laboratory characterization of a HEVA module in terms of intrinsic neutron efficiency and neutron activation.

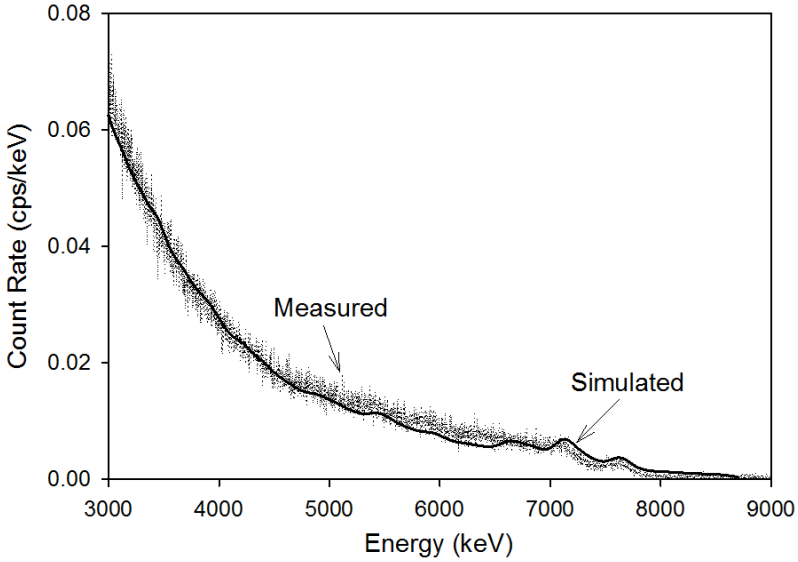


**Figure A.2**. Comparison between the simulated and measured $^{252}$Cf spectra, over high-energy indirect neutron detection region, for the experimental setup shown in Figure A.1 and described in the text.

## A.4 Neutron Activation Effects

The potential impact of activation of the NaI(Tl) detector medium was investigated, where the dominant contributor was shown to be the production of $^{128}$I via the activation of $^{127}$I. A combination of laboratory, analytical and MCNP analysis showed that the $^{128}$I bremsstrahlung spectrum will contribute approximately 10 cps in the energy region between 50 and 2000 keV, at the end of a 5-minute cylinder assay. For a 2-hour assay, the count rate may be nearly 8 times higher. It is expected, given nominal total HEVA count rates of 5 to 30 kcps during cylinder assay, that the impact of iodine activation on total HEVA count rate will not be significant. Figure A.3 shows example activation spectra collected using the same experimental configuration shown in Figure A.1.

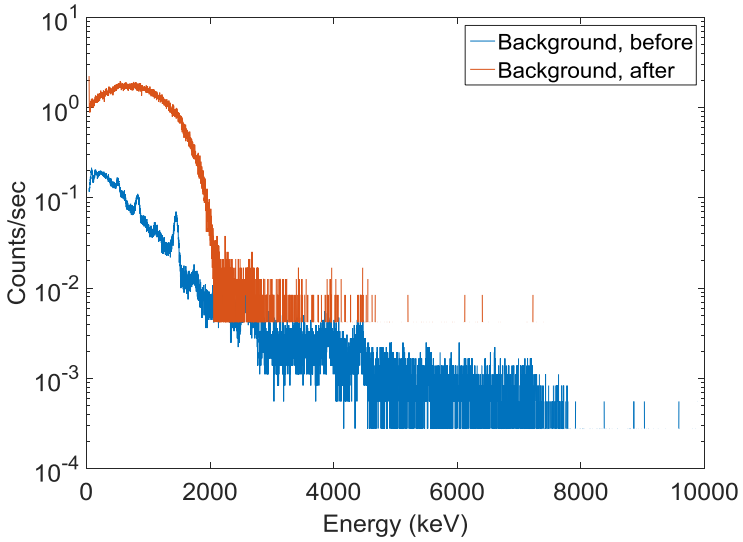


**Figure A.3**. Background spectra before and after neutron irradiation.

# Appendix B

# HEVA's Square Wave Convolute Algorithm

# Appendix B

# HEVA's Square Wave Convolute Algorithm

Applying a digital filter, such as the square wave convolute (SWC), to a raw pulse-height spectrum is a relatively straightforward approach to peak identification and peak-area measurement. The method is simple and computationally light-weight in the following sense: the digital filter consists of a simple function defined on a domain of width M (expressed in units of raw-spectrum channels). Convolution of the filter with the original spectrum (consisting of N channels) requires *NM* multiplications and *N(M-1)* additions, or a total of only *N(2M-1)* floating point operations. Application of the filter converts the raw spectrum into a form in which peak identification and, in principle, peak-area determination are readily achieved "by inspection," i.e., without resort to least-squares fitting or related maximum-likelihood fitting techniques. Note that the SWC technique yields a *calibration-independent* measure of peak area in a given spectrum; that is, the metric obtained from the convolute spectrum does not depend upon a calibration set of several $UF_6$ cylinders to assign an area to the peak in the raw spectrum. (A calibration set is required to determine the relationship between peak area and enrichment.) In contrast, multi-window approaches to implementing the enrichment meter method (see as an example Walton et al. 1974) leverage information from multiple cylinders, over a range of declared enrichments, to determine the proper weighting to be used in an (effective) background subtraction of continuum strength from the 186-keV peak region.

As suggested above, quantitative peak-area information can be extracted from the convolute peak shape (Op de Beeck 1975). The HEVA project team has investigated the square wave filter (Op de Beeck 1975: Janssens and Francois 1991), a symmetric, zero-area digital filter, as a means of measuring the area under the 186-keV peak in a medium-resolution spectrometer. Implementation details may be found in (Smith et al. 2010a). Figure B.1 (left panel) illustrates the shape of the square-wave filter, *g(t)*, which is fully described by a single width parameter, *M*. The variable *t* labels channel number in the pulse-height spectrum. The right panel of Figure B.1 illustrates the effect of applying the square-wave filter to a notional spectrum consisting of a pure Gaussian peak superimposed on a linear background. These figures demonstrate a key property of any symmetric, zero-area digital filter: by construction, the filter removes background components varying linearly with energy. The linearly varying background portion of the raw spectrum is effectively filtered out, yielding a flat baseline. The original Gaussian peak in the raw spectrum is replaced by a characteristic, non-Gaussian convolute peak-shape consisting of a positive-going central peak region plus negative-going side troughs. Janssens and Francois (1991) reported an analytical expression for this characteristic convolute shape when the peak in the raw spectrum is Gaussian. The position of the central peak of the convolute spectrum coincides with the position of the Gaussian in the original spectrum. The positions of the two side-troughs approximately mark the points in the original spectrum at which the Gaussian peak returns to the level of the linear continuum in the raw spectrum.

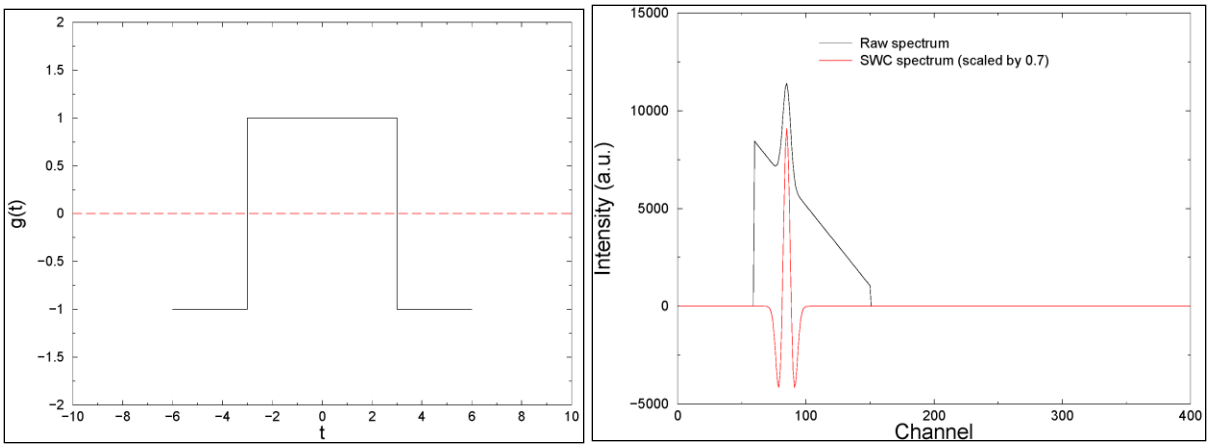


**Figure B.1**. Left panel: Illustration of square-wave filter shape for filter width M = 6. Right panel: Effect of the filter applied to a simple "toy" spectrum consisting of a Gaussian peak superimposed on a linear background.

# Appendix C

# PNEM Wiring Diagram

# Appendix C
# PNEM Wiring Diagram

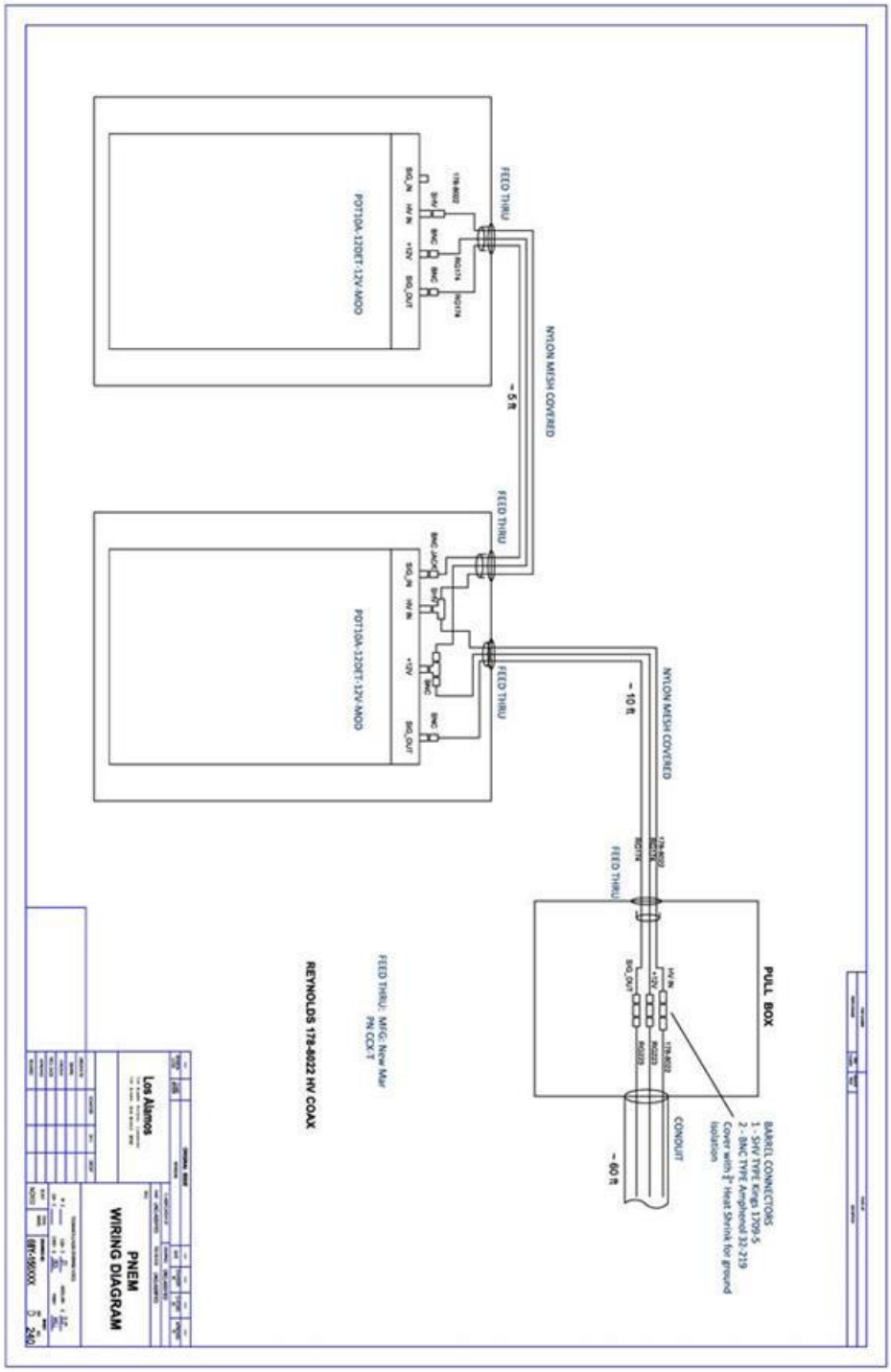

# Appendix D

# UCVS Security Plan

# Appendix D

# UCVS Security Plan

## D.1 Control

### D.1.1 Physical Protection

Access to the control system located on-site at Westinghouse Fuel Fabrication Facility (WFFF) will be subject to multiple physical protections. The computer cabinet, located inside the operator control room, will be secured with a keyed lock. Physical access will be limited to local support personnel from Savannah River National Laboratory (SRNL) and key staff at WFFF (e.g., security staff and information technology [IT] manager).

### D.1.2 Computer Access

Terminal access to the system will require a username and password. USB Mass Storage feature is disabled on the control system to prevent usage of thumb drives and other external media. The DVD/CD drive is similarly disabled by the operating system.

### D.1.3 Remote Desktop

Remote Desktop connection to the UCVS computer over the cellular network will be allowed from a limited list of computers at Pacific Northwest National Laboratory (PNNL). The UCVS team will use this feature to troubleshoot any unexpected events, such as software updates and system anomalies and also for the purpose of overall system health monitoring.

## D.2 Data Transfer and Off Site Data Protection

### D.2.1 Connectivity

All data transfer between PNNL and the UCVS computer will occur through a cellular network (Verizon). The UCVS computer is not connected in any way to WFFF's network, and it does not have Bluetooth or wireless hardware.

### D.2.2 Protections in Transit

All communications between PNNL and the UCVS will be over a site-to-site virtual private network (VPN). No access over the "open" Internet will be used to transfer project-related information. Internet access is available on the UCVS machine only to download software updates.

### D.2.3 Storage at PNNL

Data at PNNL will be stored using Common Operating and Response Environment™ (CORE) software and accessed by the project team through a web interface. Data at rest are stored on encrypted data partitions, and all communication is encrypted with Secure Sockets Layer (SSL). Unsecure access to the server is not supported. Access to the CORE system from outside the PNNL-protected network requires two-factor authentication.

To facilitate use of the International Atomic Energy Agency's (IAEA's) Rainstorm protocol, a separate copy of the data will reside on a separate system within the PNNL-protected network. Access to this computer will be limited to PNNL project staff with an identified need.

## D.3 UCVS Data Acquisition Computer

### D.3.1 Virus Protection

Microsoft Forefront software is installed on the UCVS control system. Forefront is configured for both real-time protection and weekly full scans of the computer. Updates to virus and spyware definition files are performed automatically as available.

### D.3.2 Windows Updates

PNNL's default policy for Windows updates applies noncritical patches on a monthly cycle. Critical updates can be triggered out of normal patch schedule when mandated by PNNL's Site Security Officer. The UCVS systems will be configured to apply windows updates outside of WFFF's normal operating hours to avoid interruptions to data collection.

### D.3.3 Data Backup

Local data backup is facilitated by a RAID 5 array of hard drives. A USB hard drive is also in the cabinet for manual data removal, if needed.